17 February 2012 | $10

Science

AAAS

EDITORIAL

775 Science and Diplomacy
E. William Colglazier

NEWS OF THE WEEK

780 A roundup of the week's top stories

NEWS & ANALYSIS

783 Science Spared Brunt of Ax in Budget Request
Hard Times for OSTP
>> Science *Podcast*

785 Does Forewarned = Forearmed With Lab-Made Avian Influenza Strains?
Dead Reckoning the Lethality of Bird Flu
>> Science *Express Policy Forum by J. S. M. Peiris* et al.

787 Marriage Decision Highlights Same-Sex Studies

788 A Tiny Window Opens Into Lake Vostok, While a Vast Continent Awaits

NEWS FOCUS

790 Uncovering Civilization's Roots

LETTERS

794 Bad Advice, Not Young Scientists, Should Hit the Road
M. S. Cohen

Readers' Poll: Bad Advice?

Rescuing Wolves: Threat of Misinformation
L. D. Mech

Rescuing Wolves: States Not Immune to Politics
D. Johns

Response
J. T. Bruskotter et al.

796 CORRECTIONS AND CLARIFICATIONS

796 TECHNICAL COMMENT ABSTRACTS

BOOKS *ET AL.*

797 Plato's Revenge
W. Ophuls;
Eco-Republic
M. Lane; *reviewed by S. H. Ali*

798 Grand Theories and Everyday Beliefs
W. Matson, reviewed by P. W. Hughes

POLICY FORUMS

799 H5N1 Debates: Hung Up on the Wrong Questions
D. R. Perez

801 Life Sciences at a Crossroads: Respiratory Transmissible H5N1
M. T. Osterholm and D. A. Henderson

802 The Obligation to Prevent the Next Dual-Use Controversy
R. R. Faden and R. A. Karron
>> Science *Express Policy Forum by J. S. M. Peiris* et al.; *see all H5N1 coverage online at http://scim.ag/_h5n1*

PERSPECTIVES

805 A Cold Editor Makes the Adaptation
M. Öhman
>> *Report p. 848*

806 Gene Losses in the Human Genome
L. Quintana-Murci
>> *Research Article p. 823*

807 Adding Aliphatic C–H Bond Oxidations to Synthesis
M. C. White

809 Contemplating the First Plantae
F. W. Spiegel
>> *Report p. 843*

810 Mountains, Weathering, and Climate
A. Paytan
>> *Research Article p. 818*

812 Retrospective: James F. Crow (1916–2012)
W. Dove and M. Susman

CONTENTS continued >>

page 790

page 797

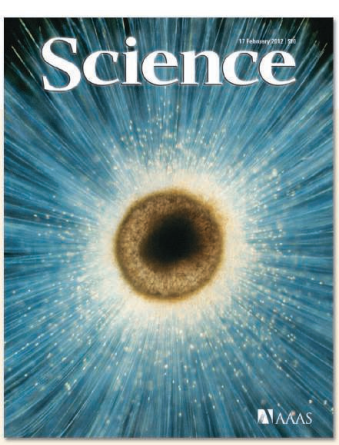

COVER

Orbulina universa, a planktonic foraminifera captured live from surface waters off Santa Catalina Island, California. Symbiotic dinoflagellates inhabit the calcite spines (length ~2.5 millimeters) radiating out from a spherical calcite shell (diameter ~0.5 millimeters). After four weeks, the shells sink to the sea floor and become part of the deep-sea microfossil assemblage. The geochemical compositions of these fossils are used to reconstruct past changes in seawater chemistry (see page 818).

Photo: Howard J. Spero, University of California, Davis

DEPARTMENTS

773 This Week in *Science*
776 Editors' Choice
778 *Science* Staff
867 New Products
868 *Science* Careers

Published by AAAS

pages 799, 801, & 802

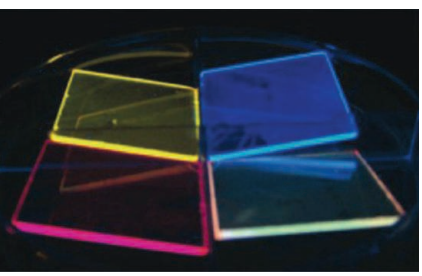

page 813

page 851

REVIEW

813 Functional Supramolecular Polymers
T. Aida et al.

RESEARCH ARTICLES

818 Lithium Isotope History of Cenozoic Seawater: Changes in Silicate Weathering and Reverse Weathering
S. Misra and P. N. Froelich
Historical changes in the lithium isotope ratio in seawater imply episodes of tectonic uplift and carbon dioxide drawdown.
>> *Perspective p. 810*

823 A Systematic Survey of Loss-of-Function Variants in Human Protein-Coding Genes
D. G. MacArthur et al.
Validation of predicted nonfunctional alleles in the human genome affects the medical interpretation of genomic analyses.
>> *Perspective p. 806;* Science *Podcast*

REPORTS

828 Unraveling the Spin Polarization of the $\nu = 5/2$ Fractional Quantum Hall State
L. Tiemann et al.
Nuclear magnetic resonance shows that an exotic state of matter may have the properties necessary for error-free quantum computing.

831 A Logic-Gated Nanorobot for Targeted Transport of Molecular Payloads
S. M. Douglas et al.
Cargoes stored in folded DNA origami are released when aptamers in the structure bind target protein molecules.

835 Supported Iron Nanoparticles as Catalysts for Sustainable Production of Lower Olefins
H. M. Torres Galvis et al.
A class of iron catalysts selectively transforms gasified biomass into the building blocks of common plastics.

838 Plate Motions and Stresses from Global Dynamic Models
A. Ghosh and W. E. Holt
Geodynamic modeling predicts where the mantle drives or resists the motion of overlying tectonic plates.

843 *Cyanophora paradoxa* Genome Elucidates Origin of Photosynthesis in Algae and Plants
D. C. Price et al.
An ancient algal genome suggests a unique origin of the plastid in the ancestor to plants, algae, and glaucophytes.
>> *Perspective p. 809*

848 RNA Editing Underlies Temperature Adaptation in K^+ Channels from Polar Octopuses
S. Garrett and J. J. C. Rosenthal
Octopus potassium channels function efficiently at different temperatures due to RNA editing and not genetic differences.
>> *Perspective p. 805*

851 Crystal Structure of a Lipid G Protein–Coupled Receptor
M. A. Hanson et al.
A channel in a lipid-dependent G protein–coupled receptor allows a ligand to access its binding site from within the plasma membrane.

856 Epithelial Nitration by a Peroxidase/NOX5 System Mediates Mosquito Antiplasmodial Immunity
G. de Almeida Oliveira et al.
Expression of nitric oxide synthase followed by peroxidase activity makes *Plasmodium* visible to the insect's complement system.

859 Structural Basis of TLR5-Flagellin Recognition and Signaling
S. Yoon et al.
Bacterially derived flagellin binds to an innate immune receptor to form a tail-to-tail heterodimeric signaling complex.

864 Survival Analysis of Faculty Retention in Science and Engineering by Gender
D. Kaminski and C. Geisler
Individual assistant professors hired since 1990 at 14 U.S. universities were tracked from time of hire to time of departure.
>> Science *Podcast*

Published by AAAS

SCIENCEONLINE

SCIENCEXPRESS

www.sciencexpress.org

Lin28b Reprograms Adult Bone Marrow Hematopoietic Progenitors to Mediate Fetal-like Lymphopoiesis

J. Yuan et al.

The RNA binding protein Lin28 drives fetal modes of immune cell development.

10.1126/science.1216557

The Transcription Factor c-Maf Controls Touch Receptor Development and Function

H. Wende et al.

A mutation known to cause cataracts also disables a specialized mechanosensory receptor in mice and humans.

10.1126/science.1214314

Influence of Synaptic Vesicle Position on Release Probability and Exocytotic Fusion Mode

H. Park et al.

Tracking of individual synaptic vesicles reveals that kiss-and-run fusion is concentrated near the center of the synapse.

10.1126/science.1216937

Observation of Quantum Criticality with Ultracold Atoms in Optical Lattices

X. Zhang et al.

Trapped low-temperature atoms model the transition between insulating and superfluid states in a more complex material.

10.1126/science.1217990

^{182}W Evidence for Long-Term Preservation of Early Mantle Differentiation Products

M. Touboul et al.

Tungsten isotopes in ancient volcanic rocks suggest sluggish mixing processes in the primitive mantle.

10.1126/science.1216351

Surveillance of Animal Influenza for Pandemic Preparedness

J. S. M. Peiris et al.

10.1126/science.1219936

>> News story p. 785; Policy Forums pp. 799, 801, and 802; see all H5N1 coverage online at http://scim.ag/_h5n1

TECHNICALCOMMENTS

Comment on "A Diverse Assemblage of Late Cretaceous Dinosaur and Bird Feathers from Canadian Amber"

C. J. Dove and L. C. Straker

Full text at www.sciencemag.org/cgi/content/full/335/6070/796-b

Response to Comment on "A Diverse Assemblage of Late Cretaceous Dinosaur and Bird Feathers from Canadian Amber"

R. C. McKellar et al.

Full text at www.sciencemag.org/cgi/content/full/335/6070/796-c

SCIENCENOW

www.sciencenow.org

Highlights From Our Daily News Coverage

Embryos Starved of Oxygen May Be 'Programmed' for Heart Disease

A rat study suggests antioxidants could help.

http://scim.ag/Embryos_Oxygen

Is Agriculture Sucking Fresh Water Dry?

Crops account for 92% of fresh water used each year, according to a new global analysis.

http://scim.ag/Fresh_Water

A Piranha-Proof Fish

Unique scales keep arapaima from becoming lunch.

http://scim.ag/Piranha-Proof

SCIENCESIGNALING

www.sciencesignaling.org

The Signal Transduction Knowledge Environment

14 February issue: http://scim.ag/ss021412

RESEARCH ARTICLE: Selective TRIF-Dependent Signaling by a Synthetic Toll-Like Receptor 4 Agonist

W. S. Bowen et al.

A single change in a synthetic lipid A mimetic may reduce the toxicity of this vaccine adjuvant.

RESEARCH ARTICLE: MNK2 Inhibits eIF4G Activation Through a Pathway Involving Serine-Arginine–Rich Protein Kinase in Skeletal Muscle

S.-I. Hu et al.

In muscle, the kinase-dependent and -independent activities of MNK2 exert a negative effect on protein synthesis pathways.

TEACHING RESOURCE: Measurement of cAMP in an Undergraduate Teaching Laboratory, Using ALPHAscreen Technology

J. D. Bartho et al.

Students measure the changes in cyclic AMP, a second messenger molecule, with a light-based assay.

ST NETWATCH: Minimum Information for Biological and Biomedical Investigations (MIBBI)

This site provides checklists that specify the metadata required for experimental data sets.

ST NETWATCH: Protein Information Resource (PIR)

Access tools for integrating genomic and proteomic information from various databases.

PODCAST

M. Peters-Golden and A. M. VanHook

The protein phosphatase activity of PTEN impairs macrophage phagocytosis of a fungal pathogen by promoting actin depolymerization.

SCIENCETRANSLATIONAL MEDICINE

www.sciencetranslationalmedicine.org

Integrating Medicine and Science

15 February issue: http://scim.ag/stm021512

RESEARCH ARTICLE: MicroRNA-21 Promotes Fibrosis of the Kidney by Silencing Metabolic Pathways

B. N. Chau et al.

MicroRNA-21 contributes to fibrosis in the kidney by posttranscriptionally regulating lipid metabolism genes.

RESEARCH ARTICLE: T-Type Calcium Channel Blockers That Attenuate Thalamic Burst Firing and Suppress Absence Seizures

E. Tringham et al.

T-type calcium channel blockers attenuate neural activity in the thalamus and suppress seizures in a genetic model of epilepsy.

RESEARCH ARTICLE: Phosphorylated α-Synuclein in Parkinson's Disease

Y. Wang et al.

An assay for detecting phosphorylated α-synuclein in CSF may help to diagnose Parkinson's disease and determine disease severity.

PERSPECTIVE: Viral and Inflammatory Triggers of Neurodegenerative Diseases

M. Deleidi and O. Isacson

Immune pathways induced by viral infections render neurons vulnerable to subsequent degeneration.

SCIENCECAREERS

www.sciencecareers.org/career_magazine

Free Career Resources for Scientists

Tooling Up: The Big Disconnect

D. Jensen

In today's biomedical industry, pinpoint hiring is the rule.

http://scim.ag/TU_Disconnect

Perspective: Bridging Your Research Into Public Health

K. Chan

A public health researcher and former bench scientist offers advice on how to implement your science in the real world.

http://scim.ag/KeeChan

SCIENCEPODCAST

www.sciencemag.org/multimedia/podcast

Free Weekly Show

On the 17 February *Science* Podcast: the gender breakdown in academic faculty, identifying mutations that give rise to disease, budgeting for science in the United States, and more.

SCIENCEINSIDER

news.sciencemag.org/scienceinsider

Science Policy News and Analysis

SCIENCE (ISSN 0036-8075) is published weekly on Friday, except the last week in December, by the American Association for the Advancement of Science, 1200 New York Avenue, NW, Washington, DC 20005. Periodicals Mail postage (publication No. 484460) paid at Washington, DC, and additional mailing offices. Copyright © 2012 by the American Association for the Advancement of Science. The title SCIENCE is a registered trademark of the AAAS. Domestic individual membership and subscription (51 issues): $149 ($74 allocated to subscription). Domestic institutional subscription (51 issues): $990; Foreign postage extra: Mexico, Caribbean (surface mail) $55; other countries (air assist delivery) $85. First class, airmail, student, and emeritus rates on request. Canadian rates with GST available upon request, GST #1254 88122. Publications Mail Agreement Number 1069624. **Printed in the U.S.A.**

Change of address: Allow 4 weeks, giving old and new addresses and 8-digit account number. **Postmaster:** Send change of address to AAAS, P.O. Box 96178, Washington, DC 20090–6178. **Single-copy sales:** $10.00 current issue, $15.00 back issue prepaid includes surface postage; bulk rates on request. **Authorization to photocopy** material for internal or personal use under circumstances not falling within the fair use provisions of the Copyright Act is granted by AAAS to libraries and other users registered with the Copyright Clearance Center (CCC) Transactional Reporting Service, provided that $30.00 per article is paid directly to CCC, 222 Rosewood Drive, Danvers, MA 01923. The identification code for *Science* is 0036-8075. *Science* is indexed in the *Reader's Guide to Periodical Literature* and in several specialized indexes.

AAAS

ADVANCING SCIENCE, SERVING SOCIETY

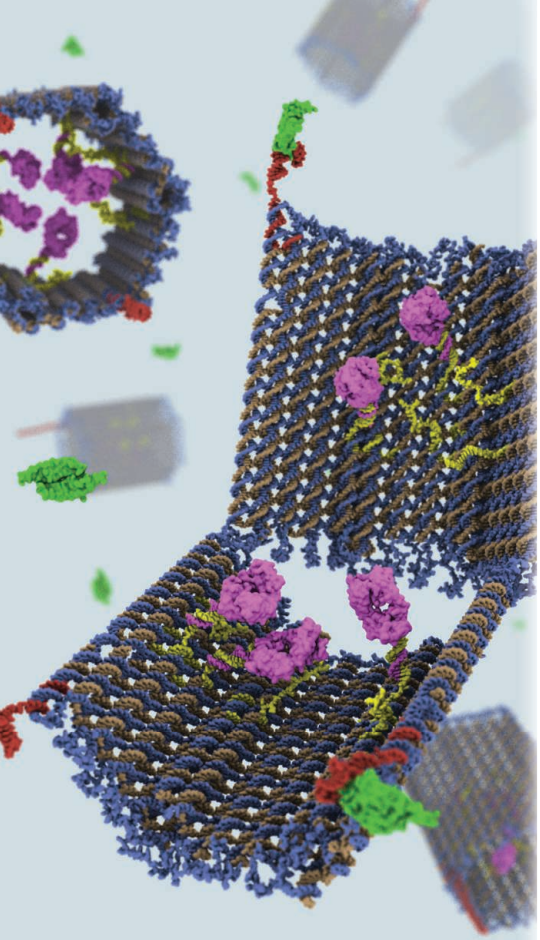

Nanorobots Deliver

DNA aptamers are short strands that have high binding affinity for a target protein that can be used as triggers for releasing cargo from delivery vehicles. **Douglas *et al.*** (p. 831) used this strategy to design DNA origami "nanorobots"—complex shaped structures created by manipulating a long DNA strand through binding with shorter "staple" strands—that could deliver payloads such as gold nanoparticles or fluorescently labeled antibody fragments. These nanorobots were designed to open in response to specific cell-surface proteins, releasing molecules that triggered cell signaling.

CREDITS (TOP TO BOTTOM): CAMPBELL STRONG, SHAWN DOUGLAS, AND GAËL MCGILL; GHOSH AND HOLT

Supramolecular Polymers Explained

While polymers are constructed from chemically bonded units, supramolecular polymers arise through reversible linkages, such as hydrogen bonding and electrostatic interactions. Recent advances in the field of supramolecular polymer science have moved from a fundamental understanding of assembly properties to the introduction of functionality, in order to exploit the particular features of this class of materials. **Aida *et al.*** (p. 813) review the specific features of supramolecular polymers that can lead to applications in a variety of fields, including: materials—in which processability and self-healing properties are of interest; biomedicine—in which the concerns are dynamic functionality and biodegradability; and hierarchical assembly and electronic systems—with an interest in unidirectionality of charge flow.

Life of Li

Because lithium primarily exists in silicate minerals on continents, the variations of Li isotopes in marine sedimentary rocks reflect the degree of silicate weathering and formation of new sediments on the seafloor, which in turn are largely controlled by climate and tectonic forces over geologic time. By analyzing sedimentary cores from eight drill sites around the world's oceans, **Misra and Froelich** (p. 818, published online 26 January; see the cover; see the Perspective by **Paytan**) assembled a 68-million-year record of the Li isotope composition of seawater. The record reveals a stepwise change in the Li isotopic ratio, suggesting that several intense episodes of tectonic uplift increased continental weathering rates and delivery of sediments to the oceans. Abrupt swings in the record at specific points in Earth's history, for example, around the time when dinosaurs became extinct, imply major changes in ocean chemistry—but their mechanisms remain enigmatic.

Driving Forces

The physical properties that control the motions of Earth's tectonic plates are difficult to predict accurately on a global scale. Large-scale geodynamic models are continually becoming more powerful, but controversies remain regarding plate-driving forces. **Ghosh and Holt** (p. 838) present a global geodynamic model that achieves a high level of accuracy in fitting surface plate motions, plate boundary deformation, and intraplate stress fields. The model identifies regions where mantle drag drives plate motion and regions where the drag resists plate motion. Based on the relative magnitude of mantle drag forces and lithospheric buoyancies contributing to the stress field, the model also quantifies absolute viscosity—a parameter that has been notoriously difficult to predict for Earth's interior.

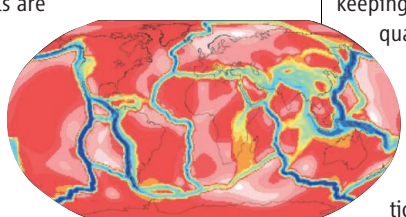

Defective Gene Detective

Identifying genes that give rise to diseases is one of the major goals of sequencing human genomes. However, putative loss-of-function genes, which are often some of the first identified targets of genome and exome sequencing, have often turned out to be sequencing errors rather than true genetic variants. In order to identify the true scope of loss-of-function genes within the human genome, **MacArthur *et al.*** (p. 823; see the Perspective by **Quintana-Murci**) extensively validated the genomes from the 1000 Genomes Project, as well as an additional European individual, and found that the average person has about 100 true loss-of-function alleles of which approximately 20 have two copies within an individual. Because many known disease-causing genes were identified in "normal" individuals, the process of clinical sequencing needs to reassess how to identify likely causative alleles.

Toward Quantum Computing

Quantum computers are expected to be able to tackle problems that would take classical computers many lifetimes to solve. Nonabelian states of matter can store quantum information in their topology, making them immune to environmental perturbations. A physical system expected to possess this unusual property is the fractional quantum Hall state at filling factor $\nu = 5/2$. **Tiemann *et al.*** (p. 828, published online 26 January) used nuclear magnetic resonance to measure the polarization of the 5/2 state and found that it is fully polarized—a finding consistent with a nonabelian state—keeping hopes for topological fault-tolerant quantum computing alive.

From Plant to Plastic

Petroleum is primarily used as fuel, but it is also used in the production of plastics. Thus, if biomass were to replace petroleum as society's carbon feedstock, a means of deriving ethylene and propylene—the principal building blocks of today's commodity plastics—would be helpful. Well-known Fischer-Tropsch (FT) catalysts can transform gasified biomass into a range of hydrocarbon derivatives, but ethylene and propylene tend to constitute a small fraction of the overall product distribution. **Torres Galvis *et al.*** (p. 835) now demonstrate a class of iron catalysts on relatively passive supports (carbon nanofibers or α-alumina) that robustly directed the FT process toward light olefins.

Continued on page 774

Downloaded from www.sciencemag.org on February 16, 2012

AAAS Travels

Wild Indonesia
August 15-29, 2012
An amazing opportunity to travel on a life-aboard boat. Discover Komodo dragons in the wild, snorkel in spectacular marine reserves, and see Liang Bua Cave (extraordinary find in 2003). Indigenous cultural groups, with beautiful dance and song, will fascinate us, as will the island biogeography of Flores. $3,690 + air.

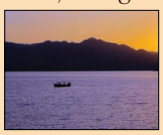

Xinjiang & Hunza
September 2-19, 2012
Discover lofty peaks and villages of the Silk Road and Karakoram, including the oasis cities of Urumqi and Kashgar, and the legendary Hunza Valley. See spectacular deserts and some of the highest peaks in the world! $3,895 + air.

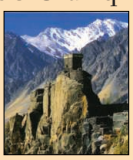

For a detailed brochure, please call (800) 252-4910
All prices are per person twin share + air

Betchart Expeditions Inc.
17050 Montebello Road
Cupertino, California 95014
Email: AAASInfo@betchartexpeditions.com
www.betchartexpeditions.com

AAAS is here –
bringing educational infrastructure to the developing world.

AAAS is helping the Rwandan government rebuild its educational infrastructure. By providing materials such as the Project 2061 *Atlas of Science Literacy*, lesson plans from Science NetLinks, and access to *Science* digital libraries, AAAS is helping the people of Rwanda work toward a future built around science and technology. If you're not yet a AAAS member, join us. Together we can make a difference.

To learn more, visit
aaas.org/plusyou/rwanda

AAAS + U = Δ

Continued from page 773

Plastid Origins

The glaucophytes, represented by the alga *Cyanophora paradoxa*, are the putative sister group of red and green algae and plants, which together comprise the founding group of photosynthetic eukaryotes, the Plantae. In their analysis of the genome of *C. paradoxa*, **Price *et al.*** (p. 843; see the Perspective by **Spiegel**) demonstrate a unique origin for the plastid in the ancestor of this supergroup, which retains much of the ancestral diversity in genes involved in carbohydrate metabolism and fermentation, as well as in the gene content of the mitochondrial genome. Moreover, about 3.3% of nuclear genes in *C. paradoxa* seem to carry a signal of cyanobacterial ancestry, and key genes involved in starch biosynthesis are derived from energy parasites such as Chlamydiae. Rapid radiation, reticulate evolution via horizontal gene transfer, high rates of gene divergence, loss, and replacement, may have diffused the evolutionary signals within this supergroup, which perhaps explains previous difficulties in resolving its evolutionary history.

Adapting to the Cold

The gating of potassium channels is temperature sensitive, suggesting that these channels must adapt to function efficiently in the extreme cold. **Garrett and Rosenthal** (p. 848, published online 5 January; see the Perspective by **Öhman**) show that the coding sequences for delayed rectifier potassium channels from an Antarctic and a tropical octopus differed at only four positions and gave functionally identical channels when expressed in *Xenopus* oocytes. A variation in temperature responses instead came from extensive messenger RNA editing. In particular, an edit that recoded an isoleucine to a valine in the pore of the Antarctic octopus channel greatly accelerated gating kinetics.

From NO to Complement

To complete their development in the mosquito, ookinetes—reproductive stages of the malaria parasite *Plasmodium*—must traverse the midgut epithelium and avoid being detected and lysed by the mosquito complement system thioester-containing protein 1 (TEP1). **Oliveira *et al.*** (p. 856, published online 26 January) identified mosquito heme peroxidase (HPX2) and a reduced form of nicotinamide adenine dinucleotide phosphate (NADPH) oxidase 5 (NOX5) as key enzymes that are induced in midgut cells during ookinete invasion that, together with nitric oxide synthase, mediate protein nitration. The HPX2-NOX5 system potentiates nitric oxide toxicity and is critical for mosquitoes to mount an effective antiplasmodial response. Epithelial nitration and TEP1-mediated lysis appear to act sequentially in parasite killing, and epithelial nitration may help to promote the mosquito complement cascade.

Flagellin Takes Its Toll

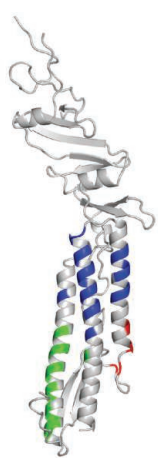

CREDIT: YOON *ET AL.*

The immune system recognizes bacterial infections by binding to conserved molecular fragments derived from the invading bacteria. Molecular mimics of these bacterial determinants have the potential to boost the immunogenicity of vaccines. **Yoon *et al.*** (p. 859) now report the crystal structure of the D1/D2 fragment of *Salmonella* flagellin, a protein critical for the motility of flagellated bacteria, with the ectodomain of zebrafish Toll-like receptor 5 (TLR5), the host receptor that binds to flagellin and signals the immune system to react. Two TLR5-flagellin heterodimers dimerized into a 2:2 tail-to-tail signaling complex. Mutational analysis and use of human TLR5 validated the signaling mechanism, which is conserved from zebrafish to humans.

Faculty Fates

Academic careers in STEM (science, technology, engineering, and math) include challenges that may differ depending on gender. **Kaminski and Geisler** (p. 864) analyzed the retention rates for tenure-track faculty at 14 U.S. universities in various disciplines. College catalogs, departmental Web sites, and other public sources of information were used to follow the academic careers of nearly 3000 STEM faculty. Except in mathematics faculties—where women left a couple of years earlier than men—generally, women and men were retained and promoted at the same rate.

Downloaded from www.sciencemag.org on February 16, 2012

E. William Colglazier is the U.S. Science and Technology Adviser to the Secretary of State, U.S. Department of State, Washington, DC.

Science and Diplomacy

THE WORLD HAS MUCH TO GAIN FROM DEVELOPING MORE KNOWLEDGE- AND INNOVATION-BASED societies and from spreading scientific values, including meritocracy and transparency, that support democracy. This fundamental assumption underlies a renewed interest in science diplomacy, along with the widespread recognition that science and technology (S&T) are strategic assets for U.S. diplomacy. My recent appointment as S&T Adviser to Secretary of State Hillary Clinton has increased my appreciation of the great potential of America's S&T capabilities for enhancing our foreign policy. S&T are strategic assets for U.S. diplomacy because all countries, regardless of their politics, culture, and worldview, respect our S&T capabilities and want to engage with U.S. scientists and engineers. This is true even of countries with which governmental relations are strained. S&T are critical to fostering innovation and economic prosperity in a highly competitive and interconnected world, and are essential for solving national and global problems.

My office, the Office of the Science and Technology Adviser to the Secretary of State (STAS), assists the Department of State but is not an operational bureau. Its goals are to strengthen the S&T knowledge base in the department, anticipate S&T issues that can affect foreign policy, advocate for science-informed decisions in all countries, and support global S&T engagement that serves U.S. interests. It works closely with the Bureau of Oceans and International Environmental and Scientific Affairs (OES), which has many policy and operational responsibilities as well as activities regarding S&T relations with other countries and organizations. OES and STAS report to Under Secretary Robert Hormats, who is a strong proponent of science diplomacy. STAS also works closely with the Office of Science and Technology at the U.S. Agency for International Development (USAID), which has expanded the role of S&T in America's international development efforts.

Last month, in public testimony to the President's Council of Advisors on Science and Technology,* I outlined 10 areas where I believe the State Department and USAID are making substantial contributions in science diplomacy. STAS is assisting in these areas by serving as an advocate inside and outside the government, adding ideas to the mix, partnering when helpful, and spearheading efforts where needed. Department activities now under way include the support of policy dialogues and programs that create knowledge-based societies worldwide, including in countries such as Colombia, South Africa, and Indonesia, which are investing heavily in education, research, and constructive policies. We also are supporting creative approaches for sourcing innovation, such as through open competitions and challenges that reach out to smart entrepreneurial people of all ages and countries. And we are working to remove barriers and garner more financial support for global S&T engagement involving U.S. federal agencies, universities, and private companies; to expand opportunities for U.S. scientists and engineers to engage in public diplomacy overseas; to promote programs that empower women in science and engineering; and to enhance fellowship programs that bring bright scientifically trained people to work at the State Department and USAID.

One of my most important goals is to encourage other governments to seek independent, objective advice from their S&T communities. The United States has benefited greatly from expert advice from the U.S. National Academies and other scientific nongovernmental organizations. The government may not always like the public advice, but it listens, and important policies are frequently influenced for the better.

Making progress in science diplomacy will require energetic international engagement by America's scientists and engineers. With that commitment, I see bright prospects for our S&T contributing significantly to our diplomacy in building a more peaceful, secure, and prosperous world.

– E. William Colglazier

10.1126/science.1220355

*www.tvworldwide.com/events/pcast/120106/.

CREDITS: (TOP) U.S. DEPARTMENT OF STATE; (RIGHT) ISTOCKPHOTO.COM

Downloaded from www.sciencemag.org on February 16, 2012

Published by AAAS

EDITED BY KRISTEN MUELLER AND JAKE YESTON

MICROBIOLOGY

Live to Divide Another Way

Bacterial cell division is classically thought of as symmetrical. Several species divide by polar budding, however, and mutations in the cell division machinery of *Agrobacterium, Brucella,* and *Sinorhizobium* trigger branching morphologies rather than filaments. Two recent papers explored this phenomenon. First, in the rod-shaped plant pathogen *Agrobacterium tunefaciens*, Brown *et al.* used time-lapse photography and observed that new daughter cells emerge strictly from the pole of the mother cell, growing by incorporation of newly synthesized cell wall. After division, there is only a small increase in mother cell length, which retains old cell wall material. Cell division in *Mycobacterium* was also shown to be asymmetrical, giving rise to slow-growing daughter cells that are less sensitive to an anti-tuberculosis drug than faster-growing but older mother cells (see Aldridge *et al.*, Reports, *Science*, 6 January 2012). Asymmetric inheritance of cell material of different ages may give bacteria multiple adaptive options by generating a variety of phenotypes, some of which will be able to escape a shift in environmental conditions and live to divide another day. — CA

Proc. Natl. Acad. Sci. U.S.A. **109**, 1697 (2011).

CELL BIOLOGY

A Collective Movement

Migratory cells are exquisitely sensitive to gradients in concentrations of molecules that provide guidance cues, and in individual cells, localized signals produce directed migration. Cells sometimes migrate as a group, however, and in this case the signaling mechanisms by which cellular movements are controlled are less clear. Inaki *et al.* tested whether one member of a group of cells could coordinate migration of the group. The authors modified border cells of the *Drosophila* ovary so that they would be unresponsive to the endogenous ligands that guide them through the activation of receptor tyrosine kinases. They then overexpressed a receptor in only one of the cells, which resulted in its being active in the absence of ligand. In an alternative approach, the authors activated the small guanosine triphosphatase Rac, which is required for migration, in only one cell. In both cases, signaling in a single cell could direct migration. These results suggest that information directing the group of cells is encoded in the difference between signals occurring in individual cells within the group; these signals appear to be different than the signals used by cells migrating on their own. — LBR

Proc. Natl. Acad. Sci. U.S.A. **109**, 2027 (2012).

PSYCHOLOGY

What Would Jesus Do?

During the past several election cycles in the United States, the association of religious views and voting preferences has been noted. This has led to claims that greater religiosity generates support for conservative policies, which generally favor lower and less progressive tax rates as well as restrictions on same-sex marriage. The take-home message has been that an individual's religious beliefs influence that person's political stance. Ross *et al.* have used a survey of roughly 500 liberal and conservative Christians to examine the converse proposition—that an individual's political views affect that person's religious beliefs. What they found was that self-described liberals and conservatives exhibited the expected views regarding higher tax rates and gay marriage. What was intriguing, however, were the views that both liberals and conservatives imputed to a contemporary Jesus: Conservatives rated Jesus as being more in favor of higher taxes on the wealthy and more opposed to gay marriage than they themselves were, with an opposite pattern for liberals. By placing more weight on issues on which they projected Jesus as being more extreme than themselves, individuals on both sides of the spectrum were able to reduce dissonance, which might be better characterized as social rather than cognitive, owing to the collective nature of religion. — GJC

Proc. Natl. Acad. Sci. U.S.A. **109**, 10.1073/pnas.1117557109 (2012).

PHYSICS

Approaching a Supermodel

Optical lattices, constructed from counter-propagating laser beams and loaded with atoms a fraction of a degree above absolute zero, are slowly fulfilling their potential of simulating solid materials. One of the long-term goals in the field is building a model of a cuprate superconductor, with its layered structure of loosely bound planes. Sommer *et al.* make a step in that direction by loading a three-dimensional (3D) gas of fermionic atoms of ^{6}Li into a 1D optical lattice; increasing the strength of the optical potential achieves a gradual crossover to a stack of uncoupled 2D layers confined to the successive troughs of the optical lattice. The authors track the formation of the bound pairs of fermions, crucial for the phenomena of superfluidity and superconductivity, by performing rf spectroscopy. As the dimensionality of the system changes, so do its properties; in line with theoretical predictions, the binding energy in the 2D system is independent of the interaction strength and equal to the binding energy in free space. Observation of superfluidity in the 2D layers is probably next on the agenda of simulating a cuprate. — JS

Phys. Rev. Lett. **108**, 45302 (2012).

CREDIT: ISTOCKPHOTO.COM

Downloaded from www.sciencemag.org on February 16, 2012

Published by AAAS

DEVELOPMENT

Developmental Dynamics Uncaged

Transcription factors are critical for proper gene regulation during development, but they have pleiotropic effects and dynamically regulate the spatial and temporal expression of many target genes. Because of the difficulty of studying this process using conventional methods, Shestopalov *et al.* devised a method to conditionally regulate the activities of several transcription factors in optically transparent zebrafish embryos. Embryos were injected with caged morpholinos targeting specific transcription factors: The RNA-targeting morpholino's repressive function is blocked initially, but exposure to UV or two-photon infrared light at specific developmental stages in specific cell populations cleaves a linker that then allows the morpholinos to block transcription factor function. Cells were then isolated and subjected to microarray analysis to determine the dynamic transcriptomes during development. As a proof of principle, the authors applied this technology to understand the activities of the No-tail transcription factor (Ntla) in axial tissues at different developmental stages. — BAP

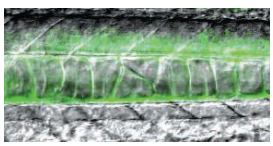

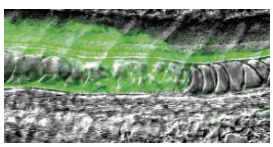

Nat. Chem. Biol. **8**, 10.1038/nchembio.772 (2012).

CHEMISTRY

More Mercury for the Money

Amalgam formation between silver and mercury has long been exploited on behalf of the silver, whether in facilitation of mining the precious metal, shaping it into jewelry, or embedding it in decayed teeth. More recently, however, there's been something of a role reversal under way, as silver particles are applied to the removal of toxic mercury contaminants from water sources. Katok *et al.* have explored the impact of silver particle size on the nature and efficiency of this process. Bulk metallic silver is known to reduce mercuric ions, with concomitant release of silver ions in a 1:2 stoichiometry. Using a range of sensitive analytical techniques, the authors found that very small (~11-nm-diameter) silver particles supported on a reduced silica substrate removed mercuric ions from aqueous solution in a ratio exceeding 1:1. The mechanism underlying this hyperstoichiometric process remains somewhat uncertain, as does the precise lattice structure of the Hg-Ag composite produced. The authors posit a catalytic role for silver ions that may be readsorbed and reduced back to the elemental state by counterions in the solution. — JSY

Angew. Chem. Int. Ed. **51**, 10.1002/anie.201106776 (2012).

ENGINEERING

Calling All Plumbers

Societal water infrastructure is in dire need of rebuilding and modernization in consideration of economic as well as human safety concerns (see Caldwell, Editorial, *Science*, 21 October 2011). For example, leaky pipes result in the loss of 7 billion gallons of clean, treated drinking water every day in the United States alone. Water distribution networks are a hodgepodge of aging original pipes, replacement pipes, and pipes made from new materials; moreover, external pressures change over time. It is therefore difficult to predict when a system—let alone an individual pipe—will fail. Malm *et al* compared two statistical models of future replacement rates in Gothenburg, Sweden, based on historical data: one that includes over 100 years of data from city archives and water utility reports, the other based on a more detailed 15-year modern record. The long-term historical model more accurately predicts some factors, including the percentage of original pipes remaining in the network; however, in the absence of archived data, service life predicted using the shorter data set was still satisfactory. Overall, system replacement needs are largely reflective of how frequently pipe rehabilitation occurred in the past, and the reasons for replacement (e.g., pipe failure versus city expansion). — NW

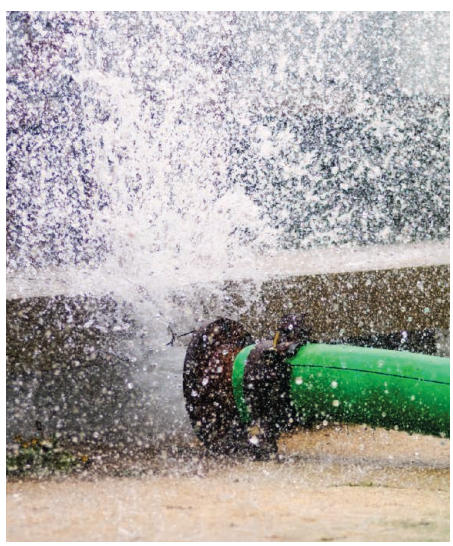

Water Res. 10.1016/j.watres.2012.01.036 (2012).

105
things you didn't (and 3 you probably shouldn't) know about some of your most respected colleagues.
One more data point on why you should spend more time at membercentral.aaas.org. There you can enjoy a feast of blogs, videos, webinars, discounts, and downloads created by and for the most insatiable brains around.
AAAS MemberCentral
membercentral.aaas.org

Downloaded from www.sciencemag.org on February 16, 2012

CREDITS (TOP TO BOTTOM): SHESTOPALOV *ET AL. NAT. CHEM. BIOL.* 8, 10.1038/NCHEMBIO.772 (2012); ISTOCKPHOTO.COM

AROUND THE WORLD

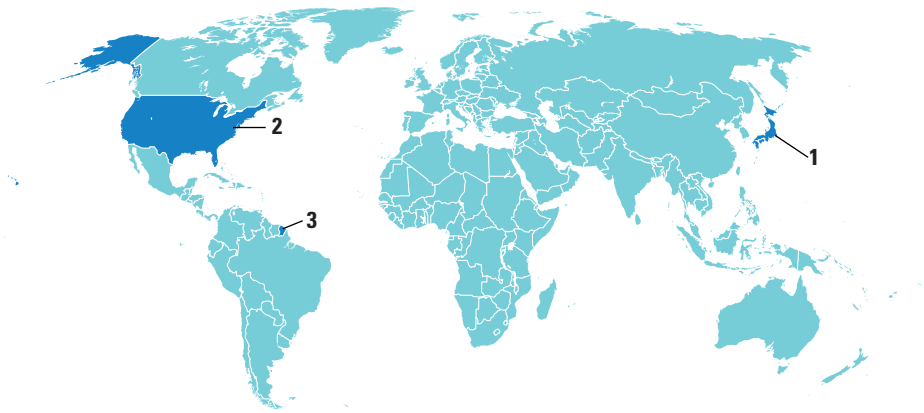

Tokyo **1**

World Bank Frets Over Urban Flooding in Asia

A new World Bank report suggests the developing countries of Asia are particularly vulnerable to flooding. "It is increasingly an Asian phenomenon," Abhas Jha, a World Bank disaster management expert, said 13 February at a report briefing in Tokyo. Over the past 30 years, the seven most destructive floods occurred in Asia, and 90% of those killed or affected by floods lived in Asia. The region also got hit with about half of the total worldwide economic loss due to flooding.

Hit hard. Urban flooding is taking a toll in Asia.

The main reason for Asia's vulnerability to floods is the movement of populations from rural areas to cities built on coasts and along rivers. The report, *Cities and Flooding: A Guide to Integrated Urban Flood Risk Management for the 21st Century*, outlines flood causes that can exacerbate heavy rains, such as deforestation and loss of wetlands, or that can increase runoff and hinder groundwater replenishment, such as paving and development.

Mitigation requires integrating the efforts of scientists, engineers, and social scientists to create hazard maps to guide urban planning and develop management strategies. The World Bank report concludes mitigation efforts should concentrate on Asia because many countries are still at an early stage of urbanization. **http://scim.ag/floodreport**

Washington, D.C. **2**

Synthetic Biology Report Being Ignored

The Obama Administration has made only modest progress toward closer oversight of the young field of synthetic biology, an outside group has concluded.

After biologist Craig Venter's team inserted a synthetic genome into a bacterial cell in May 2010, sparking concerns that such experiments could do both good and harm, the Presidential Commission for the Study of Bioethical Issues launched a review of synthetic biology's benefits and risks to human health and the environment. In December 2010, the commission made 18 recommendations in areas including risk assessment and education (*Science*, 26 November 2010, p. 1166). But according to a "scorecard" released last week by the Woodrow Wilson International Center for Scholars in Washington, D.C., the Administration has moved ahead on only 10 steps.

For example, an interagency committee has released principles for developing regulations for emerging technologies, partly fulfilling a commission recommendation to assess whether new rules are needed. But the government has not completed an inventory of federal funding for synthetic biology activities or identified a central coordinating body to track research and regulations. Many of the steps are supposed to be completed by this June.

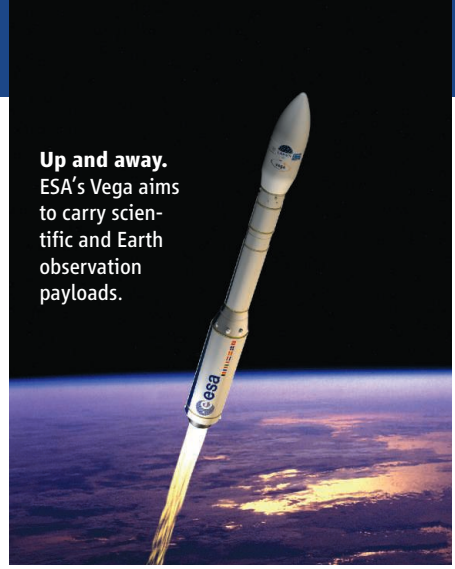

Up and away. ESA's Vega aims to carry scientific and Earth observation payloads.

Kourou, French Guiana **3**

Small Is Beautiful

The inaugural flight of Europe's new Vega rocket went off without a hitch on 13 February as mission VV01 lit up the early morning sky above the Kourou spaceport in French Guiana. Vega is a small launcher designed to carry scientific and earth observation satellites weighing from 300 to 2500 kilograms.

The European Space Agency (ESA), in collaboration with the Italian Space Agency, set out to develop the launcher 9 years ago as an alternative to sometimes-unreliable converted Russian ICBMs such as Rokot and Dnepr. Some €700 million later, Vega is ready for business. The diminutive rocket, just 30 meters tall, will be operated by the company Arianespace, alongside its medium-sized Soyuz launcher and heavy-lifting Ariane 5. "There is not anymore one single European satellite which cannot be launched by a European launcher service," ESA Director General Jean-Jacques Dordain said in a statement.

Monday's maiden flight gave nine satellites a free ride into orbit. The largest, LARES, will test the Lense-Thirring effect, a subtle orbital distortion predicted by general relativity. The rest are tiny nanosatellites built by university groups.

NEWSMAKERS

Weiler Quit NASA Over Cuts To Mars Program

The former head of NASA's science mission says the Obama Administration's attacks on ExoMars, a joint U.S.-European Mars mission, led to his resignation last September. "The Mars program is one of the crown jewels of NASA," **Ed Weiler** says. "In what irrational, Homer Simpson world would we single it out for disproportionate cuts?"

CREDITS (TOP TO BOTTOM): ESA/J. HUART, 2012; KYODO/LANDOV

Downloaded from www.sciencemag.org on February 16, 2012

Published by AAAS

In 2008, NASA and the European Space Agency (ESA) agreed to team up to send an orbiter to Mars in 2016, followed by a pair of rovers in 2018. Cuts to space science in the White House's proposed 2012 budget early in 2011 forced the two agencies to pare the two ExoMars rovers down to one, Weiler says. Then, last summer, a preliminary draft of an even more austere 2013 budget ratcheted up the pressure. Weiler says he proposed a 3% across-the-board cut, but White House budget officials insisted on gutting ExoMars. Weiler e-mailed NASA Administrator Charles Bolden saying he had had enough.

Weiler

Now, from his home in Vero Beach, Florida, Weiler says he doesn't miss the fray: "I'm glad to be here, a thousand miles away from the irrationality zone." **http://scim.ag/edweiler**

Three Q's

Glover

In January, Scottish microbiologist **Anne Glover** took office in Brussels as the first European Chief Scientific Advisor (CSA), reporting directly to European Commission President José Manuel Barroso. Glover, previously the CSA to the Scottish government, will provide the European Commission with evidence-based policy advice and will be a European spokesperson on scientific issues.

Q: What made you decide to take this job?
European science is excellent and from my point of view, looking at the future of Europe, science has to have as strong a voice as possible. My role is to raise the profile of our science both in Europe and also externally.

Q: How would you describe your task?
In very brief terms I would describe it as "big." But you can break it down into smaller pieces. We need youths to be considering their careers in science and engineering. We need the best possible evidence for policy making. We need stories of what European science has led to. Too few people realize what our science spending delivers.

Q: What lessons did you learn as a CSA in Scotland?
I noted it is very difficult to always base policy on evidence. I do appreciate that a lot more factors influence policy: ethical factors, social factors, economic factors. But where scientific evidence is not being used, there is an obligation for our policy makers and politicians to explain why they reject the evidence. I think as long as they do that, as long as there is transparency, I would be content with that. **http://scim.ag/anneglover**

Mystery Meteorite from the House of Sting

A 93-kilogram meteorite recovered 20 years ago from musician Sting's Lake House estate in the United Kingdom's rural Wiltshire may shed some light on ice-age Britain.

The meteorite landed 30,000 years ago in what would later become Sting's front yard. Sting and wife Trudie Styler bought the house in the 1990s—just after the house's previous owners, the Bailey family, loaned the meteorite to the Natural History Museum in London.

There it sat in storage until about 2 years ago, when Colin Pillinger, a planetary scientist at the Open University in Milton Keynes, U.K., took it out to study it. The meteorite was apparently preserved intact by the glaciers that once covered Britain and could provide important information about the region's ice age history, Pillinger says.

Between now and 30 March, the meteorite is on display at the Royal Society in London as part of its Objects in Space exhibit. This fall, the meteorite will go on display at Wiltshire's Salisbury Museum. http://scim.ag/stingrock

Foreign Takeover At Swedish Academy

Cannon

The Royal Swedish Academy of Sciences has selected a non-Swedish president. The Academy announced on 7 February that **Barbara Cannon**, a physiologist at the Wenner-Gren Institute for Experimental Biology at the University of Stockholm, would begin a 3-year term on 1 July. Cannon has spent her entire professional career in Sweden but has remained a citizen of her native United Kingdom. She came to Sweden for a 9-month scholarship after taking her bachelor's exam, she says, "and I've been here ever since. That's 45 years ago." Cannon, who studies the role of brown adipose tissue, was elected a member of the Academy in 1989. (Foreign members who live in Sweden have the same privi- >>

BY THE NUMBERS

3769.3 Meters that a Russian team of scientists drilled through Antarctic ice to reach the surface of subglacial Lake Vostok on 5 February (see p. 788).

92 Percentage of the world's total freshwater consumption each year attributed to agriculture, according to a study in the *Proceedings of the National Academy of Sciences*.

$333,000 Amount in Canadian dollars that Swedish hockey legend (and former captain of the Toronto Maple Leafs) Mats Sundin donated to launch two postdoctoral fellowships in developmental health at the University of Toronto and the Karolinska Institute in Stockholm.

CREDITS (TOP TO BOTTOM): © THE OPEN UNIVERSITY; NASA/BILL INGALLS; EU/SHIMERA/ETIENNE ANSOTTE; THE WENNER-GREN INSTITUTE

Downloaded from www.sciencemag.org on February 16, 2012

Published by AAAS

Armored Fish Defies Piranhas

In Amazonian rivers and lakes where piranhas swarm almost anything that moves, a 200-kilogram lungfish called the arapaima swims unmolested. A new study reveals its secret: armored scales with a supertough two-ply structure. Co-author Marc Meyers, a mechanical engineer at the University of California, San Diego, caught an arapaima (*Arapaima gigas*) while sport-fishing in Brazil and took some of its 10-centimeter scales back to his lab for testing. The scales shattered piranha teeth, Meyers and colleagues report online in *Advanced Engineering Materials*. Microscopic examination showed that the scales are made of tough but springy collagen covered with a rock-hard shell of collagen fibers cemented with calcium. Such a double-layered hard-on-soft pattern keeps cracks from growing, Meyers says. Francois Barthelat, a mechanical engineer at McGill University in Montreal, Canada, has applied the same fish-inspired pattern to forge crack-resistant glass and says similar materials could one day be used in lightweight body armor for soldiers. http://scim.ag/piranhaarmor

>>NEWSMAKERS

leges as Swedish members, she says, so her election didn't pose any bureaucratic problems.) Cannon says she hopes to be a strong advocate for basic research during her tenure. Scientists need to speak out for the inherent cultural value of research, she says. Too often, research advocates focus on possible applications, she says, but even more important is basic research that "will help us understand ourselves and our position in the universe."

FINDINGS

Former Soviet Mathematicians Edged Out U.S. Scholars

When the Soviet Union collapsed in 1991, hundreds of former Soviet mathematicians moved to the United States, displacing U.S. mathematicians in the process, a new report concludes.

Two economists—George J. Borjas of Harvard University and Kirk B. Doran of the University of Notre Dame—pored over papers published over the past 70 years. They found that 336 Russian émigrés helped fill gaps in U.S. mathematical knowledge. But the newcomers also forced aside hundreds of budding American mathematicians, relegating those young scholars to publishing in lesser journals and ultimately pushing many out of a math career. In a paper in *The Quarterly Journal of Economics*, Borjas and Doran say the American protégés of the Russian mathematicians on average enjoyed higher lifetime productivity than their peers who studied under U.S. mathematicians, but overall per capita productivity dipped among American mathematicians in the 20 years following the Soviet immigration.

Although the quality of the math itself didn't falter, many of the younger generation of mathematicians in the United States missed their shot. "The people who were displaced were on the younger side, and in mathematics, that means your period of peak productivity," Borjas says.

Science LIVE

Join us on 23 February at 3 P.M. EST for a live chat with leading experts on a hot topic in science. **http://scim.ag/science-live**

Random Sample

Young Scientists in Love

Lonely Chinese researchers isolated by shyness and long lab hours now have an online dating service designed just for them.

Building 88 (http://www.sciencedate.cn/) aims to become a "soul harbor" for young Chinese scientists, its Web site explains. Spearheaded by Science Times Media Group, which also runs the popular Chinese-language news portal Sciencenet.cn, the service takes its name from a fabled Beijing dormitory that became a meet-up spot for Chinese Academy of Sciences researchers in the 1990s.

Today's scientists lack such gathering places, says site coordinator Wu Hao, and thus have a "more intense need" for social interaction than Chinese pursuing other careers. "The social circles of young Chinese scientists are often limited to other people in their [immediate] field," Wu explains.

That may be no accident. A questionnaire Science Times distributed to 1243 young scientists revealed roughly 70% of highly educated respondents suffer from social anxiety, Wu says. Building 88 broadens the pool of potential paramours for introverts to include Chinese researchers both within China and all over the world.

Since its launch in January, the site has grown to 1000 users, most of them between the ages of 20 and 35. Whether an online portal can help draw them out of their shells is still an experiment in progress; many scientists have unusually high standards, Wu notes. And as one 31-year-old Beijing scientist puts it on his Building 88 profile: "Dating is just like scientific research: Only when you're excited about it do you get results."

CREDITS (TOP TO BOTTOM): JACOBS SCHOOL OF ENGINEERING/UCSD (2); SCIENCEDATE.CN

Downloaded from www.sciencemag.org on February 16, 2012

Published by AAAS

CREDIT: M. HICKS/*SCIENCE*

The president's men. John Holdren (*far left*) and other Administration figures at a rollout of the proposed 2013 science budget.

U.S. BUDGET

Science Spared Brunt Of Ax in Budget Request

Faced with implacable Republican opposition to his economic policies, President Barack Obama sent Congress a clear message in the 2013 budget he submitted this week: Don't cut research.

To be sure, not all agencies and programs are treated the same. Three agencies once slated for a 10-year budget doubling continue to fare well: The National Science Foundation (NSF), National Institute of Standards and Technology (NIST), and the Department of Energy's (DOE's) Office of Science research programs would receive increases of 4.8%, 14%, and 2.4%, respectively. Efforts at NSF and the Department of Education to improve science and math education would get a boost. Research within the National Oceanic and Atmospheric Administration (NOAA) would rise by 7%, and by 8% within the U.S. Geological Survey. Science at the Environmental Protection Agency would grow by 1.5%, and a small competitive research program within the U.S. Department of Agriculture would get a 23% hike.

At the same time, the National Institutes of Health (NIH), NASA's science programs, and research at the Department of Defense would basically tread water. And there are significant winners and losers within most agencies.

Of course, Obama's stern warning to Congress doesn't mean that scientists will get in the fiscal year that starts on 1 October what the president has requested for them—an overall increase of 1% in federal research and development, to $140 billion. But at a time when legislators are demanding big cuts in federal spending, it doesn't hurt that Obama has reiterated his belief that research and innovation are keys to the nation's economic recovery. "Whatever else we have to do to live within our means, no matter how much we have to cut, we are not going to stint our investment in these critical domains," presidential science adviser John Holdren said at a press briefing, paraphrasing his boss.

In most years, the White House and Congress spend the bulk of the annual budget cycle fighting over how much the government should spend. This year, however, that fight has been settled: The figure for all discretionary programs—which includes all defense and civilian science—is $1.047 trillion, a number the White House and Congress agreed upon in August as part of a 10-year plan to shrink the current $1.3 trillion annual deficit. (Obama's total budget request is for $3.8 trillion, with the bulk going to mandatory programs and service on the national debt.)

So the real fight will occur over whether the deficit can be shrunk through a combination of tax increases and spending cuts, as the White House and most Democrats propose, or by cuts alone, as most Republicans insist. With Republicans in control of the House of Representatives and Democrats leading the Senate, political observers say the chances of resolving that dispute before the November elections are slim to none.

Whenever legislators do decide to get serious about 2013, they won't have much wiggle room. The spending ceiling for 2013 is a paltry $4 billion over current levels. That steady state means any increase in one program must be offset by a decrease in another. Obama's budget, while vastly different from what House Republicans will soon draw up, clearly reflects that balancing act.

Here are some of the "tough choices" agency heads said they had to make as part of the president's 2013 request.

NIH: An 11% increase for the new National Center for Advancing Translational Sciences, including $40 million more for the Cures Acceleration Network, would be offset by a $51 million cut from the IDeA program, which supports states with relatively little NIH funding. NIH has also proposed cutting $28 million from the National Children's Study.

Despite a flat budget of $30.86 billion, NIH officials hope to make 8% more new awards next year by putting the squeeze on those already funded. Continuing grants will be cut 1% below 2012; new grants wouldn't get inflationary increases in the second, third, and fourth year; and NIH will be tougher on proposals from investigators who already have at least $1.5 million in funding.

DOE science: Three of the six programs within the science office—Basic Energy Sciences, Biological and Environmental Research, and Advanced Scientific Computing Research—would receive boosts ranging from 2.5% to 6.6%. But that growth comes at a price. In the single most dramatic cut, DOE would shutter a fusion experiment known as the Alcator C-Mod at the Massachusetts Institute of Technology in Cambridge. The tokamak and its $18-million-a-year operating budget falls

Online

sciencemag.org

Podcast interview (http://scim.ag/pod_6070) with author Jeffrey Mervis and additional online material at http://scim.ag/budget_2013.

Downloaded from www.sciencemag.org on February 16, 2012

Published by AAAS

victim to the need to pay for ITER, an international fusion reactor being built in France. The U.S. contribution for ITER increases to $150 million from $105 million this year.

DOE's nuclear physics program would see its budget fall by 3.6%, and an atom smasher known as the Relativistic Heavy Ion Collider at Brookhaven National Laboratory in Upton, New York, would run for only about 10 weeks—a third of its capacity. Similarly, the proposed budget provides $22 million for development of a new accelerator known as the Facility for Rare Isotope Beams at Michigan State University in East Lansing; university officials were expecting $55 million. Outside the science office, the budget of the 3-year-old Advanced Research Projects Agency–Energy would rise from $275 million to $350 million.

NASA: The president's request would reduce spending on planetary sciences from $1.5 billion to $1.2 billion in 2013 while taking just an $59 million nick out of NASA's overall budget, now $17.8 billion. The bulk of that reduction comes from slashing the Mars exploration program from $587 million to $360 million. The proposal also takes a bite out of the outer planets program, cutting it from $122 million to $84 million. The $5.1 billion Science Mission Directorate would drop by about $170 million.

At a budget briefing at NASA headquarters, Administrator Charles Bolden did not offer a clear explanation about why the U.S. was pulling out of the 2016 and 2018 Mars missions it had previously committed to flying in partnership with the European Space Agency. "A problematic part of the ExoMars mission is that it was another multibillion-dollar flagship mission," Bolden said. "Flagships are expensive; … we just could not afford to do another one." He declined to say whether the increased cost of a different flagship—the $8.8 billion James Webb Space Telescope—was a factor in the agency's decision to terminate ExoMars.

However, Bolden hasn't ruled out alternative medium-class missions to Mars in 2018 or 2020, when the planet's location relative to Earth will provide a convenient opportunity to land a spacecraft on its surface. The agency is talking to the European Space Agency about the possibility of collaborating on such a mission, he said, "to ensure that the next steps for the robotic Mars Exploration program will support long-term human exploration goals as well as science and meet the president's challenge to send humans to Mars in the mid-2030s."

NSF: Research and education programs would rise by slightly more than 5% at the same time funding for major new facilities would remain flat. Director Subra Suresh says his priority was "core research programs," all of which receive small boosts. A signature program begun this year to support risky multidisciplinary research would jump from $20 million to $63 million in 2013, and NSF is teaming up with the Department of Education on a joint $60 million effort to improve math education from elementary school through college.

At the same time, Suresh has proposed trimming $67 million from a dozen or so programs that "have served their purpose." He also wants to reduce spending on informal science education and shrink a long-running graduate training program aimed at fostering interdisciplinary research and education. And the lack of new starts in the agency's major research facilities program reflects Suresh's preference for finishing one project before launching a new one.

NOAA: A major satellite program would remain roughly on track, and one climate science effort would get a big boost. But a number of the agency's marine research and conservation programs would see their spending trimmed if Congress embraces the White House's proposal. An 8% increase in the agency's satellite programs includes $916 million for the Joint Polar Satellite System, a key orbiter program. Within a 7% boost to its main research arm, NOAA's Oceanic and Atmospheric Research office, competitive climate research and observation programs would get a major boost, while coastal and Great Lakes research program would drop.

NIST: This agency earned an "A" on Obama's budget report card for helping to meet the president's promise that the country will make new, high-tech products that "are invented here, manufactured here, and sold worldwide." Its budget would grow by 14%, to $857 million. The bulk of the new money, $81 million, would go to NIST's Scientific and Technical Research and Services, which would grow 14% to $648 million. More than one-half of that increase, or $45 million, would go to five measurement science initiatives totaling $90.8 million, including projects aimed at supporting biological products, nanomanufacturing, and a national "Materials Genome Initiative." Four new centers of excellence, to be chosen through a competition, would share $20 million; each is supposed to fuse government, academic, and private research.

–JEFFREY MERVIS

With reporting by Yudhijit Bhattacharjee, Adrian Cho, Jocelyn Kaiser, and David Malakoff.

Hard Times for OSTP

CREDIT: M. HICKS/SCIENCE

The Office of Science and Technology Policy (OSTP) is facing its own tough budget choices this year as it tries to coordinate research activities across the government. In November, Congress cut its 2012 budget by 30%, to $4.6 million, to demonstrate its unhappiness over U.S. scientific collaborations with the Chinese government. Representative Frank Wolf (R–VA), who chairs the House appropriations panel that sets OSTP's budget, believes the joint activities give the Chinese license to steal all manner of U.S. technology.

Science adviser and OSTP Director John Holdren acknowledged this week that the cuts have hurt his small office. About a half-dozen people have left in recent months, he says, and there's no money to replace them. The remaining employees are covering for them, he notes, adding to their already heavy workloads. Travel is practically out of the question, he says. The only saving grace is the fact that about half of OSTP's 90-person staff is on loan from other federal agencies, which are able to pick up the tab.

The president has proposed a $1.2 million boost for OSTP in his 2013 request. Even that increase, however, would leave OSTP $800,000 short of where its budget stood in 2011. In addition, Wolf and other Republicans don't appear to be in any hurry to lift the penalty they have imposed on OSTP for ignoring a congressional mandate to cease collaborating with China. So OSTP may remain short-handed for a while longer.

–J.D.M.

Downloaded from www.sciencemag.org on February 16, 2012

Published by AAAS

CREDIT: GREGORY GRAY/DEPARTMENT OF ENVIRONMENTAL AND GLOBAL HEALTH, COLLEGE OF PUBLIC HEALTH AND HEALTH PROFESSIONS

Hog-tied research. Pork producers in many locales resist active surveillance for flu.

BIRD FLU CONTROVERSY

Does Forewarned = Forearmed With Lab-Made Avian Influenza Strains?

Behind the increasingly contentious debate over whether journals should publish the full details of how two labs engineered the deadly avian influenza strain H5N1 so that it spreads more easily among ferrets, and presumably humans, lies a conundrum: Knowledge cuts both ways.

No one at the front of this protracted battle wants to stifle free scientific exchange. But two camps have formed that view risks and benefits through different lenses. Proponents of full disclosure, including the researchers who conducted the work, contend that knowing the genetic signatures of these potentially devastating viruses might prove pivotal to shoring up surveillance measures and controlling an emerging threat.

Maybe, say opponents in the other camp, but they stress that in the predominantly poor countries where H5N1 circulates, surveillance and control systems are too rudimentary, or nonexistent, to take advantage of the new knowledge. They worry that if published, that data could provide a recipe for bioterrorists to unleash a doomsday scenario.

Ideally, a robust surveillance system will detect novel flu viruses in animals when they arise, which in turn will aid control efforts with vaccines and culling, preventing economic loss to farmers and the introduction of dangerous strains to humans. Early detection of new strains in humans can similarly give public health officials a jump on fashioning an effective response. Ideally.

The reality is far messier—a point that both camps agree is troubling.

When avian influenza viruses infect and adapt to humans, they have the potential to cause devastating pandemics because we have little, if any, immunity to them. Although public health officials have documented fewer than 600 cases of H5N1 infections since it surfaced in humans in 1997, H5N1 has received intense attention because more than half of the people who had symptomatic disease died (see sidebar, p. 786). The saving grace is that it has not spread easily among people. But two labs have made the virus transmit readily among ferrets by introducing mutations or creating a "reassortant" of H5N1 and the H1N1 virus that caused the 2009 flu pandemic. Papers about the studies, stuck in limbo at *Science* and *Nature,* remain unpublished while scientists, journal editors, and public health officials weigh the benefits and risks of full disclosure.

Influenza specialists often stress that surveillance *has* improved since H5N1's emergence in Hong Kong 15 years ago. They particularly praise virologist Malik Peiris at the University of Hong Kong and colleagues, who worked on the 1997 outbreak and then began to hunt for flu viruses in birds at markets and pigs at slaughterhouses. (Peiris makes the case online in *Science* that the new experiments will help surveillance, http://scim.ag/_h5n1.) "The folks in Hong Kong are a model of what should happen in the world," says Robert Webster, who studies influenza at St. Jude Children's Research Hospital in Memphis, Tennessee, and helped Peiris launch the program.

But Hong Kong remains the exception. At a debate held 2 February by the New York Academy of Sciences about the mutant H5N1s, the state of the world's surveillance efforts received a drubbing from a member of the U.S. National Science Advisory Board for Biosecurity, which made the controversial recommendation to remove from the papers details of the genetic changes that made the virus transmissible as well as the methods the scientists used to produce those mutations. "Surveillance out there right now is like a whole lot of broken smoke alarms," said flu expert Michael Osterholm of the University of Minnesota, Twin Cities.

Veterinary microbiologist Jürgen Richt of Kansas State University, Manhattan, agrees that surveillance is wanting but says the details could indeed be put to good use. Although H5N1 primarily circulates in poor countries that have limited access to sophisticated laboratories, they widely use inexpensive and relatively simple PCR tests that could hunt for the mutations linked to transmission. "We can design surveillance screens for transmissible versus nontransmissible H5N1," Richt says. Countries that find transmissible H5N1 in animals could ramp up programs to "immediately stamp it out," he says. "We would be weeks ahead."

But having the tools only helps if countries use them properly. "We don't have the surveillance or reaction system, so how is this really going to help?" asks veterinarian Ilaria Capua, who runs an influenza reference lab for Italy at the Istituto Zooprofilattico Sperimentale delle Venezie in Padua. Capua notes that influenza programs in developing countries depend heavily on funding from the wealthy world. "There's less surveillance going on than 3 or 4 years ago, because donors have changed their priorities," she says. (Despite her surveillance concerns, Capua, who in 2006 persuaded reluctant colleagues to share H5N1 sequences in the name of spurring scientific progress, supports full publication of the new data.)

Downloaded from www.sciencemag.org on February 16, 2012

Published by AAAS

Capua works closely with Egypt, which has had more cases of human H5N1 than any country other than Indonesia. When it comes to culling H5N1-infected flocks, the primary control strategy, she notes that's easier said than done, too. "Egypt is a very poor country, they have social unrest, and they don't have the infrastructure and just cannot afford to cull the birds," she says.

Animal vaccination campaigns in poor countries, which complement surveillance and culling, similarly face huge obstacles. To combat H5N1, several countries launched massive vaccination campaigns in poultry, using more than 100 billion doses between 2002 and 2010, according to a recent review in a journal published by the World Organization for Animal Health. But birds have short life spans, and campaign success often waxes and wanes, largely dependent on how widely the vaccines are used.

Delays in moving animal samples from field to lab can also undermine the benefit of detecting dangerous strains. Several months often pass before samples from Egypt reach her lab, Capua says. Sample delays have compromised efforts in wealthy countries, too. In the United States, researchers have pushed for monitoring slaughtered pigs—the type of "active" surveillance Hong Kong does—but have met resistance from the pork industry, which took a financial beating during the 2009 pandemic and fears another backlash if the public learns that novel influenza strains infected their pigs. Hog producers wait until 3 months

Dead Reckoning the Lethality of Bird Flu

"Peter, you know there's science and there are facts, and you know you can't have your own facts."

Those fighting words came from Michael Osterholm on 2 February at the New York Academy of Sciences, where he and Peter Palese, both prominent influenza researchers, debated just how deadly the avian virus known as H5N1 is to humans. That question bears directly on the current fracas over H5N1 variants created by two labs that spread easily among ferrets, a model for human transmission (see main text). Palese, a virologist at Mount Sinai Medical Center in New York City, thinks official figures overstate the lethality of H5N1 to humans, exaggerating the risk of the new experiments. Osterholm, an epidemiologist at the University of Minnesota, Twin Cities, asserts that Palese cherry-picks studies to discount the threat. "You misrepresented the data, and that's propaganda," Osterholm charged.

The fact is, the facts aren't clear.

Without question, H5N1 kills many of those it sickens but does not spread readily among people. As of 8 February, the World Health Organization (WHO) says, H5N1 had killed 59% of the 584 confirmed cases in humans since 2003. If H5N1 artificially or naturally acquired the ability to transmit easily among mammals, jumped into humans, and remained highly pathogenic, it could trigger what Osterholm called the "worst pandemic" ever seen. Osterholm is a member of the U.S. National Science Advisory Board for Biosecurity (NSABB), which made the contentious recommendation that journals redact key details before publishing the studies to prevent aiding bioterrorists.

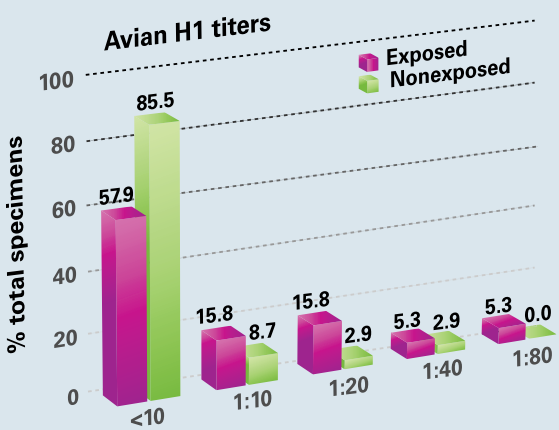

Bird's-eye view. Poultry vets (purple) had significantly higher antibodies to avian H1 strains when several dilutions were combined.

Palese says making the details freely available poses little risk and will advance the field. In a 25 January online perspective he co-authored in the *Proceedings of the National Academy of Sciences* (*PNAS*), Palese notes that WHO ignores subclinical cases of H5N1, which one recently published study suggested occurred in 45 of 800 people (5.6%) tested in rural Thailand. "Even if only a low percentage of the rural population is asymptomatically/subclinically infected, the case fatality rate that is offered by the WHO—and that is driving this controversy—is likely orders of magnitude too high," Palese's *PNAS* perspective argued.

Osterholm noted that several studies contradict the Thai report, published in the 15 October 2011 issue of *Clinical Infectious Diseases*, which he called "by far the worst one of all." Epidemiologist Gregory Gray of the University of Florida, Gainesville, who led that study, counters that it's one of the largest and most carefully done serology surveys yet published. "Is it perfect? No," Gray says. "But it's the best we can do."

Osterholm focused on the antibody assay used by Gray's group to assess exposure to H5N1. The researchers performed a "serial dilution" that mixes antibody-containing sera with inert liquid at various concentrations and then tests whether they can prevent infections in culture. More dilute solutions can stop virus only if the starting sera contain higher titers of H5N1 antibodies, so "neutralizing" titers of 1:80 are more compelling than 1:10. WHO only ascribes symptomatic cases to H5N1 if they have titers of 1:80; combining published studies of asymptomatic infection with that cutoff, prevalence is 0.48%, Osterholm says. Gray's study used a 1:10 cutoff and found an 11-fold higher prevalence.

Gray says the 1:80 cutoff makes sense in the clinic, when people have acute infections, but not in a retrospective epidemiology study. He notes that he and his colleagues analyzed villagers 2 years after H5N1 was last detected in Thailand, at which point antibody levels likely would have waned. And 1:10 was simply the minimum requirement used to define a person as positive: Titers went as high as 1:40. Their final analysis combined the various titers using a statistical technique called proportional odds modeling, validated in an earlier study of avian viruses (see graph).

Osterholm told the New York audience, "I could find a number of you in this room positive using that study design." Not so, Gray says. "We've done thousands of these, and very few people have 1:10," he says. "I'm sure there are some false positives, but it's not an egregious thing." To more precisely determine subclinical infection rates, Gray says the field needs prospective studies—which he has under way—that capture antibodies from people during and immediately after exposure.

Osterholm says NSABB didn't debate H5N1's actual lethality. "If this virus was 20-fold lower in mortality, it would still be a very, very catastrophic pandemic," he says.

But what if H5N1 is 1000-fold less lethal than WHO estimates and Palese has a valid point? Osterholm agrees that's possible but contends scientists must err on the side of caution. As he said at the debate, "We can't afford to be wrong." **–J.C.**

GRAPHIC SOURCE: ANA CAPUANO AND GREGORY GRAY/UNIVERSITY OF FLORIDA, ADAPTED FROM MYERS *ET AL.*, *CID* 45:4 (2007)

Downloaded from www.sciencemag.org on February 16, 2012

Published by AAAS

after slaughter to give samples to Webster's colleagues at St. Jude's, a compromise he says is actually a step forward. The U.S. Department of Agriculture has no mandatory active surveillance of commercial swine or poultry, but many producers have joined voluntary programs that offer financial incentives or agree to not specify the location of infected farms.

Virologist Yi Guan, who works with Peiris in Hong Kong, agrees that knowing the signatures of transmission might help but says there's often a disconnect between the influenza surveillance and control efforts in animals and humans. Vaccination makes it difficult to track the virus in poultry, so mainland China is "using humans as sentinels," he says. "First they have a human case, then they start looking for bird flu."

Cull of duty. If surveillance detects H5N1 early, killing flocks can contain it, as the United Kingdom did in 2007.

As for surveillance in humans, the benefits of the new experiments are murkier. "Once a new influenza virus begins to be transmitted between humans, whether as a result of a Mother Nature–made pandemic virus or an intentional or unintentional release of a manmade virus, it's like having a screen door on your submarine; you'll never contain it," Osterholm says.

Whether the new experimental data will help protect humans, the debate has already spotlighted the inadequacies of surveillance and control, Richt says. "This whole discussion stimulates organizations and governments to review their emergency plans if an H5N1 epidemic arises, and that's a critical point," Richt says. "These people have to rethink."

–JON COHEN

With reporting by Dennis Normile.

SOCIAL SCIENCE

Marriage Decision Highlights Same-Sex Studies

As a rookie professor in the mid-1970s, social psychologist Letitia Anne Peplau would tell students about her studies of heterosexual dating. But "when gay and lesbian students asked why I didn't talk about their same-sex relationships, I explained that there really wasn't any good research," she recalls. She set out to change that. The University of California, Los Angeles (UCLA), academic hung posters and made personal appeals to recruit gay and lesbian couples for studies. Sometimes it wasn't easy because "it hadn't been that long since many psychologists viewed homosexuality as a mental illness." Peplau never imagined, however, that her work would ultimately land her in the middle of a landmark legal battle over same-sex marriage—or as a character in an unusual movie.

"In the '70s, marriage equality simply wasn't an issue," says Peplau, who is part of a small group of social scientists who provided expert testimony in the legal jousting over California's Proposition 8, a 2008 ballot initiative that banned same-sex marriage in the state. Last week, that battle took a major turn when a three-judge federal appeals court panel voted 2-1 to find the same-sex marriage ban unconstitutional, upholding a lower court ruling. Proposition 8 "serves no purpose, and has no effect, other than to lessen the status and dignity of gays and lesbians in California," the majority wrote. The decision in *Perry* v. *Schwarzenegger*, which applies only to California, could end up as a precedent-setting case before the U.S. Supreme Court.

Even if the case doesn't go that far, it has helped highlight a growing body of research on the psychological and socioeconomic aspects of same-sex relationships. Just a few decades ago, "there were a lot of myths out there but not much research," says Lee Badgett, a labor economist at the University of Massachusetts, Amherst, who served as an expert witness in support of overturning Proposition 8. Even into the 1990s, for instance, Badgett says stereotypes suggested that gay and lesbian workers tended to earn more than heterosexuals. "There was this image of the affluent gay male couple with no kids," she says. But after combing a trove of national survey data, Badgett and others concluded that gay men actually earned less on average than their straight colleagues, while lesbians typically "earned about the same or maybe a bit more." Such results ultimately led Badgett to examine the economic costs and benefits of marriage. One intriguing finding: Couples with legal ties, same or opposite sex, tend to use less government assistance, in part because the partners can turn to each other for help in hard times, and in part because state welfare agencies tend to be stingier with couples. The bottom line, Badgett says, "is that marriage can save taxpayers money."

On the stand. Peplau's studies of same-sex couples were the subject of extensive court testimony.

Over the past decade, same-sex marriage advocates have seized on such findings to bolster their arguments. And when the conflict moved into the courts, Badgett and other academics on both sides of the issue suddenly faced requests to trade the classroom for the courtroom. But perhaps no case placed them in the spotlight like *Perry* v. *Schwarzenegger,* which kicked off in 2010 with 12 days of public testimony in the San Francisco courtroom of federal district judge Vaughn Walker. In all, opponents of Proposition 8 put nine social scientists on the stand, including psychologists, economists, and political scientists who testified about everything from the political power of homosexuals to the impact of same-sex partnerships on child rearing.

Supporters of the measure called two experts, a historian and a political scientist, who argued in part that voters had a right to promote the "optimal" family structure for bearing and raising children. Judge Walker, however, ultimately rejected much of their tes-

CREDITS (TOP TO BOTTOM): JAMIE MCDONALD/GETTY IMAGES; COURTESY OF ANNE PEPLAU

Downloaded from www.sciencemag.org on February 16, 2012

Published by AAAS

timony, finding that they "failed to build a credible factual record." (Neither replied to interview requests from *Science*.)

"It was a remarkable opportunity to discuss research in an important setting," says UCLA's Peplau, who says she was "pretty surprised" when the lawyers challenging Proposition 8 called. Some of her colleagues, however, were not: "Anne is really one of the pioneers of understanding how same-sex couples compare to heterosexual couples," says psychologist Gregory Herek of UC Davis, who also testified for the Proposition 8 challengers. In particular, he says, Peplau's work helped relationship researchers address a fundamental question: "Are the behavioral dynamics seen in heterosexual couples the result of gender differences or other factors?" Peplau's studies "essentially controlled for gender" by removing that variable, Herek says.

The answer from decades of interviews, analysis of videotaped interactions, and lab experiments, Peplau says, is that same- and opposite-sex couples appear to be more similar than different. "When you look at the factors that lead to satisfaction in a relationship, the power dynamics and other issues, you see very similar patterns," she says. "If we record a same-sex couple having a disagreement, for example, it looks really similar to a heterosexual couple."

During the 2010 trial, Peplau—who says she's been married for 32 years and voted against Proposition 8—cited such similarities in making her main point: "Marriage appears to confer a number of benefits, psychological and otherwise, … and there isn't anything in the scientific literature that suggests that gay or lesbian people would benefit less or differently than heterosexual people from access to the institution of marriage."

Such conclusions were featured in Judge Walker's August 2010 decision to declare Proposition 8 unconstitutional, and they also earned a prominent footnote in last week's 9th Circuit Court of Appeals decision, which upheld Walker's ruling on narrow constitutional grounds. Now, supporters of Proposition 8 must decide if they will ask a larger panel of 9th Circuit judges to rehear the case or appeal directly to the U.S. Supreme Court.

In the meantime, the new decision has social scientists involved in the case reflecting on their brush with history. Badgett likens the dozens of hours spent discussing her research during depositions and on the stand to a "really nightmarish dissertation defense, where someone has thought very hard about your work and how to undermine it." Others are thinking about traveling to Los Angeles in early March to see a special performance of *8*, a play based on the case, by Dustin Lance Black, an Academy Award–winning writer. Not all the researchers got included in the play, but all are featured in a 12-part Internet movie (marriagetrial.com) in which Hollywood actors reenact every day of the 2010 trial. Peplau, for example, is portrayed by Adrienne Jo Barbeau, a film veteran best known to fans for her roles in horror movies such as 1982's *Swamp Thing*. Some academics might find such attention a dubious honor, but Peplau says she was "delighted" by Barbeau's performance.

–DAVID MALAKOFF

One standard family? Proposition 8 supporters argue that opposite-sex marriages are "optimal" for children, but courts have disagreed.

POLAR SCIENCE

A Tiny Window Opens Into Lake Vostok, While a Vast Continent Awaits

They were slowed by annual evacuations and international concerns about their strategy, but after 2 decades they finally did it. On 8 February, the Russian Arctic and Antarctic Research Institute (AARI) announced that a team of its engineers and scientists had drilled through nearly 4 kilometers of Antarctic ice to open what it called a "small window" into Lake Vostok, a dark, mysterious subglacial lake that has likely been cut off from the rest of the planet for millions of years. Russian Prime Minister Vladimir Putin praised the team and promised them national awards. The "Russians are flying high with national pride, and they should be," says John Priscu, a microbiologist at Montana State University in Bozeman. It was a "major achievement" and a "real technological first," agrees David Pearce, a microbiologist at the British Antarctic Survey.

Antarctic scientists are now looking forward to finding out what's actually under all that ice. The Vostok team is one of three groups working in different parts of the continent—Priscu leads a U.S. team and Pearce is part of a British effort—that are hoping to bring back direct evidence of living organisms in the subglacial environment next year. The Russian team's success has "opened the window so that we can now do real science," Priscu adds. "We've sampled every other corner of Earth, but Antarctica is a large

At last. Russian scientists and engineers pose on 5 February, after drilling 3769.3 meters through ice to reach subglacial Lake Vostok.

CREDITS (TOP TO BOTTOM): JOHN BURGESS/NEWSCOM; AP

Downloaded from www.sciencemag.org on February 16, 2012

Published by AAAS

continent, and we've yet to sample the world beneath its ice."

Satellite data reveal that at least 200 lakes are buried beneath Antarctica's continental ice sheet. It's now routine to talk about what life might exist in the lakes, but 10 years ago, that wasn't so obvious, Priscu says. Even for hardy microbes, these liquid environments are extreme: high pressures, low temperatures, permanent darkness, and likely low availability of nutrients and oxygen. Yet in 1999, Priscu and colleagues studying an ice core taken from the then-unfinished borehole to Lake Vostok found microbes just above the lake (*Science*, 10 December 1999, p. 2141).

The Russian team began drilling the current borehole, 5G-1, in 1992. By 1998, the team had reached 3623 meters but halted for 8 years due to international concerns that they would contaminate the lake (*Science*, 28 October 2005, p. 611). By 2000, the team had a plan that would take advantage of the fact that the ice sheet floats atop the lake, and the water underneath is under pressure. Drilling fluids in the borehole normally helps keep the hole open. But when they reached the interface, the team would decrease the pressure of the drilling fluid; the water would rise up through the borehole for some distance (pushing the drilling fluids above them back up onto the surface) and freeze. The team could then extract the plug of frozen lake water.

Last week, as weather conditions were about to force their annual evacuation, the Russian team finally broke through. On 4 February, the team hit a freshwater lens sitting a few meters atop the lake; the water rose several tens of meters up into the borehole, froze, and was extracted. The next day, the team continued drilling a few more meters and reached the top of the lake. In a press release, the team's leader, Valery Lukin, announced that the lake water rose about 40 meters into the borehole; they will return to collect the ice in December, during the next Antarctic summer.

It's an exciting time, Pearce says—and, he adds, although it's frequently characterized as a race for national bragging rights, the three teams are drilling into distinct environments, which may reveal very different facets of the ice-capped continent. "If we're successful in all three next year, we'll have a much better understanding of the subglacial environment, rather than just one look-see," Pearce says.

Lake Vostok is at the center of the East Antarctic Ice Sheet and is ancient, perhaps 14 million years old. And at 1000 meters deep and 14,000 square kilometers in area, it's the seventh largest lake in the world. The Russian team is hampered by being able to sample only the surface of the lake because of the contamination concerns, notes Martin Siegert, a glaciologist at the University of Edinburgh in the United Kingdom. "Vostok is enormous," he says. "You can't appreciate the system in one go."

Siegert leads a team of British scientists preparing to drill through ice into the much smaller Lake Ellsworth, on the West Antarctic Ice Sheet near the continental divide. Lake Ellsworth is also buried under more than 3 kilometers of ice; it is only a few kilometers across and about 160 kilometers deep. "Because it's quite small, you can comprehend it well," Siegert says. It's also younger than Vostok—somewhere between 400,000 and 1.2 million years old, adding a second data point to the possible evolution of microbial life on the continent. Siegert's team is planning to use a hot-water drill to reach the lake, which creates a short-term borehole until the water refreezes but has the advantages of being quick, efficient, and, especially, clean. It'll take only a few days to drill the more than 3 kilometers to the lake's surface—and because the drilling probe is sterile, it will be able to go directly into Lake Ellsworth, collecting temperature, pressure, and salinity data throughout the water column.

The Ellsworth team is also hoping to extract 2 to 3 meters of sediment core from the bottom of the lake, to learn more about the history of the West Antarctic Ice Sheet, such as when it last broke apart. "The conditions that led to its breakup will tell us how much risk of change there is right now," Siegert says.

The team of U.S. scientists led by Priscu plans to begin hot-water drilling by December or January. They're looking at the Whillans Ice Stream, a complex hydrological feature that marks the interface between Antarctic ice and the Southern Ocean. Whillans is about 60 square kilometers across but only 10 to 20 meters deep, and is under only 800 meters of ice. It's also a relatively young, ephemeral system that fills with water from the Antarctic highlands and then flushes out to the Southern Ocean every few years.

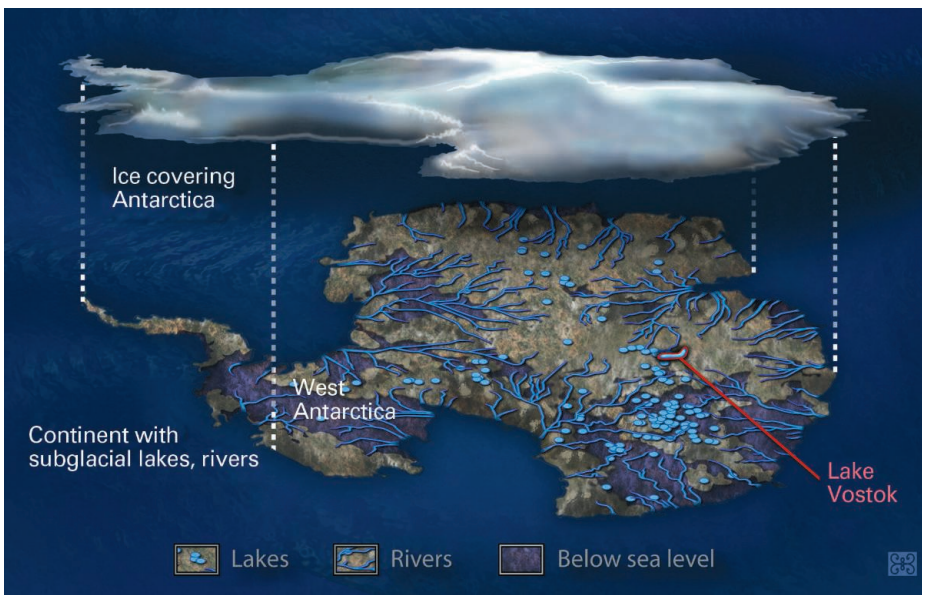

Laid bare. A complex hydrological network of rivers and lakes is thought to exist beneath Antarctica's ice.

In the 1999 *Science* paper, Priscu suggested that any life in the lake below—if similar to life in the ice above it—gets its energy from minerals such as sulfides, similar to the chemoautotrophs that live around deep-sea hydrothermal vents. Similar bacteria are likely feeding off minerals at the Whillans site, he adds, converting and consuming elements such as iron or sulfur and changing their elemental ratios through their metabolism. If subglacial microbes are as abundant and metabolically active as he suspects, Priscu says the Antarctic continent—through its sheer size—could significantly influence the chemistry of the Southern Ocean.

Even as the Russian team celebrates its achievement, they are planning their return to retrieve the hard-won core of Lake Vostok ice. The British and U.S. teams may be just behind, but don't call them runners-up. "It's not a race," Priscu says. "There's no finish line—I think that defines a race. We've been planning this as an international group for a long time."

–CAROLYN GRAMLING

CREDIT: ADAPTED FROM NATIONAL SCIENCE FOUNDATION

Downloaded from www.sciencemag.org on February 16, 2012

Published by AAAS

Uncovering Civilization's Roots

What sparked the first cities? Digs in Kuwait and Syria are reshaping how archaeologists see the first stirrings of urban life

BAHRA, KUWAIT—Camels are picking at scrub in the desert here, while archaeologist Piotr Bielinski puzzles over the jumbled remains of a 7000-year-old village in this desolate spot. Although the skyscrapers of Kuwait City form a distant backdrop 40 kilometers away, today there is little here to draw people. This site is a long walk to the Persian Gulf, has no obvious water source, and seems to lack valuable resources. In summer, the surrounding desert is a furnace, while bitter winter winds blow unimpeded from neighboring Iraq. But long ago, some 100 people created a tidy and prosperous settlement here, and the remains of their village may provide clues to the subsequent emergence of the world's first cities.

Why settle here? The riddle confronting University of Warsaw scientist Bielinski is part of an ambitious attempt to explain how humans made the momentous leap from village life to urban sprawl. That transformation first happened in Mesopotamia sometime during the 4th millennium B.C.E. in what archaeologists call the Uruk phase, named after a southern Iraq metropolis some 300 kilometers north of Bahra. But recent excavations in Kuwait, Syria, Iran, and Saudi Arabia provide mounting evidence that the origin of the urban revolution is to be found in the prior era, called the Ubaid, which began around 5500 B.C.E and lasted until about 4000 B.C.E. (see timeline, p. 792). Piecing together how and where that mysterious culture began, spread, and evolved "is a particularly hot topic right now," says Harvard University archaeologist Jason Ur. Adds University of Chicago archaeologist Gil Stein: "This is the earliest complex society in the world. If you want to understand the roots of the urban revolution, you have to look at the Ubaid."

At Bahra, archaeologists have found the oldest permanent settlement south of Mesopotamia. The finds come on the heels of a joint U.S.-Syrian discovery of a surprisingly large and sophisticated Ubaid town on the northern fringe of the Mesopotamian plain. Data from both sites contradict the old assumption that Ubaid culture was spread by precocious southern Mesopotamians who colonized their more primitive neighbors—a harbinger of the militaristic Mesopotamian empires to come. Instead, these and a handful of other sites suggest that a loose network of local peoples from the Mediterranean Sea to the Persian Gulf helped shape a way of life that eventually spawned cities.

Some archaeologists argue that crop irrigation and the resulting food surplus spurred that rise, while others cite the appearance of kings, colonial domination, or spread of a common religion. But the new Ubaid finds add weight to the hypothesis that growing contact among different groups—a so-called interaction sphere—was the spark that eventually ignited the urban revolution. "There is a direct correlation between an increase in cultural interaction and an increase in cultural complexity," says Harvard archaeologist Carl Lamberg-Karlovsky.

Although researchers agree that factors such as irrigation and trade were key to seeding civilization, the emphasis has shifted to how those ideas grew and spread. The new

CREDIT: MAHAN KALPA KHALSA

Downloaded from www.sciencemag.org on February 16, 2012

Published by AAAS

It takes a village. Warsaw's Andrzej Reiche surveys an ancient Ubaid workshop in Kuwait, home to a new way of life that eventually led to urban civilization.

Pointing south. Piotr Bielinski's dig at Bahra shows that Ubaid settlements spread south of Mesopotamia to the Persian Gulf.

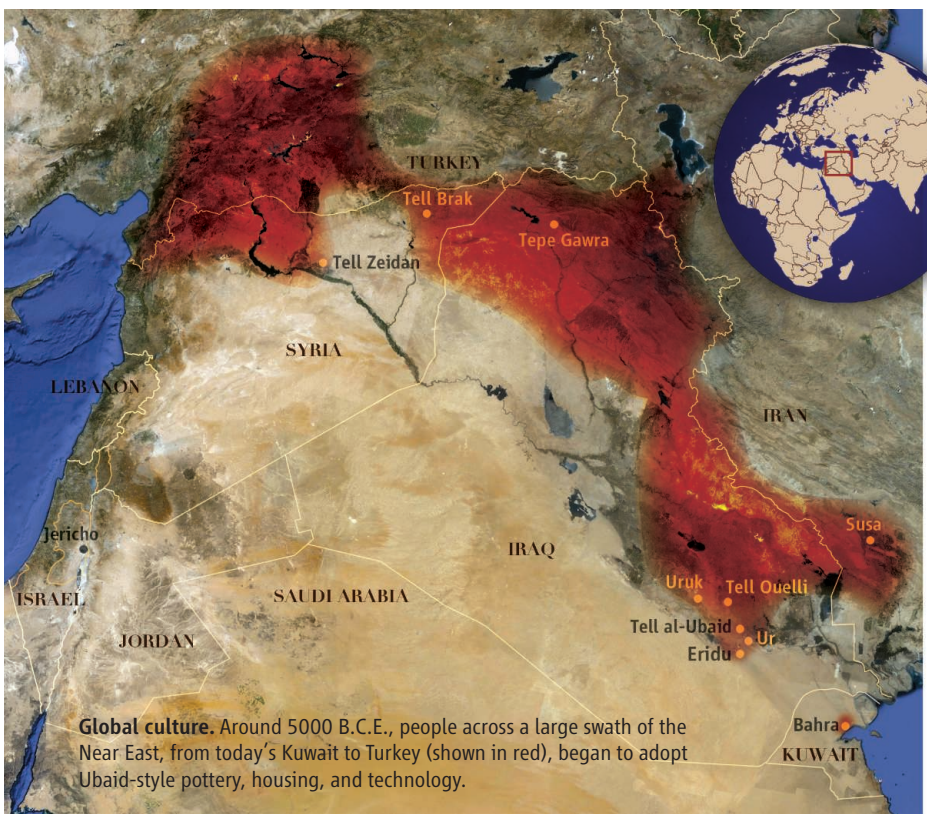

Global culture. Around 5000 B.C.E., people across a large swath of the Near East, from today's Kuwait to Turkey (shown in red), began to adopt Ubaid-style pottery, housing, and technology.

CREDITS (TOP TO BOTTOM): MAHAN KALPA KHALSA; (BASE MAP) © 2012 CNES/SPOT IMAGE; DATA: SIO, NOAA, U.S. NAVY, NGA, GEBCO; IMAGE: U.S. GEOLOGICAL SURVEY, © 2012 TERRAMETRICS, © 2010 GOOGLE

data suggest that the Ubaid was a time of mutual exchange among independent peoples rather than control asserted by a single sophisticated group. "Like the Ottoman Empire, people may have adapted in different ways," Bielinski says, his face ruddy from the sun and wind. Stein, who leads the dig in Syria, uses another analogy: "It's almost like the European Union," he says. People shared a common identity but retained their own local traditions. That view puts a radically different spin on civilization's emergence.

Deep digging

Sumer—Shinar in the Hebrew Bible—is the name of ancient southern Mesopotamia, where archaeologists discovered the first cities a century ago. One of the oldest and largest was Uruk, which expanded sometime around 4000 B.C.E. and by 3100 B.C.E. covered more than 100 hectares, boasting massive temples, a city wall, the first administrative writing system, and tens of thousands of people. Uruk pottery and trade goods from this time turn up across a wide area of the Middle East.

In the 20th century, archaeologists digging in southern Iraq began to get glimpses of pottery and buildings from an even older era, which they dubbed Ubaid after the ancient town on the southern Mesopotamian plain (see map) where it was first identified. But Ubaid remains were often buried under later cities or thick deposits of silt, Stein says. At Tell Ouelli, for example, French archaeologists dug 4.5 meters to reach Ubaid material. They found surprisingly spacious buildings but had to stop when they encountered the water table. At Eridu, which the Sumerians themselves considered the world's oldest city, excavators peeled back an extraordinary series of increasingly large and elaborate temples, which for 3000 years were built on top of what began as a modest early Ubaid structure.

The continuity of architecture from the Ubaid to Uruk is striking. Older settlements exist, such as Jericho on Palestine's West Bank or Çatalhöyük in Turkey (*Science*, 29 October 1999, p. 890). But only Ubaid sites underlie the first cities. Although the sites are relatively small and lack complex organization, the people of this era were among the first in the world to spin wool into cloth, use the wheel to manufacture distinctive pottery, irrigate their fields, and live in well-planned rectangular houses with multiple rooms. Overall, the Ubaid seems egalitarian, like previous Neolithic cultures, but archaeologists have spotted hints of social stratification. A few infant graves had many goods, and one home at Tell Abada, east of Baghdad, was several times the size of the town's smallest dwelling. That mansion was maintained for nearly 2 centuries, demonstrating not just a difference in wealth but also an ability to pass on wealth and status to succeeding generations, Stein notes.

Telltale signs of Ubaid life, such as skulls shaped in infancy by banding, have turned up in a 2000-kilometer swath from Turkey to Iran. Ubaid potsherds with bold patterns that sometimes include stylized images of dancers and animals have been found as far southeast as the Persian Gulf shore of Oman and as far northwest as the Mediterranean coast. That footprint is as large as the reach of the Uruk city-state in the 4th millennium B.C.E. "It is the first time you see the spread of material culture across so wide an area," says University of Cambridge archaeologist Joan Oates, a pioneer in Ubaid studies.

Although the plains of southern Mesopotamia have rich soil, they lack timber, stone, metals, and other natural resources. So scholars once assumed that what they termed the Ubaid expansion was the result of southern Mesopotamian traders, colo-

Downloaded from www.sciencemag.org on February 16, 2012

Published by AAAS

The Slow Birth of Cities

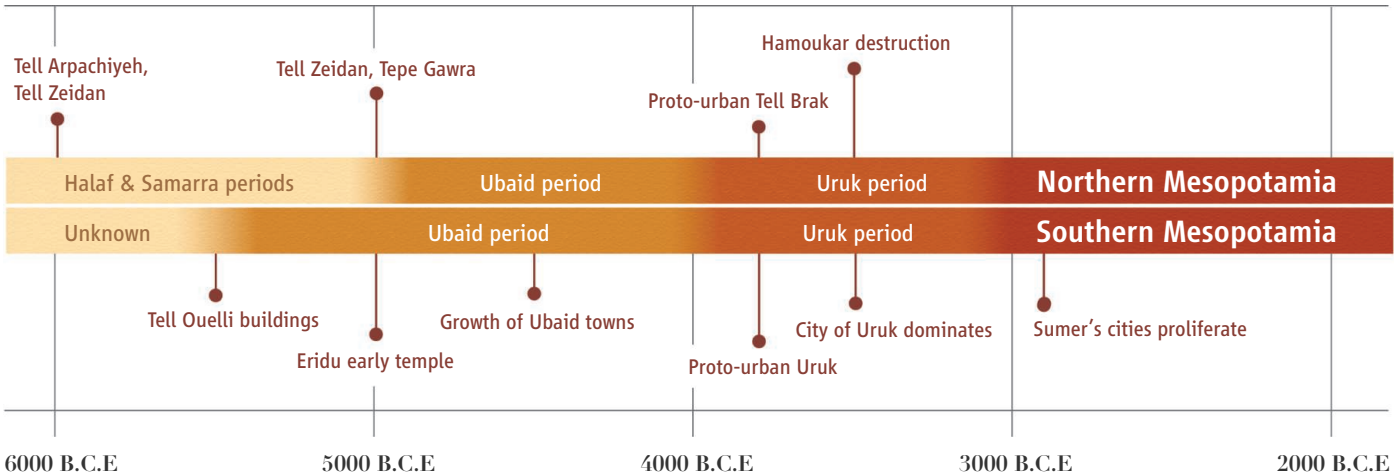

nists, or even warriors moving into other lands to gather needed resources. But discoveries of Ubaid villages and towns across northern Mesopotamia—some of which were founded even before the Ubaid began and grew larger in the 5th millennium B.C.E.—suggest indigenous development. "We can't assume [the Ubaid expansion] is the spread of people," Oates says.

Stein's dig at Tell Zeidan in northern Syria provides the latest and most definitive evidence that the Ubaid culture was more complex than once thought and that it was not simply the product of southern Mesopotamian migration. Located at the juncture of two trade routes, Tell Zeidan is made up of three large mounds covering more than a dozen hectares—at least as large as Eridu in the 5th millennium B.C.E.—and with as many as 3000 inhabitants. Elaborate stamp seals used to mark goods or rooms reveal that some people were controlling goods or access—a sign of early administrative complexity and possibly the start of a hierarchy. Smelters processed copper while craftsmen shaped obsidian into cutting tools; both kinds of raw materials came from 400 kilometers away in Anatolia. To make flint sickles for harvesting grain from their irrigated fields, the people of Tell Zeidan used bitumen from Iraq.

At another site to the north of Tell Zeidan, in today's Turkey, people built Ubaid-style houses clustered closely together as they had their Neolithic huts. That contrasts with the south, where houses were set apart from one another. Such finds, which now include sites in Iran as well, suggest that this was not a monolithic culture. "*The* Ubaid is actually *many* Ubaids that developed in tandem at roughly comparable rates," says archaeologist Guillermo Algaze of the University of California, San Diego. He envisions several independent polities exchanging goods and ideas and possibly competing with one another. He adds that the Ubaid marks "a notable advance of social complexity" across a broad area called Greater Mesopotamia.

Clues to a culture. Ubaid artifacts (*clockwise from top left*) include distinctive pottery with fanciful designs, clay female figurines, and vessels made of obsidian brought from distant sources.

Down south

By contrast with Mesopotamia, the sparsely settled Persian Gulf region has until recently attracted little attention from archaeologists. A scattering of Ubaid potsherds have turned up on the Arabian side of the gulf, but they were thought to have been left by occasional Mesopotamian traders.

Then a decade ago, a team co-led by archaeologist Robert Carter, now of University College London's campus at Doha, Qatar, excavated a substantial Ubaid encampment on the Kuwaiti coast. The team found remains of the oldest seafaring boat, complete with barnacles, as well as the oldest pierced pearl. Then in 2007, a Kuwaiti researcher turned up Ubaid potsherds 7 kilometers inland. Bielinski and his team have now excavated a stone-ringed burial chamber with more than 600 Ubaid-type beads and ornaments of shell, stone, and mother-of-pearl—an unusually large quantity and quality for this barren region. And during the past three seasons, excavators dug a 200-meter by 50-meter area revealing a series of six to eight rectangular buildings strongly reminiscent of Ubaid architecture amid a scatter of Ubaid pottery as well as a cruder red ware.

CREDITS (BOTTOM): UNIVERSITY OF CHICAGO/SYRIAN DEPARTMENT OF ANTIQUITIES

Downloaded from www.sciencemag.org on February 16, 2012

Published by AAAS

The most remarkable find was a large room with a paved stone floor and a stone podium in the middle. "At first we thought the podium might be an altar in a temple," recalls archaeologist Andrzej Reiche of Warsaw's National Museum. But given the plethora of beads and shells, "it appears this was a table in a workshop." The room contained shell beads in different states of production along with flint drills. The scale suggests to Reiche that settlers here made beads for export.

Although Bahra today is high and dry, in its heyday it was between 1 and 3 kilometers from the gulf, says archaeologist Jennifer Pournelle of the University of South Carolina in Columbia, and fresh water was likely nearby. Carter adds that Bahra appears roughly contemporaneous or slightly later than his nearby coastal site, which may have been a seasonal camp or trading center. "I would guess it was very closely related, or the same community," he adds.

The identity of Bahra's inhabitants, however, remains in dispute. Oates thinks they were Mesopotamians seeking fish, pearls, and other resources. She adds that the settlers likely brought their own fine serving ware but made the crude red clay pots for cooking. Bielinski, however, suspects that the Bahra people were locals participating in the wider Ubaid culture. He notes the use of parallel stone slab construction, a method that works well for oval-shaped houses typical of Neolithic Arabia but makes less sense for the rectangular structures of Mesopotamia. The structures, he concludes, likely were not built by experienced Mesopotamian masons but by locals seeking to emulate the fashion. As for the red ware, "it's as if the local people saw the Ubaid pottery and said, 'That's a good idea,' " Stein says.

Also, the few flints thus far found come from poor-quality sources in southern Kuwait rather than from higher-quality northern sources accessible to Mesopotamians. Bielinski cautions that it's too early to fully understand the settlement. Still, he says, "in front of an American jury I can't defend it, but this wasn't built by people from the north."

Syrian center. Archaeologists led by Chicago's Gil Stein (*top*) uncovered a rich Ubaid settlement at Tell Zeidan in northern Mesopotamia, before Syria's unrest forced a halt to the dig.

CREDITS: UNIVERSITY OF CHICAGO/SYRIAN DEPARTMENT OF ANTIQUITIES

Paving the way

Whoever the Bahra people were, both the Syrian and Kuwait finds, as well as recent discoveries of Ubaid material in Turkey, Saudi Arabia, and Iran, point to a slow but extensive transmission and sharing of goods, ideas, and technologies during this time. The twin sites in Kuwait, Carter says, nicely illustrate "this early spurt of globalization."

By 4000 B.C.E., Ubaid pottery and other materials vanish from the record across Greater Mesopotamia. But within a century or two, the protocities of Uruk in the south and Tell Brak in the north were expanding (*Science*, 9 June 2006, p. 1460). These formidable settlements had more than burgeoning populations: They controlled surrounding areas, employed administrators and craft specialists, and bore the hallmarks of central organization. Within 500 years, Uruk trade and fashions dominated an area comparable to that of the Ubaid, while other cities began to emerge elsewhere in Mesopotamia.

Ultimately, archaeologists say, the Ubaid's most important innovations were not technological but social. A new style of housing, blossoming trade, specialty jobs, temples, and growing acceptance of a budding social hierarchy changed the way people saw themselves and related to others, Bielinski says. Practical acceptance of outside ways rather than "slavish imitation" was the Ubaid way, Stein adds.

And southern Mesopotamia was not the source of the entire culture. At least one form of pottery, a greenish buff ware with black paint, seems to appear in northern Mesopotamia first. Iranian digs have revealed some of the earliest examples of banding infant skulls. The popularity of wool provided new markets for a growing number of pastoralists, who may have played a key role in transmitting goods and ideas.

In this emerging picture, the Ubaid is a dress rehearsal for the radical changes to come. Across an area of unprecedented size, a complicated mix of peoples experimented with what became the building blocks of civilization. "There were tremendous integrative forces coming into play at this time," Carter says. Despite the similarity of pots and architecture from Turkey to Oman, "it was not a homogenous cultural landscape." What began to emerge, Harvard's Lamberg-Karlovsky says, were the "technologies of social control," such as writing and organized groups of laborers that ultimately created our modern complex society.

But further exploration of the deeply buried Ubaid sites in Iraq will not be easy. Sectarian turmoil in Syria has halted the excavations at Tell Zeidan, preventing Stein's access to what he calls "archaeological heaven." And Iran remains off-limits to foreigners. Such constraints suggest that the Ubaid peoples will retain some of their ancient mystery for years to come.

–ANDREW LAWLER

Downloaded from www.sciencemag.org on February 16, 2012

Published by AAAS

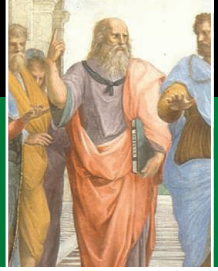

Platonic paths toward sustainable lives
797

Using information to fight influenza
799

LETTERS | BOOKS | POLICY FORUM | EDUCATION FORUM | PERSPECTIVES

LETTERS

edited by Jennifer Sills

Bad Advice, Not Young Scientists, Should Hit the Road

TYPICALLY, WHEN GRADUATE STUDENTS APPLY FOR POSTDOCS, OR postdocs apply for faculty positions at their home institutions, they are greeted with a reflexive reaction: They should diversify their training by working elsewhere. This guidance is both antiquated and damaging. It is time for a change.

Most often, this affects young scientists struggling already to balance work and personal life, perhaps with young families and multiple careers. In many cases, they have real opportunities right where they are, and the pressure to "move on" is as costly as it is arbitrary. Large institutions often have multiple labs well-suited to the student's career development, led by investigators in a position to understand and appreciate the talent of these trainees. In some cases, the trainees already work in the best lab for their own development. Others are forced by the intellectual bad habits of grant reviewers to choose between family and career. This isn't to say that the advice is always bad, but neither is it always right.

Science is a team sport: The strengths of a lab arise from the joint contributions of all of its members. These trainees may well be especially productive because of the environment they have helped to create, and the success of the lab as a whole follows suit. We should recognize and honor the importance of continuity when a group has formed an effective research unit, and should encourage young scientists to work where they are most productive. Can you imagine a private-sector environment that demands of its best workers that they find jobs at other companies, rather than nurture them toward the success of the business overall?

These are deeply institutionalized problems. As individuals, we should think carefully about the advice we give to students who want to grow right where they are. To see real change, we should look to the National Institutes of Health and the National Science Foundation to provide rational guidance on the expectations of continuing training fellowships.

MARK S. COHEN

Semel Institute for Neuroscience and Human Behavior, University of California Los Angeles, Los Angeles, CA 90095, USA. E-mail: mscohen@ucla.edu

Rescuing Wolves: Threat of Misinformation

AFTER READING THE POLICY FORUM "RESCUING wolves from politics: Wildlife as a public trust resource" (J. T. Bruskotter *et al.*, 30 September 2011, p. 1828), I would like to set the record straight. First, state governments have not shown "hostility toward wolves." Rather, each state wolf-management plan was vetted by the U.S. Fish and Wildlife Service (USFWS) and each seeks to maintain wolf numbers at or above 150% of official recovery levels. Second, although there always will be disagreement about what constitutes recovery of any imperiled species, teams of highly qualified scientists set wolf recovery criteria, and in the West, wolf numbers exceeded those goals by 500 to 600% before delisting. Third, although public opinion toward wolves is variable (*1*), state wolf-management regulations are totally different now than when wolves were deliberately exterminated (*2*, *3*). State wolf management will be monitored by the USFWS, and the wolf can be relisted anytime if necessary; strict post-delisting monitoring plans are in place for this.

Thus, the gist of the Policy Forum—that "courts must use the [Public Trust] doctrine to hold states accountable to their trust obligations" is redundant. The states, through their science-based wolf management plans, are already adhering to their public trust obligations as required by state laws for all wildlife species.

Because wolves and wolf management are contentious, no government entity can fully satisfy all viewpoints. Thus, agencies compromise by setting regulations that ensure the conservation and survival of their populations while still attempting to assert some population control. Citizens assert their control over state actions through lobbying, elections, referenda, and other legal means (*4*), and that approach is well in place.

L. DAVID MECH

Northern Prairie Wildlife Research Center, U.S. Geological Survey, Jamestown, ND 58401–7317, USA. E-mail: mechx002@umn.edu

References

1. J. T. Bruskotter, E. Toman, S. A. Enzler, R. H. Schmidt, *Bioscience* **60**, 941 (2010).
2. S. P. Young, *The Wolves of North America: Their History, Life Habits, Economic Status, and Control* (Dover Publications, New York, 1944).
3. M. J. Robinson, *Predatory Bureaucracy: The Extermination of Wolves and the Transformation of the West* (Univ. Press of Colorado, Boulder, CO, 2010).
4. C. A. Jacobson, J. F. Organ, D. J. Decker, G. R. Batcheller, L. Carpenter, *J. Wildl. Manage.* **74**, 203 (2010).

CREDIT: DON BAYLEY/ISTOCKPHOTO.COM

Downloaded from www.sciencemag.org on February 16, 2012

Published by AAAS

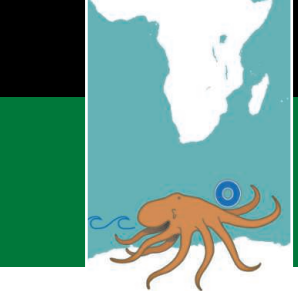

Surviving in the cold
805

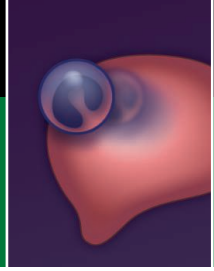

Loss of human genes
806

Readers' Poll

Bad Advice?

In his Letter, M. S. Cohen questions the wisdom of pushing graduate students and postdocs to leave their home institutions when applying for new positions. Do you agree with Cohen that this tradition is "as costly as it is arbitrary"?

Does the standard practice of applying for postdoc and new faculty positions outside one's home institution make sense?

- ❒ Yes
- ❒ No

Vote online at http://scim.ag/zWir00

Polling results reflect the votes of those who chose to participate; they do not represent a random sample of the population.

Rescuing Wolves: States Not Immune to Politics

J. T. BRUSKOTTER *ET AL*. HAVE PERFORMED A valuable service in showing how the public trust doctrine might protect species delisted from the Endangered Species Act (ESA) or otherwise not protected ("Rescuing wolves from politics: Wildlife as a public trust resource," Policy Forum, 30 September 2011, p. 1828). However, they do not provide an adequate analysis of the federal legislative delisting decision and thus do not make a persuasive case that moving the issue from federal to state courts will remove politics from decisions about wolves.

CREDIT: JOHN PITCHER/ISTOCKPHOTO.COM

Litigation in state courts under the public trust doctrine does offer the possibility of an alternative when the ESA is no longer applicable, but there are many obstacles. Although the Supreme Court and California decisions seem to support the public trust's application to wildlife protection, Bruskotter *et al*. rightly note that state courts have generally resisted or been hostile to doing so (*1*). Case law is not static, but as with civil rights and First Amendment speech, it can take decades of careful legal work to gain more just interpretations of the law (*2*). Meanwhile, state court judges who are elected [such as those in Idaho and Montana (*3*)] are statistically more likely than judges appointed for life to be swayed by public expectations (*4*).

More important, Bruskotter *et al*. do not explain why wolf opponents would respond any differently to unfavorable state court decisions than to federal ones. State legislatures can overturn court decisions by enacting statutes that replace the common law just as they can change statutes. So we are back to politics.

Litigation is an important tool in convincing governments to pay attention to the law and facts, but without extensive grassroots organizing in support of the cause being litigated, court decisions can be undermined or nullified (*5*). Only grassroots organizing can build a conservation movement strong enough to prevail with legislatures and agencies, and in protecting good case law. Unfortunately, most conservation nongovernmental organizations (NGOs) have abandoned organizing [e.g., (*6*)]. NGOs consisting of check-writers and letter-writers are no substitute for the activism that won the 8-hour work day, women's suffrage, and the end of Jim Crow (*7*, *8*).

Most polling data find that Americans favor wolf restoration by a two-to-one ratio (*9*), but if they are not organized on the issue, their voices do not count. Meanwhile, those opposed to healthy wolf populations—including some hunting and ranching groups, those with a rabid fear of wolves, and those looking to blame wolves for the consequences of sprawl, road building, and cattle consuming the forage of ungulate populations—have organized intensively (*10*).

It is the ability to reward and punish officials that determines influence (*11*). Wolves were legislatively delisted because even nominal defenders of the ESA believed they had more to fear from wolf opponents than wolf supporters. Wolf supporters were outorganized; Senator Jon Tester (D-MT) and the White House caved to the wolf opponents in hopes that such action would help Senator Tester keep his congressional seat for another term.

DAVID JOHNS

Division of Political Science, School of Government, Portland State University, Portland, OR 97207, USA. E-mail: johnsd@pdx.edu

References and Notes

1. P. Redmond, *Nat. Res. J.* **49**, 249 (2009).
2. H. A. Abraham, B. A. Perry, *Freedom and the Court* (Univ. of Kansas Press, Lawrence, KS, ed. 8, 2003).
3. L. Baum, *American Courts* (Houghton-Mifflin, Boston, ed. 6, 2008).
4. G. A. Huber, S. C. Gordon, *Am. J. Polit. Sci.* **48**, 247 (2004).
5. For example, the "wolf rider" included in PL 112-10 nullified Federal District Court Judge Malloy's rulings on the inadequacy of government wolf recovery efforts.
6. R. G. Shaiko, *Voices and Echoes for the Environment* (Columbia Univ. Press, New York, 1997).
7. S. Staggenborg, *Social Movements* (Oxford Univ. Press, New York, 2010).
8. F. F. Piven, *Challenging Authority* (Rowman & Littlefield, Lanham, MD, 2006).
9. R. Meadow, R. P. Reading, M. Phillips, M. Mehringer, B. J. Miller, *Wildl. Soc. Bull.* **33**, 154 (2005).
10. H. Herring, *High Country News* **43**, 8 (2011).
11. M. E. Kraft, S. Kamieniecki, *Business and Environmental Policy* (MIT Press, Cambridge MA, 2007).

Response

MECH'S CLAIM THAT "STATE GOVERNMENTS have not shown 'hostility toward wolves'" ignores states' recent actions with respect to wolves: Idaho's government barred its state agency from participating in wolf recovery (*1*), passed legislation demanding the removal of wolves by "whatever means necessary," and ordered state law enforcement not to assist in the enforcement of federal law protecting wolves (*2*). Wyoming held up delisting efforts by steadfastly refusing to provide any protection for wolves in the vast majority of the state (*3*)—a position Wyoming continues to maintain. Utah recently passed legislation that attempts to prevent "the establishment of a viable pack of wolves within the areas… where the wolf is not listed" and requests "immediate removal" of other wolves (*4*). In so doing, Utah's elected officials ignored public opinion (*5*) and abandoned a plan developed by the state Division of Wildlife Resources through a multistakeholder collaborative process.

Mech's confidence in states' intentions to conserve wolves is predicated on the wolf management plans developed by state wildlife agencies. However, he fails to recognize that

Downloaded from www.sciencemag.org on February 16, 2012

Published by AAAS

state agencies perform ministerial, management duties under the direction of the legislative and executive branches of government (*6*). Agencies' power over wildlife is thus constrained by elected officials (*6*), many of whom have obstructed wolf conservation, as the above examples demonstrate.

Likewise, the idea that wolves can be "relisted anytime if necessary" is dubious given Congress's willingness to remove wolves from endangered species protections by legislative rider. Furthermore, the monitoring and relisting provision of the Endangered Species Act that Mech cites extends only 5 years; after that, relisting becomes considerably less likely, especially given the U.S. Fish and Wildlife Service's recent reliance on the "warranted but precluded" finding to avoid listing species (*7*).

Finally, we believe that Mech fundamentally misinterprets our argument, which empowers wildlife managers at state agencies to act on species' behalf by reminding state elected officials that, as trustees, they have a duty to conserve wildlife—including wolves—for current and future generations.

Johns notes that we did not undertake a detailed analysis of the federal delisting decision. Indeed, such an analysis was made moot when Congress intervened and removed Endangered Species Act protection for wolves in the northern Rockies. The result: Wolf management decisions will now be made by the legislative and executive branches of states in the American West (*8*), where wolf management decisions have historically been driven by influential special interests (*2*) rather than concern for long-term conservation [e.g., (*9*)]. Because the public trust doctrine imposes an obligation on the state to "preserve the subject of the trust" for future generations (*10*), an obligation that can be enforced in a court proceeding, the doctrine provides a less political avenue to assure the long-term viability of healthy wolf populations than the state legislative or state executive branches, which are subject to the vagaries of local, short-term politics. Although we agree with Johns that elected judges can be influenced by political ideologies, judges (unlike legislators, governors, and appointed officials) are constrained by prior case law and are not free to ignore precedent for political expediency (*11*). Certainly, powerful vested interests will oppose attempts to apply the public trust doctrine to wolves; however, this does not mean that state legislatures are free to adopt legislation in defiance of their public trust obligations, nor may a state legislature or state executive substantially impair or abdicate its public trust obligation by contract or legislative action (*12*).

Finally, we agree with Johns that grassroots mobilization is an important element in species protection and may well be vital for lasting protection of wolf populations. Indeed, the record is clear that litigation can be used to influence public policy decisions (*13*), but research also suggests that the power of litigation to affect policy is enhanced when it is used as a political resource by social movement organizations in conjunction with "grassroots mobilization" (*14*). Thus, we believe that the public trust doctrine should be part of a broader movement to mobilize support for the protection of controversial wildlife populations.

JEREMY T. BRUSKOTTER,[1]* SHERRY A. ENZLER,[2]† ADRIAN TREVES[3]

[1]School of Environment and Natural Resources, The Ohio State University, Columbus, OH 43210, USA. [2]Department of Forest Resources and Institute on the Environment, University of Minnesota, St. Paul, MN 55108, USA. [3]Nelson Institute for Environmental Studies, University of Wisconsin-Madison, Madison, WI 53706, USA.

*To whom correspondence regarding response to Mech should be addressed. E-mail: bruskotter.9@osu.edu
†To whom correspondence regarding response to Johns should be addressed. E-mail: senzler@umn.edu

References

1. P. I. Wilson, *Nat. Res. J.* **39**, 543 (1999).
2. J. T. Bruskotter *et al., BioScience* **60**, 941 (2010).
3. B. J. Bergstrom, S. Vignieri, S. R. Shefield, W. Sechrest, A. A. Carlson, *BioScience* **59**, 991 (2009).
4. Utah Code Ann. §§ 23-29-101 et seq. (2010) (Wolf Management Act).
5. J. T. Bruskotter, R. H. Schmidt, T. L. Teel, *Biol. Conserv.* **139**, 211 (2007).
6. C. A. Smith, *J. Wildl. Manage.* **75**, 1539 (2011).
7. K. M. Smith, *Southeastern Environ. Law J.* **19, 119** (2010).
8. 16 U.S. Code § §1533 and 1540(g) (2010).
9. Associated Press, "Idaho Governor pulls state management of wolves in dispute over wolf hunt," *OregonLive.com* (18 October 2010); www.oregonlive.com/pacific-northwest-news/index.ssf/2010/10/idaho_governor_pulls_state_management_of_wolves_in_dispute_over_wolf_hunt.html.
10. *Greer v. Connecticut,* 161 U.S. 519, 534 (1896).
11. T. J. Miceli, *J. Legal Stud.* **38**, 157 (2009).
12. *Illinois Central Railroad Co. v. Illinois,* 146 U.S. 387, 452-53 (1892).
13. C. F. Sabel, W. H. Simon, *Harv. Law Rev.* **117**, 1015 (2004).
14. S. Enzler, *William Mary Environ. Law Pol. Rev.* **35**, 413 (2011).

CORRECTIONS AND CLARIFICATIONS

News of the Week: "Joint German-Israeli research center planned" (13 January, p. 150). Both the print version and the earlier online-only *ScienceInsider* version of this article incorrectly identified the Minerva Foundation as the funding source for the new center. The new center will be jointly funded by the Max Planck Society and the Weizmann Institute. Also, Steve Weiner, director of the Kimmel Center for Archaeological Science, is a biologist, not an archaeologist.

GE Prize Essay: "Zoom" by E. L. Aiden (2 December 2011, p. 1222). An editorial error was introduced during production. On p. 1222, the zoom for the interior of a proton was given as "10 to 16 m." The correct number is 10^{-16} m. The number has been corrected in the HTML version online.

Reports: "A composite of multiple signals distinguishes causal variants in regions of positive selection" by S. R. Grossman *et al*. (12 February 2010, p. 883). The surname of the second author was spelled incorrectly; the correct spelling is Shlyakhter. The name has been corrected in the HTML version online.

TECHNICAL COMMENT ABSTRACTS

Comment on "A Diverse Assemblage of Late Cretaceous Dinosaur and Bird Feathers from Canadian Amber"

Carla J. Dove and Lorian C. Straker

McKellar *et al*. (Reports, 16 September 2011, p. 1619) analyzed Late Cretaceous amber specimens from Canada and identified some filaments as dinosaurian protofeathers. We argue that their analysis and data do not provide sufficient evidence to conclude that such filaments are feather-like structures. Further investigation, including destructive sampling, must be carried out for more convincing conclusions.

Full text at www.sciencemag.org/cgi/content/full/335/6070/796-b

Response to Comment on "A Diverse Assemblage of Late Cretaceous Dinosaur and Bird Feathers from Canadian Amber"

Ryan C. McKellar, Brian D. E. Chatterton, Alexander P. Wolfe, Philip J. Currie

Dove and Straker question our interpretations of plumage from Late Cretaceous Canadian amber. Although we are able to refute concerns regarding both specimen taphonomy and misidentification as botanical fossils, unequivocal assignment to either birds or dinosaurs remains impossible, as we stated originally. However, reported observations and their further refinement herein are insufficient to falsify the hypothesized dinosaurian origin for protofeathers.

Full text at www.sciencemag.org/cgi/content/full/335/6070/796-c

Letters to the Editor

Letters (~300 words) discuss material published in *Science* in the past 3 months or matters of general interest. Letters are not acknowledged upon receipt. Whether published in full or in part, Letters are subject to editing for clarity and space. Letters submitted, published, or posted elsewhere, in print or online, will be disqualified. To submit a Letter, go to www.submit2science.org.

Downloaded from www.sciencemag.org on February 16, 2012

Published by AAAS

Comment on "A Diverse Assemblage of Late Cretaceous Dinosaur and Bird Feathers from Canadian Amber"

Carla J. Dove[1]* and Lorian C. Straker[1,2]

McKellar *et al.* (Reports, 16 September 2011, p. 1619) analyzed Late Cretaceous amber specimens from Canada and identified some filaments as dinosaurian protofeathers. We argue that their analysis and data do not provide sufficient evidence to conclude that such filaments are feather-like structures. Further investigation, including destructive sampling, must be carried out for more convincing conclusions.

McKellar *et al.* (*1*) recently examined Late Cretaceous amber specimens from Canada and reported stages I through V of feather evolution according to Prum's (*2*) model. They concluded that the amber specimens contained dinosaur feathers because (i) specimens UALVP 52821 [figure 1B in (*1*)] and UALVP 52822 [figure 1, C and D, in (*1*)] were comparable to nonavian dinosaur fossil compressions; and (ii) fibers in specimen TMP 96.9.334 [figure 2, A to C, in (*1*)] exhibited microstructure coiling comparable to modern birds. Because they could not identify the fibers as any organism of an "end-member" evolutionary-developmental spectrum, and the fibers occurred concurrently with modern feather types, they inferred that the fibers were dinosaurian.

The interpretations of figure 1, B to D, in (*1*); figure 2, A to C, in (*1*); and the supporting figures in (*3*) convince us that adequate analysis was not conducted on these specimens and that overstated conclusions were made on subjective observations. Other figures in (*1*) (figure 2, D to F, and figure 3) are comparable with the feather microstructure in modern birds and cannot be regarded as anything but the ultimate stage of feather evolution.

The filaments described as stage I [UALVP 52821, figure 1B in (*1*)] are an order of magnitude smaller than the filaments of compression fossils of *Sinosauropteryx prima* (*4*) with which they were compared. According to McKellar *et al.* (*1*), the largest width of the filaments in UALVP 52821 falls within the range of the *S. prima*'s integument structures; however, the cited work [(*5*), p. 1719] reported "smaller ones are considerably narrower than 0.1 mm" in diameter. This does not represent a comparable scale to the 0.027 mm [(*3*), p. 3] measurements from the specimen in amber. Further, other researchers who examined the *S. prima* impressions reported measurements no thinner than 0.05 mm and declared the fibers to be collagen and not protofeathers (*6*). Although the filament lengths of UALVP 52821 were not measured in this study, the authors report that these "are consistent with the finer filaments found in this specimen [*S. prima*], and fall within the range of observed lengths" [(*3*), p. 5].

The study reports diameter measurements for UALVP 52821 as being within the lower range of modern hair measurements (of Australian mammals), but the authors curiously excluded hair as a possible fiber based on diameter and hollowness [(*3*), pp. 3–4 and figure S1]. Our interpretation of figure S4, B to D, and figure S5B in (*3*) is that the fibers do show internal divisions and do not appear to be hollow the entire length of the filament (Fig. 1, A and B). Additionally, comparing the amber fibers to specimens of fossil hair found in Canada (TMP 96.9.998) and France (dated Early Cretaceous) does not exclusively rule out UALVP 52821 as including hair filaments based on surface texture (cross-hatching) and diameter alone [figure S4, B to E, in (*3*)]. This analysis is open to subjective interpretation based on the published images.

In the spinning disk confocal microscopy (SDCM) and laser scanning confocal microscopy (LSCM) analysis, McKellar *et al.* (*1*) state that the β-keratin autofluorescence results were influenced by background interference of the tested amber specimens, so we are confused as to why they conclude that UALVP 52821 [(*3*), p. 7)] contains β-keratin. Although the graphs have similar profiles, the intensity peaks and wavelength excitation values for β-keratin are different [figure S10, B and E in (*3*)], and we question the assumption that the materials are similar in nature.

McKellar *et al.* (*1*) explicitly state that reflective emissions of UALVP 52821 and TMP 96.9.997 are inconclusive [(*3*), pp. S7–S8] because values could be from a reflective surface when the specimen pulled away, or from fractures in the amber and not from β-keratin matrix. We feel that this represents an insufficient conclusion based on circumstantial evidence.

Another flaw in this particular analysis is that comparisons were made only to a feather in TMP 96.9.997 and not to the specimen that they reported as being hair (TMP 96.9.998). Confocal microscopy comparing the unknown fiber to the amber specimen containing hair would be more appropriate and could possibly rule out α-keratin as a component.

Because the reported stage II morphotypes [figure 1, C and D, in (*1*) and figure S5 in (*3*)] did not undergo the same analytical tests as UALVP 52821, we cannot assume that those fibers are the same [(*1*), p. 1620] and believe that the authors should have conducted similar analyses on that specimen instead of basing conclusions on visual observations.

The interpretations of fibers in TMP 96.9.334 [figure 2, A to C in (*1*)] are not analogous to modern feather microstructures of birds. Feather barbules (pennula) in modern birds are cylindrical and do not coil in both right and left directions on the same axis (Fig. 2A), nor do the twists extend distally. Twisting on modern birds only occurs on the flattened, straplike cells of bases [as shown in figure S12E in (*3*)]. McKellar *et al.*'s conclusions are invalid because (i) the amber specimen shows coiling at mid and distal positions of the fiber [figure 2A in (*1*)]; (ii) no base cell is observable; (iii) internodes are not flattened in modern birds; and (iv) figures S6A, S6B, S7A (lower arrow), and S7B (*3*) do not clearly show a rachis structure or a barb ramus, but rather seem to be a concentration of filaments focused on a central structure (observed on figure S7B). We have observed similar coiling on fibers of seed hairs (Fig. 2B), that is, *Populus trichocarpa*.

Although exploring amber specimens for clues to feather evolution may seem novel, this study lacks evidence and vigor to conclude that the fibers in UALVP 52821, UALVP 52822, and TMP 96.9.334 are dinosaurian. The analysis was not complete for each specimen, did not conclusively rule out hair or specialized plant parts as possible fibers, makes incorrect comparisons to modern feather microstructure, and cannot be cited as early stages of feather evolution. Because the topic of dinosaur feathers has been disputed, we feel that better analysis of the material in question, including destructive sampling of the amber specimens, is paramount.

Without concise identification of the various filaments depicted, there is no basis for assigning any of them to a particular group of organisms, to say nothing of dinosaurs.

[1]Smithsonian Institution, National Museum of Natural History, Division of Birds, MRC 116, Post Office Box 37102, Washington, DC 20013–7012, USA. [2]Universidade Federal do Rio de Janeiro, Instituto de Biofísica Carlos Chagas Filho, Laboratório de Ultraestrutura Celular Hertha Meyer, Ilha do Fundão, Rio de Janeiro, RJ, 21949-900, Brazil.

*To whom correspondence should be addressed. E-mail: dovec@si.edu

References and Notes

1. R. C. McKellar, B. D. Chatterton, A. P. Wolfe, P. J. Currie, *Science* **333**, 1619 (2011).
2. R. O. Prum, *J. Exp. Zool.* **285**, 291 (1999).
3. Supporting online material for (*1*).

Downloaded from www.sciencemag.org on February 16, 2012

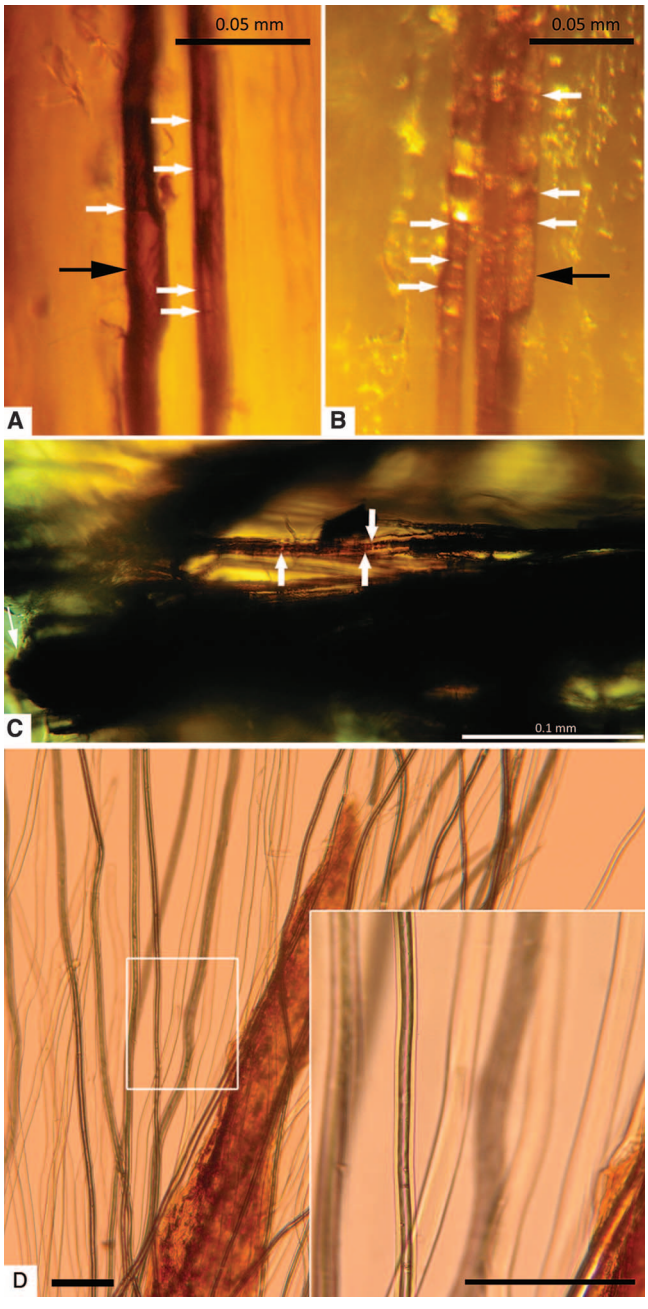

Fig. 1. (**A** to **C**) Images from (*3*) of filaments within UALVP 52821 [(A) and (B)] and UALVP 52822 (C), with white arrows added to point to our interpretation of possible internal septa, cell walls, or other features that appear as evidence to dispute hollowness. (**D**) Photomicrograph of cottonwood seed (*Populus tremuloides*) with enlarged inset showing similar overall characteristics to the filaments in the amber specimens (15 μm width and outside wall thickness is average 42% of total width). Scale bar, 0.1 mm).

4. P.-J. Chen, Z.-M. Dong, S.-N. Zhen, *Nature* **391**, 147 (1998).
5. P. J. Currie, P.-J. Chen, *Can. J. Earth Sci.* **38**, 1705 (2001).
6. T. Lingham-Soliar, A. Feduccia, X. Wang, *Proc. Biol. Sci.* **274**, 1823 (2007).

Acknowledgments: The Feather Identification Lab at the Smithsonian is funded through interagency agreements with the U.S. Air Force, the U.S. Navy, and the U.S. Federal Aviation Administration. L. C. Straker is a predoctoral fellow funded through the Coordenação de Aperfeiçoamento de Pessoal de Nível Superior/Fulbright Commission, Brazil.

4 November 2011; accepted 5 January 2012
10.1126/science.1216208

Downloaded from www.sciencemag.org on February 16, 2012

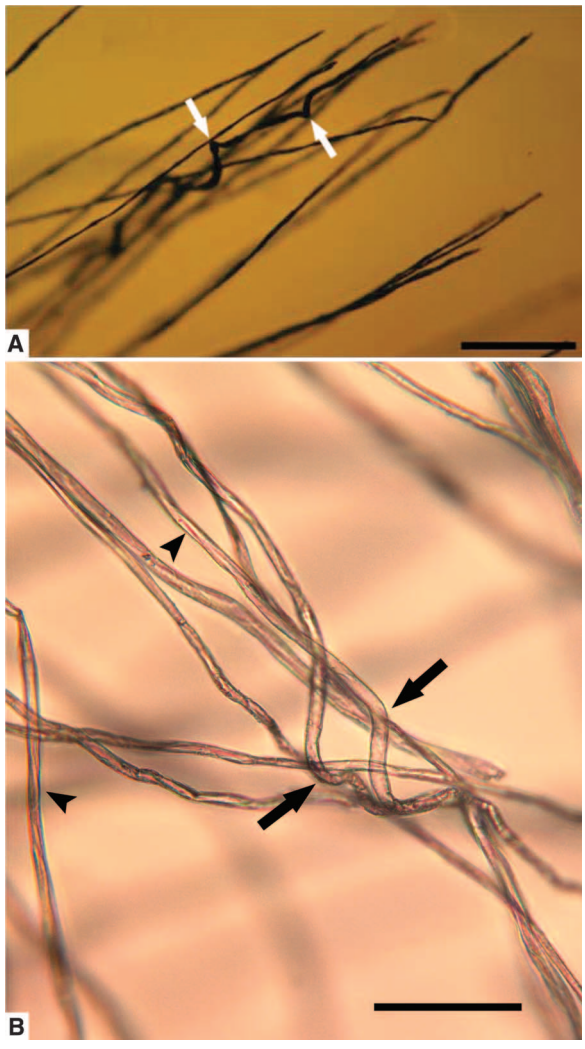

Fig. 2. Similarities of morphological characteristics of amber specimen and seed hair filaments. (**A**) Image from McKellar *et al*. (*1*) of TMP 96.9.334, with white arrows added to show the coiled distal filaments. Scale bar, 0.2 mm. (**B**) Cottonwood seed hairs (*Populus trichocarpa*) with thick arrows showing similar coiling, and arrowheads showing semiflattened areas similar to filament observed in figure 2C in (*1*) (filament width of 9 to 11 μm). Scale bar, 0.1 mm.

Downloaded from www.sciencemag.org on February 16, 2012

Response to Comment on "A Diverse Assemblage of Late Cretaceous Dinosaur and Bird Feathers from Canadian Amber"

Ryan C. McKellar,[1]* Brian D. E. Chatterton,[1] Alexander P. Wolfe,[1] Philip J. Currie[2]

Dove and Straker question our interpretations of plumage from Late Cretaceous Canadian amber. Although we are able to refute concerns regarding both specimen taphonomy and misidentification as botanical fossils, unequivocal assignment to either birds or dinosaurs remains impossible, as we stated originally. However, reported observations and their further refinement herein are insufficient to falsify the hypothesized dinosaurian origin for protofeathers.

Dove and Straker (*1*) raise concerns over whether our recent Report (*2*, *3*) of plumage from Late Cretaceous Canadian amber contains sufficient evidence to support conclusions of both avian and dinosaurian origins for inclusions. Specifically, they question two specimens (UALVP 52821 and UALVP 52822) interpreted as representatives of stages I and II in Prum's (*4*) evolutionary-developmental model, as well as a specimen (TMP 96.9.334) interpreted as representative of stage IV with specializations for water uptake. Although some uncertainty is inherent to all interpretations of fragmentary fossils, Dove and Straker's (*1*) technical concerns can be addressed readily with the specimens.

Concerning TMP 96.9.334, there is a fundamental error in their interpretation (*1*) of our paper, because we did not suggest that this specimen represents dinosaur plumage. Instead, we proposed that this specimen likely belongs to stage IV (*3*), representing Cretaceous bird plumage with structural features linked to its possible use in water uptake (*2*, *3*). Points raised (*1*) regarding fine anatomical detail are the same features that suggested to us that placement within stage IV was more appropriate than stage V. Other criticisms (*1*) represent different interpretations of our discussion and figures of specimen taphonomy (*3*).

Dove and Straker (*1*) are correct in asserting that there is no clear indication of unsegmented basal cells within TMP 96.9.334 barbules and that it is unusual to observe coiling within the segmented portion of the barbule (pennulum), because these features are unknown in modern bird feathers. As Dove has illustrated and discussed [figure 138 in (*5*)], some modern (stage V) bird plumage retains traces of segmentation or "multiple cells" within the curled basal portion of the barbule. The lack of a defined basal plate does not exclude TMP 96.9.334 from being a feather fragment, whereas the suggestion that these filaments are more comparable to *Populus* seed trichomes (*1*) is incorrect. Although coiled, trichomes are not segmented (noded) (*6*, *7*) and would not be expected to consistently straighten apically. Furthermore, Salicaceae, the family that contains *Populus,* is unknown before the latest Paleocene (*8*).

Taphonomic effects that led Dove and Straker (*1*) to critique TMP 96.9.334 were described in our original work [(*3*), p. S9], but benefit from additional clarification. The TMP 96.9.334 barbules all coil in a counter-clockwise direction. The five or so barbules (Fig. 1A) that coil clockwise have been sheared from the main mass, likely as a result of resin flow (*3*). These dislocated barbules do not indicate "coiling at mid and distal positions" (*1*), and their nodal expansions clearly indicate that they are pointing in the wrong direction. The central structure in TMP 96.9.334 is almost certainly a rachis (Fig. 1B): It is solid, not a clump of filaments, and has the appropriate size and cross-sectional shape (*9*).

Concerning UALVP 52821, Dove and Straker (*1*) chose to emphasize filament size over morphology, critiquing the match between dimensions in *Sinosauropteryx* protofeathers and the filaments in Canadian amber. Overlooking the fact that UALVP 52821 appears to contain just the distal tips of filaments (*3*), filament diameters are not "an order of magnitude smaller" (*1*) than those reported for *Sinosauropteryx*. In fact, the work (*10*) cited by Dove and Straker (*1*) contains no diameter measurements, because the

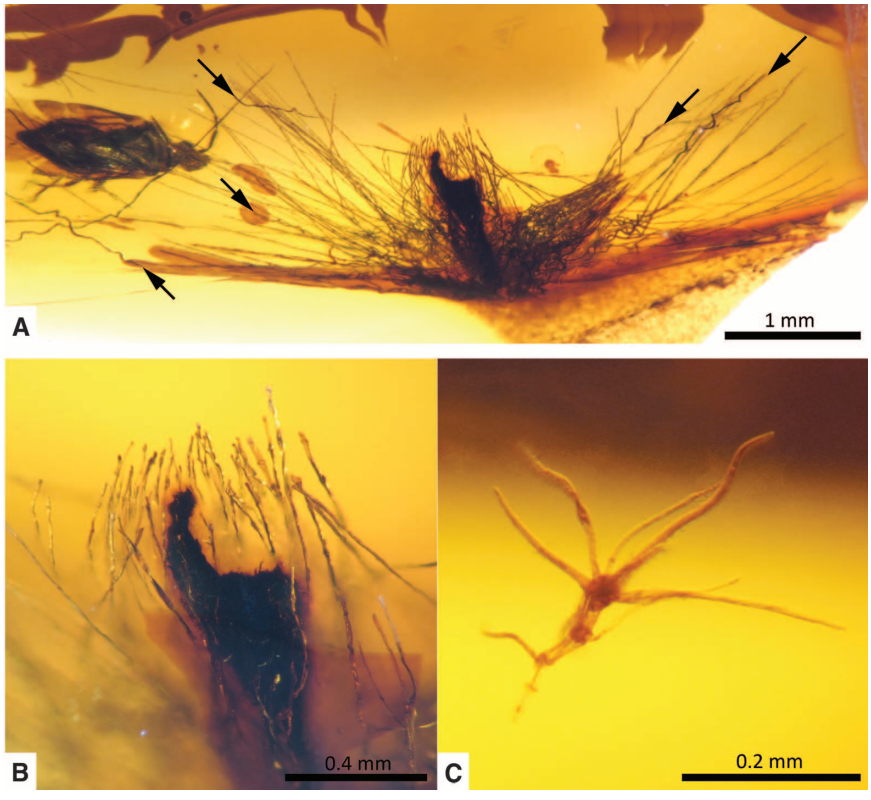

Fig. 1. Photomicrographs of TMP 96.9.334 and comparison image of a trichome preserved in Canadian amber. (**A**) Overview of TMP 96.9.334, with dislocated barbules indicated by arrows at barbule bases. (**B**) Cross section of rachis where it is truncated at the surface of the amber piece, with rachis surrounded by truncated barbule apices. (**C**) Stellate trichome (University of Alberta specimen).

[1]Department of Earth and Atmospheric Sciences, University of Alberta, Edmonton, Alberta, T6G 2E3, Canada. [2]Department of Biological Sciences, University of Alberta, Edmonton, Alberta, T6G 2E9, Canada.

*To whom correspondence should be addressed. E-mail: rcm1@ualberta.ca

Downloaded from www.sciencemag.org on February 16, 2012

authors had difficulty isolating single filaments. Later work provided generalized estimates that included smaller filaments "considerably narrower than 0.1 mm" (*11*) and cautioned that measurements may be overestimates due to filament overlap (*11*) and taphonomy (*11*, *12*). If the structures measured by Lingham-Soliar *et al*. (*12*) were indeed collagen fibers (internal structures), their measurements have no bearing on our study of integumentary structures. Subsequent work (*13*) indicated that many of the filaments surrounding *Sinosauropteryx* and *Sinornithosaurus* were pigmented and thus cannot be dismissed as collagen fibers. This also bears on the comparison between UALVP 52821 and 52822 with *Populus* trichomes [figure 1 in (*1*)]. Trichomes lack pigmentation (Fig. 1C) and are often branched or multicellular (*6*, *7*). And again, Salicaceae are unknown from the Cretaceous (*8*).

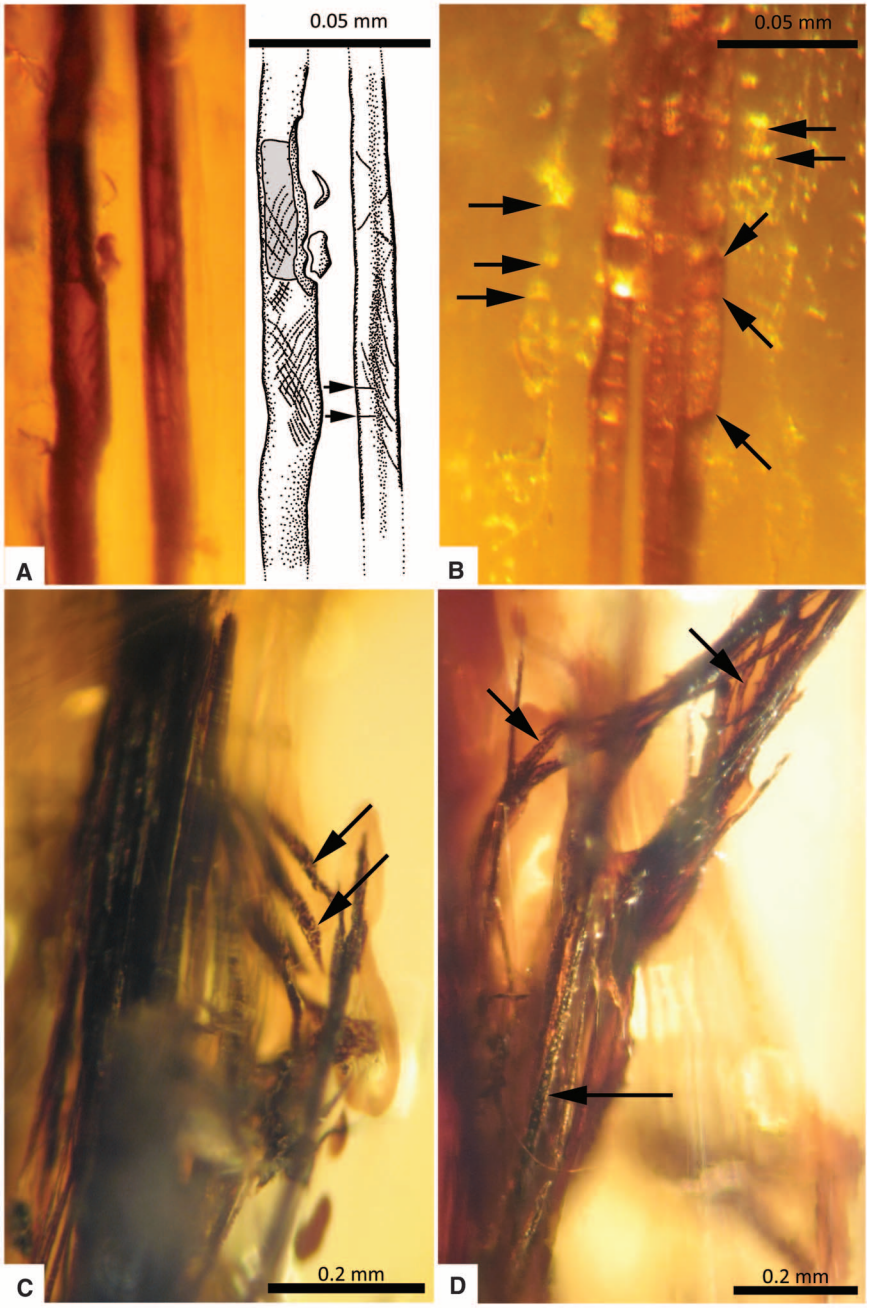

Fig. 2. Additional taphonomic details within photomicrographs of UALVP 52821 and 52822. (**A**) Diagrammatic explanation of taphonomic and structural features in UALVP 52821, bright-field image [figure S4C in (*3*)]. Stippling indicates topography, as well as the apparent cross-hatched surface or wrinkles within the outer wall of each filament. In the left filament, the gray area denotes an internal bubble in the vicinity of a large hole in the filament. In the right filament, horizontal arrows indicate cracks in the outer wall that do not extend all the way across the filament, and the filament appears to have collapsed along its midline, likely as a result of bending or torsion. (**B**) Taphonomic features in UALVP 52821 [figure S4D in (*3*)]. This is a dark-field image, highlighting surface details. Fractures within the amber appear as bright spots and are present in positions removed from the filaments (horizontal arrows); dark regions correspond to holes within the filaments (inclined arrows). (**C** and **D**) "Internal divisions" noted by Dove and Straker in UALVP 52822 (*1*) represent variations in pigmentation or cracks in the outer wall of the filament (inclined arrows) and do not appear to correspond to segmentation or internal divisions. (D) Bright spots in a linear arrangement (on the filament indicated with a horizontal arrow) appear to correspond to cross-hatching observed in UALVP 52821.

Dove and Straker (*1*) appear to advocate mammalian hair as a better match to UALVP 52821 than *Sinosauropteryx* protofeathers. Although they critique our use of diameter and hollowness as criteria for excluding mammalian hair, they overlook our most important criterion, cuticular scales. UALVP 52821 lacks cuticular scales, which was discussed at length (*3*). The internal divisions envisaged by Dove and Straker [figure 1, A to C, in (*1*)] are taphonomic artifacts (Fig. 2).

Dove and Straker (*1*) misinterpreted the results of our spinning disk confocal microscopy (SDCM) and laser scanning confocal microscopy (LSCM) analyses (*3*), which were reported as inconclusive for identifying keratin, because amber autofluorescence overwhelms any autofluorescence signal of keratin in inclusions (*3*). There is no possibility of distinguishing between α and β-keratin within this amber, and we did not claim to have identified keratin based on these analyses (*3*). Our interpretation of structure within UALVP 52821 in no way hinges upon LSCM data; the hollow, cylindrical structure of the filaments is plainly visible using light microscopy [figures S3B, S4A, and S11B in (*3*)]. We analyzed unequivocal feather fragments (TMP 96.9.997) for comparison to UALVP 52821 because the unpigmented zone of these specimens provided the best chance of detecting keratin (*3*). Keratin was not identifiable using emission profiles in TMP 96.9.997, which rendered the analysis of additional specimens futile. The same problem occurred with UALVP 52821.

We understand the recommendation for further analyses and destructive sampling (*1*). However, UALVP 52821 and UALVP 52822 are currently the only representatives of putative protofeathers in amber. The 11 plumage fragments (*2*, *3*) stem from a survey of more than 4000 inclusion-bearing pieces of amber. At a minimum, ~100,000 amber pieces were collected (*14*, *15*) over a span of decades to obtain these samples. Destructive analysis of such rare specimens is not justified when it is unlikely to produce irrefutable results (*3*). The specimens were not found with dinosaur skeletal remains, so their biological affinity will remain open to debate. At present, the evidence supports a dinosaurian source for the filaments. Dove and Straker (*1*) have suggested neither a new analytical technique nor a more parsimonious interpretation for the specimens involved.

Downloaded from www.sciencemag.org on February 16, 2012

References and Notes

1. C. J. Dove, L. C. Straker, *Science* **335**, 796 (2012); www.sciencemag.org/cgi/content/full/335/6070/796-b.
2. R. C. McKellar, B. D. E. Chatterton, A. P. Wolfe, P. J. Currie, *Science* **333**, 1619 (2011).
3. Supporting online material for (*2*).
4. R. O. Prum, *J. Exp. Zool. B* **285**, 291 (1999).
5. C. J. Dove, *Ornith. Mono.* **51**, 1 (2000).
6. J. C. T. Uphof, *Handb. Pflanzenanat*. **4**, 1 (1962).
7. E. Werker, *Adv. Bot. Res.* **31**, 1 (2000).
8. J. E. Eckenwalder, in *Biology of Populus and Its Implications for Management and Conservation*, R. F. Stettler *et al*., Eds. (NRC Research Press, Ottawa, 1996), pp. 7–32.
9. A. M. Lucas, P. R. Stettenheim, *Avian Anatomy: Integument* (U.S. Department of Agriculture, Washington, DC, 1972).
10. P.-J. Chen, Z.-M. Dong, S.-N. Zhen, *Nature* **391**, 147 (1998).
11. P. J. Currie, P.-J. Chen, *Can. J. Earth Sci.* **38**, 1705 (2001).
12. T. Lingham-Soliar, A. Feduccia, X. Wang, *Proc. Biol. Sci.* **274**, 1823 (2007).
13. F. Zhang *et al*., *Nature* **463**, 1075 (2010).
14. J. F. McAlpine, J. E. H. Martin, *Can. Ent.* **101**, 819 (1969).
15. E. M. Pike, *Palaios* **8**, 411 (1993).

Acknowledgments: Funding for this work was provided by Natural Sciences and Engineering Research Council of Canada discovery grants issued to B.D.E.C., A.P.W., and P.J.C.

6 December 2011; accepted 5 January 2012
10.1126/science.1216484

Downloaded from www.sciencemag.org on February 16, 2012

ENVIRONMENT

Learning Ecological Ethics from Plato

Saleem H. Ali

Ancient wisdom continues to provide a comforting anchorage for students and scholars across disciplines. Perhaps the most enduring source of such classical guidance comes from the Greek philosopher Plato, who lived in Athens around the 4th century BCE. The range of Plato's discourse is exemplified by how two recent books are able to use his work from very different starting points and arrive at a common argument. As the political theorist Hannah Arendt noted, central to Plato's enterprise was the elevation of philosophy over politics and ideology over iterative learning (*1*). Given the state of environmental degradation and a sense of urgency to respond to real and perceived existential threats, the Platonic approach offers an ostensible shortcut to ecological salvation. This immediacy narrative reminds one of work by ecological economist Herman Daly, particularly his book with theologian John Cobb (*2*).

William Ophuls and Melissa Lane are both attracted to Plato's certitude of ethical invocations in their work, but they make different connections with ecological goals on that basis. Although both subscribe to Plato's view that life must be lived beyond his metaphorical cave of reductionism in which inhabitants are trapped by individualism, they appear to have divergent assumptions regarding the role of scientists in this schema.

Ophuls (a political scientist) would dispense with the relatively slow and deliberative process of rationalism and focus on the normative view of natural "balance," followed by natural "limits." By this measure, the role of the scientist becomes marginal once these limits are established. Lane (a political philosopher at Princeton University) offers a more dynamic role for the scientist as a sage through this process. Her narrative also includes more contemporary examples from climate change science and cases of corporate adaptation by companies such as the carpet manufacturer Interface (*3*). In this context, she indirectly suggests that the public is detached from the scientific process itself and that the primacy of science needs to be championed regardless of consumer preferences—a supply-driven view of ecological reform with an ethical twist.

Thus Lane's treatise is more predicated in social science's traditional deference to rationalism, whereas Ophuls's work comes across as almost theological. To be fair, Ophuls notes at the outset that he offers a "provocative essay, not a scholarly treatise," and therefore his polemical tone should be taken in stride. His principal premise that the economic system should be subservient to constraints of natural systems is important and worth pursuing. However, the assumption that natural systems are somehow static in their adaptive capacity is problematic. Platonic thought cannot account for more nuanced disciplinary tangents, such as restoration or industrial ecology, that attempt to grapple with environmental constraints and human agency through innovation.

Another of Ophuls's ways of transcending rationality is revisiting James Lovelock's Gaia hypothesis as a heuristic device and tying it to Plato's concept of a "noble lie." Here I am troubled by his reluctance to deal with the darker side of such enchantments, as noted in George Williams's famed essay on the topic (*4*).

Lane makes a compelling case that the Greek vices of pleonexia (overreaching desire for more than one's share) and hubris (arrogance against natural order) need to be disparaged with the same vigor today as they were by the ancients. However, going back to the metaphor of Plato's cave, it is not so clear how to entice humanity out of that cave of self-indulgence. The Greeks noted that only necessity (ananke) could spur such movement. Yet, the light outside the metaphorical cave can also be considered in terms of finding solutions toward our challenges of sustainability. We must create incentives for people to produce technical and social innovations if we are to move toward sustainability in a pluralistic society.

Both authors acknowledge the elitism of Plato's approach. But Ophuls and Lane assume that ecological norms are logically affirmed by natural systems and hence their "virtue" offers a grassroots potential for viral inculcation, thus avoiding totalitarianism. They fail to address the question of pluralism and individual choice as ingredients for spurring technological progress that has qualitatively benefited humanity. They also neglect the broader questioning of "liberalism" on ethical terms and the insights of economic theorists such as Kenneth Arrow and Amartya Sen. Of particular interest would be revisiting Sen's classic essay "The impossibility of a Paretian liberal" (*5*).

I would also have appreciated some consideration of the critiques of Plato offered by scientists and public intellectuals such as Carl Sagan (*6*). Plato's contemporary Democritus and other Ionians, who had a more empirical approach to nature, are scarcely even referenced despite their

Plato's Revenge
Politics in the Age of Ecology
by William Ophuls
MIT Press, Cambridge, MA, 2011. 270 pp. $27.95, £19.95. ISBN 9780262015905.

Eco-Republic
What the Ancients Can Teach Us About Ethics, Virtue, and Sustainable Living
by Melissa Lane
Princeton University Press, Princeton, NJ, 2012. 255 pp. $29.95. £19.95. ISBN 9780691151243.

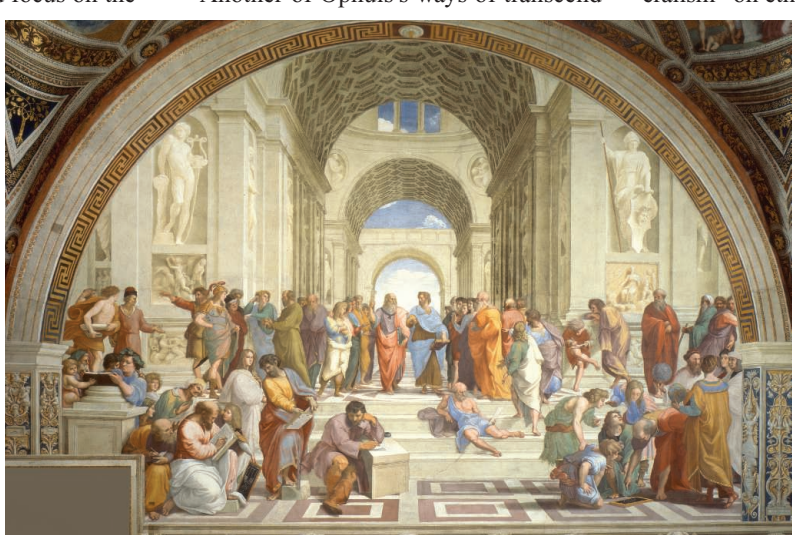

CREDIT: WIKIMEDIA COMMONS

Raphael's mural *The School of Athens* (detail, circa 1510).

The reviewer is at the Rubenstein School of Environment and Natural Resources, University of Vermont, 153 South Prospect Street, Burlington, VT 05401, USA. E-mail: saleem.ali@uvm.edu

Downloaded from www.sciencemag.org on February 16, 2012

Published by AAAS

salience to the discussion of Plato's relevance to natural laws. The reverence for natural laws that Ophuls suggests with chapter titles such as "Physics" should at least be matched with an acknowledgment that his protagonist Plato had urged the burning of all the books of Democritus and Homer because of their opposition to Pythagorean mysticism. Surprisingly, neither Lane nor Ophuls discusses works that examine Plato's view of the cosmos [such as (*7*)].

Despite such shortcomings, *Plato's Revenge* and *Eco-Republic* offer important intellectual provocation to reevaluate current inertia on environmental policy. Whether or not Plato may be our guide on these matters, the roles of science and the humanities in grappling with ecological urgency deserve to be deliberated.

References

1. D. R. Villa, *Politics, Philosophy, Terror: Essays on the Thought of Hannah Arendt* (Princeton Univ. Press, Princeton, NJ, 1999).
2. H. E. Daly, J. B. Cobb, *For the Common Good: Redirecting the Economy Toward Community, the Environment, and a Sustainable Future* (Beacon, Boston, 1989).
3. R. C. Anderson, *Mid-Course Correction: Toward a Sustainable Enterprise: The Interface Model* (Peregrinzilla, Atlanta, GA, 1998).
4. G. C. Williams, *Q. Rev. Biol.* **67**, 479 (1992).
5. A. Sen, *J. Polit. Econ.* **78**, 152 (1970).
6. C. Sagan, *Cosmos* (Random House, New York, 1980).
7. G. Vlastos, *Plato's Universe* (Univ. Washington Press, Seattle, 1975).

10.1126/science.1217178

PHILOSOPHY

Science and the Ontology of Belief

P. William Hughes

I used to believe that Maurice "The Rocket" Richard, superstar captain of the Montreal Canadiens from 1956 to 1960, was the greatest athlete who had ever lived. Even though he retired long before I was born, I had heard vivid accounts (reverently uttered) of Richard's play from my grandfather. While other hockey stars I had seen on television (such as Wayne Gretzky and Mario Lemieux) were good, they were never quite as great as I imagined The Rocket had been. I trusted my grandfather's word implicitly, and because I was obsessed with ice hockey, I knew nothing about great athletes in any other sport. What I had picked up was enough to form an opinion.

In *Grand Theories and Everyday Beliefs*, Wallace Matson addresses this strangely ubiquitous human phenomenon: we hold some beliefs very strongly despite having no firsthand evidence in their favor. Our ability to form convictions without evidence Matson terms "high belief," and he contrasts it vividly with his description of science, a system based on verified belief (as opposed to the system of in-principle-verifiable propositions á la logical positivism). Matson (a philosopher at the University of California, Berkeley) divides the book into two pieces: a fresh and intriguing detailed ontology of belief and a very broad intellectual history of scientific epistemology. The latter (which traces the development of science-as-verifiable-belief from prescientific Ionian philosophers onward) sustains Matson's theory, but it is at times uncomfortably polemical.

Grand Theories and Everyday Beliefs
Science, Philosophy, and Their Histories
by Wallace Matson
Oxford University Press, Oxford, 2011. 237 pp. $35, £22.50. ISBN 9780199812691.

Defining beliefs as "internal representations, assented to, of the way things are (or were or will be)," Matson constructs a naturalistic ontology of the concept. To do so, he divides belief into two broad categories, low and high. Low beliefs, which can be held by any organism capable of thought (including dogs, cats, and other animals having "inner lives"), are developed inductively through encounters and experience. For example, a dog may have a belief that raw beef is edible because she has eaten raw beef before and found it to be so. The capacity to form low beliefs is an evolutionary adaptation, in that low beliefs help organisms to survive and reproduce. High beliefs, on the other hand, are formed without direct experience and are gained through communication with others. Examples of high beliefs range from the trivial (Friday the 13th is unlucky) to the cultural (cosmological myths) to the world-historical (the medieval Christian idea of God's immanence). Only those organisms capable of abstract, representational language (i.e., human beings) possess the ability to hold high beliefs.

Matson thinks that high beliefs are usually false, because they rely on hearsay and anecdotal support rather than empirical verification. This presents a concrete problem. If low beliefs, being materially useful, are fitness-enhancing, why would (unreliable and arbitrary) high beliefs persist? Here Matson wades into deeply conjectural waters and invokes a group-selection hypothesis: the capacity to internalize high beliefs was "supportive of social values" in human prehistory and promoted group cohesiveness and survival. Such rampantly adaptationist evolutionary thinking is a bit convenient, but true or not, the claim represents a sound attempt at naturalistic explanation.

Once Matson identifies the capacity to form high beliefs as a natural fact of the human condition, his account of the history of scientific ideas really takes off. Although the ability to adopt others' high beliefs helped small bands of ancient humans develop cohesive identities that facilitated survival, this ability has since run amok. Not only do we now believe all manner of silly things, but baleful conflicts have resulted from disputes over the legitimacy of particular (and for Matson, arbitrary) high beliefs. A committed atheist, the author pulls no punches about religion. He considers the supernatural a myth and classifies all religious beliefs as high belief, to his mind certainly false. Matson sees science, and before it natural philosophy (as that of Thales), accounting for natural phenomena using only verifiable low beliefs (e.g., the clouds are made of vapor). His historical thesis posits that natural philosophy and science displaced culturally important high beliefs, usually inherited from a religious or supernaturalistic account (e.g., the clouds are gathered by Zeus)—the allusion to "grand theory" being made of "everyday belief." Matson's valuable history of how this process unfolded provides a series of provisional illustrations of the high belief versus low belief theory at work. However, the book's short length prevents him from treating any of the intellectual episodes with the depth and gravity they demand (e.g., Aristotle gets nine pages; Descartes, seven).

The book offers an innovative and exciting perspective on two problems important in the contemporary philosophy of science: that false beliefs are ubiquitous and that propositions have a shady ontological status—somewhere between sentences (syntactical constructions) and abstracted meaning itself. By doing away with propositions, Matson sets off in a fresh, if not entirely new, direction. (There is a trace of the old verificationist positivism in his idea of a "low belief.") His theory of how belief can function in science is stirring, as is his enthusiasm for providing a naturalistic ontology of belief. For these elements alone, *Grand Theories and Everyday Beliefs* is well worth reading.

10.1126/science.1218924

The reviewer is at Simons Laboratory, Department of Biology, Carleton University, Ottawa, ON K1S 5B6, Canada. E-mail: whughes@connect.carleton.ca

Downloaded from www.sciencemag.org on February 16, 2012

Published by AAAS

PUBLIC HEALTH AND BIOSECURITY

H5N1 Debates: Hung Up on the Wrong Questions

Information related to influenza transmissibility should be published in its entirety.

Daniel R. Perez

Over the past few months, there has been an ever-increasing debate, echoed by the media, about the wisdom of publishing the details of two studies that have looked at the respiratory transmission potential of the so-called "bird flu" (H5N1 highly pathogenic avian influenza viruses or H5N1 HPAIV). Some voices have gone as far as asking for stopping or restricting this type of research. In the next paragraphs, I would like to argue against such calls and argue that it is important for this research to be continued under the current conditions. It is also important that the information gathered from these studies finds the necessary channels to benefit public health worldwide. The attention on this issue should be redirected to the larger problem of how to eradicate a bird flu that has the capacity to affect us on a global scale.

The H5N1 bird flu emerged in Southeast Asia in the late 1990s. In 1997, it crossed to humans in Hong Kong, where 18 people were diagnosed with the virus, and the infection resulted in six fatalities (*1*). Live bird markets were associated with the source of the virus. Culling of birds from these markets prevented new human cases. Until this incident, the prevailing dogma was that HPAIVs—bird flu H5N1 being just one of them—were viruses restricted to poultry, with no direct consequences to humans. Far from being eradicated, H5N1 viruses have had an unprecedented geographic spread, not typical of HPAIVs, spreading from Southeast Asia into the Middle East, Europe, and Africa. A combination of factors has contributed to this spread, including live poultry trade and transport, other agricultural activities, the failure of poultry vaccination campaigns, and introduction of these viruses into the wild bird population. From 2003 onward, the reported human cases of H5N1 in several countries have been associated with outbreaks of the disease in domestic poultry. So far, 576 human cases and 339 resulting deaths have been reported. Countries that eradicated the disease from domestic poultry have had no additional reports of human cases (*1*).

CREDIT: SAEED KHAN/FAO

The importance of information. A duck farmer in Thailand installs a net to keep ducks and wild birds apart, a measure against spread of the avian flu virus to other birds. In places where the infrastructure for molecular analyses is not available, it is important to build the infrastructure, not deny people the information.

The H5N1 situation, however, is far from over. These viruses have continued to evolve genetically and antigenically at a pace that resembles the evolution of human influenza viruses. In Indonesia and Egypt, H5N1 is endemic in poultry and, not surprisingly, these two countries continue to report human cases (*2*). The cumulative case-fatality rate of H5N1 is 35% in Egypt and 82% in Indonesia. It is not clear whether the differences in fatality rate between these two countries are related to differences in molecular attributes of the prevalent H5N1 strains in each country, or environmental conditions and/or timing of the diagnosis and/or treatment options and regimes.

The uncontrolled spread of H5N1 viruses in poultry continues to pose a major pandemic threat. If we do not "take the bull by the horns" and make a worldwide concerted effort to help countries eradicate H5N1 viruses from domestic poultry, we will continue to face a potential H5N1 influenza pandemic (see the photo).

An influenza virus is only capable of causing a pandemic if it acquires the ability to maintain sustained human-to-human transmission (*3*). The prevailing thought is that pandemic influenza strains must transmit efficiently by respiratory droplets, particularly by droplet nuclei or aerosols. A distinctive feature of avian influenza viruses in general, and H5N1 viruses in particular, is that they are incapable of being transmitted among humans by aerosol. Because pandemic influenza strains originated in avian influenza viruses, it can be argued that past pandemic influenza viruses were once avian influenza viruses that "learned" how to jump to and transmit by aerosol in humans. Understanding the molecular attributes that make influenza viruses transmissible by aerosol is the key to predicting and/or preventing the emergence of pandemic strains.

Department of Veterinary Medicine, University of Maryland, College Park, MD 20742–3711, USA. E-mail: dperez1@umd.edu

Downloaded from www.sciencemag.org on February 16, 2012

Published by AAAS

Receptor specificity plays a major role in the ability of influenza viruses to perpetuate in the human population. Pandemic influenza strains ultimately evolve in the human population with a preference for receptors with α2,6-linked sialic acid (α2,6SA)—sialic acids bound to the adjacent galactose residue in an α2,6 conformation (*4*). In contrast, most avian influenza viruses recognize α2,3SA receptors (*4*). However, this simplistic observation does not explain the fact that the highly prevalent H9N2 strains in Eurasia and the Middle East have α2,6SA humanlike receptor specificity (*5*) but have yet to cause a pandemic, despite serological evidence showing considerable human exposure to these viruses. Likewise, this narrow approach does not explain why H5N1 viruses with typical α2,3SA avian-like receptor specificity can jump from birds to humans and replicate efficiently in the human host but fail to be transmitted among humans (*6*).

Preventing access to crucial information will hamper our ability to develop better vaccines and antivirals against these viruses.

We are certainly only making our first steps into understanding influenza transmission; we are in the infancy stage when it comes to predicting the transmission potential of influenza strains. In this regard, the independent work by Fouchier's and Kawaoka's groups showing that H5N1 can be transmitted by respiratory droplets in the ferret model is of great importance. Ferrets are considered the best animal model for predicting the transmission of influenza in humans. If there ever was a sense of complacency about H5N1 viruses, these studies are a wake-up call. More important, the molecular changes associated with this phenotype are surprisingly few, and although the combination of these changes has yet to be found in a field isolate, the mutations themselves are not unique or exclusive to the viruses produced in these two laboratories. Make no mistake, it is likely that these viruses can emerge in the field.

Nature has an uncontrolled environment and thousands of susceptible subjects at its disposal versus the handful available to scientists in the laboratory, and therefore, it is just a matter of chance for these or viruses with a similar phenotype to emerge naturally. Just as researchers use new findings to learn how to predict earthquakes and tsunamis, the key elements that have made these viruses transmissible by respiratory droplets in the laboratory must be properly communicated to help public health officials make informed decisions if they are faced with similar field viruses.

The National Science Advisory Board for Biosecurity (NSABB)—an independent expert committee that advises the U.S. Department of Health and Human Services (HHS) and other federal departments and agencies on matters of biosecurity—has recommended that "the general conclusions highlighting the novel outcome be published, but that the manuscripts not include the methodological and other details that could enable replication of the experiments by those who would seek to do harm" (*7*). Although I greatly respect the views of the NSABB, the fact that these two and other research groups have already published similar studies in the past makes it almost impossible to prevent access to details on the methodology (*8*–*14*). Preventing access to crucial pieces of information will hamper our ability to develop better vaccines and antivirals against these viruses.

The relations between receptor binding, transmissibility, and antigenic make up of the virus are intricate. Therefore, it is possible that changes that affect transmissibility can affect antigenicity and, thus, vaccine efficacy. Access to the virus sequence information could be used to increase eradication efforts if a similar field isolate is identified. The question now is not whether H5N1 viruses can be transmitted by aerosol but when it will happen in nature. In this regard, the World Health Organization highlights the importance of this research and "notes that studies conducted under appropriate conditions must continue to take place so that critical scientific knowledge needed to reduce the risks posed by the H5N1 virus continues to increase" (*15*).

The uncontrolled spread of H5N1 viruses in poultry continues to pose a major pandemic threat.

The worst mistake that we could make is to stop this type of research out of fear for the potential misuse of it. We should avoid the temptation to increase the containment levels for handling these viruses under laboratory conditions. Currently, these viruses are handled under Biosafety Level-3 (BSL3-Ag) conditions, which include biological safety cabinets, controlled access to the laboratory, protective equipment for investigators, filtration of supply and exhaust air, sewage decontamination, exit personnel showers, and facility integrity testing (*16*). This is historically the type of containment that many countries around the world use for these viruses. No containment condition is fail-proof, but it must be emphasized that there have been no human H5N1 cases reported from laboratory contamination and no accidental release into the environment from any laboratory. At present, far more people are at risk of infection with H5N1 in countries where the virus remains endemic. In these countries, backyard poultry owners and their families, from where most human cases have been reported, use no protection whatsoever. Smallpox was not defeated out of fear. Smallpox was defeated because Edward Jenner, among others, was fearless in his pursuit of controlling an infectious disease and, in the process, conferred a scientific status to the process of vaccination (*17*). We are much better prepared to confront infectious diseases now than in Jenner's time. We know a great deal more about influenza than was known during the 1918 Spanish influenza.

We were ill prepared to cope with the logistics of mass vaccine production during the 1957 and 1968 pandemics. In 2009, we dealt with an H1N1 pandemic virus that was not growing properly in eggs, the primary substrate for preparation of influenza vaccines, which caused a major delay in vaccine availability. However, through technology and the tireless efforts of dedicated virologists, an optimal vaccine against the H1N1 virus was produced. This initial roadblock triggered many countries to build their own capacity for making vaccines (*18*). The H5N1 grows well in eggs, and the United States has been committed since 1997 to making vaccine seed stocks for viruses with pandemic potential. If the laboratory variants are cross-reactive with the seed stock, then we have a vaccine candidate. If they are not, then the question becomes whether we wait or begin now stockpiling vaccines against these variants.

Yet there are still fundamental questions about influenza viruses that we must dis-

Downloaded from www.sciencemag.org on February 16, 2012

Published by AAAS

cover in order to prevent the next influenza pandemic. We failed at containing the 2009 pandemic influenza simply because, among other factors, we do not have a comprehensive understanding of what makes an influenza strain transmissible in humans. We still do not know whether an H5N1 virus that gained the capacity to transmit by respiratory droplets in ferrets can effectively transmit by the same route in humans. We do know that the potential is there, but it is not through fear that we will stop H5N1 from becoming pandemic. The pursuit of knowledge is what has made humans resilient—a species capable of overcoming our worst fears.

References

1. Y. Watanabe *et al.*, *Trends Microbiol.* **20**, 11 (2012).
2. M. D. Van Kerkhove *et al.*, *PLoS ONE* **6**, e14582 (2011).
3. J. K. Taubenberger, J. C. Kash, *Cell Host Microbe* **7**, 440 (2010).
4. M. Matrosovich, J. Stech, H. D. Klenk, *Rev. Sci. Tech.* **28**, 203 (2009).
5. M. N. Matrosovich *et al.*,*Virology* **281**, 156 (2001).
6. J. Stevens *et al.*, *Science* **312**, 404 (2006).
7. PBS NewsHour, Fearing bioterrorism, government panel asks: What research should be secret? 22 December 2011; www.pbs.org/newshour/bb/health/july-dec11/bird-flu_12-22.html.
8. E. M. Sorrell, H. Wan, Y. Araya, H. Song, D. R. Perez, *Proc. Natl. Acad. Sci. U.S.A.* **106**, 7565 (2009).
9. N. Van Hoeven *et al.*, *Proc. Natl. Acad. Sci. U.S.A.* **106**, 3366 (2009).
10. T. R. Maines *et al.*, *Science* **325**, 484 (2009).
11. T. M. Tumpey *et al.*, *Science* **315**, 655 (2007).
12. T. R. Maines *et al.*, *Proc. Natl. Acad. Sci. U.S.A.* **103**, 12121 (2006).
13. Y. Gao *et al.*, *PLoS Pathog.* **5**, e1000709 (2009).
14. E. J. Schrauwen *et al.*, *Emerg. Infect. Dis.* **17**, 200 (2011).
15. WHO Media Centre, WHO concerned that new H5N1 influenza research could undermine the 2011 Pandemic Influenza Preparedness Framework [statement], 30 December 2011; www.who.int/mediacentre/news/statements/2011/pip_framework_20111229/en/index.html.
16. Agricultural Research Service, *USDA Security Policies and Procedures for Biosafety Level-3 Facilities* (USDA, Washington, DC, 2002); www.ocio.usda.gov/directives/doc/DM9610-001.htm.
17. D. Baxby, *FEMS Immunol. Med. Microbiol.* **16**, 1 (1996).
18. A. Abelin *et al.*, *Vaccine* **29**, 1135 (2011).

Published online 19 January 2012; 10.1126/science.1219066

PUBLIC HEALTH AND BIOSECURITY

Life Sciences at a Crossroads: Respiratory Transmissible H5N1

Release of details of recent research on affecting influenza transmissibility poses far more risk than any good that might occur.

Michael T. Osterholm* and Donald A. Henderson

Two recently submitted manuscripts to *Science* and *Nature* report success in creating mutant isolates of influenza A/H5N1 that are able to be transmitted by respiratory droplet or aerosol between mammals (ferrets). The studies imply that human-to-human transmission could be possible as well. Shortly after the submission of the papers to the journals, the National Science Advisory Board for Biosecurity (NSABB) was asked by the U.S. government to address this question. The NSABB recommended that the papers not be fully published; rather, the basic results of the studies should be communicated without methods or detailed results but in sufficient detail to maximize the benefits to society of the studies' findings. In turn, these recommendations were accepted by the U.S. government and shared with the authors and the editors of *Science* and *Nature*.

Some have asserted that these recommendations represent unwarranted censorship of scientific research and that the sharing of the results, particularly the specific viral mutations, is necessary to protect global public health. They argue that sharing the virus mutation information with global influenza surveillance organizations would result in the rapid identification of a potential H5N1 pandemic virus in birds or humans. This early information might permit health authorities to quash an emerging human influenza pandemic. In addition, they believe that knowledge of the mutations could enhance H5N1 vaccine research and manufacturing.

While considering the possible merits of a wider dissemination of more complete information regarding mutational changes of the newly created H5N1 strains, one fact must be kept in mind. The current circulating strains of influenza A/H5N1, with their human case-fatality rate of 30 to 80%, place this pathogen in the category of causing one of the most virulent known human infectious diseases.

Disseminating the entirety of the methods and results of the two H5N1 studies in the general scientific literature will not materially increase our ability to protect the public's health from a future H5N1 pandemic.

Moreover, detecting an emerging pandemic virus in animals before the occurrence of a human pandemic is unrealistic; rather, the pandemic virus documentation will be "an after-the-fact record of what just happened." For example, in the six countries of the world where highly pathogenic avian influenza H5N1 is endemic (Bangladesh, Cambodia, China, Egypt, Indonesia, and Viet Nam), the quality of public and private veterinary and animal production services is variable and low in some places (*1*). These countries are not often able to detect and respond to influenza A/H5N1 infections in birds. When H5N1 isolates are obtained, little to no gene sequencing is conducted, meaning that a mutation map of possible prepandemic viruses will not be generally available. Even if such laboratory support were readily available and samples from ill birds were processed in a timely manner, these countries lack the commitment to deal vigorously with H5N1. This conclusion was recently highlighted by the United Nations Food and Agriculture Organization (*1*, *2*).

The World Health Organization (WHO) is also well aware of the magnitude of the challenge of identifying an emerging human influenza pandemic and stopping it before it spreads globally. Experiences with pan-

[1]Center for Infectious Disease Research and Division of Environmental Health Sciences, Medical School, University of Minnesota, Minneapolis, MN 55455, USA. [2]Center for Biosecurity of UPMC, University of Pittsburgh, Pittsburgh, PA 15213, USA.

*Author for correspondence. E-mail: mto@umn.edu.

Downloaded from www.sciencemag.org on February 16, 2012

Published by AAAS

demic H1N1 [influenza A(H1N1)pmd09] show the problems of a strategy based on the assumption that an emerging influenza pandemic could be identified quickly in a localized geographic area with no, or very limited, travel in or out of the pandemic zone (*3*). As a result of extensive global travel, influenza A(H1N1)pmd09 infection was already occurring in a number of countries before the first isolate was identified (*4*). That experience dashed WHO's expectations of using antiviral drugs to stop initial outbreaks of an emerging pandemic influenza virus (*3*).

With regard to H5N1 vaccine research, licensed influenza vaccines for human use, whether inactivated or live attenuated, are based on the use of the hemagglutinin and neuraminidase antigens, not on the other novel antigens that are potentially altered by mutational changes. Although H5N1 candidate vaccines using the isolates from these studies should be developed and tested, this does not require sharing all of the mutational data outside of a small select group of established researchers already working within the WHO network. Rather, the real challenge that we face in preparing for the next influenza pandemic is developing, licensing, and manufacturing 21st-century game-changing influenza vaccines that are effective against multiple strains and readily available on a global basis in time for the earliest days of the pandemic. One of us (M.T.O.) recently summarized the serious challenges we face with the relative effectiveness and availability of our current hemagglutinin antigen vaccines (*5*). First, the effectiveness of vaccines both with and without adjuvant against influenza A(H1N1)pmd09–related illness was limited despite the very close match between the circulating virus and the vaccine strain. In the United States, the effectiveness of the vaccine without adjuvant in children and adults 10 to 49 years was 59%, and for mostly vaccines with adjuvant in Europe and Canada in those primarily under 65 years of age, the median effectiveness was 72%. In addition, influenza vaccines produced for each of the last three pandemics (1957, 1969, and 2009) prevented very little disease, because supplies of vaccine were not available until after most of the cases had occurred because of lengthy manufacturing requirements (*6*–*9*).

In summary, disseminating the entirety of the methods and results of the two H5N1 studies in the general scientific literature will not materially increase our ability to protect the public's health from a future H5N1 pandemic. Even targeting dissemination of the information to scientists who request it will likely not enhance the public's health. Rather, making every effort to ensure that this information does not easily fall into the hands of those who might use it for nefarious purposes or that a biosafety accident resulting in an unintended release does not occur should be our first and highest priority. We can't unring a bell; should a highly transmissible and virulent H5N1 influenza virus that is of human making cause a catastrophic pandemic, whether as the result of intentional or unintentional release, the world will hold those who work in the life sciences accountable for what they did or did not do to minimize that risk.

References and Notes

1. Food and Agricultural Organization of the United Nations (FAO), Stamping out H5N1 avian influenza could take decades (FAO, Rome, 2011); www.fao.org/news/story/en/item/66118.
2. FAO, Approaches to controlling, preventing and eliminating H5N1 highly pathogenic avian influenza in endemic countries (Animal Production and Health Paper 171, FAO, Rome, 2011); www.fao.org/docrep/014/i2150e/i2150e.pdf.
3. WHO, WHO interim protocol: Rapid operations to contain the initial emergence of pandemic influenza (WHO, Geneva, 2007); www.who.int/influenza/resources/documents/RapidContProtOct15.pdf.
4. K. Khan *et al*., *N. Engl. J. Med.* **361**, 212 (2009).
5. M. T. Osterholm, N. S. Kelley, A. Sommer, E. A. Belongia, *Lancet Infect. Dis.* **12**, 36 (2012).
6. R. Murray, *Am. Rev. Respir. Dis.* **83**, 160 (1961).
7. R. Murray, *Bull. World Health Organ.* **41**, 495 (1969).
8. Centers for Disease Control and Prevention (CDC), H1N1 influenza vaccine doses allocated, ordered, and shipped by project area (CDC, Atlanta, GA, 2009); www.cdc.gov/h1n1flu/vaccination/vaccinesupply.htm.
9. CDC, Percentage of visits for influenza-like-illness reported by sentinel providers 2009–2010 (CDC, Atlanta, GA, 2010); www.cdc.gov/flu/weekly/weeklyarchives2009-2010/data/senAllregt52.htm.
10. M.T.O. is a member of the National Science Advisory Board for Biosecurity. His views do not represent the official policy or scientific conclusions of the NSABB. None of the information contained in this commentary resulted from his participation as a member of the NSABB.

Published online 19 January 2012; 10.1126/science.1218612

PUBLIC HEALTH AND BIOSECURITY

The Obligation to Prevent the Next Dual-Use Controversy

Ruth R. Faden[1]*† and Ruth A. Karron[2]

The recent debates over H5N1 experiments highlight current shortcomings in oversight of potential dual-use research.

For the first time, the U.S. National Science Advisory Board for Biosecurity (NSABB) has recommended that research done by two separate groups be redacted, an unprecedented caution that has unleashed debate over the proper balance of global security, public health, and the integrity of science. Currently, the avian influenza virus H5N1 is not easily transmitted from human to human, but a high mortality rate in those who have been infected with H5N1 viruses has raised fears of possible naturally occurring mutations that would increase transmissibility (*1*). This concern prompted research conducted by Fouchier and colleagues and Kawaoka and colleagues, with funding from the U.S. National Institutes of Health (NIH), to understand the molecular characteristics underlying transmissibility. However, the NSABB found sufficient cause for concern over potential use of this research by terrorists looking to unleash, rather than prevent, a lethal influenza pandemic to warrant restrictions on access to critical technical details. Although *Science* and *Nature* agreed to redact the research for publication to help prevent the misuse of this science by hostile actors, they made that agreement contingent on establishment of a mechanism to allow appropriate researchers and public health officials access to the complete information.

Although the dilemma over publication of these research projects has generated substantial concern in the bioscience community, this challenge was neither unanticipated nor previously unexamined. In part because of the anthrax attacks in 2001, the National Academy of Sciences convened a committee to analyze how best to minimize

[1]Philip Franklin Wagley Professor of Biomedical Ethics Director, Johns Hopkins Berman Institute of Bioethics, Johns Hopkins University, Baltimore, MD 21205, USA. [2]Professor, International Health, Director, Center for Immunization Research, Johns Hopkins Vaccine Initiative, Johns Hopkins Bloomberg School of Public Health, Baltimore, MD 21205, USA.

*The author was a member of the committee that generated the Fink report (*2*). †Author for correspondence. E-mail: rfaden@jhu.edu

Downloaded from www.sciencemag.org on February 16, 2012

Published by AAAS

demic H1N1 [influenza A(H1N1)pmd09] show the problems of a strategy based on the assumption that an emerging influenza pandemic could be identified quickly in a localized geographic area with no, or very limited, travel in or out of the pandemic zone (*3*). As a result of extensive global travel, influenza A(H1N1)pmd09 infection was already occurring in a number of countries before the first isolate was identified (*4*). That experience dashed WHO's expectations of using antiviral drugs to stop initial outbreaks of an emerging pandemic influenza virus (*3*).

With regard to H5N1 vaccine research, licensed influenza vaccines for human use, whether inactivated or live attenuated, are based on the use of the hemagglutinin and neuraminidase antigens, not on the other novel antigens that are potentially altered by mutational changes. Although H5N1 candidate vaccines using the isolates from these studies should be developed and tested, this does not require sharing all of the mutational data outside of a small select group of established researchers already working within the WHO network. Rather, the real challenge that we face in preparing for the next influenza pandemic is developing, licensing, and manufacturing 21st-century game-changing influenza vaccines that are effective against multiple strains and readily available on a global basis in time for the earliest days of the pandemic. One of us (M.T.O.) recently summarized the serious challenges we face with the relative effectiveness and availability of our current hemagglutinin antigen vaccines (*5*). First, the effectiveness of vaccines both with and without adjuvant against influenza A(H1N1)pmd09–related illness was limited despite the very close match between the circulating virus and the vaccine strain. In the United States, the effectiveness of the vaccine without adjuvant in children and adults 10 to 49 years was 59%, and for mostly vaccines with adjuvant in Europe and Canada in those primarily under 65 years of age, the median effectiveness was 72%. In addition, influenza vaccines produced for each of the last three pandemics (1957, 1969, and 2009) prevented very little disease, because supplies of vaccine were not available until after most of the cases had occurred because of lengthy manufacturing requirements (*6*–*9*).

In summary, disseminating the entirety of the methods and results of the two H5N1 studies in the general scientific literature will not materially increase our ability to protect the public's health from a future H5N1 pandemic. Even targeting dissemination of the information to scientists who request it will likely not enhance the public's health. Rather, making every effort to ensure that this information does not easily fall into the hands of those who might use it for nefarious purposes or that a biosafety accident resulting in an unintended release does not occur should be our first and highest priority. We can't unring a bell; should a highly transmissible and virulent H5N1 influenza virus that is of human making cause a catastrophic pandemic, whether as the result of intentional or unintentional release, the world will hold those who work in the life sciences accountable for what they did or did not do to minimize that risk.

References and Notes

1. Food and Agricultural Organization of the United Nations (FAO), Stamping out H5N1 avian influenza could take decades (FAO, Rome, 2011); www.fao.org/news/story/en/item/66118.
2. FAO, Approaches to controlling, preventing and eliminating H5N1 highly pathogenic avian influenza in endemic countries (Animal Production and Health Paper 171, FAO, Rome, 2011); www.fao.org/docrep/014/i2150e/i2150e.pdf.
3. WHO, WHO interim protocol: Rapid operations to contain the initial emergence of pandemic influenza (WHO, Geneva, 2007); www.who.int/influenza/resources/documents/RapidContProtOct15.pdf.
4. K. Khan *et al*., *N. Engl. J. Med.* **361**, 212 (2009).
5. M. T. Osterholm, N. S. Kelley, A. Sommer, E. A. Belongia, *Lancet Infect. Dis.* **12**, 36 (2012).
6. R. Murray, *Am. Rev. Respir. Dis.* **83**, 160 (1961).
7. R. Murray, *Bull. World Health Organ.* **41**, 495 (1969).
8. Centers for Disease Control and Prevention (CDC), H1N1 influenza vaccine doses allocated, ordered, and shipped by project area (CDC, Atlanta, GA, 2009); www.cdc.gov/h1n1flu/vaccination/vaccinesupply.htm.
9. CDC, Percentage of visits for influenza-like-illness reported by sentinel providers 2009–2010 (CDC, Atlanta, GA, 2010); www.cdc.gov/flu/weekly/weeklyarchives2009-2010/data/senAllregt52.htm.
10. M.T.O. is a member of the National Science Advisory Board for Biosecurity. His views do not represent the official policy or scientific conclusions of the NSABB. None of the information contained in this commentary resulted from his participation as a member of the NSABB.

Published online 19 January 2012; 10.1126/science.1218612

PUBLIC HEALTH AND BIOSECURITY

The Obligation to Prevent the Next Dual-Use Controversy

Ruth R. Faden[1]*† and Ruth A. Karron[2]

The recent debates over H5N1 experiments highlight current shortcomings in oversight of potential dual-use research.

For the first time, the U.S. National Science Advisory Board for Biosecurity (NSABB) has recommended that research done by two separate groups be redacted, an unprecedented caution that has unleashed debate over the proper balance of global security, public health, and the integrity of science. Currently, the avian influenza virus H5N1 is not easily transmitted from human to human, but a high mortality rate in those who have been infected with H5N1 viruses has raised fears of possible naturally occurring mutations that would increase transmissibility (*1*). This concern prompted research conducted by Fouchier and colleagues and Kawaoka and colleagues, with funding from the U.S. National Institutes of Health (NIH), to understand the molecular characteristics underlying transmissibility. However, the NSABB found sufficient cause for concern over potential use of this research by terrorists looking to unleash, rather than prevent, a lethal influenza pandemic to warrant restrictions on access to critical technical details. Although *Science* and *Nature* agreed to redact the research for publication to help prevent the misuse of this science by hostile actors, they made that agreement contingent on establishment of a mechanism to allow appropriate researchers and public health officials access to the complete information.

Although the dilemma over publication of these research projects has generated substantial concern in the bioscience community, this challenge was neither unanticipated nor previously unexamined. In part because of the anthrax attacks in 2001, the National Academy of Sciences convened a committee to analyze how best to minimize

[1]Philip Franklin Wagley Professor of Biomedical Ethics Director, Johns Hopkins Berman Institute of Bioethics, Johns Hopkins University, Baltimore, MD 21205, USA. [2]Professor, International Health, Director, Center for Immunization Research, Johns Hopkins Vaccine Initiative, Johns Hopkins Bloomberg School of Public Health, Baltimore, MD 21205, USA.

*The author was a member of the committee that generated the Fink report (*2*). †Author for correspondence. E-mail: rfaden@jhu.edu

Downloaded from www.sciencemag.org on February 16, 2012

Published by AAAS

the biosecurity threats posed by dual-use research of concern without undermining biomedical science. In 2004, the committee published its analysis—now popularly called the Fink report after its chair Gerald Fink—that included recommendations amounting to a new system of oversight and biosecurity risk management for the life sciences and calling for the establishment of the NSABB (*2*).

In the 8 years since [publication of the Fink] report, no coordinated system for oversight of dual-use research, either national or international, has been implemented.

The specific and immediate question posed by the H5N1 studies is how to ensure appropriate access to the details of a study when a determination has been made by NSABB that these details should not appear in the public scientific literature so as to protect against misuse. This question should not have caught the NSABB or the NIH by surprise. Although the NSABB determined that all previous studies it had been asked to review could go forward to full publication, there was always a possibility that in the next case they would find otherwise. According to the chair of the NSABB, that committee was not given the job of developing a system for distributing sensitive information (*3*). But if that is the case, then this remit should have been given to some other identified entity when the NSABB was established.

However, the current debate about these H5N1 studies is as much about whether they should have been conducted at all, as about who, after the fact, should have access to the details of the research (*4*, *5*). There are increasing calls for some kind of prospective screening to identify higher-risk research proposals and subject them to special review and oversight (*6*–*8*). The Fink report put forward one blueprint for how this might be done that included guidelines to help identify research that has the potential for diversion to offensive aggressive uses, tasking Institutional Biosafety Committees to employ these guidelines in the first stage of review of experiments, and expanding the remit and membership of NIH's Recombinant DNA Advisory Committee (RAC) to make it an appropriate body for the next stage of review. That blueprint is far from perfect. For example, whereas the Fink report rightly acknowledges that any effective system of biosecurity oversight of the life sciences must have a global structure, its recommendations for international coordination are at best underdeveloped. Nevertheless, the central point is this: In the 8 years since that report, no coordinated system for oversight of dual-use research, either national or international, has been implemented. Although the current controversy may finally spur the adoption of some kind of prospective screening process, we now run the risk that heightened public attention will result in an overcorrection that is more restrictive of the conduct or communication of biological science than appropriate concern for biosecurity requires.

In the case of the H5N1 studies, scientists and security experts have the same aim: to reduce the risk of a global, highly lethal pandemic, whether naturally occurring or the intentional consequence of bioterrorism or biowarfare. Framed this way, the dilemma becomes a familiar problem of benefit-risk assessment and risk management, in which properly constructed prospective review can play an important role. Although nations differ in their tolerance for the risks of new biotechnologies (*9*–*11*), no society does or should operate with a true "zero-risk" approach to science, just as no society can responsibly ignore the biosecurity risks posed by some work in the life sciences. The challenge is to implement effective practices to properly assess and manage these risks that allow for the vigilant stewardship of both the institution of science and public safety.

Two ethical dimensions of this challenge deserve particular mention. First, when dual-use research of concern is allowed to go forward, those responsible for managing any subsequent threats to biosecurity have a moral obligation to ensure that the results of that research are used to help reduce risks to global health. This obligation is grounded in two mutually reinforcing arguments. First, the prospect of such a benefit is at the heart of the ethical justification for conducting the research in the first place. Unless the biosecurity risk turns out to be more grave and more difficult to manage than was reasonably foreseeable, it is ethically unjustifiable to run the risks but not realize the benefits that justified their assumption. Second, particularly when there is any prospect that the research might be of near-term public health benefit, to withhold such scientific findings violates both general moral duties of beneficence to prevent harm to others and the specific forms of this duty that fall on the scientific community to use new knowledge to help prevent human suffering.

The details of the recent H5N1 studies may be of particular utility to countries where H5N1 in birds is prevalent and the risks to humans are of most immediate concern. The structure that will control access, must, as a moral matter,

Bird flu patient. Bui Thi Thao is lying in a hospital. His sister, who was the first confirmed bird flu patient in Vietnam, died the week before.

CREDIT: STRINGER/REUTERS

Downloaded from www.sciencemag.org on February 16, 2012

Published by AAAS

ensure that the global and national public health officials and scientists responsible for influenza control in these countries are included in the community of people authorized to know the research details. To do otherwise risks the ethically unacceptable prospect, if one assumes that this research turns out to have sufficient practical utility, that people will die from cases of avian flu that might otherwise have been averted (see the photo). Although current surveillance systems may not be sophisticated enough to make optimal use of these findings (*12*), that is an argument for investing in enhanced surveillance and molecular diagnostics, rather than withholding potentially valuable information. Withholding data from countries where highly pathogenic H5N1 has been detected also threatens the World Health Organization's (WHO) Pandemic Influenza Preparedness (PIP) Framework (*13*), a fragile global agreement on influenza information sharing that is vital to pandemic prevention. Established in May 2011 and adopted by all WHO member states, PIP states that laboratories conducting research on viruses obtained through WHO have an obligation to collaborate with scientists in countries where the virus originated, a response to Indonesia's position that supplies of its domestic virus strains would cease unless it was given access to the vaccines created from them (*14*).

The structure that will control access, must, as a moral matter, ensure that the global and national public health officials and scientists responsible for influenza control in these countries are included in the community of people authorized to know the research details. To do otherwise risks the ethically unacceptable prospect, if one assumes that this research turns out to have sufficient practical utility, that people will die from cases of avian flu that might otherwise have been averted.

Another ethical dimension centers on the responsibilities of individual scientists. The Fink report makes the point that all scientists have an affirmative ethical obligation to avoid contributing to the advancement of biowarfare and bioterrorism. This obligation and its implications for the conduct of scientists deserve greater attention in the life sciences literature. Fouchier and his colleagues have described their efforts to obtain consensus on the necessity of these experiments within the community of influenza virologists, to develop adequate containment facilities, and to obtain the necessary reviews and approvals from Dutch and U.S. government officials (*15*). These efforts are laudable and likely represent all of the options that were reasonably available to the investigators. However, the processes used did not have the features of the kind of review and oversight envisioned by the Fink report, including interdisciplinary and global participation.

In addition, Fouchier, Kawaoka, and more than 30 other influenza scientists recently announced a voluntary 60-day moratorium on research involving the generation of highly pathogenic H5N1 viruses that are more transmissible in mammals and on the viruses generated in the current research to give "organizations and governments around the world … time to find the best solutions for opportunities and challenges that stem from the work" (*16*). The moratorium, first suggested by the NSABB, is not the first such effort by life scientists at self-regulation. From July 1974 to February 1975, scientists refrained from conducting some types of recombinant DNA research to allow for the establishment of an appropriate oversight system in the interests of public safety (*17*). The current influenza research moratorium is not unproblematic. Sixty days may not be nearly enough time to establish a similar system for influenza research of concern, and the language used to announce the moratorium is troubling for its failure to confront the possibility that this research may pose real biosecurity concerns. Nevertheless, it illustrates one path for scientists wanting to take seriously their ethical obligation to avoid contributing to biosecurity threats while endeavoring to conduct research to protect public health.

Ethics does not demand the impossible, however; scientists cannot ensure or guarantee that their work will never be applied intentionally or accidentally to harm society. They can only take reasonable steps to minimize the chances that such harm will occur. Moreover, there are real limitations to what individual scientists or even groups of scientists can do on their own, as this recent H5N1 case illustrates vividly. Managing the biosecurity and biosafety risks posed by some life science research without unduly hampering the good that such research can produce is a classic, and daunting, collective action problem that cannot be solved without global cooperation and coordination. Just as the potential benefits of this type of research cannot be realized without providing information to international groups of scientists and public health officials with expertise in multiple disciplines (*15*), so, too, an adequate assessment of potential societal risks requires prospective review by an international body with a range of expertise, including in this case influenza virology and biosecurity. There is no doubt that there are formidable obstacles to developing such a global oversight body. But that the challenge is hard is no excuse. What we could not accomplish between 2004 and today can no longer be delayed.

References and Notes

1. WHO, Global Influenza Programme (WHO, Geneva, 2012); www.who.int/influenza/en/.
2. National Research Council, *Biotechnology Research in an Age of Terrorism* (National Academies Press, Washington, DC, 2004).
3. H. Ledford, *Nature* **481**, 9 (2012).
4. T. Inglesby, A. Cicero, D. A. Henderson, *Milwaukee-Wisconsin Journal Sentinel*; www.jsonline.com/news/opinion/benefits-of-h5n1-research-do-not-outweigh-the-risks-r93omik-137330523.html.
5. Editorial Board, An engineered doomsday, *New York Times*, 8 January 2012, p. SR10.
6. S. Connor, *Independent*, 14 December 2011; www.independent.co.uk/news/science/too-late-to-contain-killer-flu-science-say-experts-6280399.html.
7. J. D. Kraemer, L. O. Gostin, *Science* (2012); 10.1126/science.1219215
8. M. Enserink, D. Malakoff, *Science* **335**, 20(2012).
9. D. Vogel, in *Yearbook of European Environmental Law*, H. Somsen, T. Etty, J. Scott, and L. Krämer, Eds. (Oxford Univ. Press, Oxford, 2004), vol. 3, pp. 43–56; http://faculty.haas.berkeley.edu/vogel/uk%20oct.pdf.
10. S. Jasanoff, *Designs On Nature: Science and Democracy in Europe and the United States* (Princeton Univ. Press, Princeton, NJ, 2005).
11. A. E. Wohlers, *Politics Life Sci.* **29**, 17 (2010).
12. D. Butler, *Nature* **481**, 417 (2012).
13. WHO, WHO concerned that new H5N1 influenza research could undermine the 2011 Pandemic Influenza Preparedness Framework, 30 December 2011; www.who.int/mediacentre/news/statements/2011/pip_framework_20111229/en/.
14. E. Schneider, Pandemic flu preparedness: How far have we come in the last five years? An interview with Peter Clevestig and Rachel Irwin, The National Bureau of Asian Research, 14 December 2011; www.nbr.org/research/activity.aspx?id=191.
15. R. A. M. Fouchier, S. Herfst, A. D. M. E. Osterhaus, *Science* **335**, 662 (2012). 10.1126/science.1218376
16. R. A. M. Fouchier *et al.*, *Science* **335**, 400 (2012).
17. P. Berg *et al.*, *Science* **185**, 303 (1974).

Published online 9 February 2012; 10.1126/science.1219668

Downloaded from www.sciencemag.org on February 16, 2012

Published by AAAS

BIOCHEMISTRY

A Cold Editor Makes the Adaptation

Adaptation to cold temperature is mediated by RNA editing of a potassium channel in octopus neurons.

Marie Öhman

Although organisms have evolved to live in diverse conditions, closely related species often inhabit vastly different environments. This is particularly true for aquatic animals such as squid and octopus, which are common in tropical waters but are also found at the poles. These cephalopods have highly developed nervous systems, and one challenging question is how temperature-sensitive neuronal synaptic transmission has adapted to function at a near-freezing temperature. On page 848 of this issue, Garrett and Rosenthal (*1*) show that RNA editing rather than changes in the genome sequence enable potassium (K^+) channels in octopus to function at different temperatures.

Garrett and Rosenthal studied gating (opening and closing) of voltage-dependent K^+ channels, which are particularly temperature sensitive (*2*) but operate in such diverse environments as tropical temperatures and extreme cold. The activation kinetics of the K^+ channel therefore needs to be adapted for functionality in organisms with a body temperature close to 0°C. One way of achieving this is through structural changes in the channel proteins. However, when Garrett and Rosenthal compared the genome sequence of orthologous K^+ channels, they found a surprisingly high conservation between tropical and Antarctic octopus species. Thus, they concluded that cold adaptation must occur in a different way or that the channel proteins are modified posttranscriptionally.

A common post- or cotranscriptional RNA modification event in neurons is adenosine-to-inosine (A-to-I) editing (*3*) by the enzymes adenosine deaminases that act on RNA (ADARs). Because inosine is read as guanosine during translation, this editing event can change the protein code. In organisms from fruit flies to humans, A-to-I editing activity is important for normal brain development and behavior. In mammals there are two active enzymes, ADAR1 and ADAR2, which both edit mRNAs involved in neurotransmission, including those encoding the K^+ channel $K_v1.1$. There are two ADAR2 isoforms in squid (*4*), and mRNA coding for the delayed rectifier K^+ channel $K_v1.1A$ is extensively edited, affecting the action potential of the giant axon (*5*).

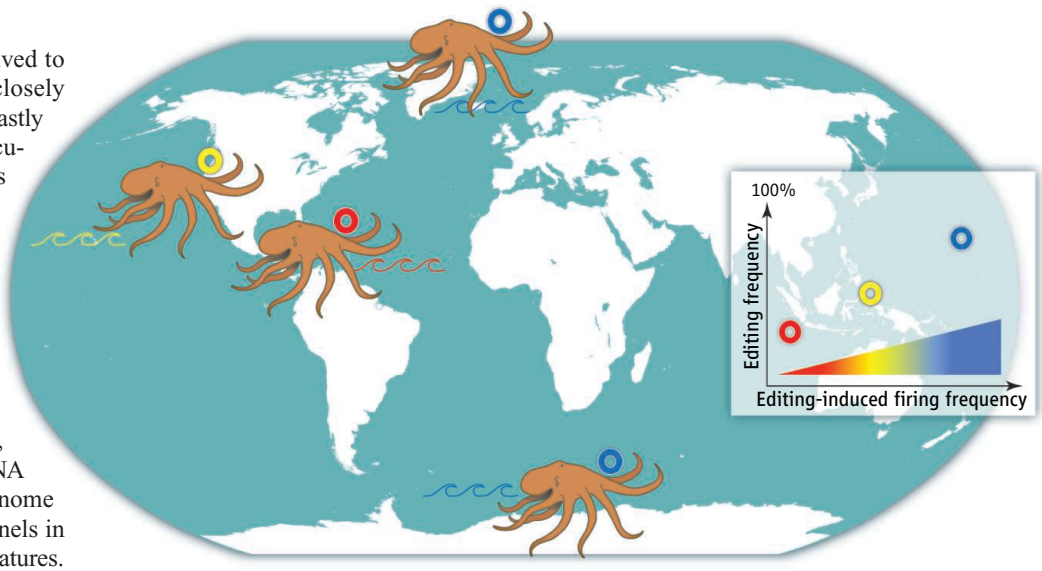

Editing on location. Temperature adaptation in octopus neurons via RNA editing. In extreme cold, the K^+ channels open and close much more slowly than in warm water. To function, Antarctic and Arctic octopus adapt their channels (blue rings) to the cold environment by increasing the action potential firing rate via high levels of RNA editing. Potassium channels in octopus from temperate (yellow) and tropical (red) species have lower levels of editing, in proportion to their temperature.

To investigate whether A-to-I editing enables cold adaptation of ion channels in cephalopods, Garrett and Rosenthal studied editing in the delayed rectifier K^+ channel in octopus from different habitats. These channels regulate many functions in neurons, such as resting potential and firing frequency (*6*). The authors identified several sites of editing within the mRNA that gave rise to amino acid changes in the K^+ channel. Four of these sites showed notable differences in the level of editing between different species. Editing at one of the sites (I321V) changes an isoleucine to a valine in the fifth transmembrane domain of the channel pore, and was observed in more than 90% of the transcripts analyzed from the Antarctic octopus, compared to only 30% in the tropical octopus. When this change was introduced as a single mutation in the genomic background of an unedited channel, the rate of channel closure more than doubled. Garrett and Rosenthal suggest this site as a candidate for cold adaptation because it accelerates the deactivation kinetics by destabilizing the open state and causes the channel to close faster. This is predicted to increase the action potential firing frequency, which is desired in the extreme cold. Indeed, when Garrett and Rosenthal analyzed mRNA editing in two Arctic octopus species, they also found extensive editing at the I321V site. Analysis of other species from tropical and temperate zones revealed that editing levels at the same site correlated well with water temperature (see the figure). Even though several other editing sites occur in the K_v1 channels, a dramatic difference in editing level was found only at the I321V site, which is the only site located in the channel pore.

Why has evolution selected RNA editing rather than changes in the genome sequence itself to achieve adaptation to cold conditions? Because RNA editing is a dynamic process, not hard-wired in the genome like genomic mutations, editing can be "tested" on sensitive processes like neurotransmission in a subset of cells without having potential deleterious effects on the entire organism.

How can the efficiency of editing only at certain sites be sensitive to temperature differences? One reasonable explanation involves the stability of the RNA structure. The ADAR enzyme acts only on a double-stranded RNA structure. The thermodynamic stability of a duplex RNA depends on both sequence and temperature (*7*). Thus, an RNA mole-

Department of Molecular Biology and Functional Genomics, Stockholm University, 106 91 Stockholm, Sweden. E-mail: marieohman@molbio.su.se

CREDIT: ADAPTED BY P. HUEY/SCIENCE

Downloaded from www.sciencemag.org on February 16, 2012

Published by AAAS

cule may be more likely to retain a double-stranded conformation favorable to editing at lower temperatures than at higher temperatures. In this way, editing frequency at certain sites can be more sensitive to external influences such as temperature, favoring the production of certain protein isoforms.

Further studies are needed to investigate whether individual octopuses can immediately respond to temperature fluctuations by varying the extent of editing, and if other conditions such as stress and access to nutrients have the same effect. Indeed, editing-related alternative protein production in response to stress has already been suggested (*8*). Recent developments in high-throughput sequencing have given us the tools to discover novel RNA editing events responding to external conditions. Cold adaptation by RNA editing might only be the tip of the iceberg.

References

1. S. Garrett, J. J. C. Rosenthal, *Science* **335**, 848 (2012); 10.1126/science.1212795.
2. B. M. Rodríguez *et al*., *J. Gen. Physiol.* **112**, 223 (1998).
3. J. E. Jepson, R. A. Reenan, *Biochim. Biophys. Acta* **1779**, 459 (2008).
4. J. P. Palavicini *et al*., *RNA* **15**, 1208 (2009).
5. J. J. Rosenthal, F. Bezanilla, *Neuron* **34**, 743 (2002).
6. O. Pongs, *FEBS Lett.* **452**, 31 (1999).
7. Z. J. Lu *et al*., *Nucleic Acids Res.* **34**, 4912 (2006).
8. K. V. Prasanth *et al*., *Cell* **123**, 249 (2005).

10.1126/science.1219300

GENETICS

Gene Losses in the Human Genome

A comprehensive survey of the human genome reveals variations that disrupt protein-coding genes.

Lluis Quintana-Murci

Characterizing variation in the human genome at the individual and population levels has provided fundamental information on population history, structure, and admixture (interbreeding), as well as on how natural selection has targeted specific genomic regions and biological functions. It also helps to clarify the contribution of genetic diversity to variation in human phenotypic traits, both benign and disease-related. Next-generation DNA sequencing is providing insights into the types of genetic variation that characterize the human genome, such as single-nucleotide polymorphisms, copy-number variants, and mobile elements, and also on the burden of deleterious variants that may be present in our genomes (*1*–*3*). On page 823 of this issue, MacArthur *et al*. (*4*) use this information to systematically investigate the true number, effects, and evolutionary properties of loss-of-function (LoF) variants located in human protein-coding genes. They estimate that an individual carries ~100 LoF variants, with ~20 genes having been completely lost.

Gene loss was proposed to be a major driver of phenotypic change and that, under certain circumstances, LoF variants can be advantageous, thereby increasing in population frequency by positive selection (the "less is more" hypothesis) (*5*). Intuitively, however, LoF variants can be obvious causes of disease, and many of them have been associated with severe, Mendelian disorders (caused by a single mutation). In this case, gene loss is deleterious, and the corresponding LoF variants will be counter-selected (a "less is less" hypothesis). Furthermore, increasing evidence suggests that LoF variants are tolerated in healthy individuals, having no impact on individual survival and therefore drifting neutrally in the population (a "less is nothing" situation). The assessment of how LoF variants are distributed across the genome, their population frequency, evolutionary properties, and phenotypic consequences is essential for understanding the impact of gene loss on human phenotypes and disease risk. In this context, MacArthur *et al*. have analyzed the three pilot data sets from the 1000 Genomes Project (*1*), together with the genome of a European individual, and identified a total of 2951 candidate LoF variants. After stringent informatic filtering and experimental genotyping of many of these variants, only 1285 were subsequently analyzed, as the remaining variants were either artifacts of sequencing, mapping, or annotation, or unlikely to cause a genuine LoF. In doing so, they provide the first comprehensive, genome-wide catalog of variants likely to disrupt protein-coding genes.

Humans carry variants that can potentially lead to gene loss (*1*, *6*, *7*). MacArthur *et al*. estimated that, depending on ethnic background, each individual's genome carries 26 to 37 variants that introduce a stop codon (which signals the termination of translation of nucleic acids into protein), with up to 6 present in the homozygous state. When considering other types of LoF variants, including those that disrupt splice-sites, large deletions, or insertions or deletions of nucleotides that change the DNA reading frame, the total number per individual is extended to 103 to 121, with ~20 present in homozygosity. A large proportion of LoF variants were enriched in low-frequency alleles, suggesting that the removal of deleterious alleles has prevented

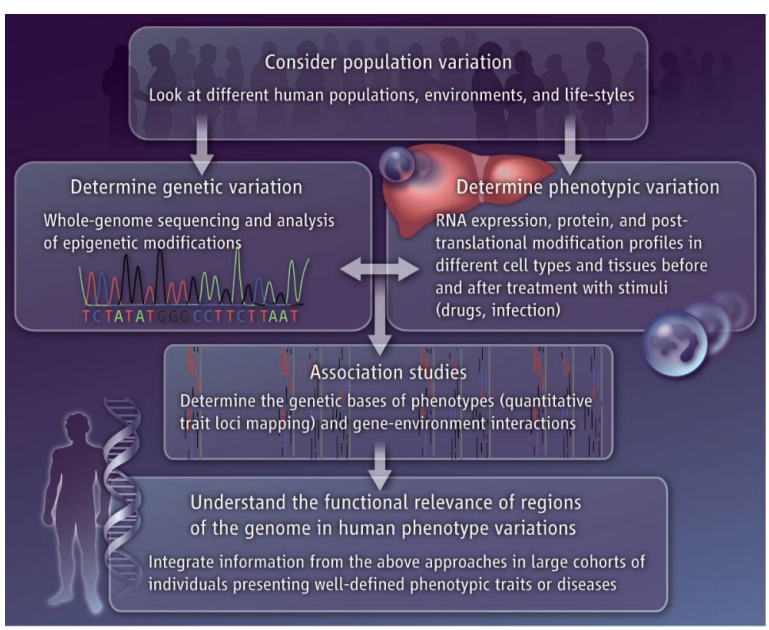

The extent of human genetic variation. A workflow is shown for integrating different information to define the impact of genetic variants on phenotype.

CREDIT: B. STRAUCH/*SCIENCE*

Institut Pasteur, Unit of Human Evolutionary Genetics, CNRS URA3012, Paris, France. E-mail: quintana@pasteur.fr

Downloaded from www.sciencemag.org on February 16, 2012

Published by AAAS

them from increasing to high frequencies. Furthermore, some have already been associated with severe human diseases, supporting the less-is-less hypothesis. Other LoF variants, which can reach higher population frequencies, fall into poorly evolutionarily conserved genes or belong to multigene families displaying high paralogous sequence identity. This suggests that the functions of the corresponding genes are highly redundant, explaining their greater tolerance for LoF variants and supporting a less-is-nothing scenario. Also, although no substantial enrichment in positive selection signals was observed among LoF variants at the genome-wide level, 20 of them fell into regions displaying signatures of positive selection, as predicted by the less-is-more hypothesis, suggesting that they may have conferred a selective advantage in human evolution.

The key question is whether LoF variants and other variants located both in coding and noncoding regions of the genome have a true impact on human phenotypes. The study of the relationship between genetic variation and intermediate molecular phenotypes, such as expression quantitative trait loci, offers new functional insights into the etiology of complex human traits and diseases (*8*). Genetic variants located in regulatory regions across the genome control gene expression (*9*, *10*), but their effects are not straightforward (*8*). Indeed, their impact on gene expression can differ between cell types and tissues (*8*, *11*, *12*). Even in the same cell type, genetic variants can modulate gene expression differently depending on the presence or absence of external stimuli, such as drugs or infectious agents (*13*–*15*). MacArthur *et al*. provide a glimpse of this by studying how a fraction of LoF variants affect gene expression, and show that a minority are associated with reduced expression of the corresponding gene. The intricate relationships observed between genetic variation and gene expression emphasize the complex ways in which genotypic variation may underlie phenotypic consequences at the physiological or pathological levels.

Whole-genome sequencing data from diverse human populations exposed to different environments and presenting different life-styles will provide a realistic picture of the extent of human genetic variation, including low-frequency and population-specific variants. Such information, combined with epigenomics, transcriptomics, and proteomics data from the same individuals and from different cell types, will help to determine the contribution of genetic variants (and the epistatic interactions among them) and environmental variables to variation in organismal traits (see the figure).

References

1. The 1000 Genomes Project Consortium, *Nature* **467**, 1061 (2010).
2. C. Stewart *et al*., *PLoS Genet.* **7**, e1002236 (2011).
3. P. H. Sudmant *et al*., *Science* **330**, 641 (2010).
4. D. G. MacArthur *et al*., *Science* **335**, 823 (2012).
5. M. V. Olson, *Am. J. Hum. Genet.* **64**, 18 (1999).
6. P. C. Ng *et al*., *PLoS Genet.* **4**, e1000160 (2008).
7. K. Pelak *et al*., *PLoS Genet.* **6**, e1001111 (2010).
8. S. B. Montgomery, E. T. Dermitzakis, *Nat. Rev. Genet.* **12**, 277 (2011).
9. S. B. Montgomery *et al*., *Nature* **464**, 773 (2010).
10. J. K. Pickrell *et al*., *Nature* **464**, 768 (2010).
11. A. S. Dimas *et al*., *Science* **325**, 1246 (2009).
12. J. E. Powell *et al*., *Genome Res.*; 10.1101/gr.126540.111 (2011).
13. L. B. Barreiro *et al*., *Proc. Natl. Acad. Sci. U.S.A.* **109**, 1204 (2012).
14. E. Choy *et al*., *PLoS Genet.* **4**, e1000287 (2008).
15. J. C. Maranville *et al*., *PLoS Genet.* **7**, e1002162 (2011).

10.1126/science.1219299

CHEMISTRY

Adding Aliphatic C–H Bond Oxidations to Synthesis

M. Christina White

Oxidations of aliphatic C–H bonds, known since the 1800s, have only recently been considered for use in organic synthesis.

Aliphatic C–H bonds are among the least reactive in organic chemistry, yet enzymes have evolved that not only oxidize them, but can discriminate between individual tertiary (3°) and secondary (2°) C–H bonds in complex molecules. Chemists considered reactivity differences between these inert bonds too minor for a small-molecule catalyst to discriminate (*1*); bio-inspired catalysts with intricate binding pockets were thought to be the only viable solution (*2*). This view pervaded because the reported examples of selective aliphatic C–H oxidations [halogenations (*3*), alkylations (*4*), aminations (*5*), hydroxylations (*6*), and dehydrogenations (*7*)] were not sufficiently high in yield or predictable in site selectivity to be useful in synthesis, except in some special cases such as steroids (see below). In the past several years, however, aliphatic C–H oxidations and simple rules for predicting their selectivities have been emerging prominently in synthetic planning. Powerful small-molecule catalysts have been invented that furnish high enough yields (>50%) to be preparatively useful and can predictably discriminate between aliphatic C–H bonds even within complex molecules that have many possible sites of oxidation.

In contrast to these newest methods, the majority of earlier intermolecular transformations were run with large excesses of substrate (generally solvent quantities), generated <1% oxidized products, and showed unexplained and/or inconsistent site selectivity trends (see the figure, panels A and B). For example, C–H hydroxylations with iron porphyrin catalysts like **1** showed poor yields and minor, unexplained site selectivities for oxidizing the most distal sites from the electron-withdrawing group on substrates (*6*). Stoichiometric organic oxidants such as methyl(trifluoromethyl)dioxirane (TFDO) (*8*) oxidized 3° C–H bonds in select substrates, such as steroids, in good yields (see the figure, panel F). However, the operational difficulty of generating stoichiometric amounts of perfluorinated reagents—and, in the case of TFDO, rapid decomposition under ambient conditions (temperatures above –20°C and visible light) to reactive free radicals (to form $\cdot CH_3$ and $\cdot CF_3$)—limited their reproducibility and use (*9*).

In certain cases, higher reactivity and control of site selectivity were obtained for intramolecular reactions (see the figure, panel C). Substrate tethers that generated carbene or nitrene species upon reacting with oxidant and rhodium (Rh) catalysts led to powerful reactions in synthesis for C–H alkylations (*10*, *11*) and aminations (*12*). Substrate-directed metalations with palladium furnished reactions for acetoxylation and iodinations (*13*, *14*). For carbene and nitrene insertion reactions, the rank order of reactivity between different C–H bond types (for example, 2° versus 3° ali-

Department of Chemistry, Roger Adams Laboratory, University of Illinois, Urbana, IL 61801, USA. E-mail: white@scs.uiuc.edu

Downloaded from www.sciencemag.org on February 16, 2012

Published by AAAS

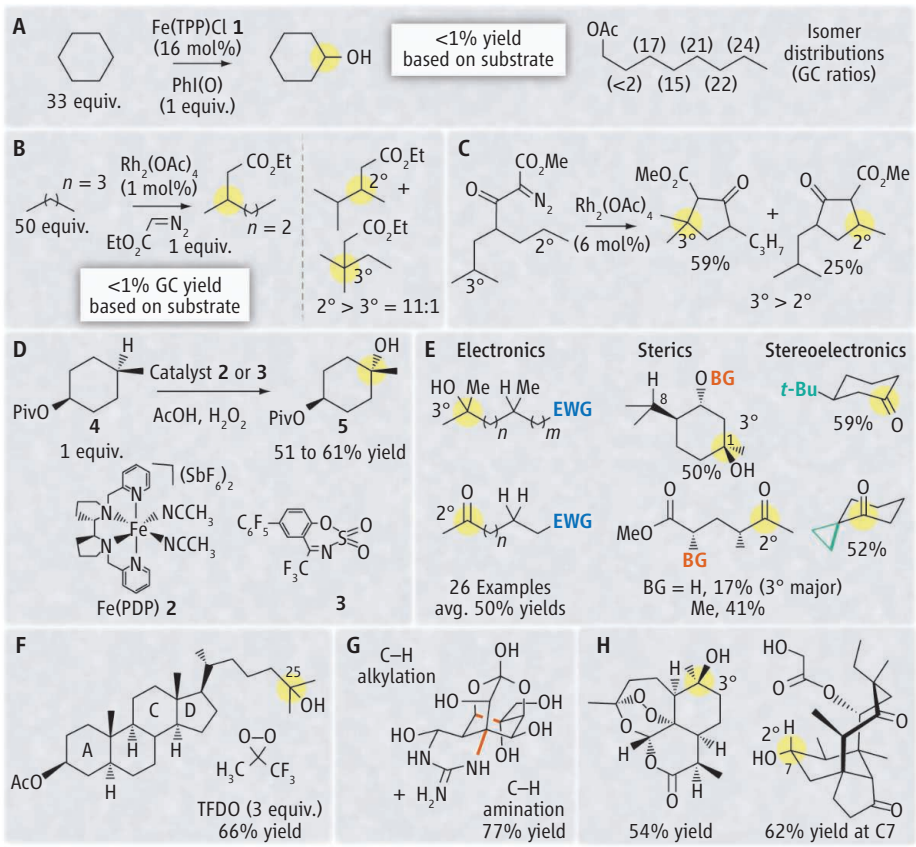

Aliphatic C–H bonds as a new functional group in synthesis. The emergence of reactions with preparative utility and rules for predictable selectivity in aliphatic C–H bond oxidations is illustrated. Unless otherwise noted, one equivalent of substrate is used, and the C–H functionalization site is shown with a yellow circle. (**A** and **B**) Intermolecular aliphatic C–H bond reactivities and site selectivities for (A) hydroxylations [Ac = acetyl, Fe(TPP)Cl **1** = iron tetraphenylporphyrin chloride; selectivities using FePPIX-DME = ferriprotoporphyrin(IX) dimethylester] and (B) alkylations (Et = ethyl); yields are based on gas chromatography (GC). (**C**) Intramolecular alkylation with improved reactivity and different site selectivity (Me = methyl). (**D**) Newer examples of intermolecular aliphatic C–H hydroxylations that achieve high yields, site selectivity, and stereoretention (Piv = pivaloyl). (**E**) Examples of how selectivity rules predict reaction sites in hydroxylations with Fe(PDP) (EWG = electron-withdrawing group; *t*-Bu = *tert*-butyl). (**F**) A 20th-century example of C–H oxidation in a steroid substrate. (**G**) New catalysts enable selective intramolecular C–H aminations [using $Rh_2(HNCOCF_3)_4$] and alkylations for synthesis of complex alkaloids such as tetrodotoxin (bonds formed shown in red). For example, in the alkylation, "complex mixtures" resulted with $Rh_2(OAc)_4$ catalyst, whereas only desired product was seen with $Rh_2(HNCOCPh_3)_4$ (Ph = phenyl). (**H**) Intermolecular hydroxylations of complex terpenes made possible with Fe(PDP); the 3° case is artemisinin and the 2° case is dihydropleuromutilone (C-7 oxidation: 42% hydroxyl, 20% ketone).

phatic) was delineated for intramolecular reactions; however, factors governing selectivities among one bond type (for example, 2° aliphatic) were unclear. Moreover, these "bond type" selectivities were often inconsistent. For example, selectivities for intermolecular Rh-carbene insertion into the less sterically hindered 2° versus 3° C–H bond conflict with those reported for an analogous intramolecular reaction (see the figure, panels B and C) (*4*, *11*). The lack of systematic studies on selectivity effects suggested that examples of site selectivity were anomalous, rather than a general reactivity trend. Moreover, it was thought that attempts to boost yields in the remarkable cases of intermolecular aliphatic C–H oxidations would diminish their site selectivity.

Preparatively useful intermolecular reactions are still lacking for many types of aliphatic C–H oxidations. However, in 2007, it was shown that a nonheme, nitrogen-coordinated iron catalyst, Fe(PDP) **2**, enabled preparative hydroxylations of aliphatic 3° C–H bonds (*15*). One equivalent of substrate could be reacted with Fe(PDP), acetic acid (AcOH), and hydrogen peroxide (H_2O_2) under ambient conditions to furnish ≥50% isolated yields of mono-oxidized products (see the figure, panel D). Fe(PDP) was later shown to catalyze preparative oxidations of 2° aliphatic C–H bonds, arguably the most difficult C–H bonds to oxidize selectively because of their bond strength and ubiquity (*16*, *17*). In 2009, a stable organocatalyst **3** was also reported that used AcOH and H_2O_2 for the preparative hydroxylation of 3° aliphatic C–H bonds (*18*).

Rules that reliably predict site selectivities of oxidation are crucial for such reactions to be adopted into late-stage synthetic planning, where C–H oxidations are most strategically powerful (*19*). With preparative utility achieved under Fe(PDP) catalysis, systematic studies could now be performed on simple substrates designed to test individually the effects of electron-withdrawing groups, sterically bulky groups, and stereoelectronic activating groups on the site selectivity of oxidation among C–H bonds of the same relative bond strengths [2° or 3° (see the figure, panel E)]. Using the highly electrophilic, bulky oxidant generated with Fe(PDP) and H_2O_2, electron-withdrawing functionality on the substrate could effectively prevent oxidation even at remote sites (up to four carbons away), and steric bulk on the substrate could shield proximal sites from oxidation. Additionally, Fe(PDP) could be directed to oxidize sites that were activated through stereoelectronic effects, such as hyperconjugative activation and relief of 1,3-diaxial interactions and torsional strain.

Perhaps the most important finding with Fe(PDP) was that the same selectivity rules that govern the differential reactivity of "traditional" functional groups (i.e., electronics, sterics, and stereoelectronics) also govern the reactivity of relatively inert C–H bonds (*15*–*17*). The generality of these predictable selectivity rules for other electrophilic, bulky oxidants has now begun to emerge (*18*, *20*). Many of the earlier examples of selectivity can now be easily, retrospectively, rationalized with these rules (*21*).

It was uncertain whether the reactivity and selectivity observed with simple substrates would translate over a range of complex-molecule settings. In addition to many more possible sites of C–H oxidation for intermolecular reactions, the presence of dense functionality and topological complexity on a substrate can markedly retard reaction rates and erode selectivities. The majority of 20th-century examples of intra- and intermolecular aliphatic C–H oxidations in complex-molecule settings were limited to steroids (see the figure, panel F). For example, with weaker organic oxidants such as TFDO, where competing 2° oxidation is not an issue, intermolecular reactions showed a striking preference for oxidation at the C-25 3° C–H bond of the C- and D-ring side chain across a range of A and B rings (*8*). However, the privileged nature of the steroid core (highly rigid and sparsely functionalized) and conflicting

Downloaded from www.sciencemag.org on February 16, 2012

Published by AAAS

rationales given for selectivities (sterics and electronics) made it difficult to see that such selectivity might be general.

Newer methods have provided extraordinary examples of predictably selective aliphatic C–H oxidations in a wide range of complex-molecule settings. In the synthesis of the alkaloid tetrodotoxin, selective intramolecular 3° aliphatic C–H alkylation and amination reactions, made possible by newer Rh-acetamide catalysts, were used to install a section of the carbon skeleton and a key amine functionality (see the figure, panel G) (*10*, *12*). The advent of Fe(PDP) catalysis enabled intermolecular aliphatic C–H oxidations to occur at both 3° and 2° sites in a wide range of complex terpenes (see the figure, panel H). Despite dense functionality, one equivalent of substrate could be used to afford preparatively useful amounts of monooxidized products (*15*–*17*).

In essence, C–H bonds have emerged as a "new" functional group for organic synthesis: They can now be specifically targeted for reactivity in a synthetic sequence. Many challenges remain, however, including the development of chemoselective catalysts that can oxidize aliphatic C–H bonds in the presence of more electron-rich functional groups (such as olefins, aromatic rings, and nitrogen atoms); preparative catalysts for intermolecular aminations, alkylations, and halogenations; and catalysts that can override biases induced by the substrate itself.

References

1. R. G. Bergman, *Nature* **446**, 391 (2007).
2. K. Godula, D. Sames, *Science* **312**, 67 (2006).
3. G. A. Russell, H. C. Brown, *J. Am. Chem. Soc.* **77**, 4578 (1955).
4. A. Demonceau, A. F. Noels, A. J. Hubert, P. Teyssie, *Bull. Soc. Chim. Belg.* **93**, 945 (1984).
5. R. Breslow, S. H. Gellman, *J. Chem. Soc. Chem. Commun.* **1982**, 1400 (1982).
6. J. T. Groves *et al*., *J. Am. Chem. Soc.* **101**, 1032 (1979).
7. R. H. Crabtree et al., *J. Am. Chem. Soc.* **101**, 7738 (1979).
8. P. Bovicelli, P. Lupattelli, E. Mincione, T. Prencipe, R. Curci, *J. Org. Chem.* **57**, 5052 (1992).
9. W. Adam, R. Curci, M. E. Gonzelez, R. Nunez, Mello, *J. Am. Chem. Soc.* **113**, 7654 (1991).
10. M. P. Doyle, Q.-L. Zhou, A. B. Dyatkin, D. A. Ruppar, *Tetrahedron Lett.* **36**, 7579 (1995).
11. D. F. Taber, R. E. Ruckle Jr., *J. Am. Chem. Soc.* **108**, 7686 (1986).
12. C. G. Espino, J. Du Bois, *Modern Rhodium-Catalyzed Organic Reactions* (Wiley-VCH, Weinheim, Germany, 2005).
13. L. V. Desai, K. L. Hull, M. S. Sanford, *J. Am. Chem. Soc.* **126**, 9542 (2004).
14. R. Giri *et al*., *Angew. Chem. Int. Ed.* **44**, 2112 (2005).
15. M. S. Chen, M. C. White, *Science* **318**, 783 (2007).
16. M. S. Chen, thesis, Harvard University (2009).
17. M. S. Chen, M. C. White, *Science* **327**, 566 (2010).
18. N. D. Litvinas, B. H. Brodsky, J. Du Bois, *Angew. Chem. Int. Ed.* **48**, 4513 (2009).
19. K. J. Fraunhoffer, D. A. Bachovchin, M. C. White, *Org. Lett.* **7**, 223 (2005).
20. W. Liu, J. T. Groves, *J. Am. Chem. Soc.* **132**, 12847 (2010).
21. T. Newhouse, P. S. Baran, *Angew. Chem. Int. Ed.* **50**, 3362 (2011).

10.1126/science.1207661

EVOLUTION

Contemplating the First Plantae

What characterized the first photosynthetic eukaryotes?

Frederick W. Spiegel

The cells of photosynthetic eukaryotes such as plants and algae contain organelles, called plastids or chloroplasts, responsible for photosynthesis. Plastids contain some DNA, a vestige of their origin from free-living cyanobacteria. On page 843 of this issue, Price *et al*. (*1*) use comparative genomics with the obscure algal protist, *Cyanophora paradoxa*, to propose a resolution to the question of how plastids have spread through the eukaryotes. By understanding the implications of their results, we may be able to picture the overall characteristics of the very first alga.

In recent decades, it has become clear that photosynthetic eukaryotes rose through endosymbiosis (*2*, *3*). In this process, a eukaryotic cell becomes inhabited by a photosynthetic cell. A complex set of events ensues, including transfer of genes from the colonizer's genome to the host's nuclear genome. This is followed by the evolution of mechanisms that allow proteins encoded by these transferred genes back into the colonizer so that it can still photosynthesize. The result is a chimeric organism in which the colonizer has become the plastid. If the colonizer was a cyanobacterium, the chimera is said to be the product of primary endosymbiosis. If the colonizer was a photosynthetic eukaryote, the chimera is the product of secondary or higher-order endosymbiosis (*2*, *3*). Because of their complex genetic histories, the relationships among chimeric organisms can be difficult to interpret (*3*). It can also be challenging to infer relationships between photosynthetic eukaryotes and their closest relatives that never had plastids.

Phylogenetic data suggest that all plastids in today's photosynthetic eukaryotes can be traced back to just two different cyanobacterial colonizers (*3*). One of these colonizers led to the primary plastids in the photosynthetic amoeba *Paulinella* (*3*), but this is not the focus of Price *et al*., who investigate primary endosymbiotic events thought to have occurred more than a billion years ago. Today's Glaucophyta (~13 species, including *C. paradoxa*), red algae (~6000 species), and green algae and land plants (over 300,000 species) all have primary plastids descended from one cyanobacterial ancestor (*1*, *2*). All other eukaryotic algae have secondary or higher-order plastids derived from either red or green algae (*1*–*3*). The data have been equivocal as to how many times that cyanobacterium colonized eukaryotic hosts. According to the Plantae hypothesis, it entered only one protist; the resulting chimera became the sole ancestor to the eukaryotic supergroup Plantae (or Archaeplastida), which contains the glaucophytes, red algae, and land plants and green algae. Alternative "non-Plantae" hypotheses suggest that the cyanobacterium that was ancestral to the plastids of glaucophytes, red algae, and land plants and green algae must have colonized different protists more than once (*4*-*7*).

Acceptance of the Plantae hypothesis requires that Plantae be monophyletic and that it cannot include any secondarily photosynthetic algae or any primitively plastid-free eukaryotes. In other words, a well-supported phylogeny must show that only the glaucophytes, red algae, and land plants and green algae evolved from one chimeric ancestor.

To test this hypothesis, Price *et al*. compare genomes from the most complete set of photosynthetic eukaryotes to date. They provide a number of independent lines of evidence, including data about genes that are independent of the plastids. All their data strongly support the Plantae hypothesis.

The glaucophytes are the most species-poor Plantae. Many phylogenies show them branching most basally in Plantae, that is, diverging before the separation of the reds and the greens (*2*). In such cases, we often have a careless tendency to think of the species-poor branch as "primitive" in all

Department of Biological Sciences, SCEN 601, 1 University of Arkansas, Fayetteville, AR 72701, USA. E-mail: fspiegel@uark.edu

Downloaded from www.sciencemag.org on February 16, 2012

Published by AAAS

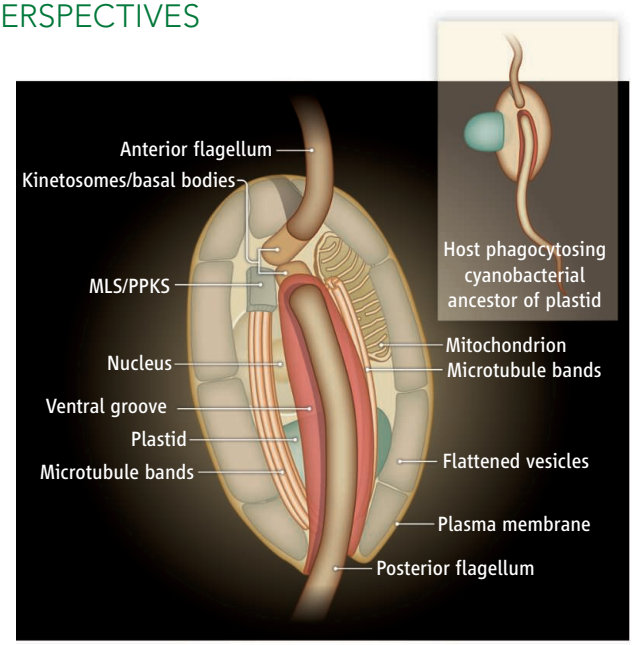

Hypothetical first alga in Plantae. After a phagocytic host was colonized by a cyanobacterium (**inset**), the chimeric first alga (shown in ventral view) probably had the following characters (*5*, *9*–*15*): a nucleus, mitochondrion, flagella, and sex found in all major lineages of eukaryotes; a ventral groove supported by microtubule bands shared by *Cyanophora,* Excavata, SAR (Stramenopila, Alveolata, and Rhizaria), and Amoebozoa; a band of microtubules with a laminated structure at its proximal end (multilayered structure/parakinetosomal structure, abbreviated as MLS/PPKS) shared by these groups and streptophyte greens; and flattened vesicles underlying the plasma membrane shared by glaucophytes, SAR, and Hacrobia. Unique features of the first alga were the primary plastid and loss of phagocytosis.

respects and the species-rich lineage as completely "advanced." However, all organisms are mosaics of inherited homologous characters. Some characters were derived after a common ancestor had undergone speciation and are unique to the lineage in which they appear. Some characters were derived in the last common ancestor of the lineage and its sibling lineages and are unique to that set of lineages. Some characters, the most primitive set, were those that the common ancestor inherited from its ancestors deeper in the phylogeny and are shared widely. We need an independently derived phylogeny to be able to tell what category a homology falls into.

Price *et al*. show unambiguously that *C. paradoxa* has both primitive and derived genomic characters. Some are indicative of its membership in Glaucophyta to the exclusion of other Plantae. Others are indicative of its inclusion in Plantae to the exclusion of other eukaryotes. Finally, there are some that are indicative of being eukaryotic. Most important, Price *et al*. show that the plastids of glaucophytes are not completely primitive with respect to the plastids of other Plantae (*8*, *9*). *C. paradoxa* is, as should be expected, a mosaic of characters. The authors also note that, despite the wealth of data at their disposal, they could not resolve which of the three major lineages of Plantae branched basally with respect to the other two. Thus, the glaucophytes may not even have a position in the Plantae tree of life to allow them to be considered "primitive."

Price *et al*. do not discuss the appearance or life history of the original Plantae, but their conclusion that Plantae is monophyletic allows us to do just that, because their data are independent of morphological and life cycle characters. By comparing features of members of Plantae with those shared with organisms in other major eukaryotic lineages (*9*-*15*), some of the characteristics of the first alga can be postulated (see the figure).

Some of the traits inferred for the first Plantae (see the figure) may also provide clues to the properties of eukaryotes in general 1 to 1.5 billion years ago. Careful examination of the literature on protist cells, combined with phylogenomic results such as those of Price *et al*., may elucidate the evolutionary events in eukaryotes at all levels, from the molecular to the morphological.

Lynn Margulis, who championed the idea that eukaryotic cells were chimeras of hosts and endosymbionts long before the hypothesis was accepted, died on 22 November 2011 (*16*). It is a shame that she missed out on this most recent vindication of her tenacity. It is nice that an obscure protist (her preferred term was protoctist) was so integral in advancing the story of how plastids spread through the eukaryotes.

References

1. D. C. Price *et al*., *Science* **335**, 843 (2012).
2. P. J. Keeling, *Am. J. Bot.* **91**, 1481 (2004).
3. C. X. Chan, J. Gross, H. S. Yoon, D. Bhattacharya, *Plant Physiol.* **155**, 1552 (2011).
4. H. Nozaki *et al*., *Mol. Biol. Evol.* **24**, 1592 (2007).
5. V. Hampl *et al*., *Proc. Natl. Acad. Sci. U.S.A.* **106**, 3859 (2009).
6. D. Baurain *et al*., *Mol. Biol. Evol.* **27**, 1698 (2010).
7. C. J. Howe *et al*., *Phil. Trans. R. Soc. B.* **363**, 2675 (2008).
8. M. Sato *et al*., *Planta* **229**, 781 (2009).
9. J. P. Mignot *et al*., *J. Protozool.* **16**, 138 (1969).
10. A. G. B. Simpson, A. J. Roger, *Curr. Biol.* **14**, R693 (2004).
11. S. M. Adl *et al*., *J. Eukaryot. Microbiol.* **52**, 399 (2005).
12. F. W. Spiegel, *Proc. Biol. Sci.* **278**, 2096 (2011).
13. F. W. Spiegel *et al*., *Protoplasma* **132**, 115 (1986).
14. N. Okamoto *et al*., *PLoS ONE* **4**, e7080 (2009).
15. F. Burki *et al*., *PLoS ONE* **2** (8), e790;10/1371/journal.pone.0000790 (2007).
16. M. Schaechter, *Science* **335**, 302 (2012).

10.1126/science.1218515

GEOCHEMISTRY

Mountains, Weathering, and Climate

Adina Paytan

Changes in the lithium isotope composition of seawater over the past 70 million years elucidate the links between weathering and climate.

Earth is sustained as a habitable planet through close interactions and feedbacks among the lithosphere, hydrosphere, atmosphere, and biosphere (*1*). These interactions occur through material and energy transfer between Earth's reservoirs, referred to as global biogeochemical cycles, and result in chemical and physical changes within each reservoir. Seawater chemistry has varied through Earth's history in response to changes in global climate and tectonics (*2*, *3*), making past records of seawater chemistry a powerful archive for reconstructing how these interactions and feedbacks changed over time. On page 818 of this issue, Misra and Froelich (*4*) report how the lithium isotopic composition of seawater (δ^7Li_{SW}), recorded in shells of tiny organisms living in the ocean, has changed over the past 70 million years. The results illustrate the tight interplay among the location of mountain belts, mountain erosion processes, and climate.

Earth and Planetary Sciences Department, University of California, Santa Cruz, CA 95064, USA. E-mail: apaytan@ucsc.edu

CREDIT: ADAPTED BY P. HUEY/*SCIENCE*

Downloaded from www.sciencemag.org on February 16, 2012

Published by AAAS

The Li isotope record reported by Misra and Froelich reveals a 9‰ increase in δ^7Li_{SW} over the past 50 million years, suggesting a general increase in continental weathering and erosion. The observed increase is not monotonous, but rather shows periods of rapid change punctuated by times of little or no change.

Continental weathering, and specifically the weathering of silicate rocks, involves the drawdown of the greenhouse gas carbon dioxide from the atmosphere:

$$CaSiO_3 + 2CO_2 + 2H_2O \rightarrow CaCO_3 + SiO_2 + CO_2 + 2H_2O$$

Changes in weathering rates thus affect climate (*5*, *6*). The general increase in weathering over this time interval has been previously recognized from Sr, Os, and Ca isotopes and other records (*3*). However, interpretation of these weathering proxy records in relation to climate change is difficult, because each of these proxies is controlled by multiple processes that do not directly result in atmospheric CO_2 consumption (see table S1). The Li isotope record is unique in that it responds specifically to the changes in weathering of silicate rocks.

Furthermore, changes in δ^7Li_{SW} reveal information about the weathering regime. Li can be transported to the ocean as dissolved Li ions in river water, or these Li ions may attach to clay particles that are also transported with the river flow. When all of the Li is delivered as ions in solution, its isotopic signature reflects the Li in the silicate rocks from which it was derived (1.7‰). But as Li is incorporated into the clay particles, ^6Li is preferentially taken out of solution, leaving the river Li enriched with the heavier isotope ^7Li. Under these conditions, δ^7Li delivered to the ocean in solution is high (21‰) and, all else being constant, δ^7Li_{SW} also increases. Thus, δ^7Li_{SW} is sensitive to river clay particle load, which in turn is related to the weathering regime.

Weathering rates and the associated solute and particle transport to the ocean depend mainly on topography (high relief enhances weathering) and climate (greater rainfall and higher temperatures enhance weathering) (*7*). Flat terrains do not erode much regardless of climate, and erosion of high mountains in dry climate is also low. Weathering of high mountains in warm and wet climates is dominated by intense chemical weathering with little particle transport, whereas high mountains in cool and wet climates exhibit high physical and chemical weathering, high denudation rates, and higher river particle loads.

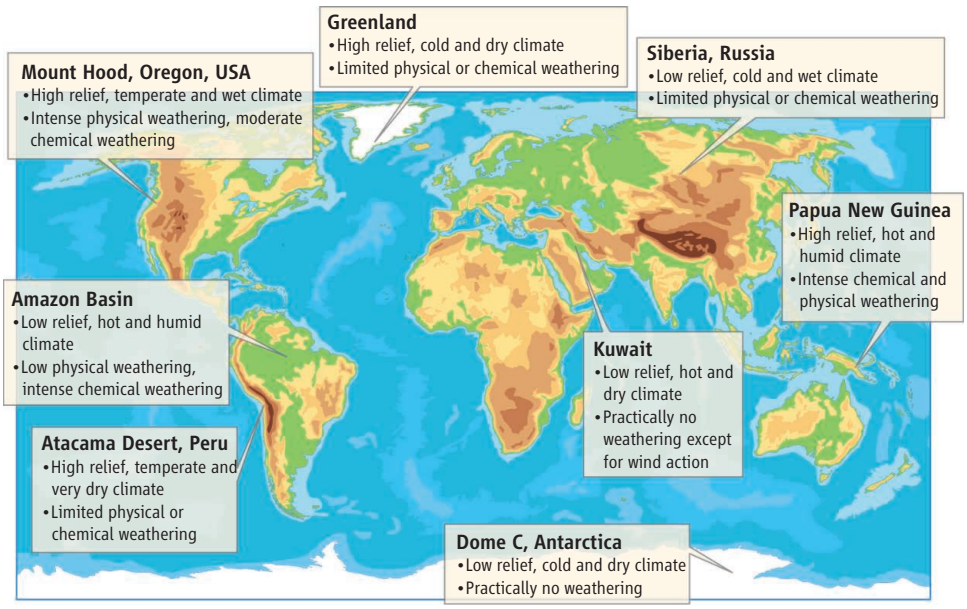

Weathering around the world. Weathering regimes differ around the world depending on both topography and climate. In the geologic past, the locations of mountain regions relative to climatic zones have been different, changing the overall weathering regimes. Misra and Froelich's record of the Li isotope composition of seawater can track such changes in weathering regime.

All these different weathering regimes occur around the world at any given time, but the relative proportion of the different weathering processes on a global scale can vary in space and time depending on the location of mountain ranges relative to climate belts (see the figure). Changes in the slope of the δ^7Li_{SW} curve reveal different weathering regimes: δ^7Li_{SW} will increase during periods of high physical weathering of silicate rocks and mountain denudation but will plateau when chemical weathering dominates. The plateaus may thus indicate high chemical weathering, which can be associated with higher rates of CO_2 drawdown. The record thus provides insight into the links among weathering regimes, mountain denudation, and climate on continental scales.

However, enhanced weathering of silicate rocks associated with either weathering regime consumes atmospheric CO_2, muddling the relation between Li isotopes and climate records (*8*). Moreover, as with all other proxies used to reconstruct past conditions on Earth, the system is underconstrained. The reservoirs participating in the global rock cycle are numerous, and fluxes between them are mostly unknown. Therefore, assumptions about their change must be made to solve the mass balance equations, and the proposed solutions are never unique.

One of the exciting opportunities provided by Misra and Froelich's study is the possibility of constructing coupled models that will better resolve the system. Different isotopes and elements are sensitive to distinct sets of forcing mechanisms or processes, and modeling Sr, Os, Li, and Ca isotopes as well as Sr/Ca and Mg/Ca and potentially other isotopes such as Pb, Hf, and Nd (*9*) together may thus constrain possible solutions (see table S1). Hf isotopes in particular also respond to weathering regimes (*10*). Additional proxies for processes that respond to changes in weathering and denudation, such as phosphate delivery to the ocean and related changes in ocean productivity (*11*) or records of the accumulation of weathering products such as soil clays (*12*) or sediments (*13*), could also be considered. This approach may reveal how the combination of different processes changed over time and how these processes are linked to climate.

References

1. R. A. Berner *et al.*, *Am. J. Sci.* **283**, 641 (1983).
2. H. D. Holland, *Treat. Geochem* **6**, 369 (2003).
3. G. E. Ravizza, J. C. Zachos, *Treat. Geochem.* **6**, 551 (2003).
4. S. Misra, P. N. Froelich, *Science* **335**, 818 (2012); 10.1126/science.1214697.
5. J. C. G. Walker, P. B. Hays, J. F. Kasting, *J. Geophys. Res.* **86**, 9776 (1981).
6. R. A. Berner, E. K. Berner, in *Tectonic Uplift and Climate Change*, W. F. Ruddiman, Ed. (Plenum, New York, 1997), pp. 353–365.
7. A. J. West *et al.*, *Earth Planet. Sci. Lett.* **235**, 211 (2005).
8. J. C. Zachos *et al.*, *Science* **292**, 686 (2001).
9. K. W. Burton, *J. Geochem. Explor.* **88**, 262 (2006).
10. T. van de Flierdt *et al.*, *Earth Planet. Sci. Lett.* **259**, 432 (2007).
11. G. M. Filippelli, *Geology* **25**, 27 (1997).
12. J. D. Milliman, R. H. Meade, *J. Geol.* **91**, 1 (1983).
13. L. A. Derry, C. Franc-Lanord, in *Tectonic Uplift and Climate Change*, W. F. Ruddiman, Ed. (Plenum, New York, 1997), pp. 289–312.

Supporting Online Material

www.sciencemag.org/cgi/content/full/science.1218342/DC1
Table S1

10.1126/science.1218342

CREDIT: (MAP) ISTOCKPHOTO.COM

Downloaded from www.sciencemag.org on February 16, 2012

Published by AAAS

RETROSPECTIVE

James F. Crow (1916–2012)

A population geneticist is remembered by colleagues for his generosity, clarity, and influence in the field, as well as in policy matters involving genetics.

William Dove and Millard Susman

James Franklin Crow pioneered population genetics and influenced policy in human genetics. He was a scholar, citizen, and friend, who touched the lives of students, colleagues, musicians, and many others. He was born on 18 January 1916 in Phoenixville, Pennsylvania. After receiving his bachelor's degree from Friends University in 1937 and his Ph.D. in genetics from the University of Texas at Austin in 1941, he joined the faculty at Dartmouth College. In 1948, he moved to the University of Wisconsin–Madison, where he remained fully active until his death on 4 January 2012 at the age of 95.

Jim's own research began with studies in the fruit fly *Drosophila* that included speciation, insecticide resistance, and mutation load. He then addressed issues in human genetics, including the impact of inbreeding and the age-dependence of mutation rates in males. When molecular data became available, his research with Motoo Kimura led to the neutral theory of molecular evolution. As his Madison colleague Bret Payseur noted, "Jim remained concerned that some of the fundamental controversies raised in the early years of population genetics were not resolved by advances in molecular biology and mathematical theory."

Crow considered his students to be his legacy. The lecture notes for Jim's General Genetics course were so lucid and up-to-date that students preferred "Crow's Notes" to their textbooks. "Notes" appeared in eight editions and was translated into several languages. Together with Kimura, Jim wrote *Introduction to Population Genetics Theory*, an instant classic.

By 1961, when he was elected to the United States National Academy of Sciences (NAS), Crow had established himself as an intellectual leader and effective administrator by serving as chair of the Medical Genetics Department. He chaired NAS committees that reviewed the mutational effects of radiation and environmental chemicals, and when the human genome project brought issues in forensic science to the fore, he was tapped for more committee leadership by the NAS and the Department of Justice. Jim's skill at leading cantankerous committees and delivering reports on time was legendary. According to Chief Justice Shirley Abrahamson of the Wisconsin Supreme Court, "his ability to teach, to listen, and to think 'outside the box' made him a respected leader."

To his colleagues at the University of Wisconsin, Jim was consistently supportive. He was a mentor to Mike Culbertson, "long before there was a formal mentoring program." Colleagues received much more than minimal feedback. When Sean Carroll recently drafted a book on evolution, he had hoped that Jim might glance at some parts to see if they were historically and scientifically accurate. Instead, Sean received "20 pages of typed notes, with several references to classic work, anecdotes, and other gems of evolutionary genetics." Many were perplexed that Jim could be so productive yet was so recklessly generous with his time. His daughter Cathy has explained that Jim never allowed himself to get hung up on trivia. "He was hard-working and careful, but he was not a perfectionist."

Jim retired from the faculty in 1986, but until the end of his life, he was still going to seminars, reading the literature, and writing. The editor of *Genetics*, Jan Drake, invited Jim and one of us (W.D.) to generate a monthly series of essays called Perspectives. This 22-year partnership worked by eschewing perfectionism. Each year, the "two birds" would divide up responsibilities. The magic ingredient was one of forgiveness: Editorial meetings were entitled "Let's exchange our mea culpas." University of Oregon geneticist Frank Stahl has said that, "I was confident that my contributions would be treated with constructive criticism delivered in a most palatable manner."

For Jim, music was a lifelong passion; he played viola in the Madison Symphony Orchestra for 45 years. He said, "I chose the viola because groups always need a violist." Sally Chisholm, violist for the Pro Arte Quartet, described him also as an "immensely influential" philanthropist, supporting music in Madison. Jim was still performing for fellow residents in his retirement community at age 95.

Throughout 2012 the journal *Genetics* will publish essays honoring Jim's contributions to science and to society. Interviews have been published by *BioEssays* and by The University of California, Los Angeles–Johns Hopkins Oral History of Human Genetics Project. His achievements are reflected in the honors bestowed on him, including membership in the U.S. National Academy of Sciences, the American Academy of Arts and Sciences, the Japan Academy, the Royal Society of London, the U.S. Institute of Medicine, and the American Philosophical Society.

Reflections from his colleagues and friends can best illustrate how James Crow will be remembered. Harvard geneticist Matthew Meselson has described him as, "One of the greats. Jim brought a rare clarity to all his work." Jan Klein, formerly of the Max-Planck-Institut für Biologie in Tübingen, Germany, has said that, "Jim will remain as perhaps the last of a generation of gentleman-scientists—'gentleman' in the sense of a courteous, gracious man with a strong sense of honor and a strong respect for the past." And University of Wisconsin colleagues Rayla Temin and Don Waller have said that, "He made you happy just to be in the aura he cast" and that no colleague was "warmer or more encouraging, nor respected more." Indeed, Jim Crow will be immortalized in the histories related by those who knew him as a scholar, citizen, and friend.

10.1126/science.1219557

PHOTO CREDIT: W. HOFFMANN, 1995

Laboratory of Genetics, McArdle Laboratory for Cancer Research, University of Wisconsin, Madison, WI 53706, USA. E-mail: dove@oncology.wisc.edu; msusman@wisc.edu

Downloaded from www.sciencemag.org on February 16, 2012

Published by AAAS

Functional Supramolecular Polymers

T. Aida,[1,2] E. W. Meijer,[3] S. I. Stupp[4,5,6,7]*

Supramolecular polymers can be random and entangled coils with the mechanical properties of plastics and elastomers, but with great capacity for processability, recycling, and self-healing due to their reversible monomer-to-polymer transitions. At the other extreme, supramolecular polymers can be formed by self-assembly among designed subunits to yield shape-persistent and highly ordered filaments. The use of strong and directional interactions among molecular subunits can achieve not only rich dynamic behavior but also high degrees of internal order that are not known in ordinary polymers. They can resemble, for example, the ordered and dynamic one-dimensional supramolecular assemblies of the cell cytoskeleton and possess useful biological and electronic functions.

Synthetic polymers used extensively in technology and everyday life are macromolecules in which small structural units are connected by covalent bonds. In a supramolecular polymer, building blocks of any size could be connected through noncovalent linkages, such as hydrogen bonds or electrostatic interactions, to create a coiled chain or ordered filament. Living systems make use of this concept extensively; one example is the cell cytoskeleton in which long ordered filaments of protein monomers form and depolymerize dynamically for vital cell functions. A synthetic platform of functional supramolecular polymers could be an extraordinary source of innovation with impact in areas ranging from energy and medicine to environmental sustainability.

The development of supramolecular chemistry, defined by Lehn as the chemistry beyond the molecule, has offered a framework to design highly interactive molecules (*1*). This framework has led to a plethora of exciting structures ranging from simple guest-host systems based on molecular recognition to complex self-assembled supramolecular objects (*2*), crystalline networks (*3*), and monolayers (*4*). In polymer chemistry, these controlled interactions have been used to create liquid crystalline materials (*5*) and intriguing architectures in block copolymer assemblies (*6*). Strong unidirectional interactions among molecules can not only recreate some of the key properties of covalent polymers, but they also add functionality based on two basic principles: (i) shape persistence and order within one-dimensional (1D) assemblies and (ii) the dynamics of noncovalent bonds. Louis Henry in 1878 initially proposed the idea of molecular polymerization by associative interactions (*7*), but it was Fouquey *et al*. in 1990 who designed and synthesized the first example of a linear supramolecular polymer based on hydrogen bonding among small molecules (*8*). More recently, strategies were developed to create large and ordered assemblies of molecules in the form of 2D structures and other discrete nanoscale objects (*2*, *9*).

There are at least two distinct types of supramolecular polymers, based largely on the mechanism of their formation (*10*). In one case, a random coil is formed without internal order in close analogy to common polymers (random-coil supramolecular polymers). Such coils form through an isodesmic supramolecular polymerization similar to stepwise growth of macromolecules and are characterized by high polydispersity. A second type of supramolecular polymer is a shape-persistent nanostructure of molecular units with a high degree of internal order (ordered supramolecular polymers). This type of polymer has no analogy to common covalent polymers and is formed by the cooperative (nucleation-elongation) self-assembly of monomers leading to ordered 1D structures. One example is the assembly of macrocycles into nanofibers (*11*), as well as rigid nanofibers based on peptides (*12*). The field of functional supramolecular polymers discussed here involves proper design of building blocks to achieve not just 1D assembly of molecules but actual function as well. Figure 1 shows four molecular units designed to form supramolecular architectures with mechanical (Fig. 1, A and B), biological (Fig. 1, C and D), and optical (Fig. 1, E and F) or electronic functionalities (Fig. 1, G and H).

Tuning the strength and directionality of interactions among molecular units is the key feature that defines the field of supramolecular polymer materials. When the lifetime of these bonds is too short ($\tau < 1$ μs), a robust 1D assembly that resembles a polymer does not exist, whereas too long a lifetime ($\tau > 1$ min) yields materials without interesting dynamic behavior. In an intermediate range of bond lifetimes lies the opportunity to create materials with properties such as adaptability, responsiveness, self-repair, and unique processing options. Highly ordered supramolecular polymers also have the possibility of undergoing well-defined transitions between states of short and long bond lifetimes due to the self-assembly mechanism involved in their formation.

Supramolecular Forms of Contemporary Polymeric Materials

Interest in coil-like supramolecular polymers was triggered by the discovery that small molecules assembled by secondary interactions into long chains can yield materials with mechanical properties that were, until then, exclusively connected to covalent macromolecules (*13*). The first of these polymers are based on self-complementary quadruple hydrogen bonding units with lifetimes on the order of 0.1 to 1 s in solution at room temperature. This approach was used by Sijbesma *et al*. to prepare these small molecules with two ureidopyrimidinone (UPy) termini separated by a spacer (Fig. 1, A and B). These small molecules behave like macromolecules in dilute and concentrated solution as well as in the bulk (Fig. 2, A to C). In solution, they obey the classical theories of polymer physics and possess an interesting equilibrium between cyclic and linear polymers. Virtual molecular weights of more than 500,000 daltons were reached at room temperature, combining excellent mechanical properties in the solid state with low viscosities at elevated temperatures where hydrogen-bond lifetimes shorten considerably. The molecular explanation for this interesting combination is rooted in the possibility of supramolecular chains moving like a reptile (reptation), as conceived by de Gennes (*14*), but also breaking and reforming their bonds with other partners at elevated temperature. Copolymers can easily be formed in these coil-like supramolecular polymers by adding other molecules; this approach has been illustrated in systems that optimize composition for energy transfer in materials designed to serve as white-light—emitting diodes (Fig. 2D) (*15*). Also the length distribution of chains generated by supramolecular polymers and, therefore, their physical properties can be modified through changes in designed interactions among the monomers. Systems based on UPy monomers have been found to obey predictions by Flory for covalent condensation polymers yielding a polydispersity index, M_w/M_n, equal to 2 under thermodynamic equilibrium (*16*).

The fascinating elasticity of rubbery materials proved to be an extremely interesting platform for the supramolecular approach (*17*). A rubbery matrix can be held together by intermolecular interactions along two orthogonal directions, that of the main chain and that of the side chains leading to cross-links. These types of supramolecular elastomers exhibit self-healing behavior as first

[1]Department of Chemistry and Biotechnology, School of Engineering, University of Tokyo, 7-3-1 Hongo, Bunkyo, Tokyo 113-8656, Japan. [2]RIKEN Advanced Science Institute, 2-1 Hirosawa, Wako, Saitama 351-0198, Japan. [3]Institute for Complex Molecular Systems, Eindhoven University of Technology, P. O. Box 513, 5600 MB Eindhoven, Netherlands. [4]Department of Materials Science and Engineering, Northwestern University, 2220 Campus Drive, Evanston, IL 60208, USA. [5]Department of Chemistry, Northwestern University, 2220 Campus Drive, Evanston, IL 60208, USA. [6]Department of Medicine, Northwestern University, Chicago, IL 60611, USA. [7]Institute for BioNanotechnology in Medicine, Northwestern University, 303 East Superior, Chicago, IL 60611, USA.

*To whom correspondence should be addressed. E-mail: s-stupp@northwestern.edu

Downloaded from www.sciencemag.org on February 16, 2012

reported by Cordier *et al*. (*18*). In this work, the chemical system involved biologically derived monomers polymerized through multiple hydrogen bonds. These cross-linked supramolecular polymers showed full strain recovery after extension under load but, in contrast to conventional covalent rubbery materials, exhibited self-healing behavior toward their original strength and elasticity after two fracture surfaces of a sample were brought into contact for a given period of time. In other systems, ultraviolet light absorption was shown to result in mechanical healing behavior in supramolecular polymers formed through metal-ligand interactions (*19*). If polymer backbone formation and cross-links were to be based on very different intermolecular interactions, it would be possible to modulate elasticity or to switch it on or off through temperature changes or other external forces.

The reversible nature of chain-forming interactions in supramolecular polymers also offers unique opportunities in recycling of materials. In principle, these materials could be recycled by simply purifying their monomers without requiring depolymerization. The chemical structure difference between repeating unit and polymer indeed vanishes, and it is only the changes in lifetime of non-covalent bonds as a result of changes in temperature or other external stimuli that determines the state of matter. This will be specially possible and important in materials designed mostly for mechanical functions and utilized in large scale. In the ordered supramolecular polymers discussed below for biological and electronic functions, bond reversibility will be more complex because large monomers and strong interactions are likely to be involved.

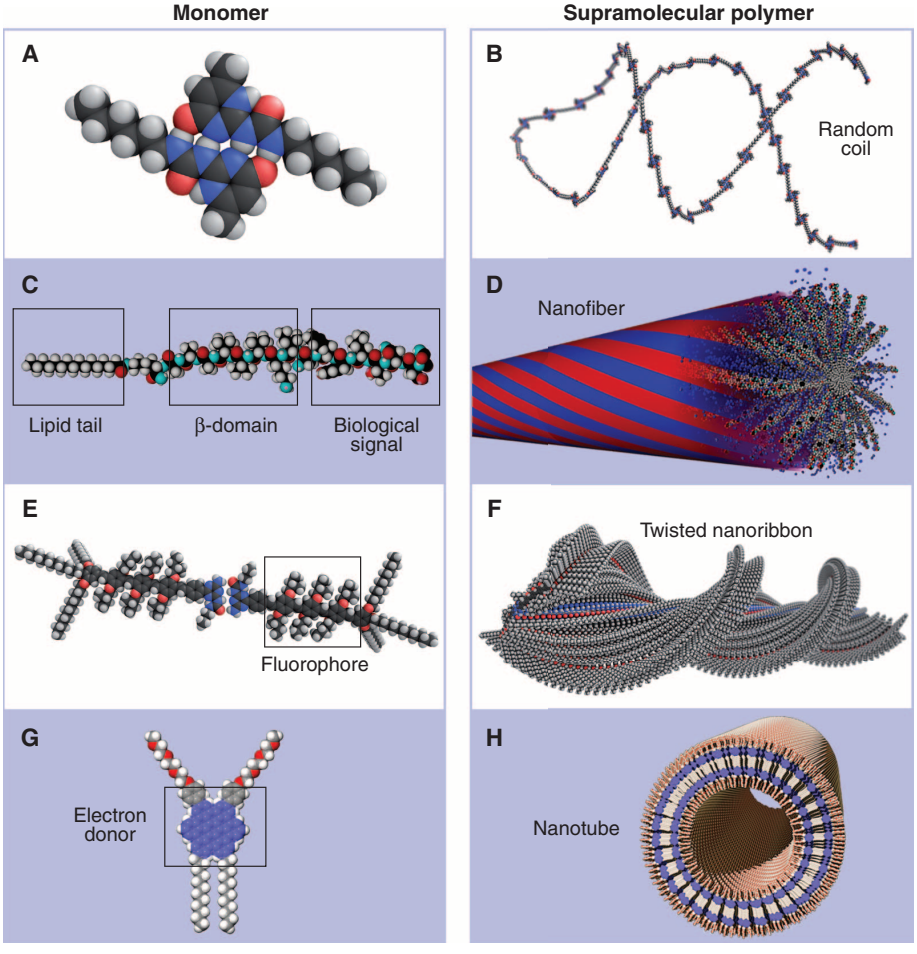

Fig. 1. Molecular representation of four different monomers and the corresponding supramolecular polymers formed after their aggregation through specific interactions. The first pair (**A** and **B**) is a ureidopyrimidinone monomer capable of forming quadruple hydrogen bonds to assemble a random-coil supramolecular polymer. The second pair (**C** and **D**) is a peptide amphiphile monomer composed of three segmental domains: a sequence bearing a biological signal, a domain containing amino acids with a strong tendency to form β sheets, and a hydrophobic alkyl tail. The idealized structure of this ordered supramolecular polymer formed by these monomers is a cylindrical aggregate in which twisted β sheets (red) collapse through hydrophobic interactions among alkyl chains, thus displaying high densities of the biological signal. The blue regions represent water domains present in the interior of the supramolecular assembly (in real dynamic structures the peptide amphiphile and water domains are not expected to have a characteristic periodicity). The third monomer is based on the fluorophore oligo(phenylene vinylene), substituted by alkyl groups for solubility and also chiral centers. One terminus of the monomer is capable of forming quadruple hydrogen bonds to create stable dyads. The ordered supramolecular polymer takes the form of a twisted ribbon with defined chirality (**E** and **F**). The last monomer is based on a hexabenzocoronene core that can behave as an electron donor, substituted by phenyl triethylene glycol and dodecyl chains (**G** and **H**). The ordered supramolecular polymer formed from this monomer is a nanotube with a wall thickness defined by the dimension of monomeric units.

Biomedical and Biomimetic Opportunities with Ordered Supramolecular Polymers

Signaling cells with bioactive filaments. Signaling of cells with biocompatible artificial structures will provide many opportunities to cure disease and improve quality of life for the world's population through regenerative medicine. If these artificial structures are to be placed in the human body, they should signal and then biodegrade into nutrients or be safely eliminated. A supramolecular polymer could be a rigid assembly of molecules displaying multiple signals to receptors in high-density and highly directed geometry, but composed of water soluble monomers. Furthermore, the supramolecular polymer could also be reconstructed by the cell to fit the necessary geometry by easily rupturing and reforming in situ its noncovalent bonds, an opportunity obviously not accessible with covalent chains (Fig. 3, A and B).

Figure 3A schematically depicts a rigid filamentous supramolecular polymer that displays signals spatially to receptors over long distances on the cell surface. These rigid assemblies of small molecules could also recruit the multiple receptors necessary in the raft structures of cell membranes. Figure 3B illustrates how the rupture of noncovalent bonds in the supramolecular polymer could adapt its architecture to the high binding affinities of receptors for the signals displayed on the artificial nanostructure. To create a vast number of such supramolecular polymers, we need self-assembly codes that lead to rigid filaments. The functional form of peptide-based supramolecular polymers has been extensively developed by Hartgerink *et al*. in peptide amphiphiles, molecules containing peptide segments covalently bonded to lipidlike hydrophobic segments (Fig. 3, C to E) (*20*, *21*). These supramolecular polymers have been shown to be highly bioactive in vivo when designed to promote biological events such as regeneration of axons in the injured spinal cord (*22*), the growth of blood vessels (*23*), and the regeneration of bone and cartilage (*24*–*26*). In other work by Jun *et al*. (*27*), peptide amphiphile supramolecular polymers have been engineered as cell scaffolds that integrate substrates for enzymes that can degrade the matrix with biological adhesion signals to promote cell viability, migration, and proliferation.

An example of complex function in ordered supramolecular polymers was their use to promote the rapid and selective differentiation of

Downloaded from www.sciencemag.org on February 16, 2012

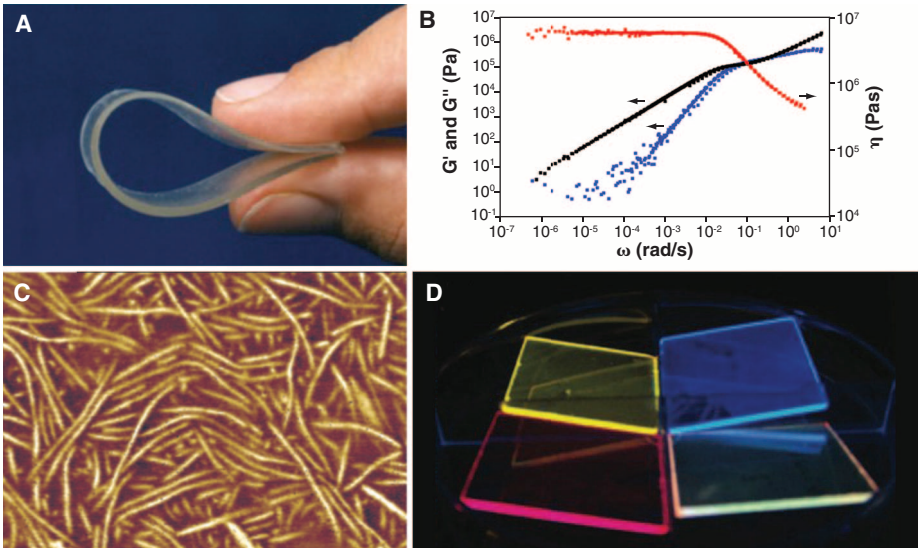

Fig. 2. Supramolecular polymers based on random-coil chains with excellent mechanical properties. (**A**) Rubbery material of a small molecule based on two ureidopyrimidinone moieties separated by a flexible spacer. (**B**) Plots of storage modulus (G′) and loss modulus (G″) as a function of frequency for a material similar to that shown in (A) but containing a stiff and short spacer between ureidopyrimidinone units. ω, angular frequency; η, dynamic viscosity in pascal-seconds. (**C**) Atomic force micrograph of supramolecular polymers that form nanofibers due to lateral hydrogen bonding of a urea group adjacent to a ureidopyrimidinone unit; these materials behave mechanically as thermoplastic elastomers. (**D**) Light-emitting films based on supramolecular copolymers formed by monomers with molecular segments that have different fluorescent properties. A large variety of films can be obtained and even white light emission is possible in these systems when a specific ratio of three different components leads to association of monomers into a random terpolymer.

neural stem cells into neurons without the development of astrocytes (*28*). This selective differentiation was achieved in a supramolecular polymer capable of displaying up to 10^{15} signals/cm^2 of the pentapeptide laminin signal IKVAV. The actual signal density is dependent on the internal level of hydration and bundling of the filamentous assemblies. The observed differentiation required assemblies in which nearly 50% of the peptide amphiphile monomers used to create a filamentous network contained the biological signal (Fig. 3D). In another example, the supramolecular filaments have been used to promote blood vessel formation with heparin-displaying nanofibers that bind the proteins vascular endothelial growth factor and fibroblast growth factor (*23*). The regeneration of cartilage was triggered by nanofibers that displayed peptides discovered by phage display that can bind the protein transforming growth factor β1 (*25*). In approaches using proteins bound to the supramolecular poly-

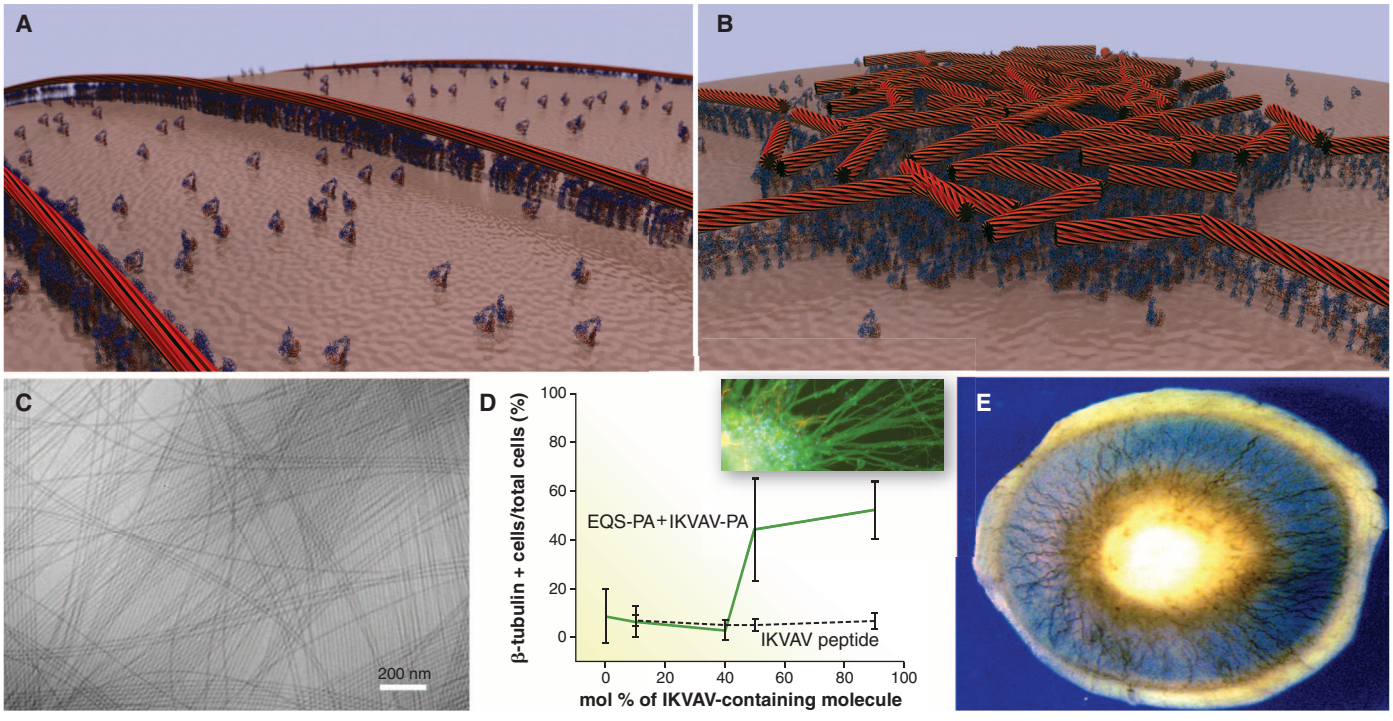

Fig. 3. (**A**) Schematic representation of a bioactive supramolecular filament displaying high densities of biological signals that bind to receptors on the cell surface. The high signal density and stiffness of the ordered supramolecular polymer should be effective at recruiting and colocalizing large numbers of receptors for effective signaling. (**B**) Strong interactions between molecular signals and cell receptors could reconstruct a noncovalent supramolecular assembly with relatively weak bonds to match a raft of receptors. (**C**) Cryo–electron micrograph image of peptide amphiphile nanofibers. (**D**) Plot of the number of neurons developed from a population of neural stem cells upon contact with supramolecular nanofibers containing various mole percents of monomer displaying the bioactive pentapeptide signal IKVAV (the number of cells is obtained counting β-tubulin III–positive cells, a marker for neuronal lineage). (Inset) A cluster of neural stem cells undergoing differentiation into neurons (green indicates the presence in the cells of β-tubulin III). The dotted curve in the main panel shows that adding various mole percents of the soluble IKVAV signal to a network of nonbioactive supramolecular polymers has no effect on differentiation of the neural stem cells. Error bars indicate ± 1 SD. (**E**) Rat cornea showing the growth of many new blood vessels 7 to 10 days after peptide amphiphile nanofibers that display heparin and bind angiogenic growth factors were placed in the tissue.

Downloaded from www.sciencemag.org on February 16, 2012

mer, the large real state on the rigid assembly can accommodate the nanoscale footprint of a growth factor or antibody to trigger a specific signal transduction pathway or to target a specific cell for therapeutic purposes. It is also important that supramolecular polymers put together through noncovalent interactions will not only be likely to biodegrade at faster rates than covalent polymers, but monomer design will also allow fine tuning of their half-life.

Biomimetic dynamic structures. The potential in supramolecular systems to achieve dynamic functions derives inspiration from the cell cytoskeleton. The reversible association of protein monomers to dynamically create and dissolve a skeleton of stiff filaments inside microscopic gels suggests many ideas for synthetic systems. In cells this fascinating process in which supramolecular polymers form and depolymerize rapidly not only controls cell migration, attachment, and division, but also serves as a highway for internal transport of molecules to specific compartments (*29*). If suitable chemistry could be developed to create biomimetic analogs, one could imagine many possibilities for novel functions. One example would be soft materials that stiffen or deliver chemicals reversibly with chemical or photonic stimuli.

Hierarchical structures. The use of noncovalent interactions to design functional materials will be greatly enhanced if the supramolecular structure codes can be extended beyond a single assembly of molecules defined as the polymer. A number of examples of supramolecular hierarchical structures have been reported recently. Cylindrical assemblies of peptide amphiphiles were found to crystallize spontaneously or were triggered to do so reversibly by x-ray photons that create charge on surfaces of the supramolecular filaments (*30*). In this case, the hexagonal crystal formed as a result of repulsive electrostatic forces among the supramolecular polymers trapped mechanically by the networks they formed. In another example, bundles of dozens of peptide amphiphile cylindrical nanofibers formed through a mechanism analogous to a 2D Rayleigh instability and, consequently, self-ordered into an aqueous liquid crystal at exceedingly low concentrations in the range of 0.5% by weight (*31*). These solutions of bundled supramolecular polymers can be sheared by a human hand into orientational monodomains of arbitrary macroscopic length. Their potential functions in aligning large populations of cells or promoting electrical connections among cardiac cells has been demonstrated. These hierarchical systems may serve as scaffolds for wires to repair parts of the brain, heart, and spinal cord. As recently shown, hierarchical supramolecular polymers could also incorporate in their building blocks the multimeric association of molecules observed in biological systems such as the collagen triple helix (*32*).

In a final example of hierarchical structure, positively charged supramolecular peptide filaments in dilute aqueous solution come into contact with dilute solutions of oppositely charged biopolymers with an average molar mass in the range of millions of daltons and assemble into a membrane with speeds in the range of milliseconds (*33*). The supramolecular rigid filaments screened by polymer chains bearing opposite charge assemble into a dense layer that serves as a diffusion barrier to prevent the chaotic mixing of both solutions. This remarkably ordered structure formed by a hierarchical structure of supramolecular polymers is permeable to large molecules such as proteins. The miniaturization of this process to the micrometer scale is a potential platform demonstrated recently to create the scaffold of synthetic cells with filamentous surfaces (*34*).

Electronic Functions in Ordered Supramolecular Polymers

Semiconducting nanofibers. π-Conjugated molecules that self-assemble by stacking have the potential for developing semiconducting nanowires that transport charge carriers unidirectionally over long distances (*35*, *36*). Nearly a decade ago, several pioneering examples of such electroactive nanowires (*37*–*41*) were reported, many of which used π-conjugated aromatic units in conjunction with hydrogen-bonding motifs. For example, mono- and bithiophene derivatives carrying urea functionalities self-assemble into nanofibers, which display highly mobile charge carriers on pulse radiolysis (*37*). The self-complementary quadruple hydrogen-bonding motifs (*13*), when coupled with oligo(*p*-phenylenevinylene) derivatives (Fig. 1), are useful for supramolecular electronics (*38*). Meanwhile, a different strategy to create electroactive 1D nanostructures by making use of molecules with architectures that include rodlike, coil-like, and dendritic segments (dendron rodcoils) has been reported (*39*, *40*). These molecules polymerize into ribbons through hydrogen bonding and π-stacking interactions.

More recent studies have focused on ordered supramolecular polymers based on very large monomeric units with extended π-conjugated motifs to attain high charge mobilities (*42*, *43*). In this context, Wu *et al*. initiated work on coronene derivatives, which have attracted attention as monomers for functional supramolecular polymers (*44*). Xiao *et al*. reported that contorted hexabenzocoronene (HBC) (molecular graphene) derivatives with eight long paraffinic side chains self-assemble into 1D single-crystalline nanofibers that can be used to create field-effect transistors (*42*). Because of strong π-stacking interactions among the molecular units, these 1D nanostructures form without the involvement of any other interactions.

Semiconducting nanotubes. The design strategy to create supramolecular nanotubes can be very different from that used for nanofibers because they derive from the polymerization of units into sheetlike objects. Hill *et al*. reported that an amphiphilic HBC, carrying triethylene glycol (TEG)–appended phenyl groups on one side and dodecyl side chains on the other, self-assembles into several graphite-like nanotubes that are tens to hundreds of micrometers long with a wall thickness of 3 nm (Fig. 1H) (*45*). Thus, these supramolecular nanotubes are characterized by a

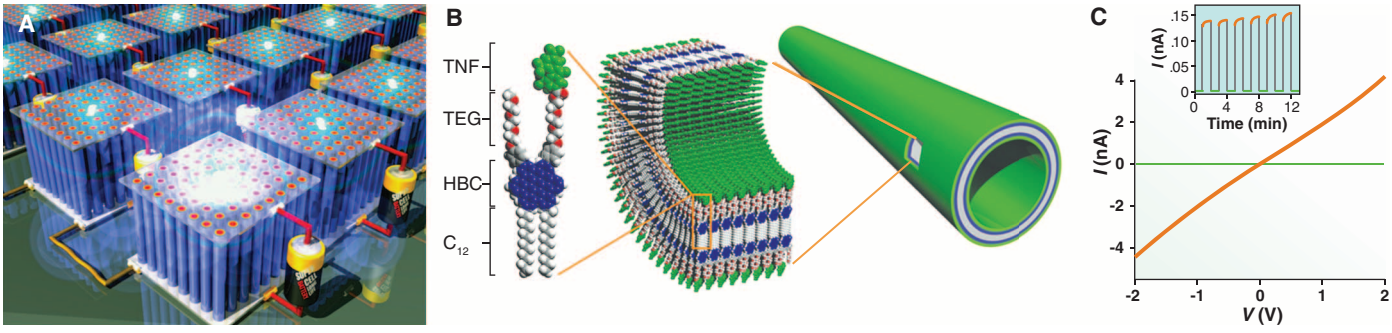

Fig. 4. (**A**) Schematic representation of the vision for photovoltaic devices containing large bundles of aligned semiconducting ordered supramolecular polymers with built-in *p*/*n*-heterojunctions. (**B**) Molecular graphics representation of the monomer and the resulting supramolecular nanotube containing a coaxial *p*/*n*-heterojunction. The donor moiety in the monomer is HBC (blue), and the acceptor is trinitrofluorenone (TNF, green); other parts of the monomer structure include TEG (red) and dodecyl (C_{12}, white) chains for solubility. (**C**) Current-voltage (*I*-*V*) profiles of supramolecular coaxial nanotubes films at ambient temperature with photoirradiation (orange) and without (green) [wavelength λ = 300 to 650 nm]. (Inset) Modulation of electric current using photoirradiation of a cast film of photoconductive nanotubes at room temperature. A large current increase is observed with illumination (orange) versus without (green).

Downloaded from www.sciencemag.org on February 16, 2012

very large aspect ratio and have a uniform, open-ended hollow space that is 14 nm wide. The oxidized nanotube across a 180-nm–gap electrode displays an electrical conductivity of 2.5 megohms at 285 K (*45*). From a suspension of long nanotubes, it is possible to obtain a macroscopic fiber a few centimeters in length consisting of unidirectionally oriented nanotubes. Because of this alignment, the doped macroscopic fiber displays a clear anisotropy in electrical conductivity (*46*). Graphite-like supramolecular nanotubes with a variety of surface functional groups in their TEG termini can be fabricated through this strategy (for example, chemically reactive groups, metal-binding functions, and chromophores) (*47*). When an asymmetric center is incorporated into the ether side chains, nanotubes (*48*) and even nanocoils with one-handed helical chirality are formed. Didraga *et al*. reported the formation of a supramolecular nanotube with a bilayer wall based on a *J*-aggregated amphiphilic cyanine dye (*49*). By means of polarization-resolved near-field scanning optical microscopy, such a red-shifted exciton emission can be detected directly from a single piece of the supramolecular nanotube (*50*).

Photoconductive nanowires and device applications. One of the interesting functions for ordered electronically active supramolecular polymers would be photovoltaic activity. Although examples of such functional systems are still limited, work reported so far is creating a foundation and vision for this field (Fig. 4A). The nanowire polymers required must contain electron-donating (D) and accepting (A) components, either properly located in a single 1D object or in different ones within a suitable electron-transfer distance for exciton splitting after light absorption. The D and A components must assemble into individual *p*- and *n*-type semiconducting arrays (*p*/*n*-heterojunction) in such a way that the photogenerated holes and electrons can efficiently move toward opposite electrodes. Ordered supramolecular polymers would offer the possibility to more precisely design the heterojunctions in contrast to the common approach that relies on phase separation. One of the challenges is to avoid unfavorable charge-transfer D/A interactions at distances on the scale of molecular dimensions. In pioneering work, a D-A-D supramolecular triad, consisting of oligo(*p*-phenylenevinylene) (D) and perylene bisimide (A), was found to self-assemble into nanofibers that presumably consist of segregated D and A arrays (*51*, *52*). Although radical anions and cations could be generated photochemically in the nanofiber, they recombined within 60 ps (*51*).

Recently, a design strategy for photoconductive nanotubes with a coaxial *p*/*n*-heterojunction based on HBC units was successfully elaborated (*53*). In this supramolecular structure, a molecular layer of the electron acceptor trinitrofluorenone laminates a graphite-like tubular wall of HBC units that are electron donors (Fig. 4B). This coaxial *p*/*n*-heterojunction structure enables photocurrent generation with a large on/off ratio greater than 10^4 (Fig. 4C). It is interesting to note that at high concentrations of the building blocks, the anticipated charge-transfer interactions prevail, and only ill-defined microfibers form that hardly display a photocurrent (*53*). When a fullerene is used in these structures as the acceptor, the resultant carbon-rich coaxial nanotube shows, upon light illumination, an ambipolar charge-carrier transport profile, where the intratubular mobility is as large as the intersheet mobility in graphite. Furthermore, the nanotube shows a photovoltaic response (*54*), although the overall device performance is not satisfactory for practical use. More recently, this assembling strategy was extended to the formation of a graphite-like nanotube with a linear D/A heterojunction using a surface–cross-linked HBC nanotube as the seed and a fluorinated HBC as the monomer (*55*). Matile and co-workers proposed a zipper-type supramolecular copolymerization of positively and negatively charged D-A dyads from initiating groups immobilized on a gold substrate (*56*, *57*). This approach has the potential to yield aligned systems on electrode surfaces with many tunable properties. Generally speaking, a key issue to consider is the essential difficulty in aligning ordered supramolecular polymers unidirectionally over macroscopic length scales to create devices, and here is where approaches to hierarchical supramolecular structures described in the previous section could become useful.

Future Outlook

Functional supramolecular polymers offer a great platform for materials that integrate order and dynamics to achieve functions such as high responsivity to stimuli, environmental adaptation, and self-repair capacity. It is also clear that an important direction in this platform is to explore functionality in hybrid systems with nanoscale structures of both supramolecular and covalent polymers. Similarly, materials that couple supramolecular and inorganic structures remain largely unknown but have potential, as evidenced by a recent report on semiconducting systems (*58*). Finally, the platform for supramolecular polymers could also transition into 2D and even 3D complex systems (*34*, *59*) to craft novel functions of interest in sustainability, electronics, and health.

References and Notes

1. J. M. Lehn, *Angew. Chem. Int. Ed. Engl.* **29**, 1304 (1990).
2. S. I. Stupp *et al*., *Science* **276**, 384 (1997).
3. G. B. Gardner, D. Venkataraman, J. S. Moore, S. Lee, *Nature* **374**, 792 (1995).
4. A. Ulman, *Chem. Rev.* **96**, 1533 (1996).
5. T. Kato, J. M. J. Frechet, *J. Am. Chem. Soc.* **111**, 8533 (1989).
6. B. G. G. Lohmeijer, U. S. Schubert, *Angew. Chem. Int. Ed.* **41**, 3825 (2002).
7. L. Henry, *Ann. Soc. Sci. Brux.* **3**, 267 (1878).
8. C. Fouquey, J.-M. Lehn, A.-M. Levelut, *Adv. Mater.* **2**, 254 (1990).
9. S. I. Stupp, S. Son, H. C. Lin, L. S. Li, *Science* **259**, 59 (1993).
10. T. F. A. De Greef *et al*., *Chem. Rev.* **109**, 5687 (2009).
11. J. D. Hartgerink, J. R. Granja, R. A. Milligan, M. R. Ghadiri, *J. Am. Chem. Soc.* **118**, 43 (1996).
12. S. G. Zhang, *Nat. Biotechnol.* **21**, 1171 (2003).
13. R. P. Sijbesma *et al*., *Science* **278**, 1601 (1997).
14. P. G. de Gennes, *J. Chem. Phys.* **55**, 572 (1971).
15. R. Abbel *et al*., *J. Am. Chem. Soc.* **131**, 833 (2009).
16. S. A. Schmid *et al*., *J. Am. Chem. Soc.* **131**, 17696 (2009).
17. H. Kautz, D. J. M. van Beek, R. P. Sijbesma, E. W. Meijer, *Macromolecules* **39**, 4265 (2006).
18. P. Cordier, F. Tournilhac, C. Soulié-Ziakovic, L. Leibler, *Nature* **451**, 977 (2008).
19. M. Burnworth *et al*., *Nature* **472**, 334 (2011).
20. J. D. Hartgerink, E. Beniash, S. I. Stupp, *Science* **294**, 1684 (2001).
21. J. D. Hartgerink, E. Beniash, S. I. Stupp, *Proc. Natl. Acad. Sci. U.S.A.* **99**, 5133 (2002).
22. V. M. Tysseling-Mattiace *et al*., *J. Neurosci.* **28**, 3814 (2008).
23. K. Rajangam *et al*., *Nano Lett.* **6**, 2086 (2006).
24. A. Mata *et al*., *Biomaterials* **31**, 6004 (2010).
25. R. N. Shah *et al*., *Proc. Natl. Acad. Sci. U.S.A.* **107**, 3293 (2010).
26. E. D. Spoerke, S. G. Anthony, S. I. Stupp, *Adv. Mater.* **21**, 425 (2009).
27. H. W. Jun, V. Yuwono, S. E. Paramonov, J. D. Hartgerink, *Adv. Mater.* **17**, 2612 (2005).
28. G. A. Silva *et al*., *Science* **303**, 1352 (2004).
29. D. A. Fletcher, R. D. Mullins, *Nature* **463**, 485 (2010).
30. H. G. Cui *et al*., *Science* **327**, 555 (2010).
31. S. M. Zhang *et al*., *Nat. Mater.* **9**, 594 (2010).
32. L. E. R. O'Leary, J. A. Fallas, E. L. Bakota, M. K. Kang, J. D. Hartgerink, *Nat. Chem.* **3**, 821 (2011).
33. R. M. Capito, H. S. Azevedo, Y. S. Velichko, A. Mata, S. I. Stupp, *Science* **319**, 1812 (2008).
34. D. I. Rożkiewicz, B. D. Myers, S. I. Stupp, *Angew. Chem. Int. Ed.* **50**, 6324 (2011).
35. A. P. H. J. Schenning, E. W. Meijer, *Chem. Commun.* **2005**, 3245 (2005).
36. L. C. Palmer, S. I. Stupp, *Acc. Chem. Res.* **41**, 1674 (2008).
37. F. S. Schoonbeek *et al*., *Angew. Chem. Int. Ed.* **38**, 1393 (1999).
38. A. El-ghayoury, E. Peeters, A. P. H. J. Schenning, E. W. Meijer, *Chem. Commun.* **2000**, 1969 (2000).
39. A. Ajayaghosh, S. J. George, *J. Am. Chem. Soc.* **123**, 5148 (2001).
40. E. R. Zubarev, M. U. Pralle, E. D. Sone, S. I. Stupp, *J. Am. Chem. Soc.* **123**, 4105 (2001).
41. B. W. Messmore, J. F. Hulvat, E. D. Sone, S. I. Stupp, *J. Am. Chem. Soc.* **126**, 14452 (2004).
42. S. X. Xiao *et al*., *J. Am. Chem. Soc.* **128**, 10700 (2006).
43. B. El Hamaoui *et al*., *Chem. Commun.* **2007**, 2384 (2007).
44. J. S. Wu, W. Pisula, K. Müllen, *Chem. Rev.* **107**, 718 (2007).
45. J. P. Hill *et al*., *Science* **304**, 1481 (2004).
46. Y. Yamamoto *et al*., *Adv. Mater.* **18**, 1297 (2006).
47. W. Jin *et al*., *J. Am. Chem. Soc.* **130**, 9434 (2008).
48. W. Jin *et al*., *Proc. Natl. Acad. Sci. U.S.A.* **102**, 10801 (2005).
49. C. Didraga *et al*., *J. Phys. Chem. B* **108**, 14976 (2004).
50. D. M. Eisele, J. Knoester, S. Kirstein, J. P. Rabe, D. A. Vanden Bout, *Nat. Nanotechnol.* **4**, 658 (2009).
51. A. P. H. J. Schenning *et al*., *J. Am. Chem. Soc.* **124**, 10252 (2002).
52. E. H. A. Beckers *et al*., *J. Am. Chem. Soc.* **128**, 649 (2006).
53. Y. Yamamoto *et al*., *Science* **314**, 1761 (2006).
54. Y. Yamamoto *et al*., *Proc. Natl. Acad. Sci. U.S.A.* **106**, 21051 (2009).
55. W. Zhang *et al*., *Science* **334**, 340 (2011).
56. A. L. Sisson *et al*., *Angew. Chem. Int. Ed.* **47**, 3727 (2008).
57. N. Sakai, R. Bhosale, D. Emery, J. Mareda, S. Matile, *J. Am. Chem. Soc.* **132**, 6923 (2010).
58. M. Sofos *et al*., *Nat. Mater.* **8**, 68 (2009).
59. Q. Wang *et al*., *Nature* **463**, 339 (2010).

Acknowledgments: Experimental work featured in this Review was supported by the Japan Science and Technology Agency and RIKEN (T.A.'s laboratory); the Dutch National Science Foundation NWO and ERC (E.W.M.'s laboratory); and the U.S. Department of Energy Basic Energy Sciences Program (grants DE–FG02-00ER45810 and EFRC Non-Equilibrium Research Center DE-SC0000989), the NIH (grants NIDCR: 2R01DE015920-06 and NIBIB: 2R01EB003806-06A2), and the NSF (grant DMR-1006713) (S.I.S.'s laboratory). We thank M. Seniw (Northwestern Univ.) for the preparation of figures and A. Tayi (Northwestern Univ.) and K. Pieterse (Eindhoven Univ. of Technology) for assistance with the preparation of the manuscript.

10.1126/science.1205962

Downloaded from www.sciencemag.org on February 16, 2012

Lithium Isotope History of Cenozoic Seawater: Changes in Silicate Weathering and Reverse Weathering

Sambuddha Misra[1]*† and Philip N. Froelich[2]

Weathering of uplifted continental rocks consumes carbon dioxide and transports cations to the oceans, thereby playing a critical role in controlling both seawater chemistry and climate. However, there are few archives of seawater chemical change that reveal shifts in global tectonic forces connecting Earth ocean-climate processes. We present a 68-million-year record of lithium isotopes in seawater (δ^7Li_{SW}) reconstructed from planktonic foraminifera. From the Paleocene (60 million years ago) to the present, δ^7Li_{SW} rose by 9 per mil (‰), requiring large changes in continental weathering and seafloor reverse weathering that are consistent with increased tectonic uplift, more rapid continental denudation, increasingly incongruent continental weathering (lower chemical weathering intensity), and more rapid CO_2 drawdown. A 5‰ drop in δ^7Li_{SW} across the Cretaceous-Paleogene boundary cannot be produced by an impactor or by Deccan trap volcanism, suggesting large-scale continental denudation.

Lithium, the lightest of the alkali elements, is a conservative cation in seawater. The residence time of Li in seawater (~1.2 million years) is much shorter than for the other major alkalis (Na^+ and K^+) but is much longer than the oceanic mixing time (~1000 years), so that Li in seawater is well mixed and homogeneous vertically and laterally in both concentration (ratio to salt) and in isotopic composition ($[Li]_{SW} \approx 26$ μM; $\delta^7Li_{SW} = 31$‰) (*1*) (fig. S1). Lithium is a trace component in continental and seafloor rocks, and unlike other recorders of oceanic chemistry changes (namely Sr and Os), it is hosted almost exclusively in silicate minerals. Because of the large relative mass difference between its two stable isotopes (^6Li and ^7Li), low-temperature Li isotope fractionation exhibits a very large range, making Li a powerful tracer of low-temperature geochemical processes. Among continental granites, mid-ocean ridge basalt (MORB), marine authigenic aluminosilicate clays (MAACs), dissolved Li sources and sinks to and from the sea, and seawater itself, the spread in δ^7Li values is more than 31‰—an enormous isotopic range.

The Li isotopic composition of seawater reflects a balance between input and removal fluxes and their isotopic compositions. The two dominant sources of dissolved Li to seawater are rivers (low-temperature chemical weathering of continental silicate rocks) and hydrothermal (HT) fluxes from mid-ocean ridge spreading centers (high-temperature weathering of oceanic silicate rocks) (*2*–*6*). The removal of Li from seawater is entirely by incorporation into marine sediments and low-temperature altered oceanic crust (AOC) via formation of Li-, Mg-, and Fe-bearing MAACs ("reverse weathering") (*7*–*13*) (Fig. 1 and Table 1). The ^7Li enrichment of seawater (much heavier than all sources) requires the existence of marine reverse weathering that produces secondary clays bearing Li that is isotopically much lighter than

[1]Geochemistry Group, National High Magnetic Field Laboratory, and Department of Earth, Ocean and Atmospheric Sciences, Florida State University, Tallahassee, FL 32310, USA. [2]Froelich Education Services, 3402 Cameron Chase Drive, Tallahassee, FL 32309, USA.

*Present address: Department of Earth Sciences, University of Cambridge, Cambridge CB2 3EQ, UK.
†To whom correspondence should be addressed. E-mail: sm929@cam.ac.uk

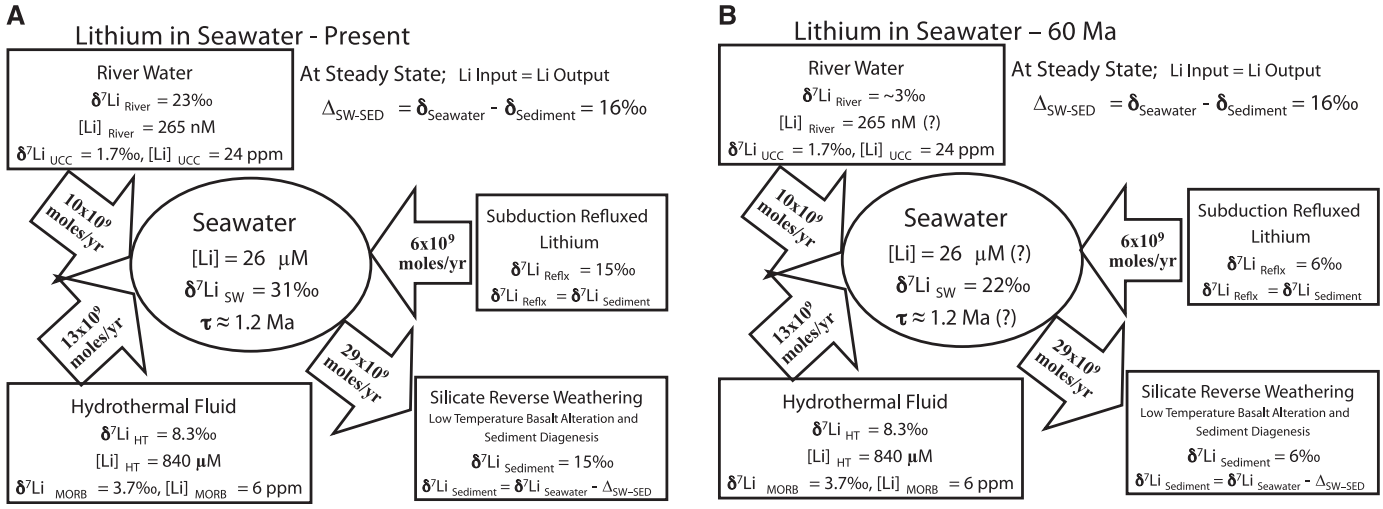

Fig. 1. (**A**) Box model of Li cycle in modern ocean (Table 1). At steady state, the input and output fluxes and isotopic compositions balance each other. The total input flux of Li to the ocean (F_{Input}) is the sum of riverine (F_{Riv}), hydrothermal (F_{HT}), and subduction reflux (F_{Reflx}). The outgoing flux (F_{Sink}) is the sum of Li removal via MAAC and AOC formation during reverse weathering. The mass balance is numerically expressed as $F_{Input} = F_{Riv} + F_{HT} + F_{Reflx} = F_{Sink}$. The isotopic composition of the input flux (δ^7Li_{Input}) is a flux-weighted average of the compositions of rivers (δ^7Li_{Riv}), hydrothermal fluids (δ^7Li_{HT}), and refluxed Li (δ^7Li_{Reflx}). The composition of the output flux (δ^7Li_{Sink}) is dependent on the seawater δ^7Li_{SW} value and has a constant offset from seawater ($\Delta_{Seawater-Sink} = \delta^7Li_{SW} - \delta^7Li_{Sink} = 16$‰). Steady-state isotope balance is expressed as $F_{Input} \times \delta^7Li_{Input} = F_{Sink} \times (\delta^7Li_{SW} - \Delta_{SW-Sink})$. (**B**) One possible steady-state isotope mass balance for the Paleocene-Eocene (P-E) Ocean (60 Ma) when δ^7Li_{SW} was 22‰, 9‰ lighter than today. F_{Riv} is set at modern values and δ^7Li_{Riv} is then constrained to lie near δ^7Li_{UCC}, reflecting congruent weathering of the peneplained transport-limited continents (*29*, *30*) plus perhaps dissolution of the basaltic Deccan Traps and North Atlantic Igneous Provinces. This P-E scenario is an end-member paradigm. Variants of this scenario in which river and hydrothermal fluxes are allowed to vary are explored in text S4 and fig. S10. These alternative scenarios demonstrate that the river condition is constrained to remain between 2‰ and 6‰ regardless of changes in river Li fluxes, hydrothermal fluxes, or seawater Li concentrations.

Downloaded from www.sciencemag.org on February 16, 2012

the seawater from which their Li is derived. Secular variations in δ^7Li_{SW} must thus reflect imbalances between the sources and sinks of Li to and from the ocean, driven by perturbations in the global silicate weathering and reverse-weathering cycles (*14*, *15*).

Seawater lithium budget. The fluxes of river Li and HT Li to the sea are comparable in magnitude but isotopically very distinct. High-temperature HT vent fluids (>350°C) are highly enriched in Li above seawater ($[Li]_{HT} \approx 840$ μM) but are only slightly fractionated from their source rocks ($\delta^7Li_{HT} \approx 8.3$‰; $\delta^7Li_{MORB} \approx 3.7$‰). The ~4‰ enrichment of HT Li above MORB is probably because of ^6Li sequestration in HT Mg-rich greenstone alteration minerals (asbestos) during various stages of hydrothermal recirculation at mid-ocean ridges. In contrast, riverine Li ($\delta^7Li_{Riv} \approx$ 23‰) is ~21‰ heavier than continental source rocks (upper continental crust; $\delta^7Li_{UCC} = 1.7$‰) (*3*, *4*, *16*, *17*) (figs. S2 to S5 and text S1).

Modern-day riverine dissolved Li displays a large spread in concentration and isotopes. Only about one-fifth of continentally weathered Li is carried in the dissolved load. The remainder is carried as Li in secondary clays (*2*, *6*) (fig. S3). The large isotopic offset (21‰) observed between δ^7Li_{Riv} and δ^7Li_{UCC} is a function of chemical weathering intensity (*18*, *19*). The preferential uptake of ^6Li into secondary aluminosilicate clay minerals and oxides formed during weathering and transport drives δ^7Li_{Riv} much heavier than the average continental crust. The partitioning of riverine Li into dissolved and secondary phases as a function of weathering intensity and weathering regimes determines both dissolved Li flux ($F_{Riv\text{-}Li}$) and δ^7Li_{Riv}. Peneplained terrains, especially those in the tropics with transport-limited regimes, exhibit congruent weathering, little or no secondary dioctahedral clay formation to entrap and transport cations, and hence dissolved Li isotope ratios that reflect their source silicate bedrocks. High-relief terrains (uplifted mountains and downcutting high plateaus) with weathering-limited regimes exhibit high physical and chemical weathering and denudation rates with extreme incongruent weathering, large rates of secondary clay formation that carry most of the weathered Li down rivers, and hence dissolved Li isotopes ratios that are ^7Li-enriched relative to their source rocks (*5*, *20*, *21*) (text S1).

At steady state, marine Li removal processes must balance the fluvial and hydrothermal inputs. We group the Li removal processes together and term them "reverse weathering" (*13*). Preferential removal of ^6Li into marine clays, similar to that on continents, leads to a large removal-induced fractionation. This reverse weathering–driven fractionation, representing "light" fractionation from the seawater Li source of about 16‰ ($\Delta_{SW\text{–}Sink} \approx 16$‰), drives seawater isotopically heavy (*11*, *12*) (text S1). Without this removal-induced Li isotope fractionation, seawater would simply reflect the flux-weighted isotope ratio of its sources ($\delta^7Li_{Input} \approx 15$‰). For a steady-state ocean, this removal-driven fractionation puts a boundary condition on composition of the input fluxes because δ^7Li_{SW} must remain about 16‰ heavier than δ^7Li_{Inputs}. This characteristic of Li isotopes in seawater with its large isotopic separation is unique.

The removal of Li by low-temperature reverse-weathering reactions includes MAAC formation in sediments (*22*) and low-temperature seafloor basalt alteration (AOC formation) (*7*, *8*, *16*), both of which involve formation of Mg-rich smectites (*9*–*11*), and Fe-rich aluminosilicates in muddy shallow-water sediments (*23*). Lithium is prone to substitute for octahedral Mg in both high-temperature and low-temperature "clays." Low-temperature weathering (<250°C) of ridge flank

Table 1. Best estimates of dissolved Li input and output fluxes and their compositions from published results (text S1).

Input/output	Lithium flux (10^9 moles/year)	Average δ^7Li (‰)	References
Inputs			
Rivers, F_{Riv}	10	23	(*2*, *5*, *6*)
Hydrothermal vents, F_{HT}	13	8.3	(*3*, *4*)
Subduction reflux, F_{Reflx}	6	15	(*10*, *26*, *27*)
Total input, F_{Input}	29	15	
Outputs			
Basalt alteration (AOC), F_{AOC}	8	15	(*7*, *8*, *17*, *26*)
Sediment uptake (MAAC), F_{MAAC}	20	15	(*9*, *10*, *14*, *26*, *27*)
$\Delta_{Seawater\text{–}Sediment}$ ($\delta^7Li_{SW} - \delta^7Li_{Sink}$)		16	(*10*, *11*)
Total reverse weathering, F_{Sink}	29	15	

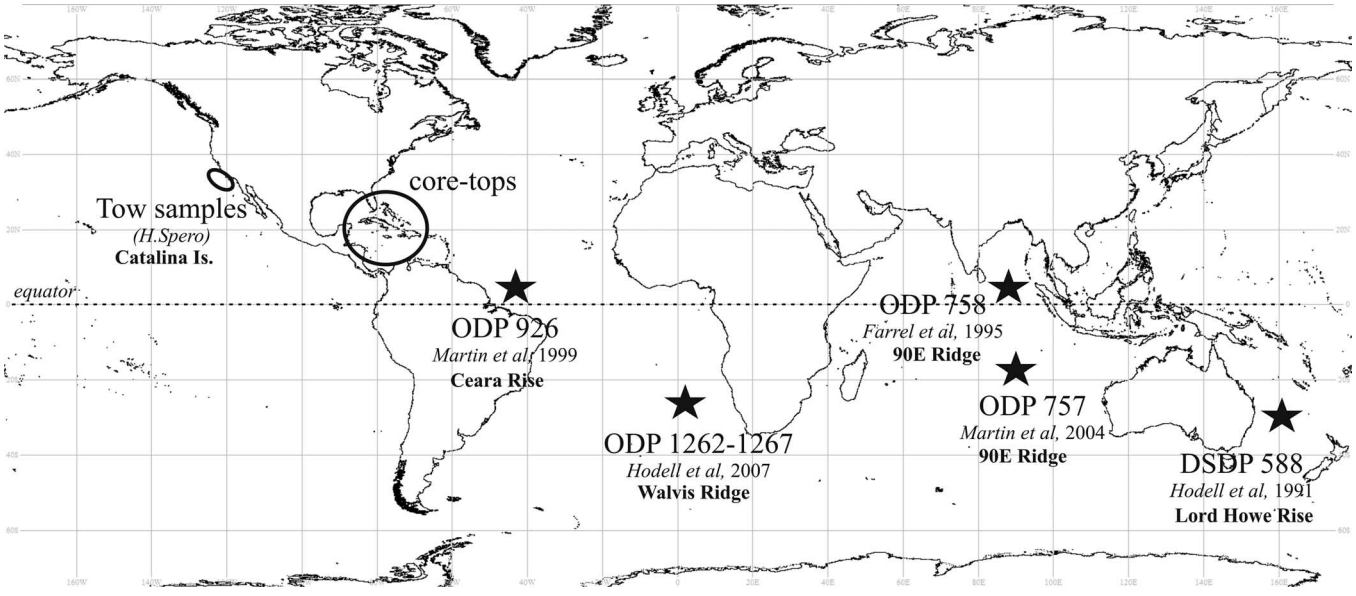

Fig. 2. DSDP/ODP drill sites 588, 757, 758, 926, 1262, 1263, 1265, and 1267, with preexisting high-resolution seawater strontium isotope records, from which the foraminifera samples for this work were collected (*25*) (text S2 and table S1).

Downloaded from www.sciencemag.org on February 16, 2012

basalts away from spreading centers acts as a net sink for Li. In many respects, Li is a crustally recycled cation (*4*, *8*, *9*), being sourced to the ocean from HT circulation at the ridge axis and then reconsumed into basalts during low-temperature alteration off axis. In today's ocean, MAAC is responsible for ~70% and AOC for ~30% of the total marine lithium removal by reverse weathering (Table 1).

Seawater lithium isotope record. Our seawater Li isotope record was constructed by analyzing chemically cleaned planktonic foraminifera that incorporate trace quantities of seawater dissolved Li into their calcium carbonate tests during growth in the surface ocean ($[Li^+]_{Foram} \approx 1$ to 2 ppm). This intrinsic lattice-bound Li isotope ratio is independent of temperature and Li concentration (*15*). The analytical challenges associated with precise δ^7Li determinations from mass-limited foraminifera samples (<1 mg) without contamination and laboratory fractionation artifacts were overcome by developing new methods (*24*, *25*). We have validated the application of foraminifera as faithful recorders of δ^7Li_{SW} (fig. S6) without significant diagenetic overprints (text S3). We selected eight Deep Sea Drilling Project (DSDP)–Ocean Drilling Program (ODP) sites with existing high-resolution Sr isotope records, minimal diagenesis, and good chronologies (Fig. 2). We analyzed age- and species-overlapping foraminifera samples (n = 301) at a resolution of 500,000 to 1 million years, which included both individual species and bulk foraminifera (Fig. 3).

We make six important assumptions for mass balance calculations that drive the observed changes in δ^7Li_{SW}: (i) In contrast to previous δ^7Li_{SW} mass balance studies (*7*, *15*), we include a Li "subduction reflux" term that recognizes solutions resulting from dewatering and breakdown of MAAC in the downgoing slab during subduction and expulsed via the decollement back to the ocean (*26*, *27*) (Table 1 and text S1). This subduction reflux of Li from the convergent margins is held constant over time at ~6×10^9 moles of Li per year (the present-day value), and its isotopic composition is set at a constant offset from contemporaneous seawater ($\delta^7Li_{Reflx} = \delta^7Li_{SW} - \delta^7Li_{Sink}$). This estimate of subduction reflux terms is based on instantaneous steady-state balances, whereas on the real Earth there is a time delay of 50 to 100 million years between sediment deposition and crustal subduction. However, this flux of Li from MAAC and AOC breakdown has a minor influence on seawater Li mass and isotope budgets. (ii) Initially, for simplicity, we take the fluvial dissolved $F_{Riv\text{-}Li}$ as constant over the Cenozoic (this constraint is later dropped). Nevertheless, from the early Paleogene to the present, the river-borne total weathered Li flux (suspended + dissolved) has increased by ~300% as a result of increased orogeny. More important, increasingly incongruent chemical weathering of the continents has changed the dominant Li-bearing phase in rivers from dissolved Li in the Paleocene to suspended Li (in clays) today. This weathering-driven redistribution of riverine Li flux has changed the ratio of dissolved to suspended partitioning from 4:1 in Paleocene to 1:4 today. (iii) δ^7Li_{HT} is kept at the modern-day value of 8.3‰. (iv) $F_{HT\text{-}Li}$ is kept constant over the Cenozoic (*28*). (v) Fractionation of Li upon removal from seawater during reverse weathering ($\Delta_{SW\text{-}SED} = \delta^7Li_{SW} - \delta^7Li_{Sink} \approx 16‰$) is kept constant because the processes of Li removal, whether sediment-hosted or by alteration of oceanic crust, likely has not changed over the Cenozoic. (vi) The removal flux of Li out of the ocean (F_{Sink}) has remained near steady state with the inputs and exhibits first-order removal kinetics with respect to the Li concentration of seawater (Li_{SW}). Our interpretation of changes in δ^7Li_{SW} is based on the weathering and reverse-weathering processes that have the largest δ^7Li fractionation factors and thus the highest likelihood to be the main drivers not only of ocean δ^7Li_{SW} change but also other changes in oceanic and atmospheric chemistry and climate driven by silicate weathering (*29*, *30*) (text S4).

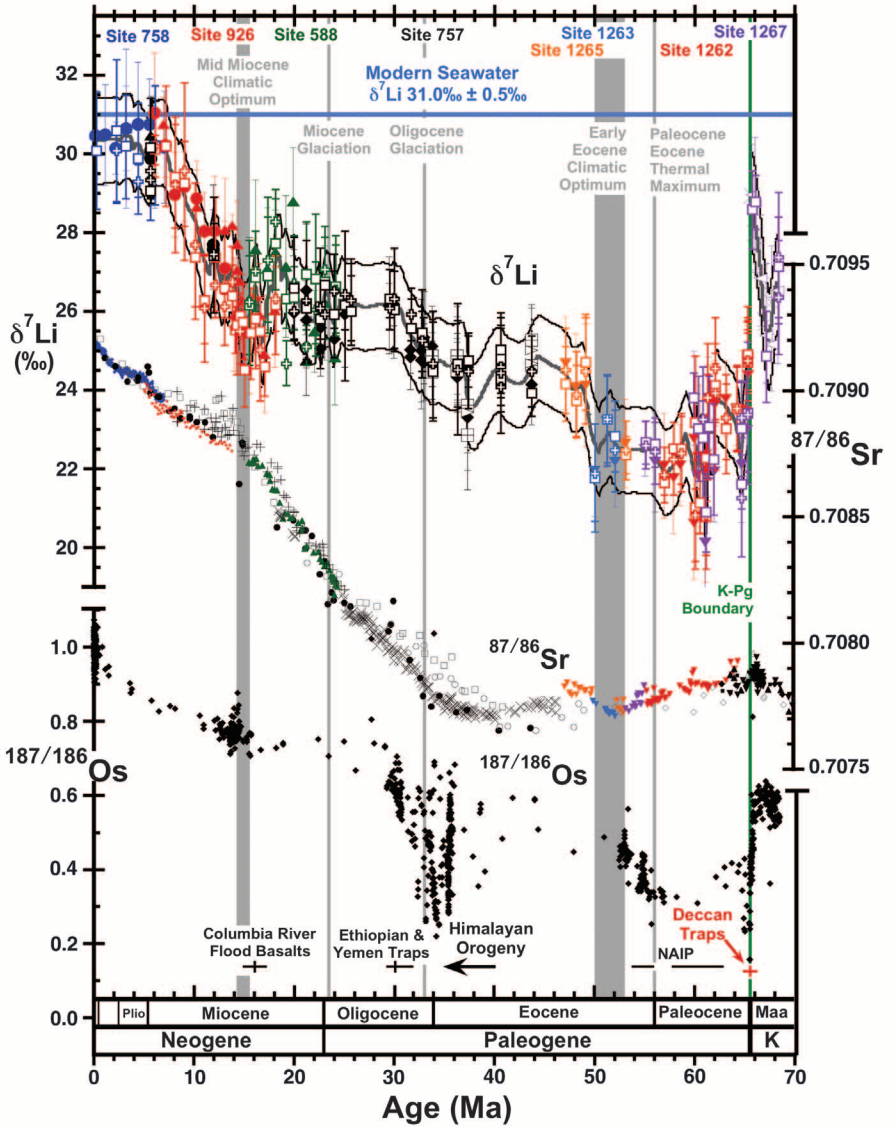

Fig. 3. Late Cretaceous to Holocene Li isotope record (covering 68 million years) and published values of seawater records for $^{87}Sr/^{86}Sr$ and $^{187}Os/^{186}Os$. Lithium isotope values (δ^7Li), expressed as per mil (‰) variation from NIST L-SVEC standard (SRM 8545) (*25*), are plotted on the top left y axis. The error bars represent 2σ uncertainty associated with each quintuplicate measurement. The gray line represents 5-point running mean of δ^7Li_{Foram} record; the two parallel black lines are the corresponding ±2σ uncertainty based on the average SD of all δ^7Li_{Foram} measurements (σ = ±0.55‰, n = 301). The individual foraminifera species symbols are listed in fig. S8. Foraminiferal Li and Sr data are color-coded according to drill sites and are plotted on the same age chronology (*33*, *50*–*53*). The Cretaceous-Tertiary (K-Pg) boundary is set at 65.68 Ma (*54*). The Cenozoic marine Os isotope record ($^{187}Os/^{186}Os$) is plotted on the bottom left y axis (*34*, *35*) (text S2). Because of osmium's short residence time in the ocean and its isotopic sensitivity to impacts and mantle sources (LIPs), the $^{187}Os/^{186}Os$ record reflects large abrupt shifts that are not discernable in either the $^{87}Sr/^{86}Sr$ or $^7Li/^6Li$ records.

Downloaded from www.sciencemag.org on February 16, 2012

Our seawater Li isotope record is consistent with previous Neogene reconstructions from chemically cleaned planktonic foraminifera (*15*, *31*) (fig. S7). Also, our two paleo-δ^7Li_{SW} records from individual species and from bulk foraminifera are indistinguishable from one another (fig. S8). This similarity implies an absence of biogenic fractionation (vital effects) in δ^7Li_{SW} recorded by different species of foraminifera (both extant and extinct), despite strong discrimination against Li by foraminifera [lithium distribution coefficient $K^D_{Li(Calcite-Seawater)} = (Li/Ca)_{Calcite}/(Li/Ca)_{Seawater} \approx 4.2 \times 10^{-3}$ mol/mol] and large variations in observed $(Li/Ca)_{Foram}$ (fig. S6). Also, fossil foraminifera from different drill sites at different paleolatitudes and paleodepths and under markedly different calcite preservation states display no offset or memory effects or diagenetic resetting (text S3 and fig. S9). The absence of any systematic differences in foraminifera-based δ^7Li_{SW} values between samples for both individual species and bulk foraminifera samples of the same age from different drill sites demonstrates that within the resolution of the present record, dissolved Li in seawater was isotopically homogeneous, and cleaned bulk foraminifera can be used to reconstruct the long-term evolution of δ^7Li_{SW}. Our modern foraminifera δ^7Li_{SW} appear to average ~1‰ lighter than seawater (fig. S6).

Results and interpretations. Our paleo-δ^7Li_{SW} record exhibits a 9‰ rise during the past 60 million years, implying a shift in chemical weathering of continental rocks consistent with the seawater $^{87}Sr/^{86}Sr$ record (Fig. 3). The isotope record shows no change over the past 6 million years; thus, the Li content and δ^7Li_{SW} of modern seawater are presumed to be near steady state (Fig. 1). Although our Li isotope record is similar to the seawater Sr isotope history, the Cenozoic δ^7Li_{SW} does not exhibit the monotonically increasing trend of seawater $^{87}Sr/^{86}Sr$. The rise in δ^7Li_{SW} during the Cenozoic is nonlinear, punctuated by transient flat steady states and quasi-linear rises that may coincide with major climatic and tectonic events (*32*). The history of δ^7Li_{SW} over the past 60 million years can be divided into periods of stepped rises (Fig. 4). From 52 to 47 million years ago (Ma), 35 to 31 Ma, and 14 to 6 Ma, the average rate of increase in δ^7Li_{SW} ($\Delta\delta^7Li_{SW} / \Delta t$) is ~ 0.4‰ ± 0.1‰ per million years (2σ). The net result is a 9‰ rise in δ^7Li_{SW} during the past 60 million years. We argue that this increase in δ^7Li_{SW} is caused primarily by increases in δ^7Li_{Riv} (text S4 and fig. S10) that drive increases in the isotopic value entering the sea. Within several residence times (several million years), the marine reverse-weathering removal sink must adjust to obtain a new balance. The mechanism for this clay formation feedback is likely linked to the aluminum source from the continents (clays) and changes in the lithium and magnesium concentrations of seawater (Li_{SW}/Mg_{SW}).

Seawater $^{87}Sr/^{86}Sr$ and $^{187}Os/^{188}Os$ are dependent on differences in isotopic compositions (no isotope fractionation) in their continental (radiogenic) and mantle (nonradiogenic) sources to the ocean (Fig. 3) (*32*–*35*). However, weathering of continental carbonates and redissolution of marine carbonates (for Sr) and weathering of organic-rich black shales and the rain of cosmic dust (for Os) complicate the uplift and continental runoff connections because these elements are not hosted solely in silicates, in contrast to Li (*2*, *36*, *37*). Increased silicate weathering during the Cenozoic has also been suggested from the records of seawater $\delta^{44/40}Ca$ (*38*) and Sr/Ca (*39*), but both suffer from nonsilicate sources and sinks. The sulfur isotope history of seawater (*40*), an ocean redox record of S burial in marine sediments, suggests an oceanic anoxic event near the Paleocene-Eocene Thermal Maximum best explained as an increase in sediment sulfide burial, but is mute on changes in tectonics and weathering. Lithium is unique in tagging processes involving silicates, which is the key to carbon dioxide consumption during weathering and thus the connection between uplift tectonics and climate (*15*, *29*, *41*, *42*).

The Paleocene-Eocene δ^7Li_{SW} minimum. Isotope and mass balance estimates for the mid-Paleocene δ^7Li_{SW} minimum (~22‰), based on our understanding of the modern-day oceanic Li cycle (Fig. 1B), predict an extremely light δ^7Li_{Riv} (~2 to 6‰) reflecting near-congruent weathering of the UCC regardless of secular changes in the Li river flux (text S4 and fig. S10). The early Cenozoic hothouse climate—with high sea levels,

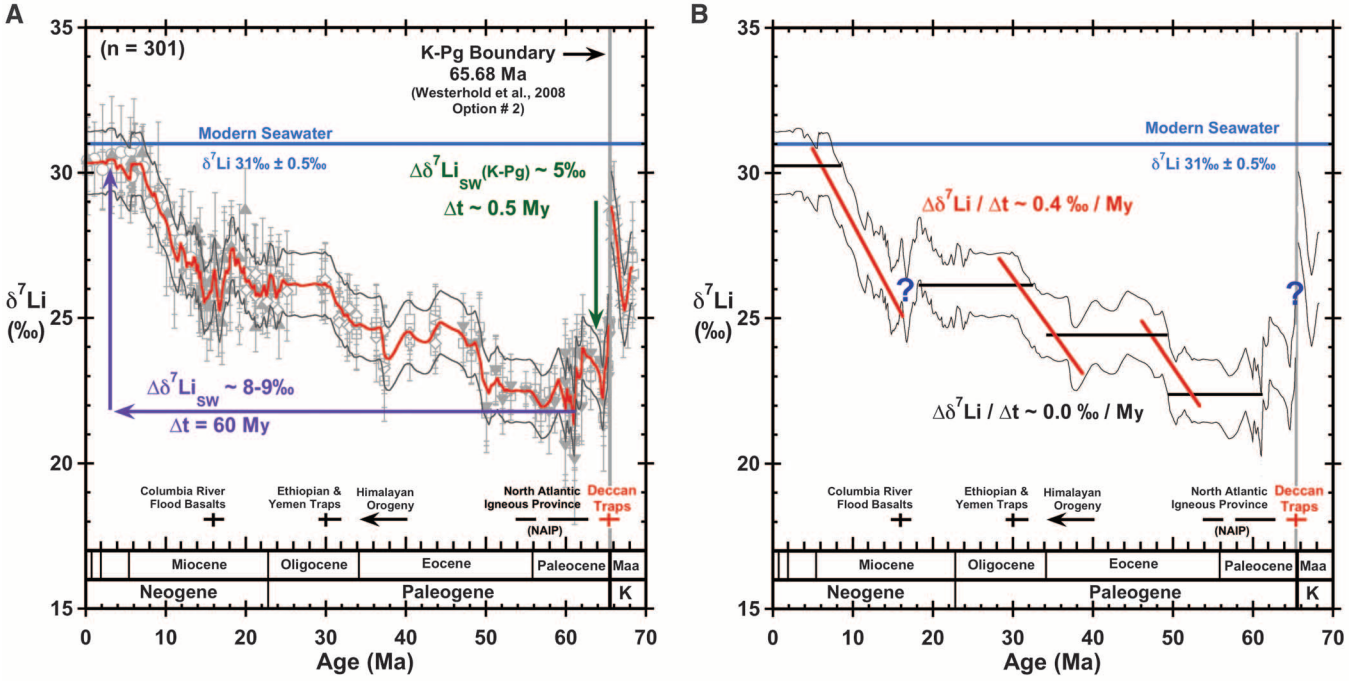

Fig. 4. (**A**) The 5-point running mean of all δ^7Li_{Foram} values from all foraminiferal Li isotope ratio analyses (red line) plotted according to their average age with 2σ uncertainty (the two parallel gray lines) (Fig. 3). The vertical green downward arrow marks the rapid drop in δ^7Li across the K-Pg boundary. The horizontal and vertical purple arrows reflect the overall 9‰ rise in δ^7Li_{SW} during the Cenozoic. (**B**) The ~9‰ rise in δ^7Li_{Foram} over the last 60 million years has been divided into four distinct periods of steady state (black horizontal lines, $\Delta\delta^7Li/\Delta t \approx 0.0$‰ per million years) and three periods of rapid increase in δ^7Li_{SW} (red lines, $\Delta\delta^7Li/\Delta t \approx 0.4$‰ per million years).

Downloaded from www.sciencemag.org on February 16, 2012

swamp continents, and cation-depleted peneplained continents dominated by neotropical congruent weathering and high weathering intensity under hot rainy conditions—is consistent with this interpretation. Low-latitude rivers during this period probably carried sparse suspended material or secondary clays. Thus, the cations delivered to the ocean were mostly in the dissolved load. The implication is that over the Cenozoic the proportion of dissolved Li flux to the ocean decreased (while clay Li increased) and its isotopic value (δ^7Li_{Riv}) increased as the chemical weathering regime of the continents became more weathering limited because of tectonic uplift in the rain belts (e.g., the Himalayas). The interpretation of the Mg/Ca change in seawater, which implies a slowdown in HT fluxes with time, is not inconsistent with the direction of change of our Li isotope record, but the magnitude of HT changes required seems unreasonable (text S4).

The δ^7Li_{SW} minimum in the early Cenozoic may have also been influenced by the northward migration of India carrying the recently erupted Large Igneous Province (LIP) Deccan Traps across the equatorial rain belt (*43*, *44*). LIPs probably have a Li concentration and δ^7Li composition similar to MORB (6 ppm; 3.7‰). Because basalts are aluminum-deficient relative to granites, they weather very rapidly (*45*) and highly congruently (few secondary cation-bearing clays to fractionate Li isotopes) (*12*). Thus rapid chemical dissolution of the Deccan basalts during the 10-million-year equatorial passage in a geological period of much more intense equatorial rainfall (*46*, *47*) may have played a part in depressing δ^7Li_{SW} during the Oligocene. The subaqueous extent of the Deccan eruptions is unknown; thus, its impact on depressing δ^7Li_{SW} cannot be quantified. Similarly, eruption of the LIP North Atlantic Igneous Provinces (NAIP) may also have contributed to subaqueous dissolution of basalts (*45*) and had a similar impact on δ^7Li_{SW} during the Oligocene. It is also likely that quiescence of active mountain building in the rain belts and absence of uplift into orographic rain-catching mountains such as the Andes, Himalayas, and Rockies minimized the early Cenozoic occurrences of transport-limited weathering regimes that are today responsible for formation and transport of secondary clays to the sea and fractionation of the fluvial dissolved river Li flux toward heavy values.

During the Cenozoic climate cooling caused by increased CO_2 drawdown, higher tectonic activity in the rain belts shifted the dominant continental weathering regime from transport-limited (congruent) to weathering-limited (incongruent), which led to heavier Li dissolved flux to the oceans and more weathered Li carried in clays (*14*). Thus, the similarity of our δ^7Li_{SW} record with the global ocean bottom water $\delta^{18}O$ (temperature and ice volume) record is perhaps not accidental (fig. S11). This interpretation suggests that the rises in δ^7Li_{SW} punctuated with stable plateaus every 10 million years or so since the late Eocene might reflect periods of active uplift and denudation followed by periods of tectonic inactivity, at least in the low-latitude rain belts where most continental chemical weathering is expected to occur (Fig. 3). This scenario of Cenozoic continental silicate weathering is different from a monotonically increasing continental chemical weathering regime after initiation of the Himalayan uplift as suggested by the seawater Sr isotope history (*32*, *33*). Coupled Sr and Li isotope models may lead to a better understanding of secular changes in chemical weathering of continental silicates and carbonates and the importance of cation-bearing clay fluxes to the sea in the CO_2-consumption term of climate models (*41*).

The Cretaceous-Paleogene boundary (KTB) δ^7Li_{SW} event. An abrupt 5‰ drop in δ^7Li_{SW} occurs in less than 500,000 years across the Cretaceous-Paleogene (Tertiary) boundary (K-Pg or KTB), simultaneous with the seawater iridium and osmium isotope spikes (Fig. 3) (*44*). This rapid drop in δ^7Li_{SW} must be due to a large instantaneous delivery of isotopically light Li to the sea comparable to the Li content of the entire Cretaceous ocean. It is probably not due to fast addition of Li to seawater from congruent weathering of freshly erupted Deccan Traps ($\delta^7Li_{Basalt} \approx 3.7‰$) (*43*). Given the inventory of Li in seawater today (~3.4×10^{16} moles) and the possibility that this may have been higher in the Cretaceous, the Li mass of the Chicxulub bolide (~10 km diameter; ~9×10^{11} moles of Li) carrying chondritic δ^7Li (~2‰) or even the 200-km impact crater itself (~4.5×10^{14} moles of Li) are insufficient Li (*48*, *49*), even if the chondrite or the granite/gneiss basement of the impact crater were presumed to be instantly pulverized and dissolved congruently into the ocean. The cause of this large fast δ^7Li_{SW} drop across the K-Pg boundary remains enigmatic. We are working on a hypothesis that suggests that this drop in δ^7Li_{SW} exactly at the K-Pg boundary might be due to massive continental denudation and acid rain weathering of continental soils that were partially incinerated and deforested by the impact aftermath and washed into the sea.

Conclusions. With increased mountain building and changes in continental silicate chemical weathering regimes through the Cenozoic, the isotopic signature of riverine dissolved δ^7Li increased from about 3‰ to 23‰. The partitioning of river-borne Li shifted from dissolved Li to clay Li as a result of increasingly incongruent weathering of silicate rocks and secondary clay formation. Overall, this scenario requires that the uplift- and weathering-driven cooling of the climate shifted the global weathering pattern from transport-limited to weathering-limited, increasing secondary clay mineral formation during weathering. As a result of preferential retention of ^6Li by secondary clays, the δ^7Li of river-borne Li became progressively heavier, driving seawater to its present heavy value. An increase in total Li weathered and delivered to the sea (clay Li plus dissolved Li), if extended to the weathering intensity of the major igneous cations stored in the sea (Na, K, and Mg), suggests faster CO_2 drawdown due to more rapid weathering rates. Direct quantification of the influences of forward chemical weathering of continental silicate rocks and reverse weathering of marine silicates on δ^7Li_{SW} might provide alternative estimates of atmospheric CO_2 consumption by the silicate weathering and reverse-weathering cycles (*42*).

References and Notes

1. W. S. Broecker, T. Peng, *Tracers in the Sea* (Lamont-Doherty Geological Observatory, Columbia University, 1982).
2. M. R. Palmer, J. M. Edmond, *Geochim. Cosmochim. Acta* **56**, 2099 (1992).
3. L. H. Chan *et al.*, *Geochim. Cosmochim. Acta* **58**, 4443 (1994).
4. H. Elderfield, A. Schultz, *Annu. Rev. Earth Planet. Sci.* **24**, 191 (1996).
5. Y. Huh, L.-H. Chan, L. Zhang, J. M. Edmond, *Geochim. Cosmochim. Acta* **62**, 2039 (1998).
6. J. Gaillardet, J. Viers, B. Dupré, in *Treatise on Geochemistry*, H. D. Holland, K. K. Turekian, Eds. (Pergamon, Oxford, 2003), pp. 225–272.
7. W. E. Seyfried Jr., X. Chen, L. H. Chan, *Geochim. Cosmochim. Acta* **62**, 949 (1998).
8. L. H. Chan, J. Edmond, G. Thompson, K. Gillis, *Earth Planet. Sci. Lett.* **108**, 151 (1992).
9. L. H. Chan, W. P. Leeman, T. Plank, *Geochem. Geophys. Geosyst.* **7**, Q06005 (2006).
10. R. H. James, M. D. Rudnicki, M. R. Palmer, *Earth Planet. Sci. Lett.* **171**, 157 (1999).
11. N. Vigier *et al.*, *Geochim. Cosmochim. Acta* **72**, 780 (2008).
12. A. Verney-Carron, N. Vigier, R. Millot, *Geochim. Cosmochim. Acta* **75**, 3452 (2011).
13. F. T. Mackenzie, R. M. Garrels, *Am. J. Sci.* **264**, 507 (1966).
14. H. D. Holland, *The Chemical Evolution of the Atmosphere and Oceans* (Princeton Univ. Press, Princeton, NJ, 1984).
15. E. C. Hathorne, R. H. James, *Earth Planet. Sci. Lett.* **246**, 393 (2006).
16. R. L. Rudnick, S. Gao, in *Treatise on Geochemistry*, H. D. Holland, K. K. Turekian, Eds. (Pergamon, Oxford, 2003), pp. 1–64.
17. P. B. Tomascak, C. H. Langmuir, P. J. Le Roux, S. B. Shirey, *Geochim. Cosmochim. Acta* **72**, 1626 (2008).
18. R. F. Stallard, J. M. Edmond, *J. Geophys. Res.* **92**, 8293 (1987).
19. J. M. Edmond, M. Palmer, C. Measures, B. Grant, R. Stallard, *Geochim. Cosmochim. Acta* **59**, 3301 (1995).
20. Y. Huh, L. H. Chan, J. M. Edmond, *Earth Planet. Sci. Lett.* **194**, 189 (2001).
21. B. Kisakűrek, R. H. James, N. B. W. Harris, *Earth Planet. Sci. Lett.* **237**, 387 (2005).
22. L. H. Chan, J. C. Alt, D. A. H. Teagle, *Earth Planet. Sci. Lett.* **201**, 187 (2002).
23. P. Michalopoulos, R. C. Aller, *Science* **270**, 614 (1995).
24. S. Misra, P. N. Froelich, *J. Anal. At. Spectrom.* **24**, 1524 (2009).
25. See supplementary material on *Science* Online.
26. T. Plank, C. H. Langmuir, *Chem. Geol.* **145**, 325 (1998).
27. Y. Li, J. E. Schoonmaker, in *Treatise on Geochemistry*, H. D. Holland, K. K. Turekian, Eds. (Pergamon, Oxford, 2003), pp. 1–35.
28. D. B. Rowley, *Geol. Soc. Am. Bull.* **114**, 927 (2002).
29. M. E. Raymo, W. F. Ruddiman, P. N. Froelich, *Geology* **16**, 649 (1988).
30. J. Zachos, M. Pagani, L. Sloan, E. Thomas, K. Billups, *Science* **292**, 686 (2001).
31. J. M. Hall, L.-H. Chan, W. F. McDonough, K. K. Turekian, *Mar. Geol.* **217**, 255 (2005).
32. J. Hess, M. L. Bender, J. G. Schilling, *Science* **231**, 979 (1986).
33. D. A. Hodell, P. A. Mueller, J. R. Garrido, *Geology* **19**, 24 (1991).

Downloaded from www.sciencemag.org on February 16, 2012

34. B. Peucker-Ehrenbrink, G. Ravizza, *Terra Nova* **12**, 205 (2000).
35. B. Peucker-Ehrenbrink, G. Ravizza, in *The Geologic Time Scale*, F. M. Gradstein, J. G. Ogg, M. D. Schmitz, Eds. (Cambridge Univ. Press, Cambridge, 2012), chapter 8; 10.1016/B978-0-444-59425-9.00008-1.
36. J. M. Edmond, *Science* **258**, 1594 (1992).
37. B. Peucker-Ehrenbrink, R. E. Hannigan, *Geology* **28**, 475 (2000).
38. E. M. Griffith, A. Paytan, K. Caldeira, T. D. Bullen, E. Thomas, *Science* **322**, 1671 (2008).
39. C. H. Lear, H. Elderfield, P. A. Wilson, *Earth Planet. Sci. Lett.* **208**, 69 (2003).
40. A. Paytan, M. Kastner, D. Campbell, M. H. Thiemens, *Science* **304**, 1663 (2004).
41. R. A. Berner, A. C. Lasaga, R. M. Garrels, *Am. J. Sci.* **283**, 641 (1983).
42. F. T. Mackenzie, L. R. Kump, *Science* **270**, 586 (1995).
43. V. Courtillot, P. R. Renne, *C. R. Geosci.* **335**, 1 (2003).
44. D. V. Kent, G. Muttoni, *Proc. Natl. Acad. Sci. U.S.A.* **105**, 16065 (2008).
45. S. R. Gislason, E. H. Oelkers, A. Snorrason, *Geology* **34**, 49 (2006).
46. C. Jaramillo, M. J. Rueda, G. Mora, *Science* **311**, 1893 (2006).
47. M. T. Clementz, J. O. Sewall, *Science* **332**, 455 (2011).
48. L. W. Alvarez, W. Alvarez, F. Asaro, H. V. Michel, *Science* **208**, 1095 (1980).
49. P. Schulte *et al.*, *Science* **327**, 1214 (2010).
50. J. W. Farrell, S. C. Clemens, L. Peter Gromet, *Geology* **23**, 403 (1995).
51. E. E. Martin, H. D. Scher, *Earth Planet. Sci. Lett.* **220**, 25 (2004).
52. E. E. Martin, N. J. Shackleton, J. C. Zachos, B. P. Flower, *Paleoceanography* **14**, 74 (1999).
53. D. A. Hodell *et al.*, *Geochem. Geophys. Geosyst.* **8**, Q09001 (2007).
54. T. Westerhold *et al.*, *Palaeogeogr. Palaeoclimatol. Palaeoecol.* **257**, 377 (2008).

Acknowledgments: We thank the U.S. National Science Foundation (MG&G), American Chemical Society (Petroleum Research Fund), and The Francis Eppes Society of Florida State University for providing financial support. We sincerely thank S. Clemens, D. Hodell, E. Hathorne, E. Martin, E. Thomas, W. Landing, and H. Spero for providing samples. The manuscript greatly benefited from the constructive reviews of M. Bender, V. Salters, M. Humayun, A. Paytan, P. Pogge von Strandmann, and an anonymous reviewer. We are very thankful to B. Peucker-Ehrenrbrink and G. Ravizza for providing the osmium isotope data from GTS 2012 (in press). We also thank H. Elderfield, I. N. McCave, and A. Galy for helpful discussions. Tabulated data are provided on *Science* Online.

Supporting Online Material

www.sciencemag.org/cgi/content/full/science.1214697/DC1
Materials and Methods
SOM Text
Figs. S1 to S11
Table S1
References (*55*–*157*)

30 September 2011; accepted 17 January 2012
Published online 26 January 2012;
10.1126/science.1214697

A Systematic Survey of Loss-of-Function Variants in Human Protein-Coding Genes

Daniel G. MacArthur,[1,2*] Suganthi Balasubramanian,[3,4] Adam Frankish,[1] Ni Huang,[1] James Morris,[1] Klaudia Walter,[1] Luke Jostins,[1] Lukas Habegger,[3,4] Joseph K. Pickrell,[5] Stephen B. Montgomery,[6,7] Cornelis A. Albers,[1,8] Zhengdong D. Zhang,[9] Donald F. Conrad,[10] Gerton Lunter,[11] Hancheng Zheng,[12] Qasim Ayub,[1] Mark A. DePristo,[13] Eric Banks,[13] Min Hu,[1] Robert E. Handsaker,[13,14] Jeffrey A. Rosenfeld,[15] Menachem Fromer,[13] Mike Jin,[3] Xinmeng Jasmine Mu,[3,4] Ekta Khurana,[3,4] Kai Ye,[16] Mike Kay,[1] Gary Ian Saunders,[1] Marie-Marthe Suner,[1] Toby Hunt,[1] If H. A. Barnes,[1] Clara Amid,[1,17] Denise R. Carvalho-Silva,[1] Alexandra H. Bignell,[1] Catherine Snow,[1] Bryndis Yngvadottir,[1] Suzannah Bumpstead,[1] David N. Cooper,[18] Yali Xue,[1] Irene Gallego Romero,[1,5] 1000 Genomes Project Consortium, Jun Wang,[12] Yingrui Li,[12] Richard A. Gibbs,[19] Steven A. McCarroll,[13,14] Emmanouil T. Dermitzakis,[7] Jonathan K. Pritchard,[5,20] Jeffrey C. Barrett,[1] Jennifer Harrow,[1] Matthew E. Hurles,[1] Mark B. Gerstein,[3,4,21]† Chris Tyler-Smith[1]†

Genome-sequencing studies indicate that all humans carry many genetic variants predicted to cause loss of function (LoF) of protein-coding genes, suggesting unexpected redundancy in the human genome. Here we apply stringent filters to 2951 putative LoF variants obtained from 185 human genomes to determine their true prevalence and properties. We estimate that human genomes typically contain ~100 genuine LoF variants with ~20 genes completely inactivated. We identify rare and likely deleterious LoF alleles, including 26 known and 21 predicted severe disease–causing variants, as well as common LoF variants in nonessential genes. We describe functional and evolutionary differences between LoF-tolerant and recessive disease genes and a method for using these differences to prioritize candidate genes found in clinical sequencing studies.

Genetic variants predicted to severely disrupt protein-coding genes, collectively known as loss-of-function (LoF) variants, are of considerable scientific and clinical interest. Traditionally, such variants have been regarded as rare and having a high probability of being deleterious, on the basis of their well-established causal roles in severe Mendelian diseases such as cystic fibrosis and Duchenne muscular dystrophy. However, recent studies examining the complete genomes of apparently healthy subjects have suggested that such individuals carry at least 200 (*1*, *2*) and perhaps as many as 800 (*3*) predicted LoF variants. These numbers imply a previously unappreciated robustness of the human genome to gene-disrupting mutations and have important implications for the clinical interpretation of human genome–sequencing data.

Comparison of reported LoF variants between published genomes is complicated by differences in sequencing technology, variant-calling algorithms, and gene annotation sets between studies (*4*, *5*), and by the expectation that LoF variants will be highly enriched for false positives. The basis for this predicted enrichment is that strong negative natural selection is expected to act against the majority of variants inactivating protein-coding genes, thereby reducing the amount of true variation at these sites relative to the genome average, whereas sequencing error is expected to be approximately uniformly distributed; as a result, highly functionally constrained sites should show lower levels of observed polymorphism and substantially higher false-positive rates (*4*). To date, no large-scale attempt has been made to validate the LoF variants reported in published human genome sequences.

LoF variants found in healthy individuals will fall into several overlapping categories: severe recessive disease alleles in the heterozygous state; alleles that are less deleterious but nonetheless have an impact on phenotype and disease risk; benign LoF variation in redundant genes; genuine variants that do not seriously disrupt gene function; and, finally, a wide variety of sequencing

[1]Wellcome Trust Sanger Institute, Hinxton CB10 1SA, UK. [2]Discipline of Paediatrics and Child Health, University of Sydney, Sydney, NSW 2006, Australia. [3]Program in Computational Biology and Bioinformatics, Yale University, New Haven, CT 06520, USA. [4]Department of Molecular Biophysics and Biochemistry, Yale University, New Haven, CT 06520, USA. [5]Department of Human Genetics, University of Chicago, Chicago, IL 60637, USA. [6]Departments of Pathology and Genetics, Stanford University, Stanford, CA 94305–5324, USA. [7]Department of Genetic Medicine and Development, University of Geneva Medical School, 1211 Geneva 4, Switzerland. [8]Department of Haematology, University of Cambridge and NHS Blood and Transplant, Cambridge CB2 0PT, UK. [9]Department of Genetics, Albert Einstein College of Medicine, Bronx, NY 10461, USA. [10]Department of Genetics, Washington University School of Medicine, Saint Louis, MO 63110, USA. [11]Wellcome Trust Centre for Human Genetics, University of Oxford, Oxford OX3 7BN, UK. [12]BGI-Shenzhen, Shenzhen 518083, China. [13]Program in Medical and Population Genetics, Broad Institute of Harvard and MIT, Cambridge, MA 02142, USA. [14]Department of Genetics, Harvard Medical School, Boston, MA 02115, USA. [15]IST/High Performance and Research Computing, University of Medicine and Dentistry of New Jersey, Newark, NJ 07103, USA. [16]Molecular Epidemiology Section, Leiden University Medical Center, 2300 RC Leiden, Netherlands. [17]The European Nucleotide Archive, European Molecular Biology Laboratory–European Bioinformatics Institute, Hinxton CB10 1SD, UK. [18]Institute of Medical Genetics, School of Medicine, Cardiff University, Heath Park, Cardiff CF14 4XN, UK. [19]Human Genome Sequencing Center, Baylor College of Medicine, Houston, TX 77030, USA. [20]Howard Hughes Medical Institute, University of Chicago, Chicago, IL 60637, USA. [21]Department of Computer Science, Yale University, New Haven, CT, USA.

*To whom correspondence should be addressed. E-mail: macarthur@atgu.mgh.harvard.edu
†These authors contributed equally to this work.

Downloaded from www.sciencemag.org on February 16, 2012

and annotation artifacts. Distinguishing between these categories will be crucial for the complete functional interpretation of human genome sequences.

Obtaining and filtering candidate LoF variants. We identified 2951 candidate LoF variants using whole-genome sequencing data from 185 individuals analyzed as part of the pilot phase of the 1000 Genomes Project (*2*), as well as detailed analysis of high-coverage whole-genome sequencing data from a single anonymous European individual (*6*). The individuals represented three population groups: Yoruba individuals from Ibadan, Nigeria (YRI); 60 individuals of Northern and Western European origin from Utah (CEU); and 30 Chinese individuals from Beijing and 30 Japanese individuals from Tokyo who were analyzed jointly (CHB+JPT).

We adopted a definition for LoF variants expected to correlate with complete loss of function of the affected transcripts: stop codon–introducing (nonsense) or splice site–disrupting single-nucleotide variants (SNVs), insertion/deletion (indel) variants predicted to disrupt a transcript's reading frame, or larger deletions removing either the first exon or more than 50% of the protein-coding sequence of the affected transcript. We further subdivided these variants into "full" LoF variants predicted to affect all known protein-coding transcripts of the affected gene and "partial" variants affecting only a fraction of known coding transcripts. All annotation was performed against the Gencode v3b annotation (*7*) with the algorithm VAT (*8*).

We then subjected our candidate list to a series of stringent informatic and experimental validation steps (*9*). Informatic filtering was based on local sequence context (such as the presence of highly repetitive sequence), gene annotation (such as variants affecting noncanonical splice sites or located close to the end of the affected open reading frame), analysis of the effects of nearby variants (such as neighboring SNVs altering the predicted functional effect of the candidate LoF variant), and measures of sequence read mapping and quality (fig. S1). Where possible, thresholds for filtering were derived from the experimental validation experiments below.

We validated all candidate LoF SNVs and indels that were not excluded by other filters and for which we could design assays ($n = 1877$) with experimental genotyping using three Illumina genotyping arrays and 819 custom Sequenom assays run, where possible, on all 185 samples from the low- and high-coverage 1000 Genomes pilot projects. Large deletions had previously been subjected to extensive validation (*10*). All LoF variants identified in NA12878 were assessed by comparison with independent 454 sequencing and array-based data from the same individual, as well as targeted capillary sequencing of variants in highly repetitive regions. Finally, 786 variants were reexamined by complete manual reannotation of the 689 affected gene models by experienced curators, using the HAVANA annotation pipeline (*7*), to identify annotation errors and flag variants unlikely to profoundly affect gene function. All 589 candidate LoF variants identified in NA12878 were subjected to independent genotype validation and complete gene model reannotation.

As expected, the proportion of likely sequencing and annotation errors in the initial candidate set was high, with overlapping sets of 25.0, 26.8, and 11.1% examined LoF variants being excluded as representing likely sequencing or mapping errors, annotation or reference sequence errors, and variants unlikely to cause genuine LoF, respectively. Candidate LoF variants removed by filtering tended to be more common than high-confidence variants (Fig. 1A). False-positive rates due to sequencing errors (Fig. 1B) were higher for LoF variants than for missense and synonymous variants in the CHB+JPT and YRI populations

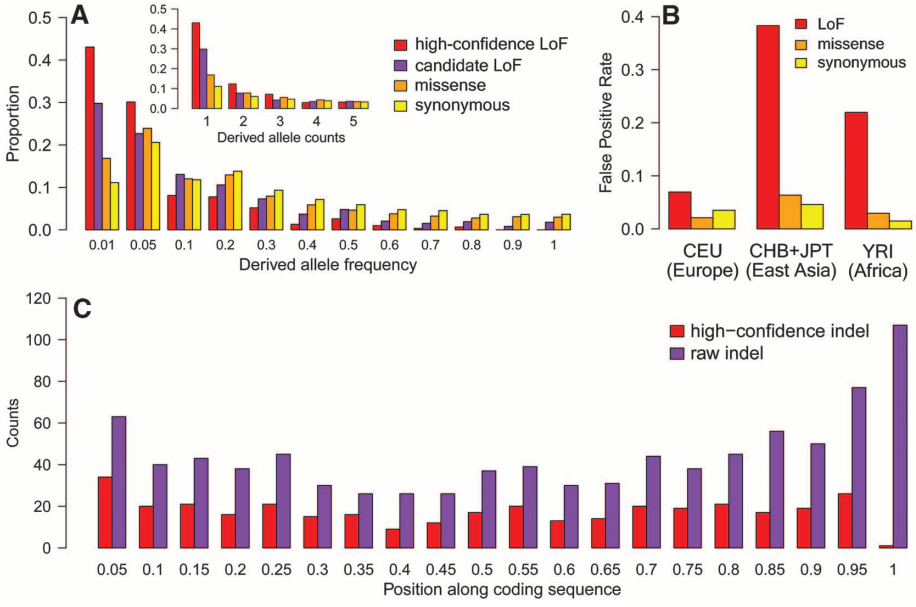

Fig. 1. (**A**) Derived allele frequency distribution in the CEU population for raw and high-confidence LoF variants, compared to missense and synonymous coding variants. (Inset) Distribution of the proportion of SNVs in each class at low allele counts (1 to 5). (**B**) False-positive rates (based on independent array genotyping) for LoF variants filtered for annotation artifacts and frequency-matched missense and synonymous SNVs. (**C**) Distribution of frameshift indels along the coding region of affected genes, before and after filtering.

Table 1. Numbers of LoF variants before and after filtering. Total numbers of candidate LoF variants and average number of LoF sites per individual (homozygous sites in parentheses) are shown for each LoF class. For large deletions, numbers represent total number of genes predicted to be inactivated.

Variant type	Before filtering					After filtering				
	Total	1000G low-coverage average per individual			NA12878	Total	1000G low-coverage average per individual			NA12878
		CEU	CHB+JPT	YRI			CEU	CHB+JPT	YRI	
Stop	1111	85.7 (21.8)	113.4 (26.7)	109.1 (23.7)	115 (25)	565	26.2 (5.2)	27.4 (6.9)	37.2 (6.3)	23 (2)
Splice	658	80.5 (29.5)	98.1 (35.6)	89.0 (30.4)	95 (32)	267	11.2 (1.9)	13.2 (2.5)	13.7 (1.9)	12 (1)
Frameshift indel	1040	217.8 (112.1)	225.5 (121.7)	247.2 (118.7)	348 (159)	337	38.2 (9.2)	36.2 (9.0)	44.0 (8.0)	38 (11)
Large deletion	142	32.4 (12.2)	31.2 (11.8)	31.4 (9.7)	31 (5)	116	28.3 (6.2)	26.7 (5.9)	26.6 (5.5)	24 (4)
Total	2951	416.4 (175.6)	468.2 (195.8)	476.7 (316.0)	654 (286)	1285	103.9 (22.5)	103.5 (24.3)	121.5 (21.7)	97 (18)

Downloaded from www.sciencemag.org on February 16, 2012

($P < 10^{-8}$ for all comparisons) and significantly higher than for missense variants in CEU ($P < 0.05$). Because most variants in a given genome are common, the comparatively high rate of annotation errors among high-frequency LoF variants meant that filtering resulted in a large reduction in LoF variants per individual (Table 1).

We identified several sources of false-positive LoF annotation that will require careful consideration in clinical sequencing projects. For instance, the predicted functional effect of a nonsense or frameshift variant can be altered by other nearby variants on the same chromosome (table S1 and fig. S2), and predicted splice-disrupting SNVs and indels can be rescued by nearby alternative splice sites (fig. S3). Both nonsense SNVs and frameshift indels are enriched toward the 3′ end of the affected gene, consistent with a greater tolerance to truncation close to the end of the coding sequence (Fig. 1C); putative LoF variants identified in the last 5% of the coding region were thus systematically removed from our high-confidence set, with the single exception of a known LoF indel in the *NOD2* gene. There is also a discernible peak close to the 5′ end of genes, suggesting that some disrupted transcripts are rescued by transcriptional reinitiation at an alternative start codon (Fig. 1C).

Notably, 415 (32.3%) of our high-confidence LoF variants are partial LoF variants, affecting only a subset of the known transcripts from the affected gene, meaning that functional protein may still be produced. We chose not to discard such cases, as it is currently impossible to assess the relative functional importance of different transcripts for most genes, and partial LoF mutations have previously been shown to be causal in Mendelian diseases (*11*).

In total, 43.5% (1285/2951) of our candidate LoF variants survived filtering. The resulting catalog of high-confidence LoF variants is not complete: The 1000 Genomes pilot projects had low power to detect extremely rare variants (*2*), and we will not have detected certain classes of LoF variants, such as large gene-disrupting duplications, noncoding variants that disrupt gene expression or splicing regulation, or coding variants that destroy protein function without overtly disrupting an open reading frame (such as missense SNVs or in-frame indels). Several known LoF variant–containing genes such as *ACTN3* (*12*) and *CASP12* (*13*) were labeled as "polymorphic pseudogenes," meaning that the reference genome contains nonfunctional allele of the gene, whereas in other haplotypes the gene is functional (*14*); it is likely that we missed LoF variants in other uncharacterized genes from this class.

Nonetheless, this catalog represents the largest available set of high-confidence human variants predicted to disrupt protein-coding genes. We note that the majority of the LoF variants identified here are novel: 70% of the high-confidence LoF SNVs and indels were not present in dbSNP before the 1000 Genomes pilot project.

The true number of LoF variants in an individual genome. Using the systematically curated list of variants from NA12878, we estimate that this anonymous individual with European ancestry carries 97 LoF variants, with 18 present in a homozygous state (Table 1 and table S2). These numbers, though still indicating an unexpected tolerance for gene inactivation in humans and being considerably higher than those based on genotyping known nonsense SNVs alone (*15*), are substantially lower than most previously published estimates based on whole-genome sequencing [e.g., (*2*, *3*, *16*)] and provide a benchmark for further studies of individual variation in functional gene content. This analysis also provides a robust estimate of different variant classes on gene inactivation: for instance, we find that 39% of genes inactivated in the NA12878 genome are the result of frame-shifting indels, a potentially serious concern given that indels are typically undercalled using short-read sequencing approaches (*2*). Over a quarter (28.7%) of the LoF SNVs and indels in NA12878 affect only a subset of the known transcripts from the affected genes, emphasizing the need to consider alternative splicing in the annotation of functional effects.

Properties of LoF variants and affected genes. LoF SNVs are markedly enriched for low-frequency alleles compared to synonymous and missense SNVs (Fig. 1A), suggesting that many LoF variants are deleterious to human health and hence are prevented from increasing in frequency by purifying natural selection. The number of high-confidence LoF variants per individual is 25% higher in the YRI (Nigerian) sample than in the three non-African populations ($P = 5.0 \times 10^{-21}$; Table 1), suggesting a higher level of variation in functional gene content in African individuals consistent with their greater overall genetic diversity. However, we caution that larger samples with more homogeneous sequencing quality across populations will be required to confirm this finding and assess its likely functional impact.

We compared the properties of genes carrying at least one high-confidence LoF variant with those of other protein-coding genes. Genes containing high-confidence LoF alleles are relatively less evolutionarily conserved, showing a higher ratio of protein-altering to silent substitutions in coding regions between human and macaque ($P = 2.8 \times 10^{-52}$) and less evolutionary conservation in their promoter regions (GERP score; $P = 3.7 \times 10^{-16}$). On average, they have more closely related gene family members (paralogs) than other genes ($P = 0.0058$) and show greater sequence identity to paralogs ($P = 0.0068$), suggesting that

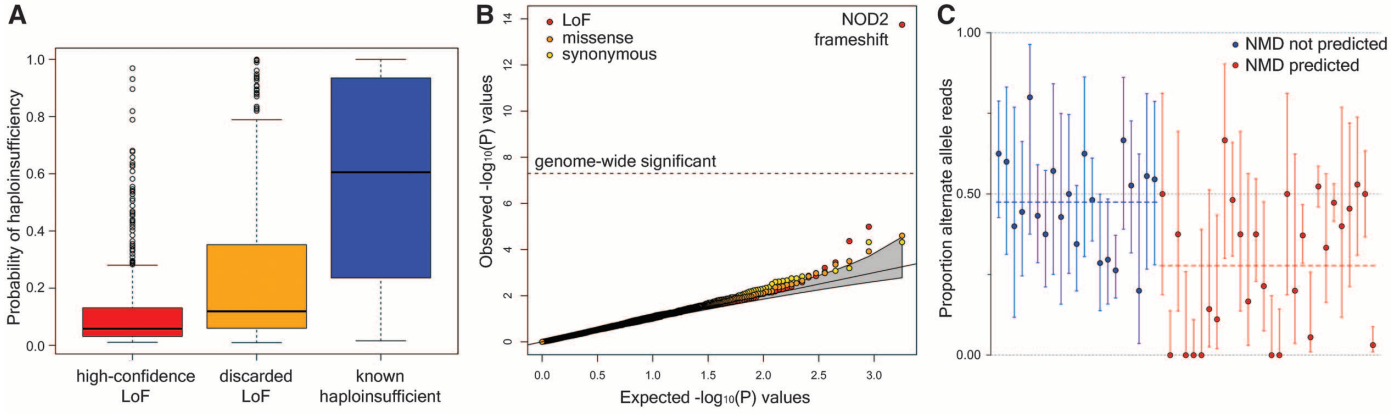

Fig. 2. (**A**) Estimated probability of haploinsufficiency (presence of disease due to heterozygous loss of function), using a model trained with an independent set of LoF deletions as well as a set of known haploinsufficient genes. (**B**) Association of coding variants with complex disease risk. Observed $-\log_{10}(P)$ values for disease association in 17,000 individuals from seven complex disease cohorts and a shared control group, following imputation of variants identified by the 1000 Genomes low-coverage pilot, are plotted against the expected null distribution for all LoF variants and frequency-matched missense and synonymous SNPs. (**C**) Allele-specific expression analysis of nonsense variants, using RNA sequencing data from 119 lymphocyte cell lines. Circles show the proportion of LoF-carrying reads spanning each site across all heterozygous individuals. Variants predicted to cause nonsense-mediated decay (NMD, red) and those predicted to escape NMD (blue) are arbitrarily ordered by genome position within each class. Blue and red dashed horizontal lines indicate mean values in each class. Error bars, 95% confidence interval.

Downloaded from www.sciencemag.org on February 16, 2012

in many cases their function may be partially redundant and also increasing the possibility that LoF variants may be gained or lost through the process of gene conversion (*17*), as has recently been reported for disease mutations (*18*). They also have lower connectivity in both protein-protein interaction ($P = 6.8 \times 10^{-6}$) and gene interaction ($P = 4.2 \times 10^{-19}$) networks, suggesting that LoF-containing genes are generally less central to key cellular pathways, although there are caveats to this interpretation (*9*). LoF-containing genes are strongly enriched for functional categories related to olfactory reception and depleted for genes implicated in protein-binding, transcriptional regulation, and anatomical development (table S8).

We estimated the probability that heterozygous inactivation of a given gene will be deleterious (a state known as haploinsufficiency) using a combination of functional and evolutionary parameters (*9*, *19*). Our filtering process disproportionately removed candidate LoF variants with a higher predicted probability of haploinsufficiency, *P*(HI), consistent with the majority of putative LoF variants in highly functionally constrained genes being artifactual (Fig. 2A). High-confidence LoF variants remaining after filtering have significantly lower *P*(HI) than variants discarded by our filters ($P = 2.1 \times 10^{-16}$) or known haploinsufficient genes ($P = 1.8 \times 10^{-73}$).

We identified 365 genes with multiple candidate LoF variants. The majority of the genes with three or more independent LoF variants were found to represent systematic sequencing errors: for instance, the *CDC27* gene contained 10 separate candidate splice-disrupting variants, all of which were found to represent mapping errors due to an inactive gene copy absent from the human reference sequence. Most of these variants were removed by filtering (table S3). Of the remaining genes, some likely represent genes drifting toward inactivation in the population: for instance, the *VWDE* gene contains four separate high-confidence LoF variants, with 42.7% of the sequenced 1000G samples carrying at least one nonfunctional copy of this gene.

Effects of LoF variants on human phenotypes and disease risk. The high-confidence LoF set includes many known LoF variants reported to have effects on human traits (table S4). We also found a number of previously uncharacterized LoF variants likely to have phenotypic effects. For instance, we identified three separate LoF variants in *PKD1L3* and one in *PKD2L1*; the protein products of these two genes form a putative sour taste receptor complex (*20*, *21*), so these variants may underlie variation in sour taste sensitivity between humans.

Our high-confidence LoF set includes many variants relevant to severe human disease. We identified 26 known recessive disease-causing mutations in our high-confidence LoF set, including mutations associated with the severe early-onset conditions Leber congenital amaurosis, harlequin ichthyosis, osteogenesis imperfecta, and Tay-Sachs disease (table S5). We also identified 21 strong candidates for novel disease-causing mutations: high-confidence LoF variants affecting all known transcripts of genes in which other null mutations have been convincingly associated with Mendelian disease, including adult-onset muscular dystrophy, Charcot-Marie-Tooth disease, and mucolipidosis (table S6). With one exception (a variant associated with transplant graft-versus-host disease), no individuals were homozygous for the putative disease-causing alleles.

Given the evidence for the presence of known deleterious variants, we hypothesized that LoF variants may also be enriched for association with risk of common, complex diseases. We investigated this hypothesis by imputing genotypes for 417 LoF SNVs and indels into a total of 13,241 patients representing seven complex diseases such as Crohn's disease and rheumatoid arthritis, along with 2938 shared controls, who had previously been subjected to genome-wide single-nucleotide polymorphism (SNP) genotyping (*22*). We confirmed a previously known frameshift indel in the *NOD2* gene associated with Crohn's disease, with a genome-wide significant imputed *P* value of 1.78×10^{-14} (two orders of magnitude more significant than the best tag SNP). However, no other LoF variants achieved genome-wide significance, and there was no overall excess of association signals in LoF variants compared to other coding variants (Fig. 2B). Because our catalog is expected to contain most genuine LoF variants at greater than 5% frequency, this result suggests that common gene-disrupting variants play a minor role in complex disease predisposition.

One explanation for the paucity of common LoF variants associated with complex disease risk is purifying selection, which is expected to prevent most severely deleterious alleles from reaching high population frequencies; this is consistent with the skew toward low frequencies among high-confidence LoF variants (Fig. 1A). In addition, genes containing homozygous LoF variants have more gene family members (median 5 versus 3; $P = 3.76 \times 10^{-3}$) and are less

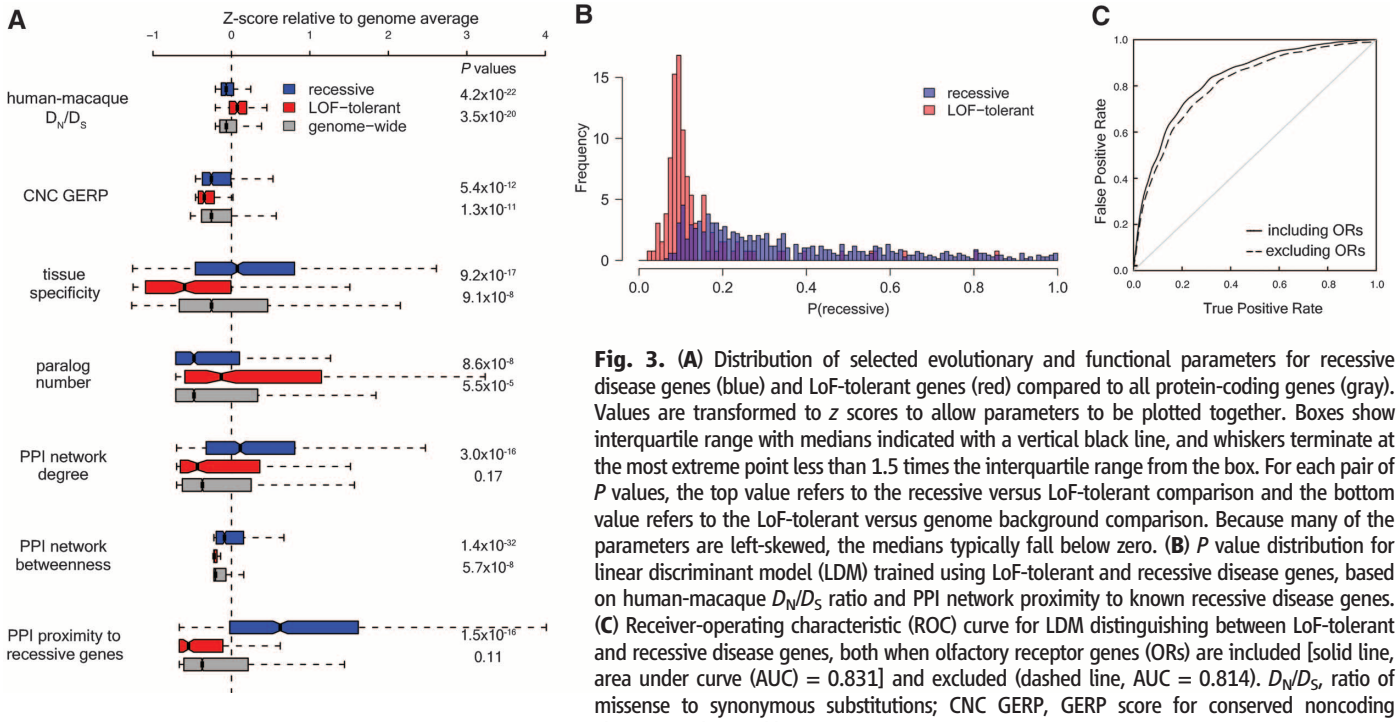

Fig. 3. (**A**) Distribution of selected evolutionary and functional parameters for recessive disease genes (blue) and LoF-tolerant genes (red) compared to all protein-coding genes (gray). Values are transformed to *z* scores to allow parameters to be plotted together. Boxes show interquartile range with medians indicated with a vertical black line, and whiskers terminate at the most extreme point less than 1.5 times the interquartile range from the box. For each pair of *P* values, the top value refers to the recessive versus LoF-tolerant comparison and the bottom value refers to the LoF-tolerant versus genome background comparison. Because many of the parameters are left-skewed, the medians typically fall below zero. (**B**) *P* value distribution for linear discriminant model (LDM) trained using LoF-tolerant and recessive disease genes, based on human-macaque D_N/D_S ratio and PPI network proximity to known recessive disease genes. (**C**) Receiver-operating characteristic (ROC) curve for LDM distinguishing between LoF-tolerant and recessive disease genes, both when olfactory receptor genes (ORs) are included [solid line, area under curve (AUC) = 0.831] and excluded (dashed line, AUC = 0.814). D_N/D_S, ratio of missense to synonymous substitutions; CNC GERP, GERP score for conserved noncoding elements within 50 kb of gene; PPI, protein-protein interaction.

Downloaded from www.sciencemag.org on February 16, 2012

conserved between macaque and human ($P = 1.87 \times 10^{-4}$) than genes containing only heterozygous LoF variants, suggesting greater redundancy in genes affected by high-frequency loss of function. Similarly small effects on complex disease risk have previously been noted for large, common copy-number variations, another class of variant with a high prior probability of functional impact (*23*).

Genotype imputation and case-control association studies have low power to detect associations for low-frequency variants, so further experiments involving direct genotyping of LoF variants in large disease cohorts will be required to characterize the impact of rare LoF variation on human complex disorders.

Effects of nonsense SNVs on gene expression. We examined the impact of validated nonsense SNVs on gene expression using RNA sequencing data generated from lymphoblastoid cell lines of 119 samples from two populations (*24*, *25*). Comparison of the relative expression of the LoF and functional alleles within experimentally genotyped heterozygous individuals (Fig. 2C and table S7) revealed a statistically significant reduction in expression from the LoF allele in 8/49 (16.3%) of variants with sufficient sequencing depth to be assayed. As expected, this reduction in expression is most common for variants predicted to trigger nonsense-mediated mRNA decay (NMD), a cellular process that degrades premature stop codon–containing transcripts: 7/28 (25.0%) of predicted NMD-triggering variants show significant evidence of decay, compared to 1/21 (4.8%) of predicted NMD-evading variants, and the proportion of reads mapping to the alternate allele was significantly lower for predicted NMD-triggering variants (median 0.352 versus 0.481; $P = 0.0023$). However, most predicted NMD-triggering variants have no detectable effect on gene expression.

These results provide functional confirmation of true loss of gene function for a minority of LoF variants. In addition, they demonstrate that the most widely used algorithm for NMD prediction (*26*) is an imperfect indicator of the effects of nonsense SNVs on RNA expression.

Natural selection on LoF variants. We explored whether LoF variants as a class showed evidence of recent positive selection, as expected under the "less is more" hypothesis of adaptive gene loss proposed by Olson (*27*). We examined the overlap between high-confidence LoF variants and regions showing potential signatures of positive selection using frequency spectrum and haplotype length–based tests on 1000 Genomes pilot data (*2*). In contrast to the "less is more" hypothesis, LoF variants overlapped with positively selected regions no more often than frequency-matched synonymous SNVs. However, we have identified 20 high-confidence LoF variants in candidate regions for positive selection that warrant further analysis (table S10).

In some cases, selection for gene inactivation may act through the accumulation of multiple rare LoF variants rather than increased frequency of a specific LoF allele. We identified one potential example of this: In addition to a relatively common nonsense SNV in the *CD36* gene reported to be the target of positive selection in African populations (*28*), we identified two rare, novel splice-disrupting SNVs in the same gene. All three of these variants were specific to the Yoruban (YRI) population, suggesting that multiple null alleles for *CD36* may be accumulating in African populations under the influence of selection.

Using LoF-tolerant genes to predict the probability of disease causation for novel variants. Homozygous inactivation of a gene can have a range of phenotypic effects: At one end of the spectrum are severe recessive disease genes, while at the other end are genes that can be inactivated without overt clinical impact, referred to here as LoF-tolerant genes. Clinical sequencing projects seeking to identify disease-causing mutations would benefit from improved methods to distinguish where along this spectrum each affected gene lies.

Genes homozygously inactivated in 1000 Genomes Project samples are likely to fall close to the LoF-tolerant end of the spectrum. These genes therefore represent a comparison group that can be used to define the functional and evolutionary characteristics that distinguish these genes from severe recessive disease genes.

We examined the 253 genes containing validated LoF variants that were found to be homozygous in at least one individual. These LoF-tolerant genes are significantly less conserved and have fewer protein-protein interactions than the genome average (Fig. 3A). They are also enriched for functional categories related to chemosensation, largely explained by the enrichment of olfactory receptor genes in this class (13.0% versus 1.4% genome-wide), and depleted for genes involved in embryonic development and cellular metabolism (table S8).

We then identified parameters that could be used to classify candidate genes along the disease/LoF-tolerant spectrum. We first removed olfactory receptors from the LoF-tolerant set, as these genes could be easily excluded as candidates for most severe Mendelian diseases, leaving 213 LoF-tolerant genes to compare with 858 known recessive disease genes. These two gene categories were found to display marked differences in a wide range of properties (Fig. 3A).

We developed a linear discriminant model based on human-macaque conservation and proximity to recessive disease genes in a protein-protein interaction network to classify genes into LoF-tolerant and recessive disease classes (Fig. 3, B and C). Although insufficient to definitively discriminate between the two classes, this algorithm could be used to prioritize candidates identified by sequencing recessive disease patients for replication and functional follow-up. We have calculated a recessive disease probability score for each protein-coding gene in the genome for use in such analyses (*9*).

Conclusions. Here we describe a stringently filtered catalog of variants disrupting the reading frame of human protein-coding genes, including the majority of such variants present at a population frequency of 1% or greater. Because large numbers of candidate LoF variants are present in the genomes of all individuals, but are highly enriched for a variety of sequencing and annotation errors, there is a need for caution in assigning disease-causing status to novel gene-disrupting variants found in patients. More reliable reference gene sets will help: Reference sequence and automated gene annotation errors accounted for 44.9% of candidate LoF variants in our deeply characterized individual genome, but most of these have now been corrected as a result of this project and other manual annotation efforts.

Our stringent filtering of the LoF variants found in a single high-quality human genome suggests that a typical "healthy" genome contains ~100 genuine LoF variants, with most of them carried in the heterozygous state. Given that humans (*29*) and other species (*30*) have been estimated to carry fewer than five recessive lethal alleles per genome, it seems likely that the majority of LoF variants found in an individual genome are common variants in nonessential genes, although these may still have an effect on human phenotypic variation. Nonetheless, the signature of strong purifying selection against high-confidence LoF variants as a class, and the discovery of numerous known and predicted severe recessive disease alleles, indicates that many LoF alleles with large effects on human fitness exist at low frequency in the human population. Large sequencing and genotyping projects will be required to uncover the full spectrum of these variants and their effects on human disease risk.

We have found that LoF-tolerant and recessive disease genes have differing functional and evolutionary properties, allowing us to develop a potential approach for prioritizing novel candidate recessive disease variants identified in patient samples for functional follow-up. As further examples of LoF-tolerant genes are obtained from high-throughput sequencing studies, the power of this type of classification approach is likely to grow considerably.

Finally, we note that our catalog of validated LoF variants comprises a list of naturally occurring "knockout" alleles for more than 1000 human protein-coding genes, many of which currently have little or no functional annotation attached to them. Identification and systematic phenotyping of individuals homozygous for these variants could provide valuable insight into the function of many poorly characterized human genes.

References and Notes

1. P. C. Ng *et al.*, *PLoS Genet.* **4**, e1000160 (2008).
2. The 1000 Genomes Project Consortium, *Nature* **467**, 1061 (2010).
3. K. Pelak *et al.*, *PLoS Genet.* **6**, e1001111 (2010).
4. D. G. MacArthur, C. Tyler-Smith, *Hum. Mol. Genet.* **19**, (R2), R125 (2010).
5. S. Balasubramanian *et al.*, *Genes Dev.* **25**, 1 (2011).
6. M. A. DePristo *et al.*, *Nat. Genet.* **43**, 491 (2011).

Downloaded from www.sciencemag.org on February 16, 2012

7. J. Harrow *et al.*, *Genome Biol.* **7** (suppl. 1), S4, 1 (2006).
8. http://vat.gersteinlab.org/
9. See supporting material on *Science* Online.
10. R. E. Mills *et al.*; 1000 Genomes Project, *Nature* **470**, 59 (2011).
11. A. Uzumcu *et al.*, *J. Med. Genet.* **43**, e5 (2006).
12. D. G. MacArthur *et al.*, *Nat. Genet.* **39**, 1261 (2007).
13. Y. Xue *et al.*, *Am. J. Hum. Genet.* **78**, 659 (2006).
14. Z. D. Zhang, A. Frankish, T. Hunt, J. Harrow, M. Gerstein, *Genome Biol.* **11**, R26 (2010).
15. B. Yngvadottir *et al.*, *Am. J. Hum. Genet.* **84**, 224 (2009).
16. J. R. Lupski *et al.*, *N. Engl. J. Med.* **362**, 1181 (2010).
17. J. M. Chen, D. N. Cooper, N. Chuzhanova, C. Férec, G. P. Patrinos, *Nat. Rev. Genet.* **8**, 762 (2007).
18. C. Casola, U. Zekonyte, A. D. Phillips, D. N. Cooper, M. W. Hahn, *Genome Res.* 10.1101/gr.127738.111 (2011).
19. N. Huang, I. Lee, E. M. Marcotte, M. E. Hurles, *PLoS Genet.* **6**, e1001154 (2010).
20. Y. Ishimaru *et al.*, *Proc. Natl. Acad. Sci. U.S.A.* **103**, 12569 (2006).
21. A. L. Huang *et al.*, *Nature* **442**, 934 (2006).
22. Wellcome Trust Case Control Consortium, *Nature* **447**, 661 (2007).
23. D. F. Conrad *et al.*, *Nature* **464**, 704 (2010).
24. S. B. Montgomery *et al.*, *Nature* **464**, 773 (2010).
25. J. K. Pickrell *et al.*, *Nature* **464**, 768 (2010).
26. E. Nagy, L. E. Maquat, *Trends Biochem. Sci.* **23**, 198 (1998).
27. M. V. Olson, *Am. J. Hum. Genet.* **64**, 18 (1999).
28. A. E. Fry *et al.*, *Hum. Mol. Genet.* **18**, 2683 (2009).
29. A. H. Bittles, J. V. Neel, *Nat. Genet.* **8**, 117 (1994).
30. A. R. McCune *et al.*, *Science* **296**, 2398 (2002).

Acknowledgments: T. Shah provided the Pyvoker software used for manual assignment of genotypes based on intensity clusters; S. Edkins was involved in the Sequenom validation; and the genotyping groups at Illumina, the Wellcome Trust Sanger Institute, and The Broad Institute of Harvard and MIT provided raw intensity data for the three Illumina arrays used for genotyping validation. The work performed at the Wellcome Trust Sanger Institute was supported by Wellcome Trust grant 098051; D.G.M. was supported by a fellowship from the Australian National Health and Medical Research Council; G.L. by the Wellcome Trust (090532/Z/09/Z); E.T.D. and S.B.M. by the Swiss National Science Foundation, the Louis Jeantet Foundation, and the NIH–National Institute of Mental Health GTEx fund; K.Y. by the Netherlands Organisation for Scientific Research (NWO) VENI grant 639.021.125; and H.Z., Y.L., and J.W. by a National Basic Research Program of China (973 program no. 2011CB809200), the National Natural Science Foundation of China (30725008, 30890032, 30811130531), the Chinese 863 program (2006AA02A302, 2009AA022707), the Shenzhen Municipal Government of China (grants JC200903190767A, JC200903190772A, ZYC200903240076A, CXB200903110066A, ZYC200903240077A, and ZYC200903240080A), and the Ole Rømer grant from the Danish Natural Science Research Council, as well as funding from the Shenzhen Municipal Government and the Local Government of Yantian District of Shenzhen. M.B.G. and C.T.-S. contributed equally to this work as senior authors. J.K.P. is on the scientific advisory board of 23andMe, and R.A.G. has a shared investment in Life Technologies. Raw sequence data for the 1000 Genomes pilot projects are available from www.1000genomes.org, and a curated list of the loss-of-function variants described in this manuscript is provided in the supporting online material.

Supporting Online Material

www.sciencemag.org/cgi/content/full/335/6070/823/DC1
Materials and Methods
Figs. S1 to S5
Tables S1 to S10
References (*31*–*71*)
Data Files S1 to S3

10 October 2011; accepted 11 January 2012
10.1126/science.1215040

REPORTS

Unraveling the Spin Polarization of the ν = 5/2 Fractional Quantum Hall State

L. Tiemann,[1,2]* G. Gamez,[1] N. Kumada,[1] K. Muraki[1,2]*

The fractional quantum Hall (FQH) effect at filling factor ν = 5/2 has recently come under close scrutiny, as its ground state may possess quasi-particle excitations obeying nonabelian statistics, a property sought for topologically protected quantum operations. However, its microscopic origin remains unknown, and candidate model wave functions include those with undesirable abelian statistics. We report direct measurements of the electron spin polarization of the ν = 5/2 FQH state using resistively detected nuclear magnetic resonance. We find the system to be fully polarized, which unambiguously rules out the most likely abelian contender and lends strong support for the ν = 5/2 state being nonabelian. Our measurements reveal an intrinsically different nature of interaction in the first excited Landau level underlying the physics at ν = 5/2.

When a highly correlated two-dimensional electron system (2DES) is placed under a strong perpendicular magnetic field B at low temperature, the interplay between quantum mechanics and the interelectron interaction produces spectacular effects. When the filling factor ν, the ratio between the number of electrons (n_s) and the number of magnetic flux quanta [$n_\phi = (e/h)B$; e: electron charge; h: Planck's constant], takes particular "magic" rational values p/q (p, q: integer), an energy gap forms based purely on electron correlation and makes the system's transverse (Hall) resistance invariant to small perturbations (*1*). In these fractional quantum Hall (FQH) phases, small variations of n_s or n_ϕ generate quasiparticles with a fractional charge $e^* = \pm e/q$ (*2*). The composite-fermion (CF) model (*3*), in which an electron is transformed into a fictitious particle by merging it with an even number of flux quanta, explains FQH effects for odd values of q. The most notable FQH state with an even denominator observed to date, the ν = 5/2 FQH state (*4*), cannot be described within this simple CF picture, and it has recently come under close scrutiny as it may support something even more tantalizing: a nonabelian state of matter (*5*–*7*). Charge excitations from this potential nonabelian state would be carried by quasiparticles whose interchange takes the system from one of its many ground states to another, whereas the interchange of ordinary abelian quasiparticles only adds a phase to their wave functions. This unusual property, specific to nonabelian states, is proposed as the foundation for topological quantum computation that would be robust against environmental decoherence (*8*). Both nonabelian (*5*, *9*, *10*) and abelian (*11*) states have been proposed for ν = 5/2, but experimental efforts (*12*–*16*) have not discriminated clearly between them. Two most probable wave function candidates that emerged through quasiparticle tunneling experiments on ν = 5/2 (*13*) are the nonabelian anti-Pfaffian state (*9*, *10*) and the abelian (331) state (*11*). One can discriminate between them by measuring the spin polarization of the state (*17*–*19*), as the former is fully polarized, and the latter unpolarized (*18*, *19*).

We perform this measurement using a 100-μm-wide Hall bar (Fig. 1A) with the 2DES confined to a 27-nm-wide gallium arsenide (GaAs) quantum well. A back gate enables us to tune the electron density n from 0.5×10^{15} to 4.2×10^{15} m^{-2}. At $n = 4.2 \times 10^{15}$ m^{-2}, the longitudinal resistance R_{xx} and the Hall resistance R_{xy} show a well-developed ν = 5/2 FQH state at 12 mK, along with pronounced FQH features at ν = 7/3 and 8/3, indicating a high sample quality (*20*) (Fig. 1B).

Our measurement of the spin polarization exploits the hyperfine interaction that intrinsically exists between the magnetic moments of the atoms constituting the GaAs quantum well and the spins of the electrons confined therein. When the 2DES has a nonzero spin polarization P, nuclei in contact with the 2DES experience a local magnetic field, which shifts their nuclear resonance frequency to a lower value by an amount proportional to P (Knight shift K_s). We measure K_s using the resistively detected nuclear magnetic resonance (RD-NMR) technique (*21*), where the resonant absorption of radio frequency (rf) and the resultant change in the nuclear polarization

[1]NTT Basic Research Laboratories, NTT Corporation, 3-1 Morinosato-Wakamiya, Atsugi 243-0198, Japan. [2]ERATO Nuclear Spin Electronics Project, Japan Science and Technology Agency (JST), Kawaguchi 332-0012, Japan.

*To whom correspondence should be addressed. E-mail: lars.tiemann@gmail.com (L.T.); muraki.koji@lab.ntt.co.jp (K.M.)

Downloaded from www.sciencemag.org on February 16, 2012

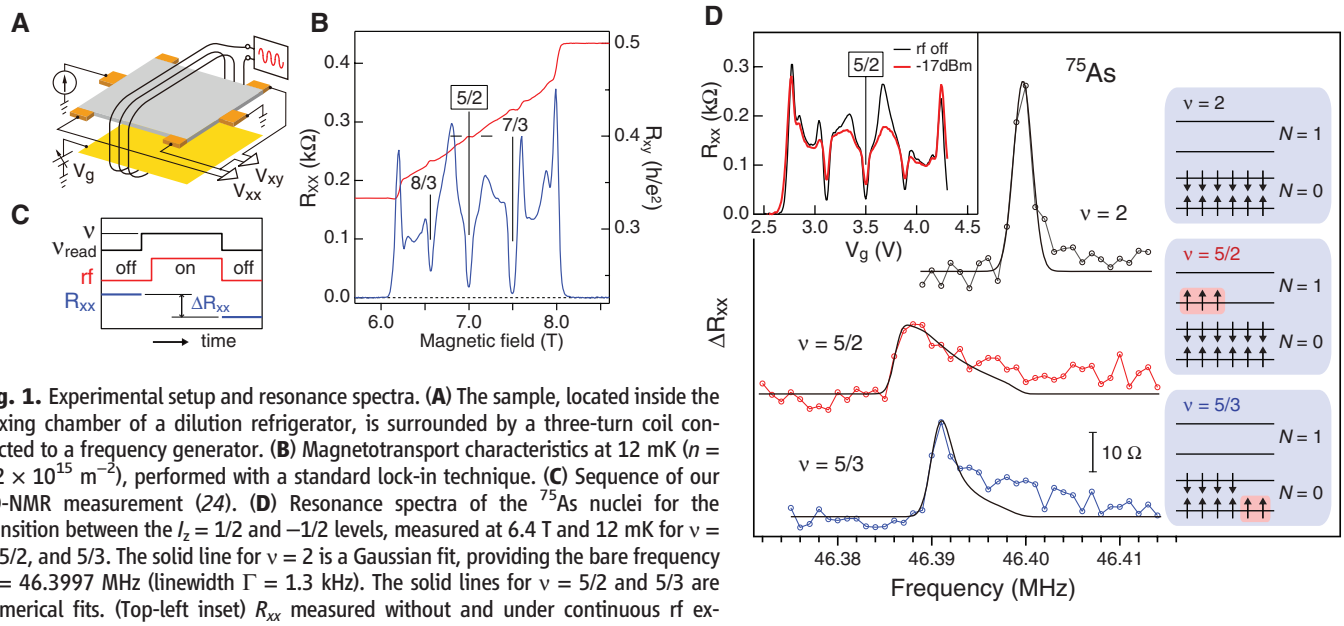

Fig. 1. Experimental setup and resonance spectra. (**A**) The sample, located inside the mixing chamber of a dilution refrigerator, is surrounded by a three-turn coil connected to a frequency generator. (**B**) Magnetotransport characteristics at 12 mK (n = 4.2 × 10^{15} m^{-2}), performed with a standard lock-in technique. (**C**) Sequence of our RD-NMR measurement (*24*). (**D**) Resonance spectra of the ^{75}As nuclei for the transition between the I_z = 1/2 and −1/2 levels, measured at 6.4 T and 12 mK for ν = 2, 5/2, and 5/3. The solid line for ν = 2 is a Gaussian fit, providing the bare frequency f_0 = 46.3997 MHz (linewidth Γ = 1.3 kHz). The solid lines for ν = 5/2 and 5/3 are numerical fits. (Top-left inset) R_{xx} measured without and under continuous rf excitation with −17 dBm, the output power we used to obtain spectra. (Right insets) LL energy diagrams and their occupations. The number of electron spins that can contribute to K_s (highlighted in red) is 1.5 times larger at ν = 5/2 than at ν = 5/3.

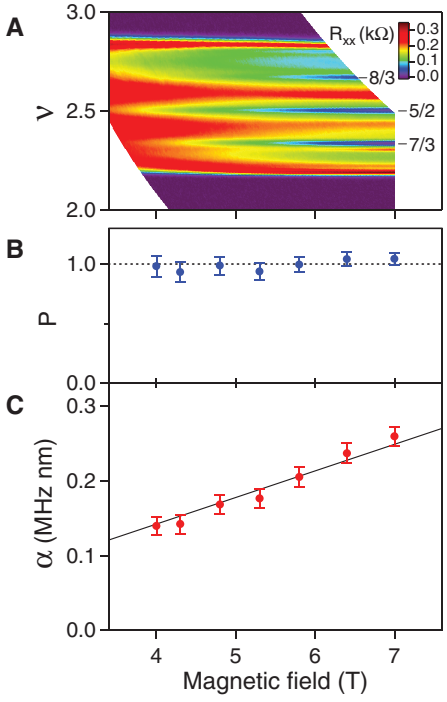

Fig. 2. Magnetic-field dependence of Knight shift and spin polarization at ν = 5/2. (**A**) Mapping of R_{xx} plotted as a function of B and ν. (**B**) Polarization calculated as $P = \alpha/\alpha_{full}(B)$. (**C**) Parameter α deduced from the fitting of resonance spectra measured at ν = 5/2 at different values of B. The solid line represents a function $\alpha_{full}(B) \propto B$ obtained from a linear fit. [For the estimation of error bars, see (*24*).]

$\langle I_z \rangle$ are detected as a change in R_{xx} that originates from the coupling between $\langle I_z \rangle$ and the electron Zeeman energy $E_Z \propto (B + b_0 \cdot \langle I_z \rangle)$ mediated by the hyperfine interaction (b_0: constant). To deduce P from the NMR spectrum measured at ν = 5/2, we also measure states with known spin polarizations at ν = 2 and 5/3 at the same B, from which the bare unshifted resonance frequency of the nuclei and the proportionality factor between P and K_s are deduced. Standard RD-NMR, however, is not directly applicable: At ν = 2 and 5/3, R_{xx} is zero, whereas at ν = 5/2, it only showed nonresonant heating effects. We therefore use the back gate to switch to a different filling factor ν_{read} with finite R_{xx} and sensitivity to read out the resonant rf absorption at ν as a change in R_{xx} at ν_{read} (Fig. 1C) (*22*). We used ν_{read} = 0.59 to 0.65, where R_{xx} becomes highly sensitive to tiny perturbations in E_Z due to the competition between differently spin-polarized FQH ground states (*23*, *24*). The ν = 5/2 FQH state remains well developed during our NMR measurements (Fig. 1D).

Figure 1D shows resonance spectra of the ^{75}As nuclei measured for three different filling factors at 6.4 T. The top spectrum was measured at ν = 2, where the 2DES is unpolarized because equal numbers of spin-up and spin-down electrons fill the two lowest Landau (LL) levels, (N = 0, ↑) and (N = 0, ↓) (right inset). The peak's center thus marks the unshifted resonance frequency of the ^{75}As nuclei. When RD-NMR is performed at ν = 5/2 (= 2 + 1/2), we find that the resulting resonance spectrum is Knight shifted to a lower frequency, indicating a nonzero polarization. We compare the ν = 5/2 spectrum with the spectrum at ν = 5/3 (= 2 − 1/3), a FQH state whose effective spin polarization is equal to that of the fully polarized ν = 1/3 Laughlin state (*2*). We accessed different values of ν by changing the number of electrons while keeping B constant. Thus, the Knight shift for ν = 5/2 should be 1.5 times larger than that for ν = 5/3, if both states are fully polarized (right insets).

For an accurate determination of the spin polarization, we take account of the spectral shape for each ν. The spectra for ν = 5/2 and 5/3 are asymmetrically broadened, reflecting the local electron density (determined by the probability density of the subband wave function $|\Psi_\nu(z)|^2$) that varies along the z direction. We fit these spectra by calculating the Knight shift $K_s(z) = \alpha_\nu \cdot |\Psi_\nu(z)|^2$ for each nucleus and then integrating over z, with α_ν the fitting parameter representing the size of the Knight shift (*24*). Taking the electron densities contributing to the polarization into account, we find that $\alpha_{5/2}/\alpha_{5/3}$ = 1.56 obtained from the fit corresponds to a polarization ratio of $P_{5/2}/P_{5/3}$ = 1.04. This clearly shows that the ν = 5/2 FQH state is fully polarized.

An open question is whether the ν = 5/2 FQH state remains fully polarized as the Zeeman energy is decreased. When we fit the ν = 5/2 spectra measured at different values of B, the obtained parameter α follows a linear function reflecting the density of electrons contributing to K_S that is proportional to B (Fig. 2C). This result indicates that the polarization is constant, independent of the Zeeman energy between 4.0 and 7.0 T (Fig. 2B). Mapping R_{xx} over the same range of B shows that the ν = 5/2 FQH minimum evolves continuously (Fig. 2A). The absence of a singularity is consistent with the system being polarized over the entire density range.

With these measurements, which provide direct evidence of full polarization at ν = 5/2, we are able to exclude all unpolarized or partially polarized states as the correct description of the ν = 5/2 state. Moreover, we can unambiguously rule out the abelian (331) state (*11*), which had remained one of the most likely candidates through quasiparticle tunneling experiments (*13*). Other abelian models had already been ruled

Downloaded from www.sciencemag.org on February 16, 2012

out (*13*). Therefore, the remaining most likely models contain only nonabelian states, the anti-Pfaffian state (*9*, *10*), its particle-hole conjugate the Pfaffian state (*5*), and the $U(1) \times SU_2(2)$ state (*25*), which are all spin polarized and therefore consistent with our results. Although recent optical experiments suggest an unpolarized system (*26*) or partially polarized domains developing at $\nu = 5/2$ (*27*), its true ground state, as we have shown, is fully spin polarized (supplementary online text).

To better understand the physics behind the $\nu = 5/2$ FQH state and its polarization, we have explored other states in the $N = 1$ and $N = 0$ LLs (Fig. 3A) and mapped out the entire range of experimentally accessible ν at 6.4 T (Fig. 3, B and C). In the $N = 0$ LL between $\nu = 2$ and 1/3, α exhibits a complicated oscillatory pattern reflecting the various CF ground states (*28*). The dashed line in Fig. 3C represents the value of α expected for full polarization at each value of ν, calculated on the basis of three data points near $\nu = 5/3$. In addition to $\nu = 5/3$, other fully polarized quantum Hall states such as $\nu = 1$, 2/5, and 1/3 show maxima approaching the line of full polarization (*24*), whereas unpolarized FQH states such as $\nu = 4/3$ exhibit minima approaching zero. By contrast, in the $N = 1$ LL, α increases linearly for $\nu \geq 2.2$ across $\nu = 7/3$, 5/2, and up to 8/3, indicating that the system is fully polarized over the range investigated here (Fig. 3B).

Because this measurement is performed at constant B, neither the Zeeman energy ($\propto B$) nor its ratio to the Coulomb energy ($\propto B^{1/2}$) can account for these qualitative differences between the $N = 0$ and $N = 1$ LLs. Thus, the contrasting behavior reflects the character of the interparticle interaction (*29*). Notable examples can be found at half fillings. CFs do not pair up at and near $\nu = 1/2$ or 3/2 due to the strong repulsion at short distances (*30*), and the system is well described as a compressible Fermi sea of CFs, which naturally accounts for its partial polarization (*28*). At $\nu = 5/2$, the weak repulsion at short distances is believed to be essential for the pairing of CFs and the formation of the $\nu = 5/2$ FQH state (*30*, *31*).

The properties of unpaired CFs at $\nu = 5/2$, the parent state of the $\nu = 5/2$ FQH state, can be examined through RD-NMR measurements at elevated temperatures (Fig. 4B). Although the $\nu = 5/2$ FQH state has vanished at 150 mK (Fig. 4A), its polarization is unaffected and remains nearly maximal up to 200 mK, before it starts to gradually drop (Fig. 4C), in contrast to the polarization at $\nu = 3/2$ being constant. The robustness of the high polarization to temperature is seen in the entire $N = 1$ LL (Fig. 4D). Fitting the data in Fig. 4C by using a simple noninteracting CF model (*32*) yields a CF effective mass m_{CF} of $(2.68 \pm 0.24)m_e$ and $(0.71 \pm 0.05)m_e$ for $\nu = 5/2$ and 3/2, respectively (m_e: electron mass in vacuum). In this simple picture, the high spin polarization is explained in terms of the large m_{CF} in the $N = 1$ LL, making the Fermi level smaller than E_Z. It is thus tempting to consider the large m_{CF} to be

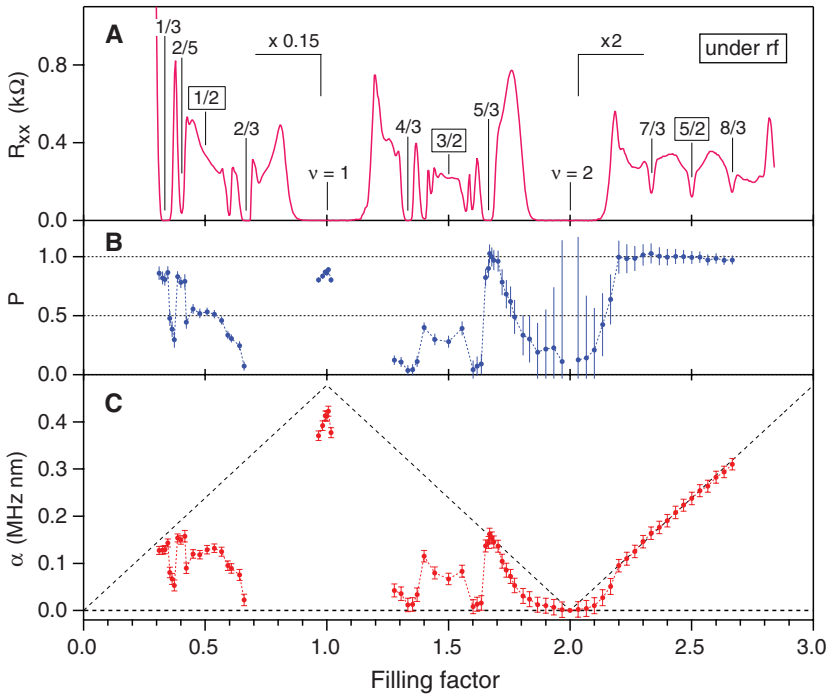

Fig. 3. RD-NMR at different filling factors. (**A**) R_{xx} measured under continuous application of rf with the same power (–17 dBm) as used for the RD-NMR measurement. (**B**) Polarization P calculated as $P = \alpha/\alpha_{full}(\nu)$. (**C**) Parameter α deduced from fitting the spectra (e.g., fig. S2) measured at 6.4 T and 12 mK. The dashed line represents the value $\alpha_{full}(\nu)$ expected for full polarization at each value of ν (*24*).

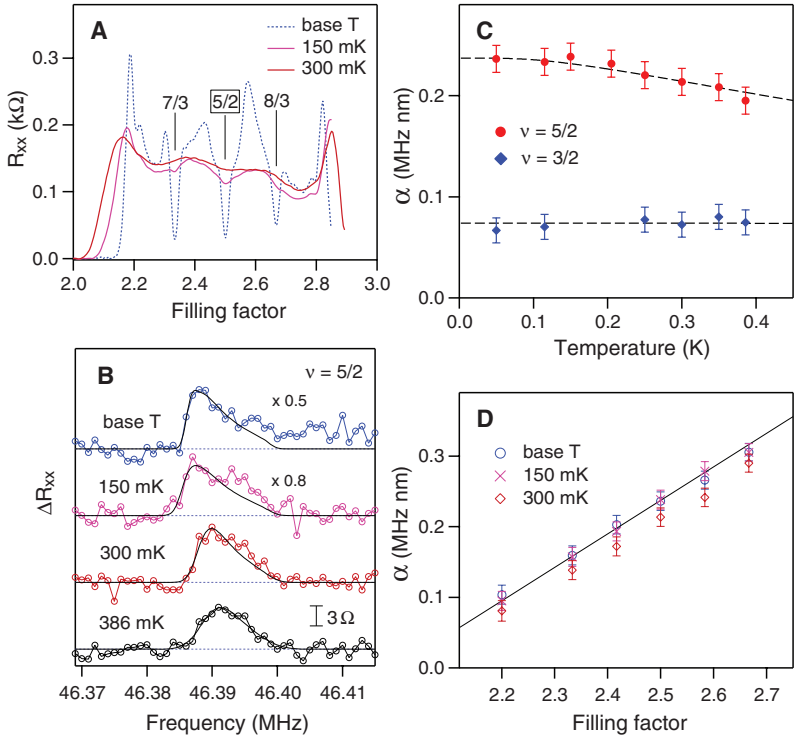

Fig. 4. Temperature dependence of Knight shift and polarization. (**A**) Magnetotransport characteristics at different temperatures and 6.4 T. (**B**) Resonance spectra measured at $\nu = 5/2$ at different temperatures. (**C**) Parameter α deduced from the fitting of resonance spectra measured at $\nu = 5/2$ and 3/2 at different temperatures. The dashed line represents a fitting based on a noninteracting CF model (*24*, *32*). (**D**) Parameter α for various values of ν in the $N = 1$ LL at different temperatures. The solid line represents the value expected for full polarization as determined from the data in Fig. 3C.

Downloaded from www.sciencemag.org on February 16, 2012

essential in the pairing of CFs and the formation of the ν = 5/2 FQH state at low temperature.

Our NMR experiments have demonstrated maximal spin polarization for the ν = 5/2 FQH state over a wide range of electron densities. These measurements are consistent with the nonabelian Pfaffian state (*5*) and the anti-Pfaffian state (*9*, *10*), while unambiguously ruling out the unpolarized (331) state (*11*), which had been the most likely abelian contender (*13*). However, the exciting prospect of topologically protected quantum operations using the ν = 5/2 FQH state awaits a direct experimental demonstration of its nonabelian nature.

References and Notes

1. D. C. Tsui, H. L. Stormer, A. C. Gossard, *Phys. Rev. Lett.* **48**, 1559 (1982).
2. R. B. Laughlin, *Phys. Rev. Lett.* **50**, 1395 (1983).
3. J. K. Jain, *Phys. Rev. Lett.* **63**, 199 (1989).
4. R. L. Willett *et al.*, *Phys. Rev. Lett.* **59**, 1776 (1987).
5. G. Moore, N. Read, *Nucl. Phys. B* **360**, 362 (1991).
6. M. Greiter, X. G. Wen, F. Wilczek, *Nucl. Phys. B* **374**, 567 (1992).
7. C. Nayak, F. Wilczek, *Nucl. Phys. B* **479**, 529 (1996).
8. C. Nayak, S. H. Simon, A. Stern, M. Freedman, S. Das Sarma, *Rev. Mod. Phys.* **80**, 1083 (2008).
9. M. Levin, B. I. Halperin, B. Rosenow, *Phys. Rev. Lett.* **99**, 236806 (2007).
10. S.-S. Lee, S. Ryu, C. Nayak, M. P. A. Fisher, *Phys. Rev. Lett.* **99**, 236807 (2007).
11. B. Halperin, *Helv. Phys. Acta* **56**, 75 (1983).
12. M. Dolev, M. Heiblum, V. Umansky, A. Stern, D. Mahalu, *Nature* **452**, 829 (2008).
13. I. P. Radu *et al.*, *Science* **320**, 899 (2008).
14. R. L. Willett, L. N. Pfeiffer, K. W. West, *Proc. Natl. Acad. Sci. U.S.A.* **106**, 8853 (2009).
15. V. Venkatachalam, A. Yacoby, L. Pfeiffer, K. West, *Nature* **469**, 185 (2011).
16. A. Bid *et al.*, *Nature* **466**, 585 (2010).
17. R. Morf, *Phys. Rev. Lett.* **80**, 1505 (1998).
18. I. Dimov, B. I. Halperin, C. Nayak, *Phys. Rev. Lett.* **100**, 126804 (2008).
19. A. E. Feiguin, E. Rezayi, K. Yang, C. Nayak, S. Das Sarma, *Phys. Rev. B* **79**, 115322 (2009).
20. G. Gamez, K. Muraki, ν=5/2 fractional quantum Hall state in low-mobility electron systems: Different roles of disorder; available at http://arxiv.org/abs/1101.5856 (2011).
21. W. Desrat *et al.*, *Phys. Rev. Lett.* **88**, 256807 (2002).
22. N. Kumada, K. Muraki, Y. Hirayama, *Phys. Rev. Lett.* **99**, 076805 (2007).
23. J. H. Smet *et al.*, *Nature* **415**, 281 (2002).
24. Materials and methods are available as supporting material on *Science* Online.
25. X. G. Wen, *Phys. Rev. Lett.* **66**, 802 (1991).
26. M. Stern *et al.*, *Phys. Rev. Lett.* **105**, 096801 (2010).
27. T. D. Rhone *et al.*, *Phys. Rev. Lett.* **106**, 196805 (2011).
28. I. V. Kukushkin, K. von Klitzing, K. Eberl, *Phys. Rev. Lett.* **82**, 3665 (1999).
29. F. D. M. Haldane, *Phys. Rev. Lett.* **51**, 605 (1983).
30. V. W. Scarola, K. Park, J. K. Jain, *Nature* **406**, 863 (2000).
31. N. Read, D. Green, *Phys. Rev. B* **61**, 10267 (2000).
32. N. Freytag, M. Horvatić, C. Berthier, M. Shayegan, L. P. Lévy, *Phys. Rev. Lett.* **89**, 246804 (2002).

Author contributions: L.T. performed all the RD-NMR and transport measurements presented in this paper. G.G. performed transport measurements to optimize the samples. N.K. advised on the RD-NMR measurements. K.M. grew heterostructures and fabricated samples. L.T. and K.M. analyzed the data and wrote the paper.

Supporting Online Material

www.sciencemag.org/cgi/content/full/science.1216697/DC1
Materials and Methods
Supplementary Text
Figs. S1 and S2
References (*33*–*45*)

2 August 2011; accepted 19 January 2012
Published online 26 January 2012;
10.1126/science.1216697

A Logic-Gated Nanorobot for Targeted Transport of Molecular Payloads

Shawn M. Douglas,* Ido Bachelet,* George M. Church†

We describe an autonomous DNA nanorobot capable of transporting molecular payloads to cells, sensing cell surface inputs for conditional, triggered activation, and reconfiguring its structure for payload delivery. The device can be loaded with a variety of materials in a highly organized fashion and is controlled by an aptamer-encoded logic gate, enabling it to respond to a wide array of cues. We implemented several different logical AND gates and demonstrate their efficacy in selective regulation of nanorobot function. As a proof of principle, nanorobots loaded with combinations of antibody fragments were used in two different types of cell-signaling stimulation in tissue culture. Our prototype could inspire new designs with different selectivities and biologically active payloads for cell-targeting tasks.

The DNA origami method (*1*), in which a multiple-kilobase single-stranded "scaffold" is folded into a custom shape by interaction with hundreds of oligonucleotide "staple" strands, has proved to be extremely versatile for creating custom two- and three-dimensional assemblies (*2*–*4*) that can template precise arrangement of diverse components (*5*–*7*). DNA can also be used to construct devices that perform robotic tasks such as sensing, computation, and actuation (*8*–*11*). Recently, a three-dimensional DNA origami box integrating both structural and computational components was described (*12*). Inspired by these advances, we sought to design a robotic DNA device capable of selectively interfacing with cells to deliver signaling molecules to cell surfaces.

Using cadnano, a computer-aided design tool for DNA origami (*13*), we created a nanorobot in the form of a hexagonal barrel with dimensions of 35 nm × 35 nm × 45 nm. The barrel consists of two domains that are covalently attached in the rear by single-stranded scaffold hinges, and can be noncovalently fastened in the front by staples modified with DNA aptamer–based locks (Fig. 1A). Initial self-assembly proceeds in a one-pot reaction in which 196 oligonucleotide staple strands direct a 7308-base filamentous phage–derived scaffold strand into its target shape during a thermal-annealing ramp of rapid heating followed by slow cooling (*14*).

A clasp system based on DNA locks and DNA keys was previously used to control the opening of the lid on a DNA box (*12*). To operate our device in response to proteins, we designed a DNA aptamer–based lock mechanism that opens in response to binding antigen keys (Fig. 1, B and C). Our lock system was inspired by aptamer beacons (*15*) and structure-switching aptamers (*16*), which typically undergo target-induced switching between an aptamer-complement duplex and an aptamer-target complex. We incorporated aptamer-complement duplexes on the left and right sides of the front of the barrel, such that the aptamer strands are attached to one domain and partially complementary strands are attached to the other domain. When both aptamers recognize their targets, the lock duplexes dissociate, and the nanorobot—acting as an entropic spring—undergoes a drastic reconfiguration to expose its previously sequestered surfaces. We found that shorter duplexes gave better sensitivity and faster activation rates, but at a cost of increased spontaneous activation (see text S2). We chose a lock duplex length of 23 base pairs (bp) for subsequent experiments because it displayed similar sensitivity to a shorter 16-bp duplex (activation at 10 pM) without the unacceptable loss in sensitivity observed for longer duplexes (30, 37, and 44 bp required 1 nM).

Payloads that were premodified by covalent attachment to the 5′ end of a 15-base single-stranded DNA oligonucleotide linker were loaded inside the nanorobot. To enable multivalent interaction with surface receptors for potent cell stimulation (*17*), we aimed to load at least two payload molecules per robot. Twelve payload attachment sites were arranged in an inward-facing ring in the middle of the barrel (Fig. 1, A and C) to enable different payload orientations and spacings. The sites are staple strands with 3′ extensions

Wyss Institute for Biologically Inspired Engineering and Department of Genetics, Harvard Medical School, Boston, MA 02115, USA.

*These authors contributed equally to this work.
†To whom correspondence should be addressed. E-mail: http://arep.med.harvard.edu/gmc/email.html

Downloaded from www.sciencemag.org on February 16, 2012

that are complementary to a linker sequence attached to the intended cargo (Fig. 1D). After nanorobot folding and purification, cargo loading was carried out by adding linker-modified payload in molar excess to attachment sites and incubating at room temperature for 12 hours. Two types of cargo were loaded: 5-nm gold nanoparticles covalently attached to 5′-thiol–modified linkers (*18*), and various Fab′ antibody fragments that were covalently attached to 5′-amine–modified linkers using a HyNic/4FB coupling kit (Solulink, San Diego, California). We used negative-stain transmission electron microscopy (TEM) to analyze the device in closed and open states, with and without cargo (Fig. 1F). We observed by manual counting that on average four attachment sites were populated when loading gold nanoparticles, and three sites were populated when loading antibody fragments (fig. S11).

One obstacle to overcome in constructing a "spring-loaded" device was to ensure assembly to high yield in its closed state. Like hands that set a mousetrap, two "guide" staples were incorporated adjacent to the lock sites that span the top and bottom domains of the device (Fig. 1E). The guide staples include 8-base toehold overhangs and could be removed after folding and purification steps by adding a 10:1 excess of fully complementary strands to the mixture (*19*). We observed that folding with the aid of guide staples increased the yield of closed robots from 48% to 97.5%, as assessed by manual counting of nanorobots images by TEM (fig. S17).

To examine nanorobot function, we selected a payload such that robot activation would be coupled to labeling of an activating cell (Fig. 2A). Robots loaded with fluorescently labeled antibody fragments against human leukocyte antigen (HLA)–A/B/C were mixed with different cell types expressing human HLA-A/B/C and various "key" combinations (described below) and were analyzed by flow cytometry. In the absence of the correct combination of keys, the robot remained inactive. In the inactive state, the sequestered antibody fragments were not able to bind the cell surface, resulting in a baseline fluorescence signal. However, when the robot encountered the proper combination of antigen keys, it was freed to open and bind to the cell surface via its antibody payload, causing an increase in fluorescence. We used key-neutralizing antibodies in competitive inhibition control experiments to verify that nanorobots were not activated by a non–ligand-based mechanism (fig. S25).

The robot could be programmed to activate in response to a single type of key by using the same aptamer sequence in both lock sites. Alternatively, different aptamer sequences could be encoded in the locks to recognize two inputs. Both locks needed to be opened simultaneously to activate the robot. The robot remained inactive when only one of the two locks was opened. The lock mechanism is thus equivalent to a logical AND gate, with possible inputs of cell surface antigens not binding or binding (0 or 1, respectively) to aptamer locks, and possible outputs of remaining closed or a conformational rearrangement to expose the payload (0 or 1, respectively) (Fig. 2B).

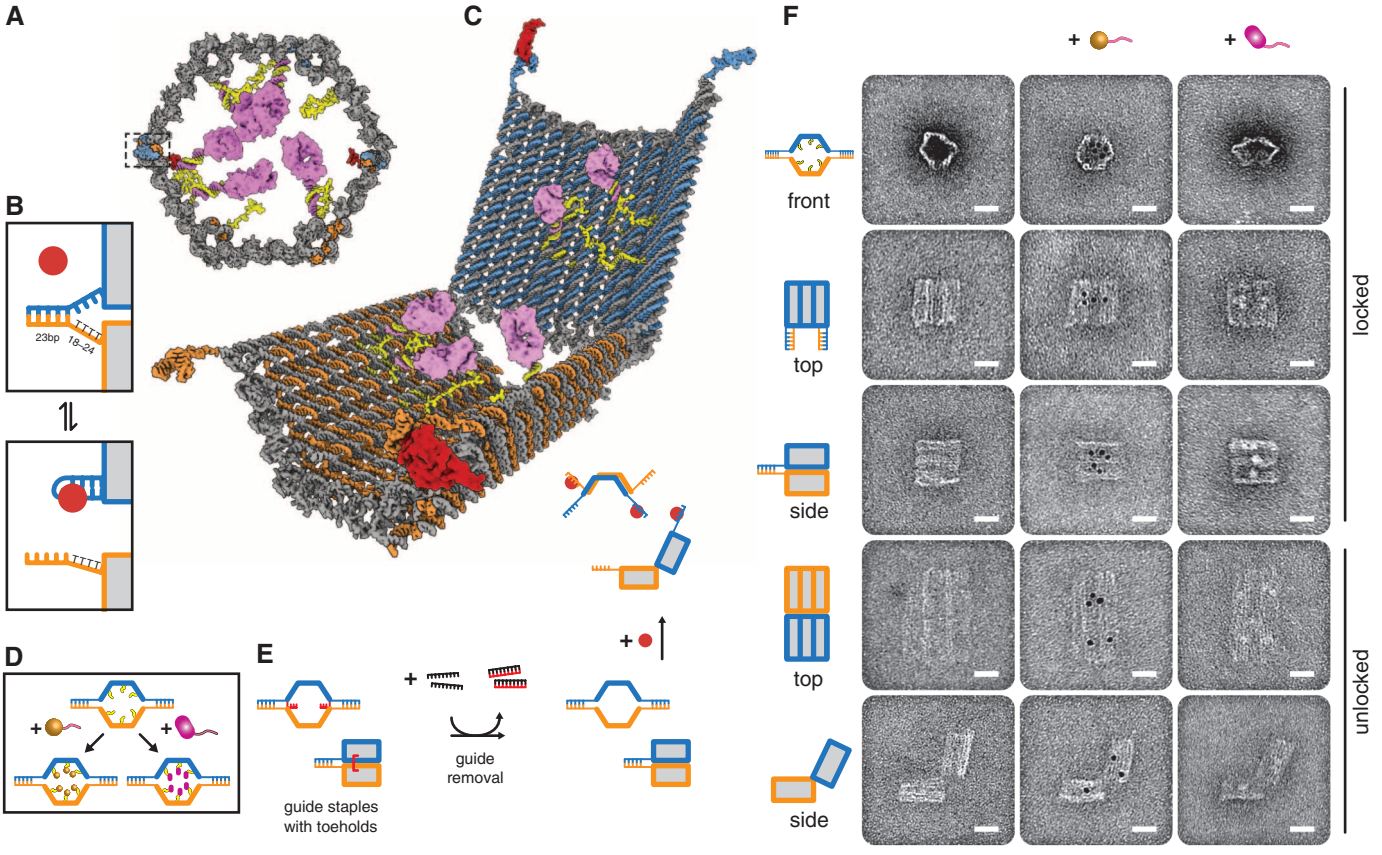

Fig. 1. Design and TEM analysis of aptamer-gated DNA nanorobot. (**A**) Schematic front orthographic view of closed nanorobot loaded with a protein payload. Two DNA-aptamer locks fasten the front of the device on the left (boxed) and right. (**B**) Aptamer lock mechanism, consisting of a DNA aptamer (blue) and a partially complementary strand (orange). The lock can be stabilized in a dissociated state by its antigen key (red). Unless otherwise noted, the lock duplex length is 24 bp, with an 18- to 24-base thymine spacer in the nonaptamer strand. (**C**) Perspective view of nanorobot opened by protein displacement of aptamer locks. The two domains (blue and orange) are constrained in the rear by scaffold hinges. (**D**) Payloads such as gold nanoparticles (gold) and antibody Fab′ fragments (magenta) can be loaded inside the nanorobot. (**E**) Front and side views show guide staples (red) bearing 8-base toeholds aid assembly of nanorobot to 97.5% yield in closed state as assessed by manual counting. After folding, guide staples are removed by addition of fully complementary oligos (black). Nanorobots can be subsequently activated by interaction with antigen keys (red). (**F**) TEM images of robots in closed and open conformations. Left column, unloaded; center column, robots loaded with 5-nm gold nanoparticles; right column, robots loaded with Fab′ fragments. Scale bars, 20 nm.

Downloaded from www.sciencemag.org on February 16, 2012

To test the generality and robustness of the aptamer-encoded logic gating, we designed six different robots using pairwise combinations of aptamer locks drawn from a set of three well-characterized aptamer sequences: 41t, against platelet-derived growth factor (PDGF) (*20*), shown in red; TE17 (*21*), shown in yellow; and sgc8c (*22*), shown in blue (Fig. 2C). The six robot versions—plus a permanently locked negative control and a no-lock positive control—were loaded with fluorescently labeled antibody to human HLA-A/B/C Fab′ and used to probe six different cell lines, each expressing different profiles of the "key" antigens recognized by the three chosen aptamers. A Burkitt's lymphoma cell line (Ramos) activated none of the robots. An acute myeloid leukemia cell line (Kasumi-1) activated all robots. A third cell line, isolated from a patient with large granular lymphocytic leukemia, aggressive NK type (NKL) (*23*), activated robots with two 41t locks, two TE17 locks, and with one 41t and one TE17 lock. The baseline negative signal for NKL cells was higher than other cell lines because of NKL background fluorescence. A fourth cell line, isolated from acute T cell leukemia (Jurkat), activated robots bearing two TE17 locks, two sgc8c locks, as well as one TE17 lock and one sgc8c lock. The fifth line was isolated from acute lymphoblastic leukemia (CCRF-CEM) and had a similar profile to Jurkat cells. Finally, a neuroblastoma cell line (SH-SY5Y) activated robots with two sgc8c locks. The lower intensity of the positive signals in the neuroblastoma cell line may be caused by the lower level of surface HLA-A/B/C expressed on these cells, and fluorescence intensities may be affected in general by expression levels of both aptamer keys and antibody payload targets.

We further examined the performance of the logic-gating mechanism in three ways. First, we tested the ability of the robot to selectively bind to a single cell type ($NKL^{PTK7+/+}$) in a mixed population of two cell types ($NKL^{PTK7+/+}$ and Ramos).

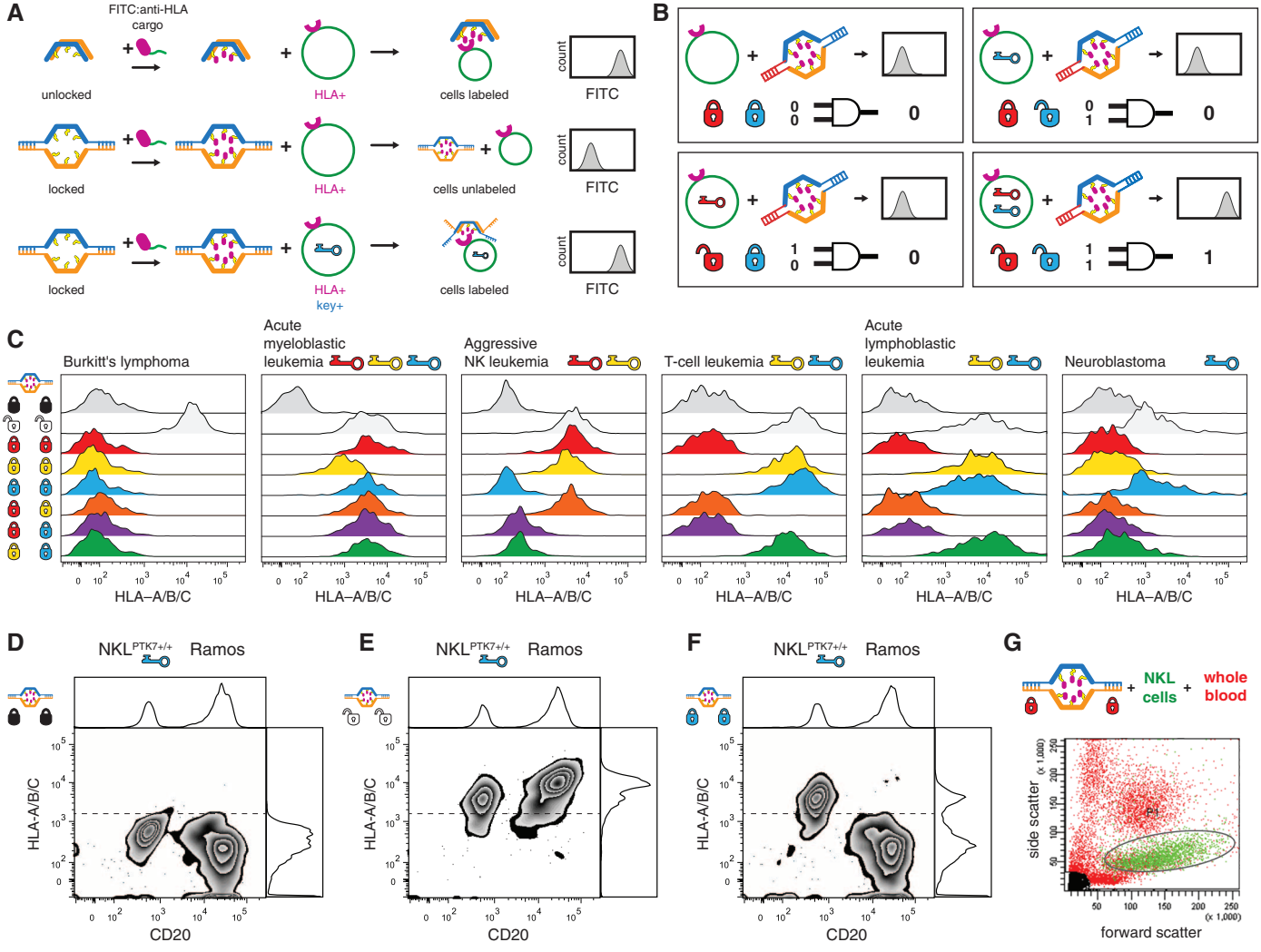

Fig. 2. Analysis of logic-gated nanorobot activation by different cell types. (**A**) Experimental scheme. Nanorobots were loaded with fluorescently labeled antibody Fab′ fragments to human HLA-A/B/C. In their unlocked state, nanorobots will bind to any cell expressing the HLA-A/B/C antigen (top). They remain inactive in the presence of key^- cells (middle) but activate upon engaging key^+ cells (bottom). (**B**) Truth table for nanorobot activation. The aptamer-encoded locks function as an AND gate responding to molecular inputs (keys) expressed by cells. Color match indicates lock-and-key match. Aptamer-antigen activation state serves as input; output is manifested as nanorobot conformation. (**C**) Eight different nanorobot versions (10 to 100 fmol, loaded with anti–HLA-A/B/C antibody fragments at a molar excess of 20) were tested with six different cell types expressing various combinations of antigen keys by incubating for 5 hours. Each histogram displays the count of cells versus fluorescence due to anti–HLA-A/B/C labeling. (**D**) NKL cells (50,000 per sample, with transiently induced expression of PTK7 ($NKL^{PTK7+/+}$), Ramos cells (100,000 per sample), fluorescein isothiocyanate (FITC)–labeled antibody to human CD20 (0.1 μg/ml), and permanently locked robots loaded with allophycocyanin–labeled antibody to human HLA-A/B/C Fab′ were incubated at room temperature for 5 hours. No labeling is observed, as locked robots remain inactive. (**E**) Unlocked robots react with both cell populations. (**F**) sgc8c-gated robots react only with the cell population expressing the PTK7 key. (**G**) Forward- versus side-scatter dot plot of 4:1 mixture of healthy human whole-blood leukocytes and NKL cells. Nanorobots loaded with anti-CD33 Fab′ payload and gated with 41t locks selectively label NKL cells. Off-target binding occurred in 0.6% of sampled cells.

Downloaded from www.sciencemag.org on February 16, 2012

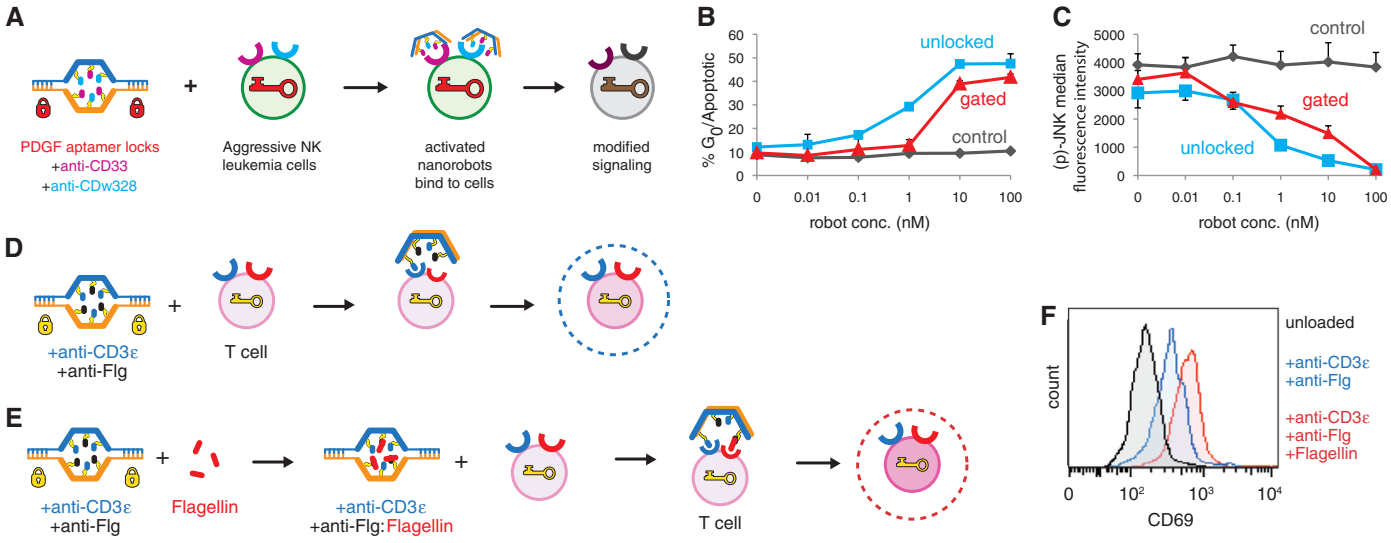

Fig. 3. Nanorobots manipulate target cell signaling. (**A**) Experimental scheme. A single dose of nanorobots loaded with an equal mixture of antibody to human CD33 and antibody to human CDw328/Siglec-7 Fab′ fragments (cyan and magenta, respectively, each at a molar excess of 10 over nanorobots) and gated by 41t locks recognizing platelet-derived growth factor (PDGF) were used to treat NKL cells at various concentrations (0 to 100 nM). Phosphorylation of JNK was measured after 72 hours by intracellular flow cytometry. (**B**) NKL cells (10,000 per sample) treated with nanorobots were analyzed after 72 hours for cell cycle distribution by propidium iodide (5 μg/ml). (**C**) Phosphorylation level of JNK as a function of robot concentration (lowest, 0; highest, 100 nM) after 72 hours. Error bars for (B) and (C) represent SEM of two biological replicates. (**D** and **E**) Incremental activation of T cells by nanorobots loaded with antibody to human CD3ε (blue) and antibody to flagellin Fab′ (black). Nanorobots (50 nM) with (E) and without (D) pre-incubation with flagellin (red; 100 pg/ml) were reacted with Jurkat T cells (pink) for 1 hour at 37°C. (**F**) Histograms showing T cell activation after nanorobot treatment, as measured by labeling with FITC-labeled antibody to CD69.

Three versions of the robot were tested: a permanently closed version in which the guide staples were not removed, an open version in which no guide staples or aptamer locks were included, and a gated version using two sgc8c locks, which we expected to target only the PTK7-expressing NKL cells (Fig. 2, D to F, and figs. S22 and S23). The gated version discriminated between the two cell types, only binding to NKL cells. Second, to further simulate physiological conditions, we mixed NKL cells with healthy whole-blood leukocytes and found that robots gated with 41t locks discriminated those NKL cells with high precision (Fig. 2G and fig. S19). Third, we examined the sensitivity of the nanorobots to cell concentration using a background of 1e6 Ramos cells, tested for the ability of an sgc8c-gated robot to bind to Jurkat$^{PTK7+/+}$ cells. Nanorobots were activated for every cell count, from 1e6 cells down to the single-cell level (fig. S24).

Finally, we investigated the ability of an activated robot to interface with cells and stimulate their signaling in separate inhibition and activation tasks. We first chose to target NKL cells using a pair of 41t locks, and loaded the robots with a combination of antibody to human CD33 and antibody to human CDw328 Fab′ fragments, which have been shown to induce growth arrest in leukemic cells (*24*). The robots induced growth arrest in NKL cells in a dose-dependent fashion (Fig. 3, A and B). The robots suppressed Jun N-terminal kinase (JNK) (Fig. 3C) and Akt (protein kinase B) signaling in this process (fig. S27). We then used T cells to test various methods of signaling pathway activation (Fig. 3, D to F). Robots loaded with combinations of antibody to human CD3ε Fab′ and antibody to flagellin Fab′ were mixed with T cells and found to induce activation (Fig. 3, D and F). Previous work has shown that flagellin can augment T cell activation (*25*). We found that our nanorobots were able to collect flagellin from a 100 pg/ml solution and induce augmented T cell activation (Fig. 3, E and F). These findings demonstrate that the robots can induce a variety of tunable changes in cell behavior. Furthermore, biologically active payloads may be bound indirectly via interactions with antibody fragments, enabling applications in which the robot carries out a scavenging task before targeted payload delivery.

References and Notes

1. P. W. K. Rothemund, *Nature* **440**, 297 (2006).
2. Y. Ke *et al.*, *Nano Lett.* **9**, 2445 (2009).
3. S. M. Douglas *et al.*, *Nature* **459**, 414 (2009).
4. H. Dietz, S. M. Douglas, W. M. Shih, *Science* **325**, 725 (2009).
5. A. Kuzuya *et al.*, *ChemBioChem* **10**, 1811 (2009).
6. N. V. Voigt *et al.*, *Nat. Nanotechnol.* **5**, 200 (2010).
7. N. Stephanopoulos *et al.*, *Nano Lett.* **10**, 2714 (2010).
8. M. N. Stojanovic, D. Stefanovic, *Nat. Biotechnol.* **21**, 1069 (2003).
9. G. Seelig, D. Soloveichik, D. Y. Zhang, E. Winfree, *Science* **314**, 1585 (2006).
10. Y. Benenson, B. Gil, U. Ben-Dor, R. Adar, E. Shapiro, *Nature* **429**, 423 (2004).
11. B. Ding, N. C. Seeman, *Science* **314**, 1583 (2006).
12. E. S. Andersen *et al.*, *Nature* **459**, 73 (2009).
13. S. M. Douglas *et al.*, *Nucleic Acids Res.* **37**, 5001 (2009).
14. See supporting material on *Science* Online.
15. N. Hamaguchi, A. Ellington, M. Stanton, *Anal. Biochem.* **294**, 126 (2001).
16. R. Nutiu, Y. Li, *J. Am. Chem. Soc.* **125**, 4771 (2003).
17. J. J. Boniface *et al.*, *Immunity* **9**, 459 (1998).
18. A. P. Alivisatos *et al.*, *Nature* **382**, 609 (1996).
19. B. Yurke, A. J. Turberfield, A. P. Mills Jr., F. C. Simmel, J. L. Neumann, *Nature* **406**, 605 (2000).
20. L. S. Green *et al.*, *Biochemistry* **35**, 14413 (1996).
21. Z. Tang *et al.*, *Anal. Chem.* **79**, 4900 (2007).
22. Y. F. Huang *et al.*, *ChemBioChem* **10**, 862 (2009).
23. M. J. Robertson *et al.*, *Exp. Hematol.* **24**, 406 (1996).
24. C. Vitale *et al.*, *Proc. Natl. Acad. Sci. U.S.A.* **98**, 5764 (2001).
25. Z. Ye, C. M. L. Lee, G. W. Sun, Y. H. Gan, *Infect. Immun.* **76**, 2541 (2008).

Acknowledgments: We thank J. Ritz for providing NKL cells; C. Reynolds for technical assistance with NKL cells; C. Strong and G. McGill for assistance with 3D visualization using Molecular Maya; A. Marblestone for helpful discussions; and J. Markson for comments on the manuscript. S.M.D. holds a Career Award at the Scientific Interface from the Burroughs Wellcome Fund and a Wyss Technology Development Fellowship, and I.B. is supported by a fellowship from the Life Sciences Research Foundation. S.M.D. and I.B. designed and performed the experiments and analyzed the data; S.M.D., I.B., and G.M.C. wrote the manuscript.

Supporting Online Material

www.sciencemag.org/cgi/content/full/335/6070/831/DC1
Materials and Methods
SOM Text
Figs. S1 to S27
Table S1

16 September 2011; accepted 12 January 2012
10.1126/science.1214081

Downloaded from www.sciencemag.org on February 16, 2012

Supported Iron Nanoparticles as Catalysts for Sustainable Production of Lower Olefins

Hirsa M. Torres Galvis,[1] Johannes H. Bitter,[1] Chaitanya B. Khare,[2] Matthijs Ruitenbeek,[2] A. Iulian Dugulan,[3] Krijn P. de Jong[1]*

Lower olefins are key building blocks for the manufacture of plastics, cosmetics, and drugs. Traditionally, olefins with two to four carbons are produced by steam cracking of crude oil–derived naphtha, but there is a pressing need for alternative feedstocks and processes in view of supply limitations and of environmental issues. Although the Fischer-Tropsch synthesis has long offered a means to convert coal, biomass, and natural gas into hydrocarbon derivatives through the intermediacy of synthesis gas (a mixture of molecular hydrogen and carbon monoxide), selectivity toward lower olefins tends to be low. We report on the conversion of synthesis gas to C_2 through C_4 olefins with selectivity up to 60 weight percent, using catalysts that constitute iron nanoparticles (promoted by sulfur plus sodium) homogeneously dispersed on weakly interactive α-alumina or carbon nanofiber supports.

Lower olefins (C_2 to C_4) are extensively used in the chemical industry as building blocks to synthesize a wide range of products such as polymers, solvents, drugs, cosmetics, and detergents. Traditionally, lower olefins have been produced by thermal or catalytic cracking of naphtha or vacuum gas oil (*1*) or from dehydrogenation of alkanes (*2*, *3*), but environmental and economic factors are currently spurring exploration of alternative routes for their production.

In recent years there has been growing interest in the development of biomass as a renewable feedstock for the production of commodity compounds (*4*, *5*). Pyrolized biomass or bio-oil can be converted catalytically to lower olefins with moderate selectivity (43% C) (*5*), although other compounds such as aromatics are also produced. Schemes put forward to produce lower olefins from synthesis gas (syngas)—a mixture of H_2 and CO obtained through biomass gasification—consist of at least two conversion steps, which involve either cracking of Fischer-Tropsch (FT)–derived hydrocarbons (*6*) or the methanol to olefins (MTO) process (*7*). Here, we consider Fischer-Tropsch to olefins (FTO) as a direct route, without intermediate steps, to transform syngas into light olefins.

For several decades, research groups have attempted to develop iron-based catalysts to direct product selectivity of the FT synthesis toward light olefins (*8*, *9*). Relative to other FT catalysts such as cobalt, iron disfavors competing formation of methane, and furthermore catalyzes the water-gas shift reaction, enabling the use of a CO-rich syngas feed without an H_2/CO ratio adjustment. Mainly unsupported (sometimes referred to as bulk) iron oxide catalysts have been investigated (*9*–*12*), and in some cases they have exhibited high selectivities toward lower olefins (up to 70 wt %) when the iron was modified by the addition of promoters (*9*). Despite these promising results, however, the bulk iron catalysts are mechanically unstable when the reaction is performed at high temperature, which is necessary to steer product selectivity to lighter hydrocarbons. Under these conditions, the undesirable Boudouard reaction, $2CO(g) \rightarrow C(s) + CO_2(g)$ (*13*), leads to the deposition of carbon, which can block the active sites and induce fragmentation of the particles in bulk iron catalysts (*14*). The poor mechanical stability of the bulk iron oxide catalysts may lead to plugging of the catalyst bed in fixed-bed operation or to fouling of separation equipment in a fluidized-bed process.

Supported iron catalysts display enhanced dispersion of the active phase and may withstand the mechanical degradation that threatens bulk iron catalysts. Research on supported iron catalysts (*15*–*21*) has met with limited success, however. Barrault *et al.* (*15*) found that iron dispersed on alumina with high surface area displayed much lower activity than did iron dispersed on alumina with low surface area. This finding points to a key aspect of supported iron catalysts—that is, their cumbersome activation. If highly dispersed iron oxide interacts strongly with an oxidic support with high surface area, the conversion of iron oxide into the active phase (iron carbide) is impeded (*14*). Other supports for iron-based FTO catalysts in addition to alumina (*15*, *16*) have been explored, such as zeolites (*18*), aluminophosphate molecular sieves (*19*), and carbonaceous materials (*20*, *21*). Table S1 summarizes the most relevant results reported in the literature regarding the development of carbon- or alumina-supported iron catalysts for the selective production of lower olefins. Iron supported on activated carbon displayed a high catalytic activity, but this was accompanied by low selectivity to light olefins (*20*) or a high deactivation rate (*21*). Many years of research have shown that supported iron catalysts display an inverse relationship between activity and selectivity (*15*).

To overcome the low activity and mechanical stability problems, we explored the use of support materials weakly interactive toward iron. As a working hypothesis, we posited that these inert supports would impart mechanical stability to the iron nanoparticles without inhibiting their activation. In particular, nanostructured carbon materials (*22*), such as carbon nanofibers (CNF) (*23*, *24*) and carbon nanotubes (*25*), boast high specific surface area, chemical inertness, and good mechanical strength.

In addition to CNF, we explored β-silicon carbide (β-SiC) and α-alumina (α-Al_2O_3) as supports. For comparison, we also examined three bulk

[1]Inorganic Chemistry and Catalysis, Debye Institute for Nanomaterials Science, Utrecht University, P.O. Box 80083, 3508 TB Utrecht, Netherlands. [2]DOW Benelux B.V., P.O. Box 48, 4530 AA Terneuzen, Netherlands. [3]Fundamental Aspects of Materials and Energy Group, Delft University of Technology, 2629 JB Delft, Netherlands.

*To whom correspondence should be addressed. E-mail: k.p.dejong@uu.nl

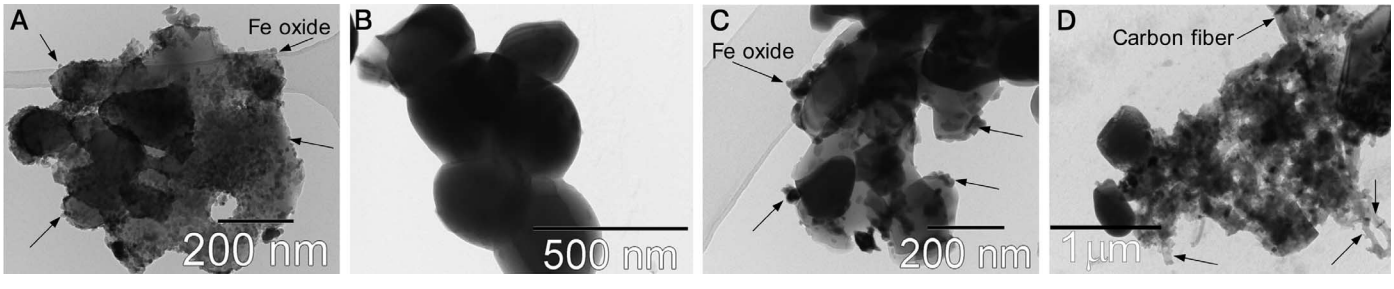

Fig. 1. TEM images of fresh and spent Fe catalysts. (**A** and **B**) The images from the fresh Fe/α-Al_2O_3 catalysts (A) show a homogeneous distribution of iron oxide nanoparticles on the support, whereas the bulk Fe-Ti-Zn-K catalyst (B) is mainly composed of aggregates of iron oxide crystals. (**C** and **D**) In images of the spent catalysts after 64 hours of reaction at 340°C, 20 bar, and a H_2/CO ratio of 1, the Fe/α-Al_2O_3 (C) showed sintering of Fe particles after reaction; the bulk spent catalyst (D) fragmented and manifested carbon fiber growth (indicated by arrows).

Downloaded from www.sciencemag.org on February 16, 2012

iron catalysts (one unpromoted and two promoted) and iron supported on conventional high-surface-area SiO_2 and γ-Al_2O_3. The supported Fe catalysts were prepared using ammonium iron citrate as precursor with a nominal iron loading of 10 wt %, whereas the bulk catalysts had an iron content higher than 30 wt % (table S2). The ammonium iron citrate used in the preparation of the supported samples contained low amounts of sulfur and sodium and efficiently introduced these promoters in the catalysts (table S3).

The use of ammonium iron citrate as the metal precursor provides a homogeneous distribution of the iron nanoparticles on the support, in contrast to the extensive clustering that is observed when using iron nitrate (*26*). Fe nanoparticle aggregation could lead to low catalytic activity and high methane selectivity, as observed when using bulk iron catalysts. Transmission electron microscopy (TEM) was used to determine the size of the iron oxide particles and their distribution on the support.

Figure 1A shows a representative TEM micrograph of the calcined Fe/α-Al_2O_3, which exhibited a homogeneous distribution of iron oxide particles (arrows). The Fe_2O_3 particle size distribution (fig. S2) was 14 ± 5 nm on this support and 5 ± 1 nm on CNF. The bulk promoted catalyst (Fe-Ti-Zn-K) consisted of large Fe_2O_3 particles (average size 400 nm), which formed aggregates resembling grape bunches (Fig. 1B).

The volume-averaged Fe_2O_3 crystallite size of the Fe catalyst precursors was calculated with the Scherrer equation using the parameters obtained by x-ray diffraction analysis (fig. S3 and table S2). Fe/SiO_2, Fe/γ-Al_2O_3, and Fe/β-SiC did not show the characteristic diffraction lines from iron oxide, indicating that the Fe_2O_3 was amorphous or that the crystallites were smaller than 4 nm (fig. S3).

The fresh catalysts were also analyzed by Mössbauer spectroscopy to determine the composition of the iron phase (tables S4 and S5). Iron was present in the form of hematite (α-Fe_2O_3) in all samples. A superparamagnetic (SPM) iron oxide phase (α-Fe_2O_3 SPM) was measured in Fe_2O_3 particles smaller than 13.5 nm (table S4 and accompanying text). Iron was highly dispersed on CNF, γ-Al_2O_3, and SiO_2, as evidenced by the presence of SPM nanoparticles exclusively. The iron oxide particles on α-Al_2O_3 and β-SiC had a broader size distribution, whereas the bulk Fe-Ti-Zn-K catalyst was primarily composed of large Fe_2O_3 particles.

The supported and bulk Fe catalysts were tested in the FT reaction at 1 bar and 350°C at low CO conversion (0.5 to 1%) to restrict secondary hydrogenation of olefins (Table 1 and fig. S4). Catalytic activity is expressed as iron time yield (i.e., the number of CO moles converted to hydrocarbons per gram of iron per second). A high initial activity was observed for Fe/β-SiC and Fe/CNF. The activity of Fe/CNF decreased continuously during the 15 hours of reaction; the activity of the Fe/β-SiC catalyst increased during the first 5 hours of reaction, then decreased slowly afterward (fig. S4A). Fe/α-Al_2O_3 exhibited a lower catalytic activity than Fe/CNF and Fe/β-SiC; however, it showed remarkable stability, as the activity remained constant over 15 hours. Fe/γ-Al_2O_3 and Fe/SiO_2 displayed a low catalytic activity, comparable to the bulk Fe catalysts (fig. S4B). The Fe-Cu-K-SiO_2 catalysts showed an initial activity approximately 4 times that of the Fe-Ti-Zn-K catalyst. Nevertheless, the iron time yield decreased rapidly to achieve comparable values after 15 hours of reaction.

One of the most important requirements for an FTO catalyst is to obtain the maximum production of the lower-olefins fraction while limiting methane selectivity to the lowest level possible. Fe/CNF and Fe/α-Al_2O_3 exhibited high selectivity toward lower olefins (~60% C) while directing comparatively little carbon to methane (<25% C)

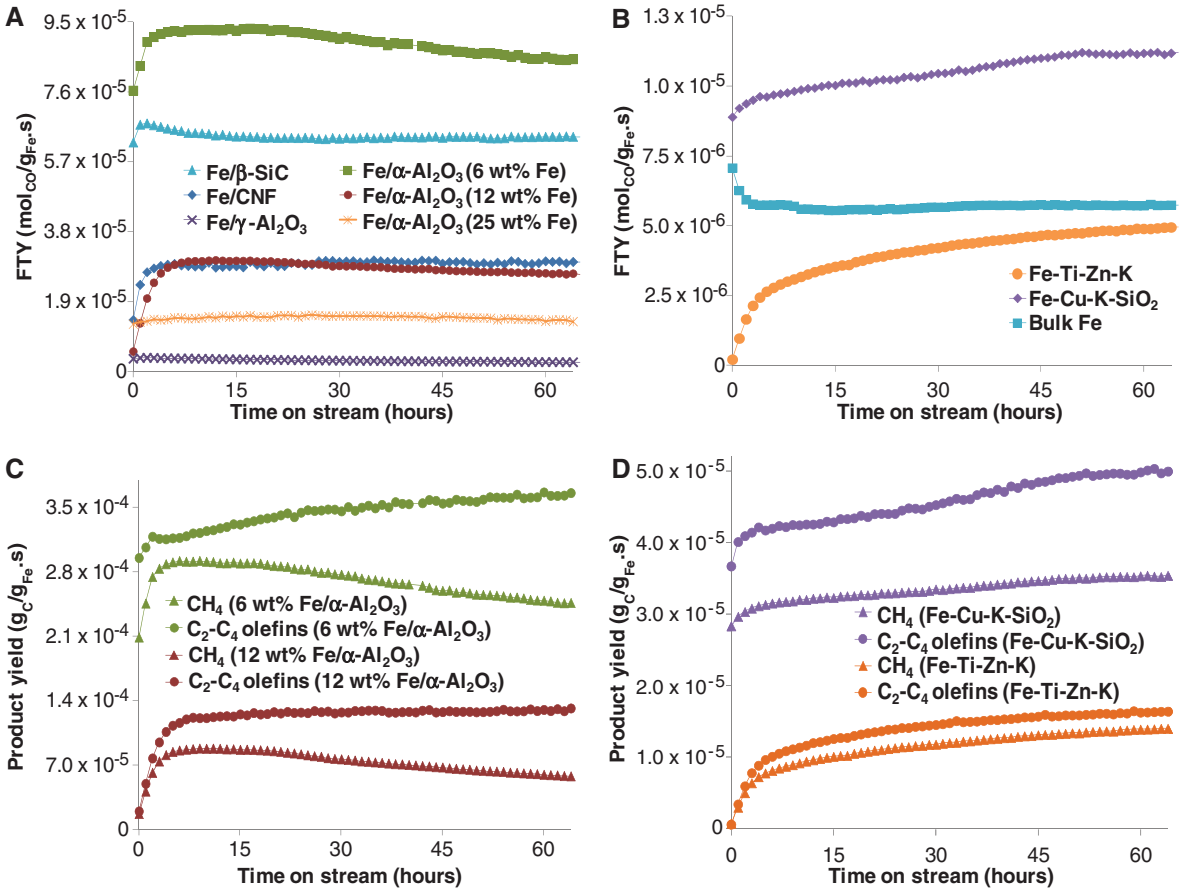

Fig. 2. (**A** to **D**) Catalytic performance of iron catalysts for the FTO process at 20 bar. Catalytic tests were carried out at T = 340°C, P = 20 bar, and a H_2/CO ratio of 1. Iron time yield is plotted above as a function of time for (A) Fe-supported catalysts and (B) bulk Fe catalysts. Methane and lower olefins yields are plotted below as a function of time for (C) Fe-supported catalysts and (D) bulk Fe catalysts. The product yields were obtained at CO conversion levels between 70 and 80%.

Downloaded from www.sciencemag.org on February 16, 2012

(Table 1). Fe/β-SiC and Fe/SiO_2 also showed high selectivity to C_2 through C_4 olefins, but the CH_4 product fraction was higher than 30% C. Fe/γ-Al_2O_3 and the bulk catalysts displayed a high selectivity to methane (>40% C), which is not desirable for their application in the FTO process.

Additional tests were carried out at 20 bar, 340°C, and an H_2/CO ratio of 1 to observe the performance of supported and bulk Fe catalysts under industrially relevant conditions (Fig. 2). In view of the promising results obtained at 1 bar, we prepared and tested additional α-Al_2O_3–supported catalysts with different iron loadings (6 and 25 wt % Fe) to study the effect of iron content on catalytic performance. Most of the catalysts showed an initial increase in activity, except for the unpromoted bulk Fe (Fig. 2B), which exhibited a decrease in activity during the first 10 hours of reaction before reaching stability. After an initial activation period, Fe/β-SiC, Fe/CNF, 25 wt % Fe/α-Al_2O_3, and Fe/γ-Al_2O_3 showed a stable catalytic activity for 60 hours. A slight decrease in activity during reaction was observed for the 6 wt % and 12 wt % Fe/α-Al_2O_3 catalysts, mainly resulting from a continuous drop in CH_4 production (Fig. 2C). The stability maintained during 60 hours fully complies with the requirements for the application of these catalysts in fluidized-bed reactors. In view of their favorable heat transfer characteristics, it is expected that these reactors will be preferred in industrial applications of the exothermic FTO process.

Table 1. Product selectivity and catalytic activity at 1 bar. Catalytic tests were performed at 350°C and a H_2/CO ratio of 1; results after 15 hours on stream are shown (CO conversion: 0.5 to 1.0%). The product mixture that was analyzed consisted of C_1 to C_{16} hydrocarbons. Iron time yield (FTY) represents moles of CO converted to hydrocarbons per mol of Fe per second; %C is defined as carbon atoms in a product with respect to the total number of C atoms in the hydrocarbon mixture. CO_2 was not measured.

Sample	FTY (10^{-6} mol_{CO}/g_{Fe}·s)	Selectivity (%C)			
		CH_4	C_2–C_4 olefins	C_2–C_4 paraffins	C_{5+}
Fe/CNF	1.41	23	61	4	12
Fe/α-Al_2O_3 (12 wt % Fe)	0.65	22	61	4	13
Fe/β-SiC	6.52	31	58	4	7
Fe/SiO_2	0.14	38	56	5	1
Fe/γ-Al_2O_3	0.07	54	44	2	0
Fe-Ti-Zn-K	0.13	83	16	1	0
Fe-Cu-K-SiO_2	0.20	43	46	2	9
Bulk Fe	0.08	76	21	2	1

Table 2. Catalytic performance at 20 bar. Catalytic tests were performed at 340°C and a H_2/CO ratio of 1; results after 64 hours on stream are shown. The product mixture that was analyzed consisted of C_1 to C_{10} hydrocarbons. FTY and selectivity are defined as in Table 1. The selectivities were calculated on hydrocarbons produced; CO conversions and CO_2 selectivities are reported in table S6.

Sample	FTY (10^{-5} mol_{CO}/g_{Fe}·s)	Selectivity (%C)				
		CH_4	C_2–C_4 olefins	C_2–C_4 paraffins	C_{5+}	Oxygenates
Fe/CNF	2.98	13	52	12	18	5
Fe/α-Al_2O_3 (6 wt % Fe)	8.48	24	35	21	10	10
Fe/α-Al_2O_3 (12 wt % Fe)	2.66	17	39	19	14	11
Fe/α-Al_2O_3 (25 wt % Fe)	1.35	11	53	6	21	9
Fe/β-SiC	6.38	35	19	39	4	3
Fe/γ-Al_2O_3	0.25	49	33	11	1	6
Fe-Ti-Zn-K	0.49	24	28	29	10	9
Fe-Cu-K-SiO_2	1.12	26	36	12	18	8
Bulk Fe	0.57	30	32	18	14	6

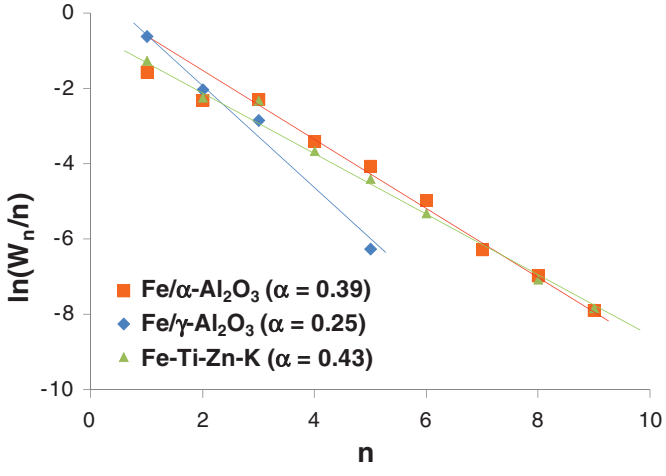

Fig. 3. Comparison of ASF plots for supported and bulk catalysts. The ASF plots are based on the product distribution obtained when performing the FT reaction at 20 bar, 340°C, and a H_2/CO ratio of 1 after 64 hours time on stream. Fe/α-Al_2O_3 has an iron loading of 12 wt %; *n* is the number of carbon atoms in a product, and W_n is the weight fraction of the product with carbon number equal to *n*.

Table 2 summarizes the activities and product selectivities measured after 64 hours of reaction at 20 bar. The CO_2 selectivity for all the samples was approximately 40% on the basis of CO converted, except for Fe/γ-Al_2O_3 (table S6). Under the selected reaction conditions, most of the catalysts had comparable CO conversion levels (77 to 81%; table S6). However, the Fe/γ-Al_2O_3 catalyst only achieved a CO conversion of 10%. The promoted catalysts prepared using supports with low interaction with iron showed high catalytic activities combined with high selectivities to the desired products. Fe/CNF and 25 wt % Fe/α-Al_2O_3 exhibited high selectivities toward C_2 through C_4 olefins (>50% C) while yielding a methane product fraction lower than 15% C. The Fe-Cu-K-SiO_2 catalyst showed a catalytic activity comparable to the 25 wt % Fe/α-Al_2O_3; however, only moderate selectivities toward lower olefins were obtained.

The Anderson-Schulz-Flory model (eq. S2) that is used to predict the product distribution indicates that the maximum selectivity achievable for the C_2-C_4 fraction, including olefins and paraffins, is approximately 50 wt %, at a chain growth probability (α) between 0.4 and 0.5, as shown in fig. S5. This model predicts that methane selectivity is about 30 wt % when this maximum C_2-C_4 selectivity is reached.

Anderson-Schulz-Flory (ASF) plots (Fig. 3 and fig. S6) show that the catalysts prepared using inert supports provide α values of ~0.4, close to the optimal value for maximum lower-olefins production. Moreover, the plots in Fig. 3 revealed lower methane selectivities relative to the values predicted from the ASF model. This can be rationalized from the simplified "surface carbide" or "alkyl" mechanism (fig. S1), which is widely accepted for the FT synthesis (*13*). In this model, following CO dissociation and carbon hydrogenation, a CH_3 group adsorbed on the catalyst surface is proposed to act as a chain initiator. The carbon chain grows by the addition of methylene monomer units (CH_2) to the adsorbed alkyl species. The chain growth is terminated by β-hydride abstraction to form α-olefins or by hydrogenation to produce paraffins. Negative deviations from the ASF prediction for methane selectivity can be expected when using iron catalysts modified

Downloaded from www.sciencemag.org on February 16, 2012

with promoters that limit the hydrogenation reactions (*8*), thus favoring chain growth and the termination step via β-hydride abstraction that cannot give rise to CH_4 production. The suppression of the methanation reaction induced by the promoters was only observed when using CNF or α-Al_2O_3 because these "inert" supports are thought to favor the proximity between iron and promoters (Na plus S), in contrast to reactive supports such as γ-Al_2O_3 that lead to more methane (Fig. 3). In the case of the bulk catalysts, CH_4 selectivities coincided with the values predicted by the ASF model or were slightly above.

Mössbauer spectroscopy of the spent catalysts after reaction at 1 bar (table S5) showed that the nature of the iron phases varied when using different support materials. Although some of the iron carbides may be oxidized after exposure to air, Fe_xC_y was detected on the samples with moderate to high catalytic activity. In contrast, the samples with the lowest catalytic activity, Fe/SiO_2 and Fe/γ-Al_2O_3, did not contain any carbides. A strong metal-support interaction clearly inhibits the formation of catalytically active iron carbides, as observed for conventional high-surface-area support materials. Note that in the size range of iron particles dispersed on inert supports (7 to 20 nm), particle size effects seem to be minimal.

TEM performed on spent catalysts revealed that the iron nanoparticles in the supported samples increased in size. The particle size distributions of the fresh and spent Fe/α-Al_2O_3 and Fe/CNF are shown in fig. S2. For Fe/CNF, changes in the catalytic activity were only observed during the first 4 hours of reaction, which suggests that the changes in the catalyst structure took place during catalyst activation and initial usage. In the case of Fe/α-Al_2O_3, the average iron nanoparticle size increased from 14 ± 5 nm to 17 ± 5 nm (Fig. 1C). The promoted bulk iron oxide showed extensive particle fragmentation and carbon filament growth, which brings about the poor mechanical stability of this catalyst (Fig. 1D).

The spent catalysts were characterized with thermogravimetric analysis to determine the extent of carbon lay-down. Carbon burn-off experiments were performed for all the samples, except for the Fe/CNF catalyst. Although extensive carbon deposition on the samples after reaction with CO-rich syngas and high temperatures could be expected, most of the samples exhibited low solid carbon formation. After 64 hours of reaction at 340°C and 20 bar, the levels of carbon lay-down measured on the spent catalysts were lower than 10 wt %. In contrast, Fe/α-Al_2O_3 (25 wt % Fe) and Fe-Cu-K-SiO_2 exhibited a higher extent of coke formation (23 wt % and 40 wt %, respectively).

The FTO process represents a strong alternative route for the sustainable production of lower olefins from biomass-derived synthesis gas. The industrial potential of this process is greatly enhanced by the reported development of active, selective, and mechanically stable catalysts that consist of promoted iron nanoparticles dispersed on weakly interactive supports. Further suppression of methane production, maximization of the C_2-C_4 olefins fraction, and reduction of carbon lay-down by addition of promoters and by optimization of physical properties (e.g., Fe particle size, distribution of Fe nanoparticles on the support) will allow us to further understand and develop the performance of these catalysts.

References and Notes

1. A. Corma, F. V. Melo, L. Sauvanaud, F. Ortega, *Catal. Today* **107–108**, 699 (2005).
2. R. Diercks *et al.*, *Chem. Eng. Technol.* **31**, 631 (2008).
3. S. Wang, Z. H. Zhu, *Energy Fuels* **18**, 1126 (2004).
4. E. L. Kunkes *et al.*, *Science* **322**, 417 (2008).
5. T. P. Vispute, H. Zhang, A. Sanna, R. Xiao, G. W. Huber, *Science* **330**, 1222 (2010).
6. X. Dupain, R. A. Krul, C. J. Schaverien, M. Makkee, J. A. Moulijn, *Appl. Catal. B* **63**, 277 (2006).
7. G. A. Olah, *Angew. Chem. Int. Ed.* **44**, 2636 (2005).
8. C. Wang, L. Xu, Q. Wang, *J. Nat. Gas Chem.* **12**, 10 (2003).
9. B. Büssemeier, C. D. Frohning, G. Horn, W. Kluy, U.S. Patent 4564642 (1986).
10. B. H. Davis, *Catal. Today* **84**, 83 (2003).
11. S. Soled, E. Iglesia, R. A. Fiato, *Catal. Lett.* **7**, 271 (1990).
12. Y. Jin, A. K. Datye, *J. Catal.* **196**, 8 (2000).
13. A. P. Steynberg, M. E. Dry, Eds., *Fischer-Tropsch Technology* (Elsevier, Amsterdam, 2004).
14. M. D. Shroff *et al.*, *J. Catal.* **156**, 185 (1995).
15. J. Barrault, C. Forquy, J. C. Menezo, R. Maurel, *React. Kinet. Catal. Lett.* **15**, 153 (1980).
16. B. G. Baker, N. J. Clark, H. MacArthur, E. Summerville, U.S. Patent 4610975 (1986).
17. D. B. Bukur *et al.*, *Ind. Eng. Chem. Res.* **29**, 1588 (1990).
18. L. Xu, Q. Wang, Y. Xu, J. Huang, *Catal. Lett.* **31**, 253 (1995).
19. M. L. Cubeiro *et al.*, *Appl. Catal. A* **167**, 183 (1998).
20. V. K. Jones, L. R. Neubauer, C. H. Bartholomew, *J. Phys. Chem.* **90**, 4832 (1986).
21. A. P. B. Sommen, F. Stoop, K. van der Wiele, *Appl. Catal.* **14**, 277 (1985).
22. K. P. de Jong, *Oil Gas Sci. Technol.* **61**, 527 (2006).
23. K. P. de Jong, J. W. Geus, *Catal. Rev., Sci. Eng.* **42**, 481 (2000).
24. E. van Steen, F. F. Prinsloo, *Catal. Today* **71**, 327 (2002).
25. W. Chen, Z. Fan, X. Pan, X. Bao, *J. Am. Chem. Soc.* **130**, 9414 (2008).
26. A. J. van Dillen, R. J. A. M. Terörde, D. J. Lensveld, J. W. Geus, K. P. de Jong, *J. Catal.* **216**, 257 (2003).

Acknowledgments: Supported by ACTS-ASPECT (NWO) and by NWO-TOP and NRSCC. We thank M. Van de Vijver for the catalytic tests at 20 bar performed at DOW Benelux, E. J. M. Hensen for his contribution in the discussion of the Mössbauer spectroscopy results, and C. van der Spek for the TEM images. ACTS-ASPECT (NWO) has filed a patent application based on the work reported here.

Supporting Online Material

www.sciencemag.org/cgi/content/full/335/6070/835/DC1
Materials and Methods
Eqs. S1 and S2
Tables S1 to S6
Figs. S1 to S6
References (*27–35*)

21 October 2011; accepted 6 January 2012
10.1126/science.1215614

Plate Motions and Stresses from Global Dynamic Models

Attreyee Ghosh* and William E. Holt

Delineating the driving forces behind plate motions is important for understanding the processes that have shaped Earth throughout its history. However, the accurate prediction of plate motions, boundary-zone deformation, rigidity, and stresses remains a difficult frontier in numerical modeling. We present a global dynamic model that produces a good fit to such parameters by accounting for lateral viscosity variations in the top 200 kilometers of Earth, together with forces associated with topography and lithosphere structure, as well as coupling with mantle flow. The relative importance of shallow structure versus deeper mantle flow varies over Earth's surface. Our model reveals where mantle flow contributes toward driving or resisting plate motions. Furthermore, subducted slabs need not act as strong stress guides to satisfy global observations of plate motions and stress.

Predicting plate motions correctly, along with stresses within the plates, has been a challenge for global dynamic models. Accurate predictions are vitally important for understanding the forces responsible for the movement of plates, mountain building, rifting of continents, and strain accumulation released in earthquakes. Previous studies have investigated these driving forces by either predicting stresses in the plates alone (*1*, *2*) or plate motions alone (*3*–*5*). Other studies have taken the important step of predicting both plate motions and stresses in a single model (*6*–*8*). However, in addition to predicting plate motions, a successful global dynamic model must also explain plate rigidity and plate boundary-zone deformation, as well as intraplate stress patterns. Furthermore, the presence of lateral viscosity variations within the top 200 km of Earth influences the coupling between lithosphere and mantle convection. A systematic investigation of this influence is needed to improve our understanding of the driving mechanisms for plate tectonics.

Geosciences Department, Stony Brook University, Stony Brook, NY 11794, USA.

*To whom correspondence should be addressed. E-mail: atreig@gmail.com

Downloaded from www.sciencemag.org on February 16, 2012

We used global dynamic models to investigate the influence of lateral viscosity variations in the lithosphere and asthenosphere on both surface motions and stresses within the plates and plate boundary zones. Our models include incorporation of the effects of topography and lithosphere structure and a lithosphere coupled with whole-mantle convection, driven by density buoyancies within the mantle. Our modeling reveals the lateral viscosity variations that are necessary for matching observations. The results further emphasize the relative contributions of (i) topography and lithosphere structure and (ii) coupling with whole-mantle convection, both of which vary over Earth's surface.

We solved the three-dimensional (3D) force balance equations after depth-integrating them from a surface of variable elevation to a common depth reference level (100 km below sea level) to obtain deviatoric stresses, strain rates, and horizontal velocities within the top 100 km of the planet (*9*). The body forces in these equations were derived from two sources: (i) topography and lithosphere density structure and (ii) density-driven convection within the mantle constrained by tomography and history of subduction. Benchmarking tests have demonstrated that despite the simplification used in this method, we are able to recover the horizontal components of stress, strain rate, and velocity in the upper 100 km of a full 3D whole-mantle convection model with better than 99% accuracy (*10*). We tested different radial and lateral viscosity variations in the lithosphere and asthenosphere, where the lateral variations were assigned based on positions of cratons and weak plate boundary zones (Fig. 1A). A relatively narrow range of viscosity models gave acceptable fits to the observations. Viscosity models that simultaneously gave a good fit to both plate motions and stresses required a stiff lithosphere (10^{23} Pa · s) with stiffer (10^{24} Pa · s) cratons (white regions in Fig. 1A) and weaker plate boundary zones (10^{20} to 10^{22} Pa · s) in the top 100 km and a moderately strong asthenosphere (300-km thickness, 10^{20} Pa · s). The successful models had keels beneath the cratons with viscosities less than 10^{23} Pa · s between depths of 100 to 200 km.

The velocity field predicted by our best-fit dynamic model in a no-net-rotation (NNR) frame shows a remarkably good fit to the NNR plate motion model defined by Global Positioning System (GPS) (Fig. 1B) (*11*). The root mean square misfit of the velocity field from our complete dynamic model (mantle flow–associated tractions plus lithosphere structure and topography) compared at 63,000 spaced points (1° by 1°) with the kinematic NNR model is ~1 cm/year. The relative contribution of motions associated with coupling with whole-mantle flow versus topography and lithosphere structure can be understood by inspection of Fig. 1C, which is based on the contribution from mantle circulation tractions only. The relative driving mechanisms of topography and lithosphere structure versus coupling with mantle flow varies from plate to plate. The India and Nazca plates have a dominant influence from coupling with mantle flow, whereas other plates and regions approach parity in the relative contribution, with mantle-flow tractions dominating slightly. It is obvious, however, that the contribution from coupling with mantle circulation alone fails to predict surface motions.

We calculated the poles of rotation (table S1) for the angular velocities of the major tectonic plates that were predicted by the dynamic model and compared them with the latest NNR kinematic model, MORVEL (Fig. 1D) (*12*). The velocity of any given patch on the surface of our dynamic model was parameterized by an angular velocity possessing a pole position. The small scatter in the pole positions for these patches (blue dots) shows that the plates are behaving almost rigidly at the stress levels output by the dynamic model and for an effective viscosity of the plates of 1×10^{23} Pa · s. A comparison of the

Downloaded from www.sciencemag.org on February 16, 2012

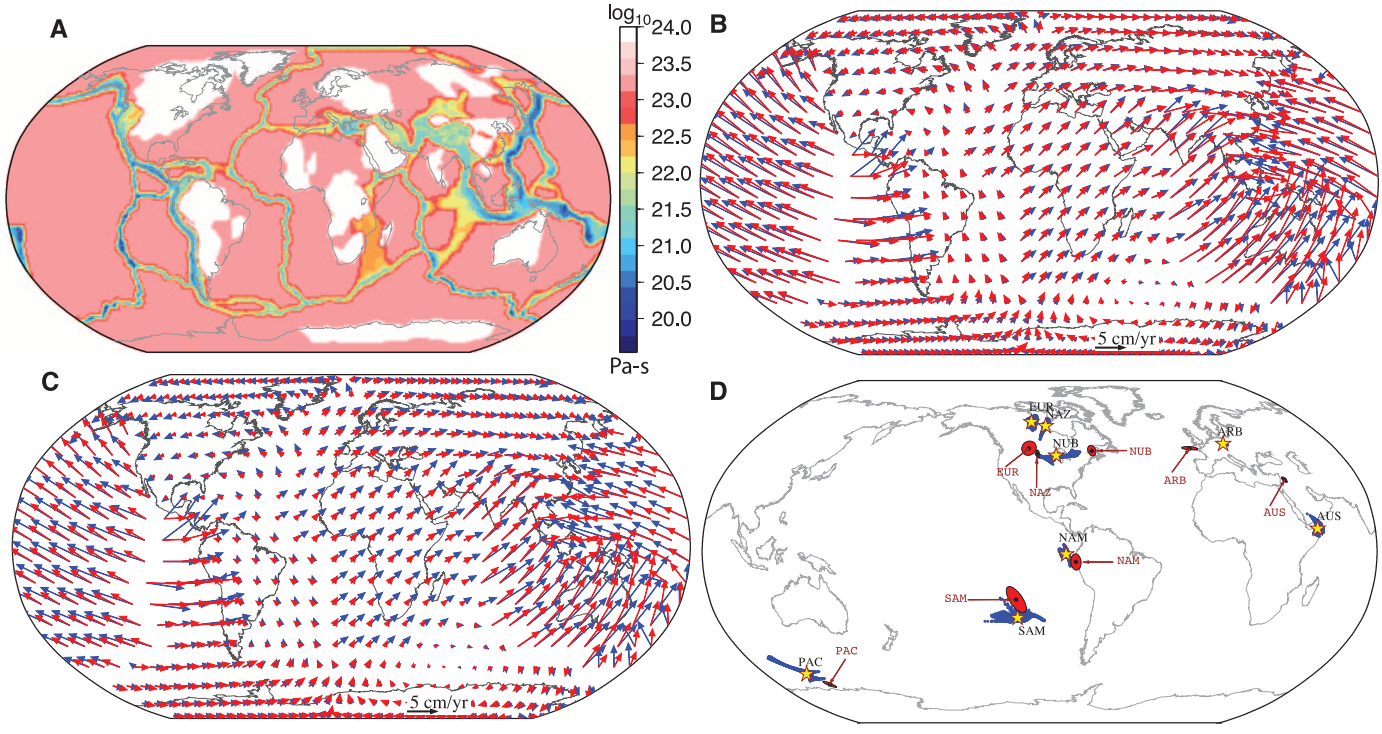

Fig. 1. (**A**) Absolute viscosity model (top 100 km) that provided a best fit to our observations. (**B**) Kinematic NNR model from (*11*) (blue arrows), along with predicted velocities from our global dynamic model (red arrows) in an NNR frame. The dynamic model includes contributions from both coupling with whole-mantle convection and lithosphere structure and topography. (**C**) Same as in (B), except the predicted velocities (red arrows) are from mantle tractions only. (**D**) Average poles of rotation of major tectonic plates (yellow stars) predicted by the dynamic model on top of individually inferred poles from relatively undeformed patches on the respective plates (blue dots). The NNR MORVEL poles from (*12*) are shown as black dots within their respective 95% confidence level error ellipses (in red). PAC, Pacific; NAM, North America; SAM, South America; ARB, Arabia; NUB, Nubia; NAZ, Nazca; EUR, Eurasia; and AUS, Australia.

poles of rotation from the NNR MORVEL model (red 95% confidence ellipse) with the average pole positions (yellow stars) shows that the predictions for the North and the South American plates are nearly perfect (Fig. 1D and table S1). The predicted poles of the Pacific, Europe, Nubia, Nazca, and Arabia plates also lie fairly close to the respective poles of the kinematic MORVEL model.

Comparison of relative surface motions provided by our best-fit dynamic model in selected frames of reference with GPS observations (*11*) shows that the dynamic model is predicting motions in both the plates and plate boundary zones (Fig. 2, A to C). The poles of rotation for the relative angular velocities predicted by the dynamic model (red stars) are, in most cases, close to angular velocities (blue stars) from the latest kinematic plate-motion estimates (*13*). The general agreement of the predicted velocities from the dynamic model to the GPS vectors demonstrates that the model is predicting the correct deformation tensor field within plate boundary zones, including diffuse plate boundary zones, which is a difficult problem for global dynamic models.

Earth's lithospheric stress field gives an indication of the driving forces that cause continental deformation and form mountain ranges and plateaus (*1*, *14*, *15*). We compared the orientation and style of our predicted deviatoric stresses with the World Stress Map (WSM) data (*16*) in the intraplate areas. Our predicted most compressive principal stresses (Fig. 3B) are in good agreement with the WSM horizontal most compressive stress (SH_{max}) directions and style (Fig. 3A). We show the stress results in three important continental deformation zones: western North America, the India-Asia collision zone, and the central Mediterranean. In western North America, deviatoric stresses from the dynamic model predict the opening of the Basin and Range Province, strike-slip along the San Andreas system, compression within the Juan de Fuca trench, and north-south compression over the Cascadia forearc (Fig. 4A). In the central Mediterranean and eastern Turkey regions, the modeled stresses (Fig. 4B) are compatible with findings of the known deformation field (*17*). The Hellenic arc displays trench-perpendicular compression, whereas clear strike-slip deformation is predicted along the North Anatolian fault. Improvement in prediction for these continental regions is possible through incorporation of the influence of smaller-scale convection (*18*). The predicted deviatoric stresses in Tibet show a predominantly strike-slip style of deformation (also mixed with normal fault-

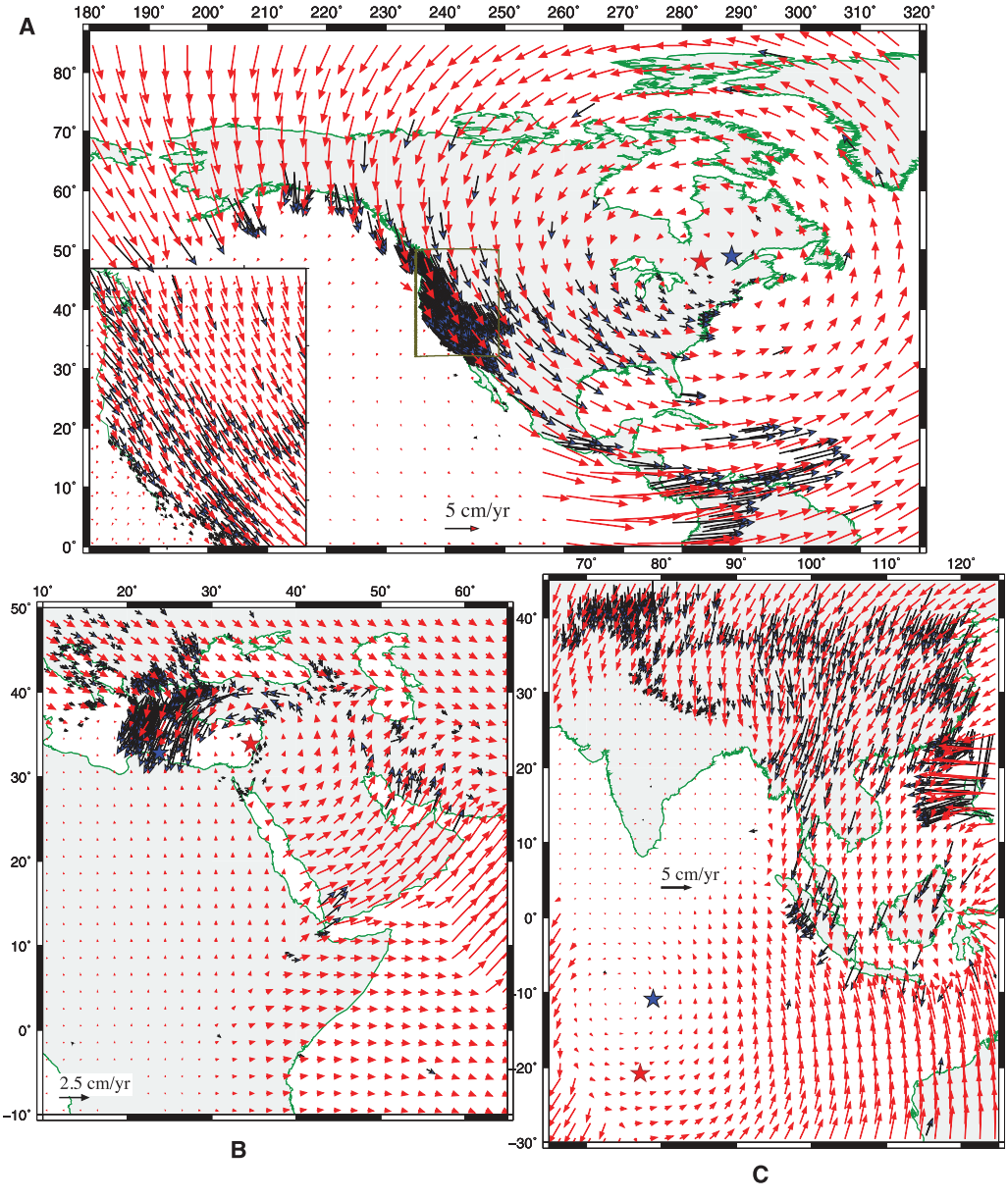

Fig. 2. (**A**) Model velocity vectors (red arrows) from our global dynamic model plotted along with GPS vectors (*11*) (blue arrows) over North America in a Pacific fixed reference frame. A zoom-in view of the western U.S. region is shown in the inset map. Poles predicted by the dynamic model (red star) and the MORVEL plate-motion model (*13*) (blue star) are shown for PAC-NAM relative motion. (**B**) Same as in (A), but with Nubia fixed. Poles are for ARB-EUR relative motion. (**C**) Same as in (A), but with India fixed. Poles are for AUS-India relative motion.

Downloaded from www.sciencemag.org on February 16, 2012

style deviatoric stress) and a rotation of SH_{max} within Tibet around the Eastern Himalayan Syntaxis region (Fig. 4C), similar to what is observed there. The contribution from topography and lithosphere structure plays an important role for these areas of continental deformation. We also compared our predicted stress orientation and style with strain-rate data from the Global Strain Rate Map (GSRM) (*19*) in the deforming areas by computing a correlation coefficient (*20*) between the predicted stress tensors and the GSRM strain-rate tensors. The comparison shows a good match in the mid-oceanic ridges, continental Africa and the Indo-Australia oceanic plate boundary zone, as well as in the Andes (fig. S1).

The traction field (*21*) that contributes to our best-fit dynamic model is long wavelength (Fig. 4D) and shows convergent flow in areas of downgoing slabs and divergent flow in places such as central Africa and the Pacific. Comparison of these tractions with surface velocities (Fig. 1B) indicates whether the tractions are driving or resisting. If mantle flow is leading plate motion, tractions are driving; if mantle flow is trailing the plate, then tractions are resistive. Tractions are driving in areas like the Nazca plate, eastern North America, the North Atlantic and Western Europe, northern and eastern Siberia, northern Africa, the Indian and Australian plates, and the Pacific plate in regions approaching the subduction zones. In these places, tractions act in similar directions to plate motions in an NNR frame, and thus mantle flow is leading the plate motion. On the other hand, in western North America, the northern part of South America, and southern Africa, tractions are resistive, as they are in a direction opposite to the NNR surface velocity. This is an important conclusion of our study that addresses the hugely controversial issue of whether mantle tractions are driving or resistive (*14*, *22*, *23*).

We also calibrated the absolute deviatoric stress magnitudes in the lithosphere verified through benchmarking using whole-mantle convection models (*10*). The average stress levels (second invariant of deviatoric stresses) within the lithosphere in our best-fit dynamic models are between 20 and 80 MPa (fig. S2). The higher stresses occur within the plates, whereas the plate boundary zones have lower values. At those stress levels, and given the predicted stress and strain-rate tensor fields, we obtain near-plate rigidity (Fig. 4E) and a close prediction to surface motions. The rigidity of the plates is evident from the low strain rates predicted in the intraplate areas, 1 to 4×10^{-9} per year (white to red areas in Fig. 4E). A goal of this study is to investigate the relative contribution of mantle flow versus lithosphere structure and topography. Although this ratio of the relative contribution varies depending on location, an average of 70% of the magnitude of lithosphere deviatoric stresses is associated with coupling with mantle flow, and the remaining 30% is associated with lithosphere structure and topography.

The issue of whether slabs remain strong (*8*) or weaken (*24*–*27*) as they subduct is still unresolved (*28*). Our convection model is solely density-driven with Newtonian viscosity; no nonlinear rheology or stiff slabs have been considered, and yet our model predicts global plate motions, as well as motions within most of the world's diffuse plate boundary zones. Our results cannot rule out the need for stiff slabs; we can only infer that they are not a necessary condition for predicting plate motions and plate boundary-zone deformation.

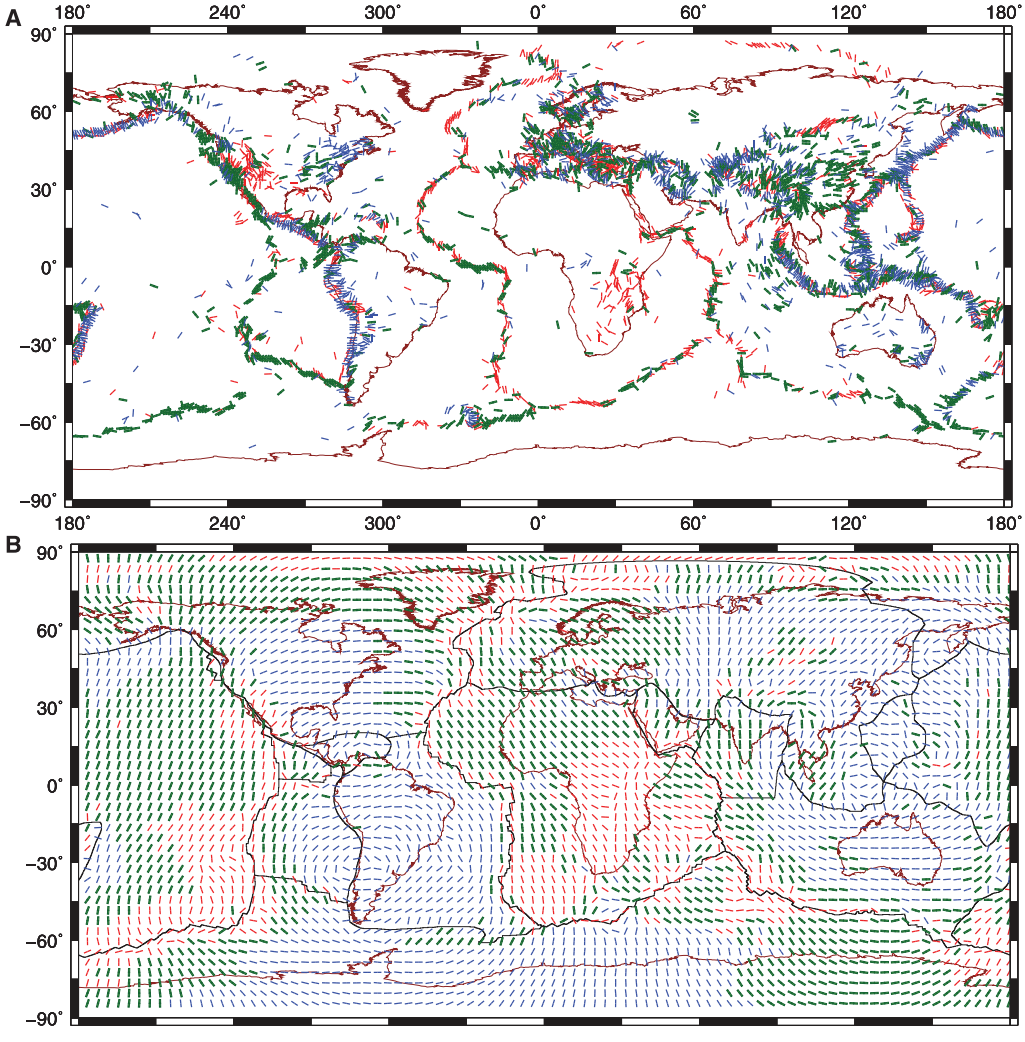

Fig. 3. (**A**) SH_{max} directions from the World Stress Map averaged within 1° by 1° areas. Red indicates a normal fault regime, blue indicates a thrust regime, and green denotes a strike-slip regime. Only SH_{max} directions where the regime was known have been used. (**B**) Most compressive horizontal principal deviatoric stress axes from our best-fitting dynamic model. The colors indicate the strain environment predicted by the deviatoric stresses in the dynamic model. Red, blue, green: same as in (A).

Downloaded from www.sciencemag.org on February 16, 2012

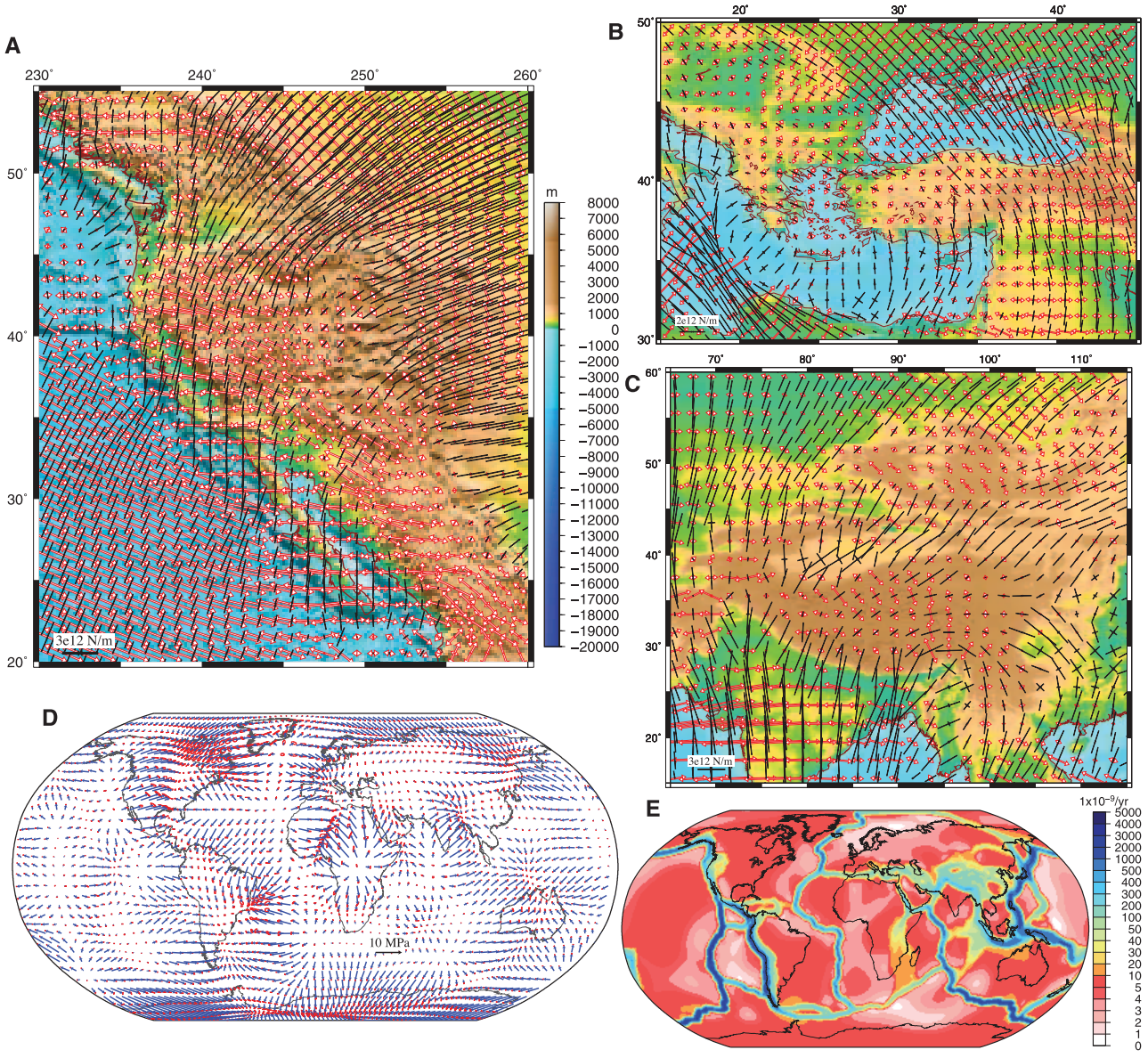

Fig. 4. (**A**) Deviatoric stress prediction in western North America plotted on top of topography. Red denotes tensional stresses, whereas black denotes compressive stresses. (**B**) Same as in (A), but in the central Mediterranean. (**C**) Same as in (A), but in the India-Asia collision zone. (**D**) Average horizontal tractions at the reference-level depth of 100 km below sea level, along with 95% confidence error ellipses, derived from nine mantle-flow models that fit the observations. The nine models possessed the narrow range of acceptable lateral viscosity variations described in the text and in (*9*). (**E**) Predicted second invariant of strain rates from our best-fitting dynamic model.

Downloaded from www.sciencemag.org on February 16, 2012

References and Notes

1. C. Lithgow-Bertelloni, J. H. Guynn, *J. Geophys. Res.* **109**, B01408 (2004).
2. P. Bird, Z. Liu, W. K. Rucker, *J. Geophys. Res.* **113**, B11406 (2008).
3. Y. Ricard, C. Vigny, *J. Geophys. Res.* **94**, 17543 (1989).
4. C. Lithgow-Bertelloni, M. Richards, *Geophys. Res. Lett.* **22**, 1317 (1995).
5. T. W. Becker, R. J. O'Connell, *Geochem. Geophys. Geosyst.* **2**, 2001GC000171 (2001).
6. B. Steinberger, H. Schmeling, G. Marquart, *Earth Planet. Sci. Lett.* **186**, 75 (2001).
7. A. Forte, R. Moucha, N. Simmons, S. Grand, J. Mitrovica, *Tectonophysics* **481**, 3 (2010).
8. G. Stadler *et al.*, *Science* **329**, 1033 (2010).
9. Methods are available as supporting material on *Science* Online.
10. A. Ghosh, W. E. Holt, L. Wen, A. J. Haines, L. M. Flesch, *Geophys. Res. Lett.* **35**, L16309 (2008).
11. C. Kreemer, D. A. Lavallée, G. Blewitt, W. E. Holt, *Geophys. Res. Lett.* **33**, L17306 (2006).
12. D. F. Argus, R. G. Gordon, C. DeMets, *Geochem. Geophys. Geosyst.* **12**, Q11001 (2011).
13. C. DeMets, R. G. Gordon, D. F. Argus, *Geophys. J. Int.* **181**, 1 (2010).
14. P. Bird, *J. Geophys. Res.* **103**, 10115 (1998).
15. A. Ghosh, W. E. Holt, L. M. Flesch, A. J. Haines, *Geology* **34**, 321 (2006).
16. O. Heidbach *et al.*, *The World Stress Map Database Release 2008* (GFZ, Potsdam, Germany, 2008).
17. S. M. Özeren, W. E. Holt, *Geophys. J. Int.* **183**, 1165 (2010).
18. C. Faccenna, T. W. Becker, *Nature* **465**, 602 (2010).
19. C. Kreemer, W. E. Holt, A. J. Haines, *Geophys. J. Int.* **154**, 8 (2003).
20. A. Ghosh, W. E. Holt, L. M. Flesch, *Geophys. J. Int.* **179**, 787 (2009).
21. By tractions we mean $-\tau_{r\theta}$ and $-\tau_{r\phi}$, which are the effective force per unit area imposed on the base of the lithosphere by mantle flow.
22. R. M. Richardson, S. Solomon, N. Sleep, *Rev. Geophys.* **17**, 981 (1979).
23. W. Bai, C. Vigny, Y. Ricard, C. Froidevaux, *J. Geophys. Res.* **97**, 11729 (1992).
24. W. C. Tao, R. J. O'Connell, *Nature* **361**, 626 (1993).
25. L. N. Moresi, M. Gurnis, *Earth Planet. Sci. Lett.* **138**, 15 (1996).
26. S. L. Bilek, C. P. Conrad, C. Lithgow-Bertelloni, *Geophys. Res. Lett.* **32**, L14305 (2005).
27. M. A. Jadamec, M. I. Billen, *Nature* **465**, 338 (2010).
28. M. I. Billen, *Annu. Rev. Earth Planet. Sci.* **36**, 325 (2008).

Acknowledgments: This study was supported by NSF grant EAR-0911300. Maps were prepared using Generic Mapping Tools version 4.5.7. We thank D. Argus and C. Kreemer for

sharing their kinematic models and GPS data for comparison with the dynamic models, L. Wen for help with using his code, and three anonymous reviewers for their comments that substantially improved the manuscript. We are grateful to UNAVCO, Incorporated Research Institutions for Seismology, NSF-EarthScope, International GNSS Service, NASA, and countless researchers for facilitation and availability of geodetic and seismic data. The codes are available as a zip file as part of the supporting online material.

Supporting Online Material

www.sciencemag.org/cgi/content/full/335/6070/838/DC1
Methods
SOM Text
Figs. S1 and S2
Table S1
References (*29*–*37*)
Computer Codes

20 September 2011; accepted 24 January 2012
10.1126/science.1214209

Cyanophora paradoxa Genome Elucidates Origin of Photosynthesis in Algae and Plants

Dana C. Price,[1] Cheong Xin Chan,[1]* Hwan Su Yoon,[2,3] Eun Chan Yang,[2] Huan Qiu,[2] Andreas P. M. Weber,[4] Rainer Schwacke,[5] Jeferson Gross,[1] Nicolas A. Blouin,[6] Chris Lane,[6] Adrián Reyes-Prieto,[7] Dion G. Durnford,[8] Jonathan A. D. Neilson,[8] B. Franz Lang,[9] Gertraud Burger,[9] Jürgen M. Steiner,[10] Wolfgang Löffelhardt,[11] Jonathan E. Meuser,[12] Matthew C. Posewitz,[13] Steven Ball,[14] Maria Cecilia Arias,[14] Bernard Henrissat,[15] Pedro M. Coutinho,[15] Stefan A. Rensing,[16,17,18] Aikaterini Symeonidi,[16,17] Harshavardhan Doddapaneni,[19] Beverley R. Green,[20] Veeran D. Rajah,[1] Jeffrey Boore,[21,22] Debashish Bhattacharya[1]†

The primary endosymbiotic origin of the plastid in eukaryotes more than 1 billion years ago led to the evolution of algae and plants. We analyzed draft genome and transcriptome data from the basally diverging alga *Cyanophora paradoxa* and provide evidence for a single origin of the primary plastid in the eukaryote supergroup Plantae. *C. paradoxa* retains ancestral features of starch biosynthesis, fermentation, and plastid protein translocation common to plants and algae but lacks typical eukaryotic light-harvesting complex proteins. Traces of an ancient link to parasites such as Chlamydiae were found in the genomes of *C. paradoxa* and other Plantae. Apparently, *Chlamydia*-like bacteria donated genes that allow export of photosynthate from the plastid and its polymerization into storage polysaccharide in the cytosol.

Eukaryote evolution has largely been shaped by the process of primary endosymbiosis, whereby bacterial cells were taken up and over time evolved into double membrane–bound organelles, the plastid and the mitochondrion [e.g., (*1*, *2*)]. The cyanobacterium-derived plastid is found in diverse photosynthetic organisms, including Glaucophyta, Rhodophyta, and green algae and their land plant descendants (the Viridiplantae). These three lineages are postulated to form the monophyletic group Plantae (or Archaeplastida) (*3*–*6*), a hypothesis that suggests the primary cyanobacterial endosymbiosis occurred exclusively in their single common ancestor. Plastid gene trees demonstrate a single origin of the Plantae (*5*, *7*); however, many nuclear, multiprotein phylogenies provide little (*8*) or no support (*9*, *10*) for their monophyly. These latter results may reflect a reticulate ancestry among genes that can mislead phylogenetic inference (*11*). Furthermore, glaucophytes retain ancestral cyanobacterial features not found in other Plantae (*12*)—such as the presence of peptidoglycan between the two bounding membranes of the plastid (*13*)—that cast doubt on their evolutionary history. It is therefore unclear whether the Plantae host and its plastid, with its associated complex machinery (e.g., for plastid protein import and solute transport) (*14*, *15*), had a single origin or multiple origins. To elucidate the evolutionary history of key algal and land plant traits and to test Plantae monophyly, we have generated a draft assembly of the ≈70 Mbp nuclear genome from the glaucophyte *Cyanophora paradoxa* CCMP329 (Pringsheim strain) (Fig. 1A).

A total of 27,921 *C. paradoxa* proteins were predicted from the genome data, and 4628 had significant BLASTp hits ($e \leq 10^{-10}$) to prokaryote and eukaryote genome data in our comprehensive local database (table S1). Using phylogenomics (*16*), we generated 4445 maximum likelihood trees from the *C. paradoxa* proteins and found that >60% support a sister-group relationship between glaucophytes and red and/or green algae with a bootstrap value ≥90% (Fig. 1B and fig. S1). The Plantae clade in many of these trees is, however, interrupted by chlorophyll *a* + *c* containing "chromalveolates." An example of this type of tree is fructose-1,6-bisphosphatase (Fig. 1C and fig. S2), which has cytosolic and plastidic isoforms. The gene for this enzyme, found in stramenopiles (e.g., diatoms) and haptophytes, originated from the red algal secondary endosymbiont that gave rise to the plastid in these taxa (*2*, *9*). This sort of intracellular gene transfer associated with endosymbiosis (EGT) has greatly enriched algal and land plant genomes (*17*, *18*).

We estimated the "footprint" of cyanobacterium-derived EGT in Plantae genomes. The proportion of cyanobacterium-derived nuclear genes varies from 18% in *Arabidopsis thaliana* (*19*) to ~7% in mesophilic red algae and 6% in *Chlamydomonas reinhardtii* (*20*, *21*). Phylogenomic analysis of the predicted *C. paradoxa* proteins showed 274 to be of cyanobacterial provenance (*22*). This constitutes ~6% of proteins in the glaucophyte that have significant BLASTp hits (i.e., 274 out of 4628), as found in other algae (*20*, *21*). BLASTp analysis identified 2029 proteins that are putatively destined for the plastid, of which 293 contain the transit sequence for plastid import [identified by the presence of phenylalanine (F) within the first four amino acids: MF, MAF, MNAF, MSAF, and MAAF] (*23*, *24*) (fig. S4B). Of these 293 proteins, 80% are derived from Cyanobacteria.

Another source of foreign genes in Plantae is horizontal gene transfer (HGT), which is not associated with endosymbiosis. Using 35,126 bacterial sequences as a query, we found 444 noncyanobacterial gene families with a common origin shared amongst Bacteria and Plantae. Among them, 15 genes are present in all three Plantae phyla. An example of a gene derived from Bacteria after an ancient HGT event that is shared by

[1]Department of Ecology, Evolution, and Natural Resources and Institute of Marine and Coastal Sciences, Rutgers University, New Brunswick, NJ 08901, USA. [2]Bigelow Laboratory for Ocean Sciences, West Boothbay Harbor, ME 04575, USA. [3]Department of Biological Sciences, Sungkyunkwan University, Suwon 440-746, Korea. [4]Institute for Plant Biochemistry, Heinrich-Heine-University, D-40225 Duesseldorf, Germany. [5]Botanical Institute, Biocenter Cologne, University of Cologne, Zülpicher Strasse 47b, 50674 Cologne, Germany. [6]Department of Biological Sciences, University of Rhode Island, Kingston, RI 02881, USA. [7]Canadian Institute for Advanced Research, Department of Biology, University of New Brunswick, Fredericton, New Brunswick E3B 5A3, Canada. [8]Department of Biology, University of New Brunswick, Fredericton, New Brunswick E3B 5A3, Canada. [9]Centre Robert Cedergren, Département de Biochimie, Université de Montréal, Montréal, Québec H3C 3J7, Canada. [10]Department of Biology/Plant Physiology, Martin-Luther-University Halle-Wittenberg, Germany. [11]Max F. Perutz Laboratories, Department of Biochemistry and Cell Biology, University of Vienna, Vienna, Austria. [12]Department of Civil and Environmental Engineering, Colorado School of Mines, Golden, CO 80401, USA. [13]Department of Chemistry and Geochemistry, Colorado School of Mines, Golden, CO 80401, USA. [14]Unité de Glycobiologie Structurale et Fonctionnelle, UMR 8576 CNRS-USTL, Université des Sciences et Technologies de Lille, 59655 Villeneuve d'Ascq Cedex, France. [15]Universités Aix-Marseille I & II, Case 932, 163 Avenue de Luminy, 13288 Marseille Cedex 9, France. [16]Faculty of Biology, University of Freiburg, Freiburg, Germany. [17]FRISYS Freiburg Initiative in Systems Biology, University of Freiburg, Freiburg, Germany. [18]BIOSS Centre for Biological Signalling Studies, University of Freiburg, Freiburg, Germany. [19]Roy J. Carver Center for Genomics, Department of Biology, University of Iowa, Iowa City, IA, 52242, USA. [20]Department of Botany, University of British Columbia, Vancouver, British Columbia V6T 1Z4, Canada. [21]Genome Project Solutions, Hercules, CA 94547, USA. [22]Department of Integrative Biology, University of California, Berkeley, CA 94720, USA.

*Present address: Institute for Molecular Bioscience, University of Queensland, Brisbane, QLD 4072, Australia.
†To whom correspondence should be addressed. E-mail: bhattacharya@aesop.rutgers.edu

Downloaded from www.sciencemag.org on February 16, 2012

Plantae is that encoding a thiamine pyrophosphate–dependent pyruvate decarboxylase family protein involved in alcohol fermentation (Fig. 1D). Another 60 genes were present in only two of the tree phyla (i.e., 24, 10, and 26 genes in Glaucophyta-Viridiplantae, Glaucophyta-Rhodophyta, and Rhodophyta-Viridiplantae, respectively) (*22*).

We sequenced the mitochondrial genome from *C. paradoxa* and from the distantly related glaucophyte *Glaucocystis nostochinearum* and generated a near-complete plastid genome sequence from *G. nostochinearum* that was added to the existing plastid genome data from *C. paradoxa* (GenBank NC_001675). The mitochondrial DNAs (mtDNAs) of *C. paradoxa* and *G. nostochinearum* share similar characteristics, including a large gene content, but differ markedly in size [Fig. 3A, tables S3 and S4, and discussion in the supporting online material (SOM)]. A concatenated multiprotein (17,049 aligned amino acid positions) phylogeny of the plastid data shows the expected monophyly of Plantae plastids (*2*, *5*, *6*) and places glaucophytes very close to the divergence point of red and green algae (fig. S5A).

Building on the support for Plantae monophyly provided by the phylogenomic analyses, we analyzed the evolution of landmark traits that are associated with plastid endosymbiosis. Previous work suggests that in red and green algae, the initial link for carbon metabolism between the

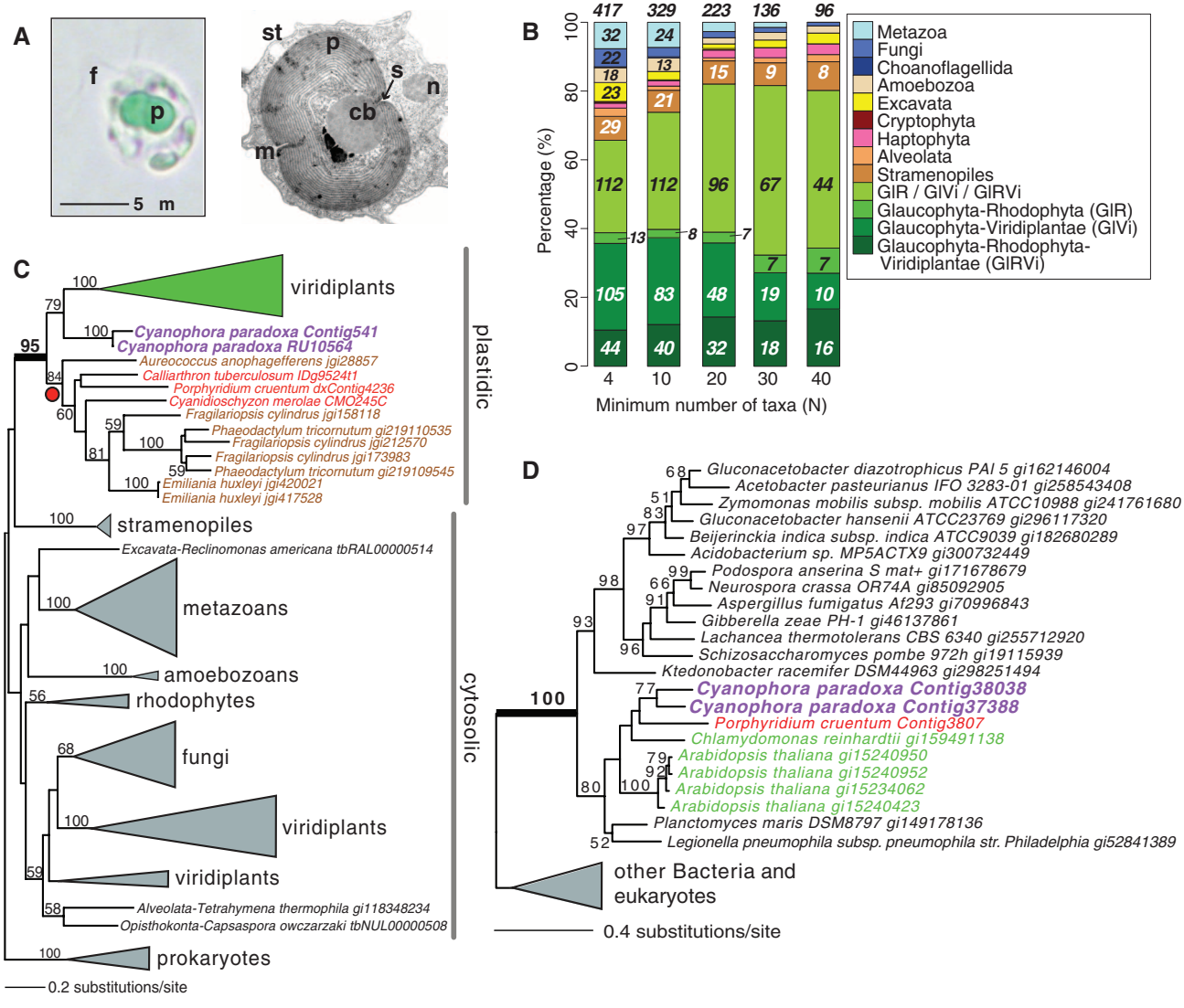

Fig. 1. (**A**) Schematic (left) and transmission electron micrograph (right) images of *C. paradoxa*. This freshwater microalga has two flagella (f) of unequal lengths, and the plastid (p) contains an electron-dense central body (cb). The nucleus (n), mitochondrion (m), starch granules in the cytoplasm (st), and peptidoglycan septa (s) formed during plastid division are also shown. (**B**) Percentage of single-protein Randomized Axelerated Maximum Likelihood (RaxML) trees (raw numbers shown in the bars) that support the monophyly of Glaucophyta (bootstrap ≥ 90%) solely with other Plantae members, or in combination with non-Plantae taxa that interrupt this clade. These latter groups of trees are primarily explained by red/green algal EGT into the nuclear genome of chromalveolates and euglenids. For each of these algal lineages, the set of trees with different numbers of taxa (*N*) ≥4, ≥10, ≥20, ≥30, and ≥40 and distinct phyla ≥3 in a tree are shown. The Plantae-only groups are Glaucophyta-Rhodophyta (GlR), Glaucophyta-Viridiplantae (GlVi), and Glaucophyta-Rhodophyta-Viridiplantae (GlRVi). Trees with evidence of EGT are shown as the single group, GlR/GlVi/GlRVi. An expanded analysis that shows the results when red or green algae are used as the query to search for support for Plantae monophyly is summarized in fig. S1. (**C**) Schematic ML phylogeny of fructose-1,6-bisphosphatase, an enzyme with cytosolic and plastidic isoforms that unites Plantae (plastid-targeted protein) and shows an example of a protein affected by EGT. The plastidic gene has been transferred from red algae to chromalveolates that contain a red algal–derived plastid, presumably through EGT (marked by the filled red circle). The full tree is shown in fig. S2. (**D**) Schematic ML phylogeny of a gene encoding a thiamine pyrophosphate (TPP)–dependent pyruvate decarboxylase family protein involved in alcohol fermentation. RAxML bootstrap support values are shown at the nodes of the trees in panels (C) and (D), in which glaucophytes, red algae, green algae, and chromalveolates are in purple, red, green, and brown, respectively.

Downloaded from www.sciencemag.org on February 16, 2012

host cell and plastid relied on sugar-phosphate transporters that evolved from existing host endomembrane nucleotide sugar transporters (NSTs) (*15*, *25*). Unexpectedly, we found that although six endomembrane-type NST genes exist in *C. paradoxa* (fig. S3), this alga lacks plastidial phosphate-translocator (PT) genes (Fig. 2A). We searched the genome for alternative candidate genes encoding homologs of bacterial carbon exporters and found two UhpC-type hexose-phosphate transporters (Fig. 2B) that are also present in red and green algae. One of these putative transporters (contig 37408) encodes a plastid-targeting signal containing a conserved phenylalanine (F) and proline (P) at the N terminus typical for *C. paradoxa* plastid-targeted proteins [e.g., (*23*)] (Fig. 2, B and C). The second UhpC homolog contains an F and a P at the N terminus and may also be plastid-targeted. These transporters are related to sequences in the parasites Chlamydiae and *Legionella*. We suggest that the UhpC gene originated in Plantae and *Legionella* species through independent HGT events from Chlamydiae. This direction of gene transfer for the prokaryotes is supported by the nested position of a single proteobacterial clade (i.e., *Legionella*) within Chlamydiae. Chlamydiae have contributed a substantial number of other genes to Plantae that are involved in plastid functions (*26*, *27*).

A second landmark trait of photosynthetic eukaryotes is the presence of protein-conducting channels (translocons) in the outer and inner envelope membranes of plastids (Toc and Tic, respectively) [e.g., (*14*)], for which there is biochemical evidence in the *C. paradoxa* plastid (*28*). We identified nuclear-encoded homologs of the major Toc75 and Tic110 translocon proteins, two Toc34-like receptors, homologs of the plastid Hsp70 and Hsp93 chaperones, and a stromal processing peptidase (table S2). This minimal set of components likely formed the ancestral plastid protein translocation system in Plantae (*29*). Candidates for additional translocon subunits Tic20 to Tic22, Tic32, Tic55, and Tic62 were also found in the glaucophyte. The presence of a conserved core of cyanobacterium-derived, homologous translocon subunits shared by *C. paradoxa* and other Plantae (i.e., Toc75, Tic20, and Tic22) or those apparently evolved de novo in the host (i.e., Toc34 and Tic110) (table S2 and fig. S4A) provides strong evidence that the primary plastid was established in a single ancestor of Plantae (*14*, *29*, *30*).

A key component of plastids is light-harvesting complex (LHC) proteins that increase the capacity to capture incoming light. Cyanobacteria, red algae, and glaucophytes use phycobilisomes (protein complexes anchored to the thylakoid) for light harvesting, but red algae also have nuclear-encoded pigment-binding proteins homologous to the typical green algal LHCs but specifically associated with photosystem I (*31*). Unexpectedly, no candidate genes with three membrane-spanning regions, characteristic of LHCs in all other photosynthetic eukaryotes, were found in *C. paradoxa*. This alga does, however, encode several members of the LHC-like (LIL) protein family that contain a single chlorophyll-binding transmembrane helix, including two copies of the "one-helix proteins" (OHPs) (see fig. S8 and SOM).

The anaerobic capabilities of *C. paradoxa* provide parallels to the well-characterized anoxic metabolism of the green alga *Chlamydomonas reinhardtii*

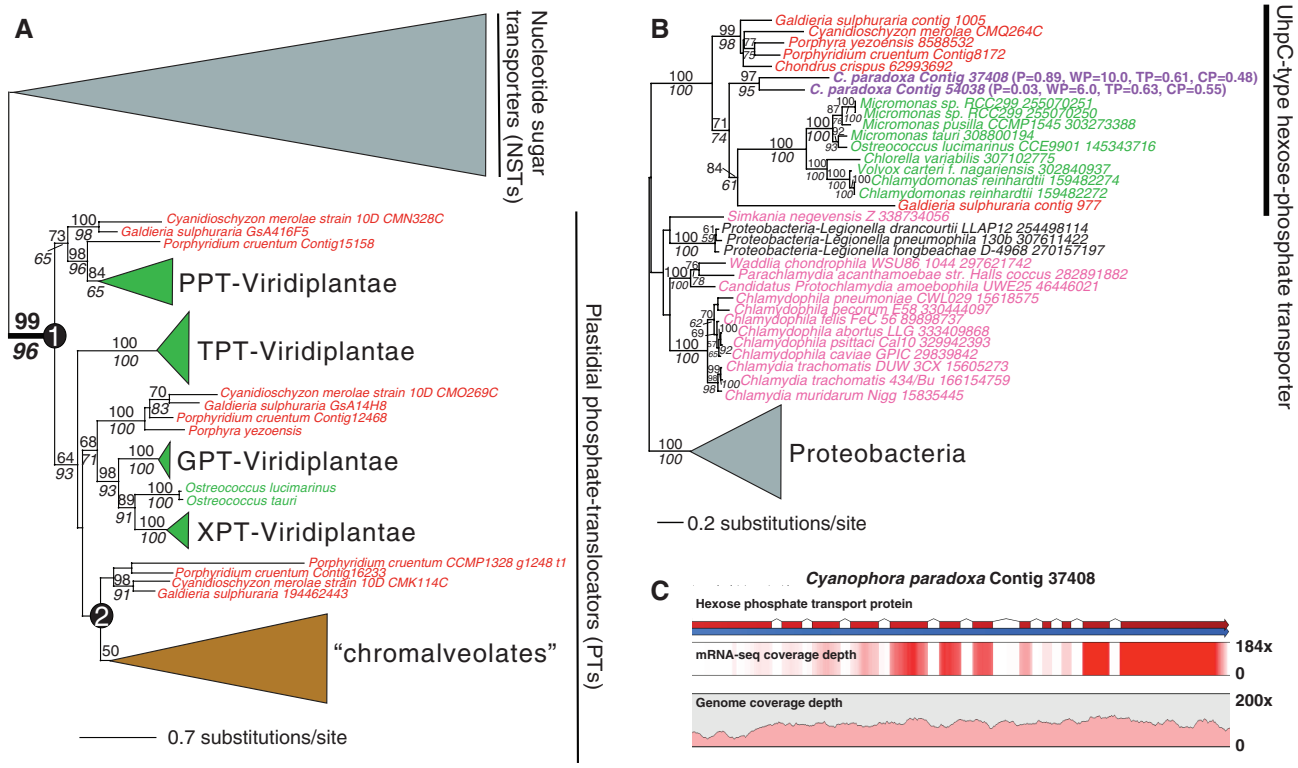

Fig. 2. (**A**) Maximum likelihood (PhyML) phylogeny of endomembrane (NST) and plastidial phosphate-translocators (PTs). PhyML bootstrap values are shown above the branches, and RAxML bootstrap values are shown below the branches in italics. Only bootstrap values ≥50% are shown. Red algae, Viridiplantae, and chromalveolates are shown in red, green, and brown, respectively. The different plastid-targeted transporters are glucose 6-phosphate translocator (GPT), phosphoenolpyruvate translocator (PPT), triose phosphate translocator (TPT), and xylulose 5-phosphate translocator (XPT). The numbers in the filled circles indicate transporters shown to the right that (1) resulted from primary endosymbiosis and (2) were transferred from the red algal secondary endosymbiont to the chromalveolate host. The full tree is shown in fig. S3. (**B**) RAxML phylogeny of UhpC-type hexose-phosphate transporters in algae, land plants, and Bacteria. RAxML bootstrap values are shown above the branches, and PhyML bootstrap values are shown below the branches in italics. Only bootstrap values ≥50% are shown. Red algae, Viridiplantae, glaucophytes, and Chlamydiae are shown in red, green, magenta, and pink, respectively. The numbers after the *C. paradoxa* contig names are bioinformatic predictions for plastid targeting of the encoded proteins with Predotar (P), WoLF PSORT (WP), TargetP (TP), and ChloroP (CP). These data suggest that contig 37408 (and perhaps also contig 54308) is destined for the *C. paradoxa* plastid. (**C**) Intron distribution, genome contig coverage, and transcriptome coverage (mRNA-seq) of *C. paradoxa* genome contig 37408 that encodes a putative plastid-targeted UhpC-type hexose phosphate transporter.

Downloaded from www.sciencemag.org on February 16, 2012

(*32*). The predicted pathways in *C. paradoxa* suggest a complex heterofermentative state in the Plantae ancestor (Fig. 3B), with retention in Chlorophyta (e.g., Chlorophyceae and Trebouxiophyceae) and losses in Streptophyta. Orthologs of fermentation enzymes encoded by the *C. paradoxa* genome can also be found in Cyanobacteria (for lactate, formate, acetate, and ethanol) and hydrogenosomal eukaryotes (for H_2, lactate, formate, and ethanol). Therefore, the complex fermentative capabilities conserved between the distantly related *C. paradoxa* and green algae (*33*) likely represent an evolutionarily advantageous combination of anoxic enzymes from the eukaryote host and the cyanobacterial endosymbiont. Genome evidence for H_2 metabolism in *C. paradoxa* is demonstrated by the presence of a [FeFe]-hydrogenase and associated maturases (HydE, HydF, and HydG).

Putative carbohydrate metabolism enzymes in *C. paradoxa* were identified using the Carbohydrate-Active enZymes (CAZy) database (*34*) annotation

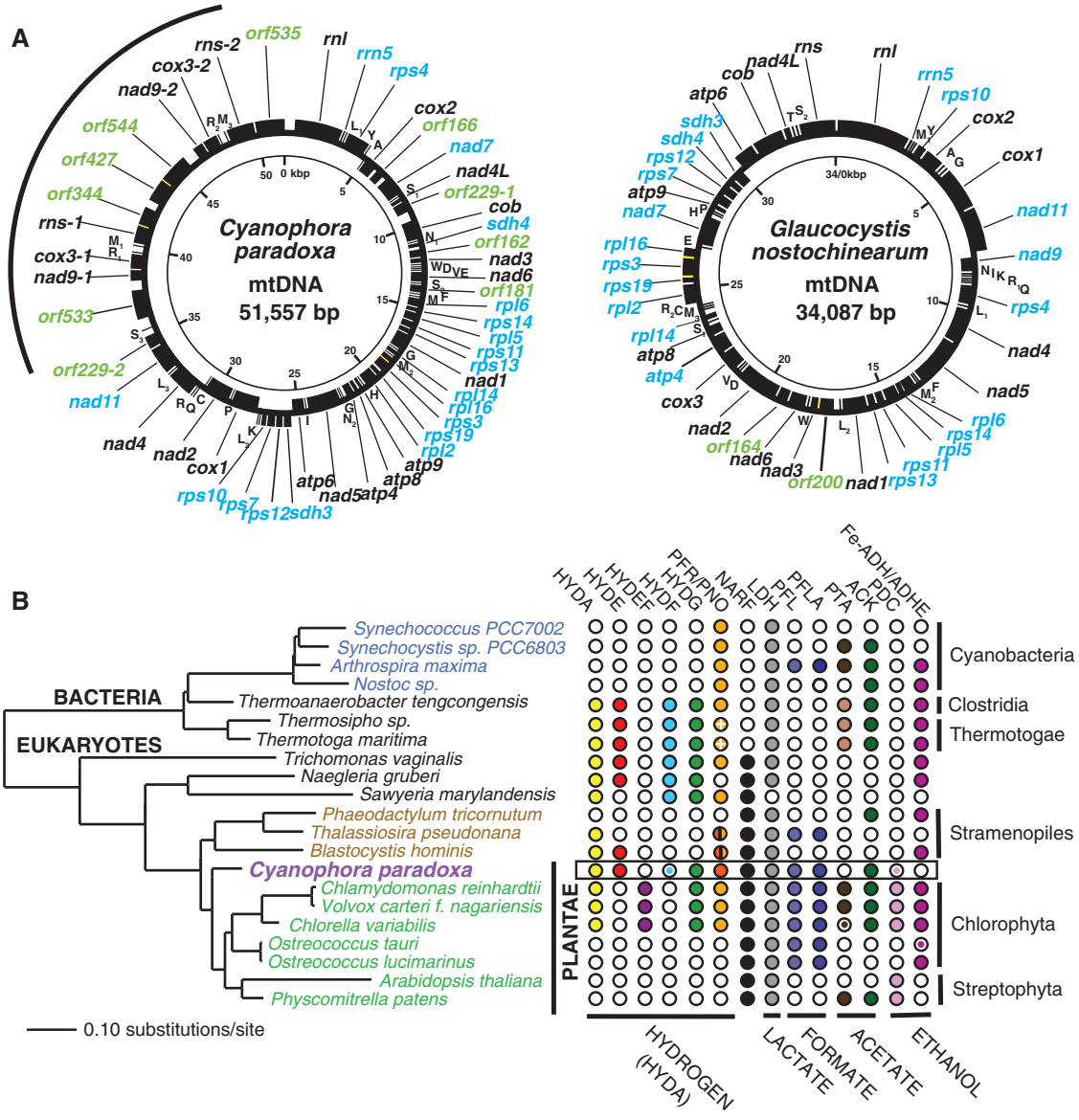

Fig. 3. (**A**) Gene maps of glaucophyte mitochondrial genomes. Black blocks indicate genes that are arranged outside and inside the circle, indicating they are transcribed clockwise and counterclockwise, respectively. tRNA gene names are abbreviated in single–amino acid letter code; subscript numbers distinguish isoacceptor tRNAs. The color-coding identifies genes that are typically present in fungal and animal mtDNAs (black); additional genes found in land plants and protists are marked in blue and unidentified ORFs in green. The arc marks the genome region with long segmental duplications in *C. paradoxa* mtDNA. (**B**) Phylogeny of small subunit rRNA of organisms with sequenced genomes that share predicted fermentative orthologs encoded in the *C. paradoxa* genome. Predicted orthologs encoded by *C. paradoxa* are shown boxed. Enzyme abbreviations are as follows: Fe-ADH, iron-containing alcohol dehydrogenase; ADHE, iron-containing alcohol/aldehyde dehydrogenase; ACK, acetate kinase; HYDA, [FeFe]-hydrogenase; HYDE, radical S-adenosylmethionine HYDA maturase; HYDF, GTPase-domain HYDA maturase; HYDEF, fused HYDE and HYDF maturase; HYDG, radical S-adenosylmethionine HYDA maturase; LDH, lactate dehydrogenase; NARF, nuclear prelamin A recognition factor; PTA, phosphotransacetylase; PDC, pyruvate decarboxylase; PFL, pyruvate:formate lyase; PFLA, pyruvate:formate lyase activase; PFR, pyruvate:ferredoxin oxidoreductase; PNO, pyruvate:NADP oxidoreductase composed of a PFR domain fused to a C-terminal NADPH-cytochrome P450 reductase domain. Filled circles indicate the presence of the indicated enzyme(s), whereas incompletely filled circles indicate support from a partial *C. paradoxa* sequence. In the case of PFR/PNO, the darker filled circle represents PNO, a divided fill represents evidence for both enzymes, and white crosses indicate the heteromeric PFRs present in the Thermotogae. Shading is also used to discriminate the single-domain type 1 (light) and multidomain type II (dark) PTA isoforms. Single-letter abbreviations for the amino acids are as follows: A, Ala; C, Cys; D, Asp; E, Glu; F, Phe; G, Gly; H, His; I, Ile; K, Lys; L, Leu; M, Met; N, Asn; P, Pro; Q, Gln; R, Arg; S, Ser; T, Thr; V, Val; W, Trp; and Y, Tyr.

Downloaded from www.sciencemag.org on February 16, 2012

Table 1. List of CAZymes (*34*) present in the *C. paradoxa* genome. GH, glycoside hydrolase; GT, glycosyl transferase; PL, polysaccharide lyase; CE, carbohydrate esterase; CBM, carbohydrate-binding module. Photosynthetic taxa are shown in the green field and nonphotosynthetic taxa in the blue field.

Species	GH	GT	PL	CE	CBM	GH+GT
Cyanophora paradoxa (glaucophyte)	84	128	3	2	24	212
Cyanidioschyzon merolae (red alga)	21	61	0	2	16	82
Ostreococcus lucimarinus CCE9901 (green alga)	30	69	0	3	23	99
Arabidopsis thaliana (land plant)	400	468	34	110	126	868
Crocosphaera watsonii WH8501 (cyanobacterium)	18	92	0	4	7	110
Dictyostelium discoideum (amoebozoan)	75	69	0	3	34	144
Saccharomyces cerevisiae S288C (yeast)	56	68	0	3	12	124

pipeline (*22*). The genome of this alga encodes ~84 glycoside hydrolases (GHs) and 128 glycosyl transferases (GTs). This is far greater than in the marine green microalga *Ostreococcus lucimarinus* CCE9901 and the extremophilic red alga *Cyanidioschyzon merolae* but less than in *Arabidopsis thaliana* (Table 1). Consistent with these results, inspection of the number of CAZy families (*22*) shows that *C. paradoxa* contains twice the number of GH families and 20% more GT families than *O. lucimarinus* and *C. merolae*. The smaller number of CAZy families in these unicellular algal lineages when compared to *A. thaliana* suggests less functional redundancy.

Many *C. paradoxa* CAZymes are involved in starch metabolism (*22*). Synthesis of the polysaccharide within Viridiplantae plastids relies on enzymes of the GT5 CAZy (*34*) family associated with glycogen synthesis in Bacteria such as adenosine diphosphate (ADP)–glucose pyrophosphorylases and ADP-glucose using starch synthases (SSs). Eukaryotes synthesize glycogen from uridine diphosphate (UDP)–glucose using either a GT3 (all fungi, some Amoebozoa, and animals) or a GT5 (alveolates, parabasalids, and Amoebozoa) type of transferase. The major *C. paradoxa* enzyme is phylogenetically related to the GT5 UDP-glucose–specific enzyme of heterotrophic eukaryotes (*35*) and has been partially purified from this alga (*36*). This suggests the absence of ADP-glucose pyrophosphorylase in *C. paradoxa*. Therefore, it was unexpected to find a second gene in the glaucophyte genome whose gene product is related to the SSIII-SSIV (GT5) type of starch synthases in Viridiplantae. This gene is phylogenetically related to glucan synthase in Chlamydiae, Cyanobacteria, and some Proteobacteria (fig. S5B) and likely played a key role in linking the biochemistry of the host and the endosymbiont. The SSIII-SSIV enzyme uses ADP-glucose in Bacteria and land plants (*35*), suggesting that *C. paradoxa* or, alternatively, the common ancestor of Viridiplantae and glaucophytes may have used both types of nucleotide sugars for starch synthesis.

Analysis of the gene-rich *C. paradoxa* genome unambiguously supports Plantae monophyly (*2*, *5*, *6*, *14*, *15*) (see discussion of Plantae branching order in the SOM), laying to rest a long-standing issue in eukaryote evolution. Plantae share many genes with an EGT or HGT origin that have essential functions such as photosynthesis, starch biosynthesis, plastid protein import, plastid solute transport, and alcohol fermentation. The alternative explanation of a polyphyletic Plantae would require the unlikely combination of a large number of independent HGT events in its major phyla followed by gene loss in all (or many) other eukaryotes. Consolidation of the Plantae allows insights into the gene inventory of their common ancestor. It is now clear that the Plantae ancestor contained many of the key innovations that characterize land plant and algal genomes, including extensive EGT from the cyanobacterial endosymbiont and retargeting of plastid-destined proteins, the minimal machinery required for plastid protein translocation, and complex pathways for fermentation and starch biosynthesis. In spite of the fact that glaucophytes retain peptidoglycan, an ancestral trait lost by all other algae (except the primary plastid in *Paulinella*) (*37*) and land plants, glaucophytes are not a lineage of "living fossils." Rather, the *C. paradoxa* genome contains a unique combination of ancestral, novel, and "borrowed" (e.g., via HGT) genes, similar to the genomes of other Plantae (*38*).

References and Notes

1. L. Margulis, *Origin of Eukaryotic Cells* (Yale University Press, New Haven, CT, 1970).
2. A. Reyes-Prieto, A. P. Weber, D. Bhattacharya, *Annu. Rev. Genet.* **41**, 147 (2007).
3. T. Cavalier-Smith, *Biosystems* **14**, 461 (1981).
4. S. M. Adl *et al.*, *J. Eukaryot. Microbiol.* **52**, 399 (2005).
5. N. Rodríguez-Ezpeleta *et al.*, *Curr. Biol.* **15**, 1325 (2005).
6. C. X. Chan *et al.*, *Curr. Biol.* **21**, 328 (2011).
7. H. S. Yoon, J. D. Hackett, G. Pinto, D. Bhattacharya, *Proc. Natl. Acad. Sci. U.S.A.* **99**, 15507 (2002).
8. F. Burki *et al.*, *PLoS ONE* **2**, e790 (2007).
9. D. Baurain *et al.*, *Mol. Biol. Evol.* **27**, 1698 (2010).
10. L. W. Parfrey *et al.*, *Syst. Biol.* **59**, 518 (2010).
11. J. W. Stiller, *Trends Plant Sci.* **12**, 391 (2007).
12. W. Löffelhardt, H. J. Bohnert, D. A. Bryant, *Plant Syst. Evol.* **11**, 149 (1997).
13. B. Pfanzagl *et al.*, *J. Bacteriol.* **178**, 332 (1996).
14. G. I. McFadden, G. G. van Dooren, *Curr. Biol.* **14**, R514 (2004).
15. A. P. M. Weber, M. Linka, D. Bhattacharya, *Eukaryot. Cell* **5**, 609 (2006).
16. A. Moustafa *et al.*, *Science* **324**, 1724 (2009).
17. W. Martin, R. G. Herrmann, *Plant Physiol.* **118**, 9 (1998).
18. J. T. Harper, P. J. Keeling, *Mol. Biol. Evol.* **20**, 1730 (2003).
19. W. Martin *et al.*, *Proc. Natl. Acad. Sci. U.S.A.* **99**, 12246 (2002).
20. N. Sato, M. Ishikawa, M. Fujiwara, K. Sonoike, *Genome Inform.* **16**, 56 (2005).
21. A. Moustafa, D. Bhattacharya, *BMC Evol. Biol.* **8**, 6 (2008).
22. The *Cyanophora paradoxa* Genome Project (http://dblab.rutgers.edu/cyanophora/home.php).
23. T. Wunder, R. Martin, W. Löffelhardt, E. Schleiff, J. M. Steiner, *BMC Evol. Biol.* **7**, 236 (2007).
24. J. M. Steiner, W. Löffelhardt, *Mol. Membr. Biol.* **22**, 123 (2005) (review).
25. C. Colleoni *et al.*, *Mol. Biol. Evol.* **27**, 2691 (2010).
26. J. Huang, J. P. Gogarten, *Genome Biol.* **8**, R99 (2007).
27. A. Moustafa, A. Reyes-Prieto, D. Bhattacharya, *PLoS ONE* **3**, e2205 (2008).
28. F. Yusa, J. M. Steiner, W. Löffelhardt, *BMC Evol. Biol.* **8**, 304 (2008).
29. J. Gross, D. Bhattacharya, *Trends Plant Sci.* **14**, 13 (2009).
30. S. Reumann, K. Inoue, K. Keegstra, *Mol. Membr. Biol.* **22**, 73 (2005) (review).
31. G. R. Wolfe, F. X. Cunningham, D. G. Durnford, B. R. Green, E. Gantt, *Nature* **367**, 566 (1994).
32. M. C. Posewitz, A. Dubini, J. Meuser, M. Seibert, M. Ghirardi, in *The Chlamydomonas Sourcebook: Organellar and Metabolic Processes*, D. Stern, Ed. (Academic Press, Oxford, ed. 2, 2009), vol. 2, pp. 217–255.
33. J. E. Meuser *et al.*, *J. Biotechnol.* **142**, 21 (2009).
34. B. L. Cantarel *et al.*, *Nucleic Acids Res.* **37** (Database issue), D233 (2009).
35. C. Plancke *et al.*, *Eukaryot. Cell* **7**, 247 (2008).
36. P. Deschamps, H. Moreau, A. Z. Worden, D. Dauvillée, S. G. Ball, *Genetics* **178**, 2373 (2008).
37. A. Reyes-Prieto *et al.*, *Mol. Biol. Evol.* **27**, 1530 (2010).
38. S. S. Merchant *et al.*, *Science* **318**, 245 (2007).

Acknowledgments: This work was made possible by grants from the National Science Foundation (MGSP 0625440 and MCB 0946528) awarded to D.B. and J.B. Partial support came from NSF grants EF 0827023 and DEB 0936884 awarded to D.B. and H.S.Y. and by BioGreen 21 (PJ008177) Rural Development Administration of South Korea awarded to H.S.Y. Air Force Office of Scientific Research grant FA9550-11-1-0211 supported work by J.E.M. and M.C.P. A.P.M.W. appreciates support from Deutsche Forschungsgemeinschaft CRC TR1. W.L. acknowledges support from the Austrian Science Foundation (P19683). G.B. acknowledges funding from Canadian Institute for Health Research operating grant MSP-14226. S.R. and A.S. acknowledge funding from the German Federal Ministry of Education and Research. G.B. acknowledges the Natural Sciences and Engineering Research Council of Canada (NSERC) for general laboratory funding. We are grateful to B. Andersen and the staff at the Provasoli-Guillard National Center for Culture of Marine Phytoplankton (CCMP) for preparing the axenic culture of *C. paradoxa*. We thank I. Plante and L. Forget for technical assistance in mtDNA cloning and sequencing and N. Beck for development of the MFannot computer program. The sequence data used to assemble the draft *C. paradoxa* genome and the Illumina mRNA-seq reads from this alga are archived at the NCBI Sequence Read Archive (SRA) under accession number SRP00920. The assembled genome and cDNA contigs, gene models, gene annotations, supporting material that is not in the SOM, and the phylogenomic results are available at (*22*). The complete *C. paradoxa* and *G. nostochinearum* mitochondrial genomes are available at NCBI under accession numbers HQ849544 and NC_015117, respectively. The partial mitochondrial genome data from *G. nostochinearum* are available at the genome Web site as part of the aligned protein data set used to infer the plastid multigene tree. We are grateful for the helpful comments of two anonymous reviewers of this manuscript.

Supporting Online Material

www.sciencemag.org/cgi/content/full/335/6070/843/DC1
Materials and Methods
SOM Text
Figs. S1 to S9
Tables S1 to S4
References

5 September 2011; accepted 5 January 2012
10.1126/science.1213561

Downloaded from www.sciencemag.org on February 16, 2012

RNA Editing Underlies Temperature Adaptation in K^+ Channels from Polar Octopuses

Sandra Garrett[1] and Joshua J. C. Rosenthal[1,2]*

To operate in the extreme cold, ion channels from psychrophiles must have evolved structural changes to compensate for their thermal environment. A reasonable assumption would be that the underlying adaptations lie within the encoding genes. Here, we show that delayed rectifier K^+ channel genes from an Antarctic and a tropical octopus encode channels that differ at only four positions and display very similar behavior when expressed in *Xenopus* oocytes. However, the transcribed messenger RNAs are extensively edited, creating functional diversity. One editing site, which recodes an isoleucine to a valine in the channel's pore, greatly accelerates gating kinetics by destabilizing the open state. This site is extensively edited in both Antarctic and Arctic species, but mostly unedited in tropical species. Thus adenosine-to-inosine RNA editing can respond to the physical environment.

Action potentials, during which the electrical potential across a cell membrane rapidly rises and falls, are the nervous system's basic unit of communication. In 1949, Hodgkin and Katz, using the squid giant axon, showed that the action potential's falling phase has steeper temperature dependence than that of the rising phase and that the membrane's return to the resting potential is particularly sensitive to temperature (*1*). Accordingly, they hypothesized that ectotherms would be forced to regulate the waveform of their action potentials to accommodate the thermal environment. As it emerged that the rising phase was due to voltage-dependent Na^+ channels, and the falling phase to voltage-dependent K^+ channels (*2*–*3*), the early observations suggested that potassium channel gating is more temperature sensitive than is sodium channel gating. This assertion has since been demonstrated (*4*). These observations also suggested that the closing kinetics of potassium channels, which determine the rate of return to rest, should be especially temperature sensitive, and this has also been shown (*5*). If K^+ channel kinetics did not adapt to temperature, the cold would make action potentials disproportionately broad and severely limit repetitive firing. Accordingly, potassium channel kinetics should be a prime target for regulation in organisms adapted to the extreme cold. This study shows that they are, but by an unsuspected mechanism.

To identify mechanisms of cold adaptation, we compared potassium channel orthologs from a tropical and an Antarctic octopus. Despite the enormous body of work on squid axons, we chose octopus as a comparative model because individuals generally have small home ranges, and species inhabit widely different thermal environments, from the poles to the equator. The Antarctic octopus was a *Pareledone sp*., which was collected from McMurdo Station (*6*), where the waters, at –1.8°C, are in equilibrium with sea ice and have been so for the past 28 to 38 million years (*7*). For comparison, we used *Octopus vulgaris* which we collected from a Puerto Rican reef at 30°C. Over the year, the temperature at this location fluctuates between ~25° and 35°C. We sequenced the ortholog of the squid delayed rectifier from each species (*8*).

On the basis of conventional natural selection, we hypothesized that the channels' genes would have evolved mutations to help tune them to their respective environments. Suprisingly, the primary sequences encoded by the two genes were virtually identical, differing at only four positions (fig. S1). They also shared 95% identity with the widely studied *Loligo* ortholog, indicating that the basic genetic template for the delayed rectifier is remarkably similar in coleoid cephalopods. To test whether the four differences affected function, each channel was expressed in *Xenopus* oocytes and characterized electrophysiologically at 2°, 15°, and 25°C. Experiments focused on opening and closing kinetics, which are the most temperature-sensitive properties, but also on the voltage dependence of opening and the rate of inactivation. Functionally, the two channels were virtually identical (Fig. 1A and table S1). As with the squid delayed rectifier, they opened rapidly in response to depolarization and exhibited a steep voltage-dependence between –20 and 20 mV. Upon repolarization, they closed quickly, following a simple exponential time course. When held at a constant depolarizing potential, both channels inactivated slowly, over the course of several seconds. There were some subtle differences. Antarctic channels opened slightly faster (Fig. 1A), but this difference was only significant at potentials near the threshold for activation. The steepness factor (Z) of their steady-state voltage dependence was also slightly smaller (table S1). Overall, however, in spite of their drastically different environments the genomically encoded channels displayed essentially the same behavior. At their respective native temperatures, Antarctic channels would open about 14 times slower and close about 60 times slower than would tropical channels (see Q_{10}s in table S1). Either the Antarctic octopus barely compensates for the cold, or post-transcriptional mechanisms are important.

Adenosine deamination, the most common form of RNA editing, is carried out by a family of enzymes known as ADARs (adenosine deaminases that act on RNA). ADARs convert adenosine (A) to inosine (I) (*9*). Because inosine is

[1]Institute of Neurobiology, University of Puerto Rico–Medical Sciences Campus, San Juan 00901, PR. [2]Department of Biochemistry, University of Puerto Rico–Medical Sciences Campus, San Juan 00936, PR.

*To whom correspondence should be addressed. E-mail: rosenthal.joshua@gmail.com

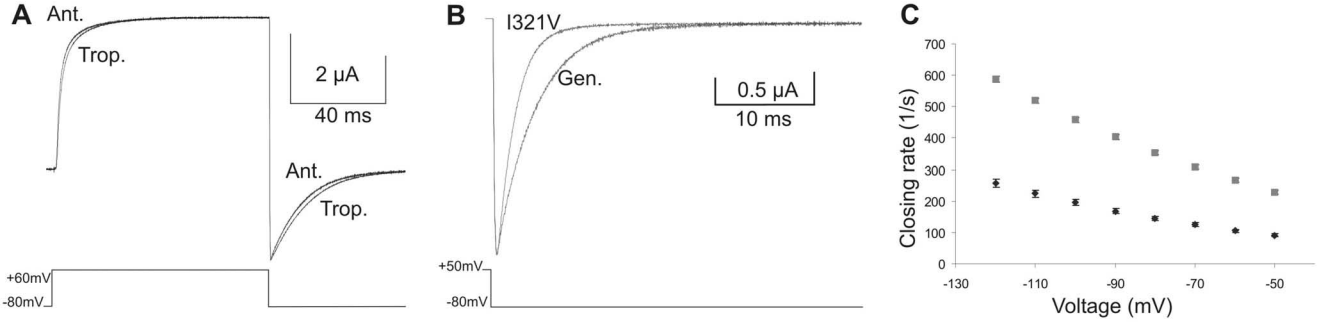

Fig. 1. RNA editing, but not gene-level differences, changes channel function. (**A**) Current traces for Antarctic and tropical K_v1 genomic channels in response to a voltage step from –80 mV to +60 mV. Traces have been scaled in order to show the near identity in opening and closing kinetics. (**B**) Representative current traces focusing on closing kinetics for genomic Antarctic and I321V edited channels. Currents were activated by a stimulus to +50 mV for 20 ms, but only their decay after a return to –80 mV is shown. (**C**) Channel closing kinetics over a range of repolarization voltages after an activating step to +50 mV. Error bars, SEM; n = 16 oocytes for genomic and 9 for I321V. ◆ indicate genomic Antarctic and ■ indicate I321V edited. All data was recorded from voltage-clamped *Xenopus* oocytes injected with cRNA for the appropriate construct, and the temperature was maintained at 15°C.

Downloaded from www.sciencemag.org on February 16, 2012

read as guanosine by the translational machinery, codons in mRNAs can change (*10*). A-to-I editing is common in the nervous system, having been identified in mRNAs encoding ion channels and receptors (*11*–*13*). Extensive editing by this mechanism has been described in squid, in which it modifies diverse mRNAs, including the squid delayed rectifier K^+ channel (*14, 15*). We compared cDNA sequences to check whether the octopus channels were edited as well. Our preliminary cloning results showed site-specific A/G variation in the electropherograms of direct sequences, which is a hallmark of A-to-I RNA editing. To investigate further, we cloned and sequenced 50 individual cDNAs from the stellate ganglia of each species and then looked for A or G variation that was not present in the gene sequence. Each species showed extensive editing. For the Antarctic octopus, there were 18 editing sites, 9 of which caused amino acid changes (fig. S1). For the tropical octopus, there were 15 editing sites, 10 of which caused amino acid changes. Of the 12 nonsilent sites, 5 were species specific, and 4 of the shared sites were edited to greatly different extents (Fig. 2A). Thus, in these channels greater species diversity is generated by RNA editing than by gene mutations.

Do the RNA edits alter channel function? Four editing sites were selected for further study because they were edited exclusively, or to a much greater extent, in one species or the other; N105G and I321V were considered candidates for cold adaptation, whereas N40S and S54G were considered candidates for warm adaptation. [In edited codons, the genomically encoded amino acid was recoded; for example, N105G indicates that asparagine at position 105 was replaced by glycine. Single-letter abbreviations for the amino acid residues are as follows: A, Ala; C, Cys; D, Asp; E, Glu; F, Phe; G, Gly; H, His; I, Ile; K, Lys; L, Leu; M, Met; N, Asn; P, Pro; Q, Gln; R, Arg; S, Ser; T, Thr; V, Val; W, Trp; and Y, Tyr.] N105G is only found in the Antarctic channel, and N40S is only found in the tropical channel. The other two sites showed greater than 50% differences in editing, with I321V highly edited in the Antarctic channel, and S54G highly edited in the tropical channel (Fig. 2A). I321V lies in the fifth transmembrane span (S5), within the pore domain (Fig. 2B) (*16*). The rest of the sites are located in the T1 domain (Fig. 2B), a region that is important for tetramerization (*17*, *18*). At the genomic level, all of these positions except S54G are nearly invariant among Kv1 channels, suggesting that they are functionally important.

To characterize their effects, each of the four edits were singly introduced into the unedited channel background (genomic) and studied at 15° and 25°C. Three of the four editing sites produced clear functional changes to a number of channel properties (table S1). The tropical edits (N40S and S54G) had similar effects: Both slowed channel opening by about 50%, and both increased the rate of inactivation by 30% for N40S and by 60% for S54G (fig. S2). These effects on gating were somewhat surprising, given that both sites are in the cytoplasmic tetramerization domain, which is thought to be physically separate from the membrane-bound voltage sensor and pore (*16*, *19*). However, others have reported that the T1 domain influences function (*20*, *21*). The Antarctic edits also altered function. N105G caused subtle changes in activation and deactivation kinetics. The most pronounced effect of all, however, was due to I321V, which more than doubled the rate of closure (Fig. 1, B and C) and produced a positive shift in the voltage dependence of opening (table S1). This effect was dominant, speeding closing when combined with other editing sites that mimicked natural editing patterns (table S1 and fig. S3) (*6*).

Because I321V was highly edited in the Antarctic species and dramatically accelerated deactivation kinetics, which underlie the action potential's afterhyperpolarization, it was a good candidate for cold adaptation. This position lies in the S5 helix, an interface between the voltage sensor and the ion conduction pathway (*16*, *22*, *23*). At negative voltages, the voltage sensor is thought to force the gate shut via contact between the S4-S5 linker and the S6 helix. At positive potentials, the voltage sensor moves away, allowing the channel to open (*22*, *24*, *25*). The open state is not stable, however, and channels flicker between open and closed conformations (*26*, *27*). Because I321V causes the channel to close faster and also shifts its voltage sensitivity to more positive potentials, we hypothesized that it destabilizes the open state. This possibility was examined directly by recording single-channel events. Representative records for both unedited and I321V Antarctic channels show that I321V channels close more frequently (Fig. 3, A and C). To quantify this phenotype, recordings were idealized by using an algorithm, and the durations of open and closed events were determined (*28*). The average open duration for the unedited Antarctic channels was twice that of I321V channels. The durations of closed events did not change, suggesting that I321V selectively affects the open to closed state transition. This idea was reinforced by a simple five-state model (Fig. 3, E and F): By doubling

A

Site	nt.	Amino acid change	Domain	Editing percentages	
				Antarctic	Tropical
1	119	N40S	T1	0	76
2	124	S42G	T1	0	10
3	160	S54G	T1	10	68
4	175	T59A	T1	0	10
5	314-315	N105G	T1	92	0
6	348	K116R	T1	16	0
7	379	K127E	T1	88	78
8	403	I135V	T1	96	80
9	499	I167V	S1	96	78
10	508	M*170V	S1	98	84
11	961	I321V	S5	92	30
12	1114	I372V	P/S6	90	82

B

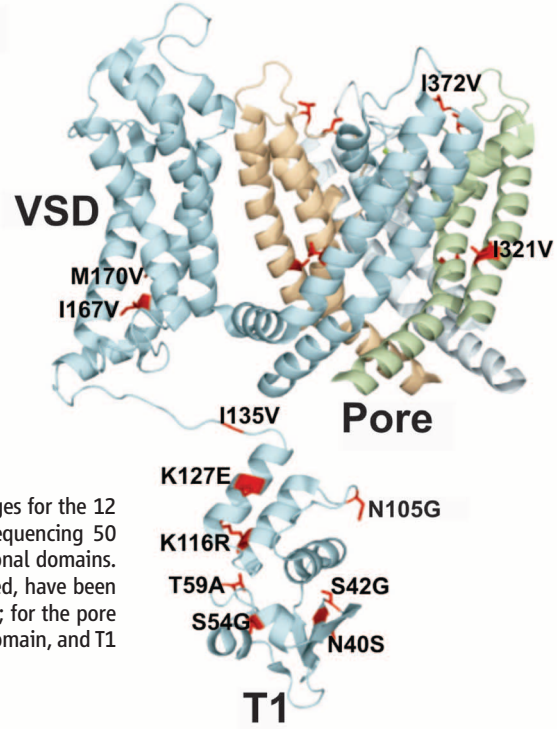

Fig. 2. mRNAs encoding octopus K_v1 channels are extensively edited. (**A**) Editing percentages for the 12 nonsilent sites found in the Antarctic and tropical octopus K_v1 channels calculated by sequencing 50 individual cDNA clones for each channel. (**B**) Octopus editing sites occur in different functional domains. Homologous positions to those altered by RNA editing in octopus K_v1 channels, shown in red, have been mapped on the $K_v1.2$ crystal structure (*23*). One full subunit of the tetramer is shown (blue); for the pore region, all four subunits are shown, each in a different color. VSD indicates voltage-sensing domain, and T1 indicates tetramerization domain.

Downloaded from www.sciencemag.org on February 16, 2012

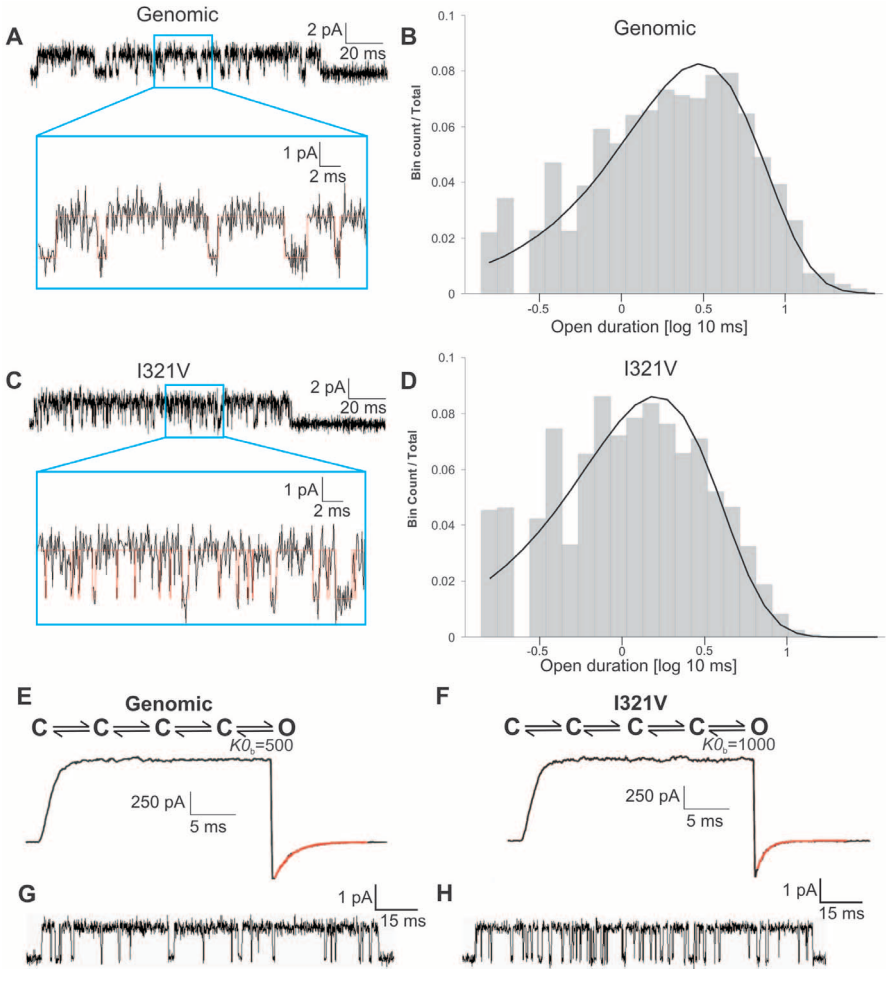

Fig. 3. The editing site I321V speeds channel-closing kinetics by destabilizing the open state. Current traces from cell-attached patches containing single (**A**) Antarctic genomic and (**C**) I321V K_v1 channels. Channels opened in response to a voltage step from −80 mV to +60 mV. I321V channels close more frequently. Overlapping red lines (insets) show idealizations of traces as a series of open and closed events. (**B** and **D**) Duration distributions of open events for genomic Antarctic and I321V channels. The average duration of open events in the genomic channel (3.42 ms) was about twice that of I321V channels (1.72 ms). (**E** and **F**) Simple five-state models for genomic Antarctic and I321V channel gating and simulations generated from the models. Doubling the backward rate constant for the final transition recapitulates both the macroscopic difference in closing kinetics and the single channel behavior (**G** and **H**) between genomic and I321V channels. Rate constants were assumed to depend exponentially on voltage: $k = k_0 e^{(zFV/RT)}$, where F is the Faraday's constant, V is voltage, R is the universal gas constant, and T is the temperature. For the above models: $k_{1f} = 700$, $z = 0.3$; $k_{1b} = 50$, $z = 1.6$; $k_{2f} = 1200$, $z = 1.8$; $k_{2b} = 25$, $z = 1.1$; $k_{3f} = 600$, $z = 0.8$; $k_{3b} = 150$, $z = 1.5$; $k_{4f} = 3000$, $z = 0.02$; k_{4b} variable, $z = 0.2$. A stochastic simulation of 1000 channels pulsed from −80mV to +60mV and back to −80mV showed faster closing with the I321V model. The maximum open probability was similar: 0.59 versus 0.55 for genomic and I321V, respectively. Closing rates (single exponential fit, overlapping red line) were similar to those obtained from room temperature experimental data: 625 and 1250 (s^{-1}) simulated kinetics versus 610 and 1423 (s^{-1}) experimental kinetics for genomic and I321V, respectively. For the single-channel simulations, the average open duration using the I321V model was half that for the genomic model.

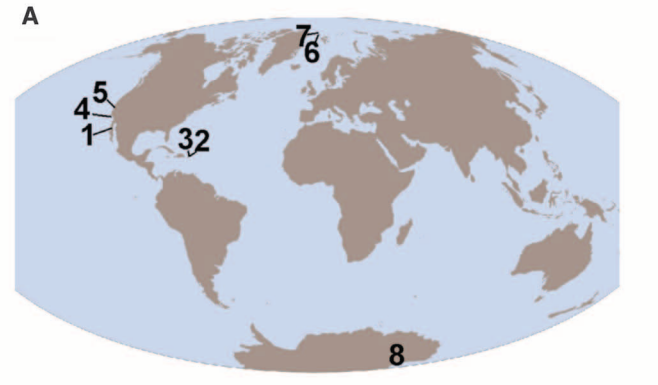

Collection sites and water temperatures for octopus species

	Species	Collection site	Water temp. (°C)
1	*Octopus digueti*	Estuary, Baja California	37
2	*Octopus defilippi*	Reef flat, Rio Grande, PR	32
3	*Octopus vulgaris*	Inshore reef, Luquillo, PR	28
4	*Octopus bimaculata*	Near shore rock ledge, Catalina Is., CA	18
5	*Octopus rubescens*	Near shore, Monterey, CA	10
6	*Benthoctopus piscatorum*	Benthic trawl, north Svalbard, Norway	0
7	*Bathypolypus arcticus*	Benthic trawl, north Svalbard, Norway	-1
8	*Pareledone sp.*	McMurdo station, Antarctica	-2

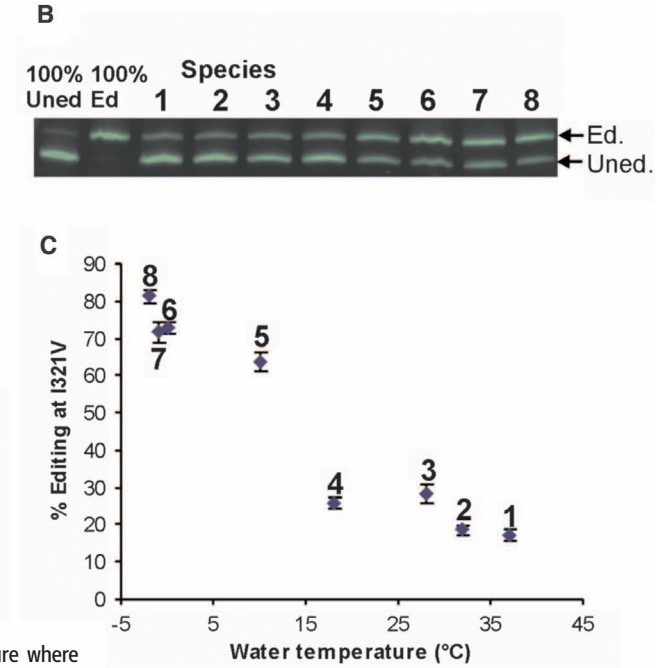

Fig. 4. The extent of editing at I321V correlates with the water temperature where octopus species were captured. (**A**) Collection sites for eight octopus species and the water temperatures and habitats at the time of capture. (**B**) Representative poison primer extension assay showing the amount of I321V editing among the eight species. (**C**) I321V editing percentages for the eight species, based on poison primer extension assays, versus water temperature at capture site. Error bars, SEM; $n = 4$ assays.

Downloaded from www.sciencemag.org on February 16, 2012

the backward rate constant for the final transition, both the macroscopic difference in closing kinetics (Fig. 3, E and F) and the single-channel difference in open duration (Fig. 3, G and H) could be recapitulated. In agreement with experimental data, the model predicts nearly identical activation kinetics and open probability for the two channels (Fig. 3, E and F). Thus, it appears that once open, I321V channels are poised to close rapidly, but the opening kinetics and other properties are preserved. In an axon, we predict that the major effect of I321V channels would be to accelerate the after-hyperpolarization, and thus shorten the refractory period, increasing repetitive firing rates.

If editing of codon I321 is indeed a cold adaptation, then we might expect other cold-adapted octopuses to make the same edit. To test this idea, we collected two Arctic species from benthic trawls northwest of the Svalbard archipelago, where water temperatures at ~0°C were similar to those in Antarctica. We also collected two more tropical species, one from Puerto Rico and one from a desert lagoon in Baja California, and two temperate species from California (Fig. 4A). Editing levels at I321V, as determined by a primer extension assay, correlated very well with the environmental temperature where the species were captured (Fig. 4, B and C). We also quantified all editing sites in the six new species using direct sequencing. Although many of the other editing sites were edited differentially among the eight species, I321V correlated most closely with temperature (table S2).

In Coleoid Cephalopods, and in other higher metazoans, A-to-I RNA editing adds a layer of complexity to the proteome. A clear advantage to this strategy is that it allows options: Different isoforms can be expressed in response to different conditions. Exactly how organisms exercise these options is largely unknown. *Drosophila* and rodents use editing to fine-tune protein function temporally, over the course of development (*29*, *30*), and spatially, in different brain regions (*12*). Here, we present evidence that RNA editing can respond to an external pressure: temperature. Although still maintaining the basic K^+ channel plan, octopuses can make fast-closing versions, and the extent of their expression can be graded. A basic question that remains is whether octopuses use editing for rapid acclimation or long-term adaptation. For each possibility, the biochemical mechanisms that impart temperature sensitivity to the editing process would be different. Others have shown that the RNA structures that drive editing evolve and generate species-specific patterns, suggesting a plausible mechanism for adaptation (*31*). Acclimation could arise from temperature-sensitive RNA structures, or temperature-dependent expression of other factors that control ADAR's access to specific editing sites.

References and Notes

1. A. L. Hodgkin, B. Katz, *J. Physiol.* **109**, 240 (1949).
2. A. L. Hodgkin, A. F. Huxley, *J. Physiol.* **116**, 449 (1952).
3. C. M. Armstrong, F. Bezanilla, E. Rojas, *J. Gen. Physiol.* **62**, 375 (1973).
4. F. Kukita, *J. Membr. Biol.* **68**, 151 (1982).
5. B. M. Rodríguez, D. Sigg, F. Bezanilla, *J. Gen. Physiol.* **112**, 223 (1998).
6. Materials and methods are available as supporting material on *Science* Online.
7. M. E. Katz *et al.*, *Science* **332**, 1076 (2010).
8. J. J. Rosenthal, R. G. Vickery, W. F. Gilly, *J. Gen. Physiol.* **108**, 207 (1996).
9. B. L. Bass, H. Weintraub, *Cell* **55**, 1089 (1988).
10. C. Basilio, A. J. Wahba, P. Lengyel, J. F. Speyer, S. Ochoa, *Proc. Natl. Acad. Sci. U.S.A.* **48**, 613 (1962).
11. T. Bhalla, J. J. Rosenthal, M. Holmgren, R. Reenan, *Nat. Struct. Mol. Biol.* **11**, 950 (2004).
12. C. M. Burns *et al.*, *Nature* **387**, 303 (1997).
13. T. Melcher, S. Maas, M. Higuchi, W. Keller, P. H. Seeburg, *J. Biol. Chem.* **270**, 8566 (1995).
14. D. E. Patton, T. Silva, F. Bezanilla, *Neuron* **19**, 711 (1997).
15. J. J. Rosenthal, F. Bezanilla, *Neuron* **34**, 743 (2002).
16. S. B. Long, E. B. Campbell, R. Mackinnon, *Science* **309**, 897 (2005).
17. A. Kreusch, P. J. Pfaffinger, C. F. Stevens, S. Choe, *Nature* **392**, 945 (1998).
18. M. Li, Y. N. Jan, L. Y. Jan, *Science* **257**, 1225 (1992).
19. W. R. Kobertz, C. Williams, C. Miller, *Biochemistry* **39**, 10347 (2000).
20. S. J. Cushman *et al.*, *Nat. Struct. Biol.* **7**, 403 (2000).
21. D. L. Minor Jr. *et al.*, *Cell* **102**, 657 (2000).
22. Z. Lu, A. M. Klem, Y. Ramu, *J. Gen. Physiol.* **120**, 663 (2002).
23. G. J. Soler-Llavina, T. H. Chang, K. J. Swartz, *Neuron* **52**, 623 (2006).
24. S. B. Long, X. Tao, E. B. Campbell, R. MacKinnon, *Nature* **450**, 376 (2007).
25. M. M. Pathak *et al.*, *Neuron* **56**, 124 (2007).
26. F. Conti, E. Neher, *Nature* **285**, 140 (1980).
27. I. Llano, C. K. Webb, F. Bezanilla, *J. Gen. Physiol.* **92**, 179 (1988).
28. F. Qin, L. Li, *Biophys. J.* **87**, 1657 (2004).
29. B. R. Graveley *et al.*, *Nature* **471**, 473 (2011).
30. H. Lomeli *et al.*, *Science* **266**, 1709 (1994).
31. R. A. Reenan, *Nature* **434**, 410 (2005).

Acknowledgments: We are grateful to T. de Lange Wenneck and the Norwegian Institute of Marine Research for the invitation to collect Arctic cephalopods aboard the RV *Jan Mayen*. We thank C. DeVries for samples of *Pareledone*. This work was supported by the National Institutes of Health (NIH) Ruth L. Kirschstein National Research Service Predoctoral Fellow Award FNS064774A, NIH 2 U54 NS039405-06, NIH R01 NS064259NIH, and the National Science Foundation (NSF) IBN-0344070. Part of the work was conducted in the Molecular Biology Core Facility at the Institute of Neurobiology that is supported by Research Centers in Minority Institutions grant G12 RR 03051. K_v1 sequences have been submitted to GenBank. The accession nos. are as follows: JQ246406, *Pareledone* sp.; JQ246407, *Octopus vulgaris*; JQ246408, *Octopus digueti*; JQ246409, *Octopus defilippi*; JQ246410, *Octopus bimaculata*; JQ246411, *Bathypolypus arcticus*; JQ246412, *Benthoctopus piscatorum*; JQ246413, *Octopus rubescens*. S.C.G. performed all experiments, participated in designing experiments, collected Arctic samples, and wrote the manuscript. J.J.C.R. participated in designing experiments; collected Antarctic, temperate, and tropical samples; and edited the manuscript.

Supporting Online Material

www.sciencemag.org/cgi/content/full/science.1212795/DC1
Materials and Methods
Figs. S1 to S3
Tables S1 to S3
References (*32*–*35*)

17 August 2011; accepted 9 December 2011
Published online 5 January 2012;
10.1126/science.1212795

Downloaded from www.sciencemag.org on February 16, 2012

Crystal Structure of a Lipid G Protein–Coupled Receptor

Michael A. Hanson,[1*] Christopher B. Roth,[1] Euijung Jo,[2] Mark T. Griffith,[1] Fiona L. Scott,[1] Greg Reinhart,[1] Hans Desale,[1] Bryan Clemons,[1] Stuart M. Cahalan,[2] Stephan C. Schuerer,[3] M. Germana Sanna,[2] Gye Won Han,[3] Peter Kuhn,[4] Hugh Rosen,[2,5*†] Raymond C. Stevens[3*†]

The lyso-phospholipid sphingosine 1-phosphate modulates lymphocyte trafficking, endothelial development and integrity, heart rate, and vascular tone and maturation by activating G protein–coupled sphingosine 1-phosphate receptors. Here, we present the crystal structure of the sphingosine 1-phosphate receptor 1 fused to T4-lysozyme ($S1P_1$-T4L) in complex with an antagonist sphingolipid mimic. Extracellular access to the binding pocket is occluded by the amino terminus and extracellular loops of the receptor. Access is gained by ligands entering laterally between helices I and VII within the transmembrane region of the receptor. This structure, along with mutagenesis, agonist structure-activity relationship data, and modeling, provides a detailed view of the molecular recognition and requirement for hydrophobic volume that activates $S1P_1$, resulting in the modulation of immune and stromal cell responses.

G protein–coupled receptors (GPCRs) convert exogenous signals into a cellular response by initiating a variety of intracellular signaling cascades. The sphingosine 1-phosphate receptor subtype 1 ($S1P_1$) (*1*) belongs to a subclass of the GPCR family originally termed the endothelial differentiation gene (EDG) family of lipid receptors. The family was later renamed to reflect activation by two distinct lipids, S1P and lysophosphatidic acid (*2*). The S1P receptor family comprises five members ($S1P_{1-5}$) with high sequence identity within the ligand-binding region, including the conserved sphingolipid binding pocket. Activation of the $S1P_1$ receptor through exogenous ligands, both physiological and pharmacological, results in inhibition of

[1]Receptos, 10835 Road to the Cure, Suite 205, San Diego, CA 92121, USA. [2]Department of Chemical Biology, The Scripps Research Institute, 10550 North Torrey Pines Road, La Jolla, CA 92037, USA. [3]Department of Molecular Biology, The Scripps Research Institute, 10550 North Torrey Pines Road, La Jolla, CA 92037, USA. [4]Department of Cell Biology, The Scripps Research Institute, 10550 North Torrey Pines Road, La Jolla, CA 92037, USA. [5]The Scripps Research Institute Molecular Screening Center, 10550 North Torrey Pines Road, La Jolla, CA 92037, USA.

*To whom correspondence should be addressed. E-mail: mhanson@receptos.com (M.A.H.), stevens@scripps.edu (R.C.S.), hrosen@scripps.edu (H.R.)
†These authors contributed equally to this work.

lymphocyte recirculation (*3*). This physiological effect was leveraged in the development of the nonselective S1P agonist prodrug FTY720 (fingolimod), recently approved for the clinical treatment of relapsing-remitting multiple sclerosis (*4*).

The structures of multiple members of the GPCR family have been determined at atomic resolution in both agonist and antagonist conformation, as well as in complex with a cognate G protein (*5*–*16*). Together, these structures help define the repertoire of structural changes associated with the class A GPCR family that are required to recognize ligands with very different physicochemical properties, yet that signal through common mechanisms. We report here the structural characterization of a lipid-sensing GPCR, the $S1P_1$ receptor fused to T4-lysozyme, in complex with the selective antagonist sphingolipid mimic (*R*)-3-amino-(3-hexylphenylamino)-4-oxobutylphosphonic acid (ML056) (*17*) to 3.35 Å using traditional x-ray diffraction data processing methods and to 2.8 Å resolution using an experimental microdiffraction data assembly method to help process data of rapidly decaying microcrystals (table S1) (*18*). Analysis of the structure, along with structure-activity and mutagenesis data, reveals key interactions associated with the binding of physiological phospho-sphingolipids and related molecules (class I ligands). In addition, we report interactions within the binding pocket that are not required for class I ligand binding or function, but that directly affect binding of class II ligands, small-molecule $S1P_1$ agonists that are not dependent on polar lipid head group interactions (*19*).

Overall, the $S1P_1$-T4L receptor structure shares many common features with previously determined receptors, including seven-transmembrane helices arranged in a structurally conserved bundle. The extracellular region for all GPCRs is composed of three loops: ECL1 between helices II and III, ECL2 between helices IV and V, and ECL3 between helices VI and VII. However, a number of distinguishing characteristics are associated with the ligand-binding pocket in the $S1P_1$ receptor (Fig. 1A). The N terminus folds over the top of the receptor and contributes binding interactions, while at the same time forming a helical cap, which limits access to the amphipathic binding pocket (Fig. 1B). Both ECL1 and ECL2 pack tightly against the N-terminal helix, further occluding ligand access to the receptor from the extracellular milieu while contributing a large surface area to the binding pocket. The limited access to the ligand-binding site from the extracellular region explains why $S1P_1$ ligands, including S1P, show slow saturation of receptor binding in the presence of excess ligand (*1*) (Fig. 1C). The ligands may gain access to the binding pocket from within the membrane bilayer, possibly through a gap between helices I and VII (Fig. 1D). This region of the receptor structure is more open than in other receptors due to a repositioning of helices I and II toward helix III in $S1P_1$ relative to other receptors, which is apparent after alignment using GPCR fold core residues (fig. S4) (*20*). A similar mode of entry has been postulated for retinal loading into opsin, as well as for the entry of anandamide into the closely related cannabinoid receptors (*21*–*23*).

The binding pocket of the $S1P_1$ receptor is highly amphipathic, reflecting the nature of its hydrophobic-zwitterionic agonist. The established roles of $R120^{3.28}$ and $E121^{3.29}$ (*24*) that interact with the zwitterionic sphingosine head group (*25*, *26*) are recapitulated in their interactions with the phosphonate and primary amine of ML056 (Fig. 2). However, a third predicted ionic interaction between $R292^{7.35}$ and the phosphate head group is not apparent in the ML056 interactions. Instead, the phosphonate head group of ML056 is surrounded by a ring of positively charged and polar residues contributed by helices III and VII, ECL2, and the N-terminal capping helix, which form a positively charged pocket that provides charge complementarity and high-affinity interactions to the phosphate group of the sphingolipids. The primary amine of ML056 is likely protonated at physiological pH, which results in a zwitterionic head group. This positive charge contributes to the binding affinity of sphingosine-containing compounds through ionic interactions with the carboxylate side chain of $E121^{3.29}$, as well as the amide carbonyl of $N101^{2.60}$ (helix II). The involvement of $N101^{2.60}$, Y29, and K34 (*27*) in the binding of sphingosine-like head groups was not previously predicted. We, therefore, verified their involvement through mutagenesis coupled with signaling assays (table S3).

The phenyl acyl tail of ML056 inserts into a largely aromatic pocket consisting of residues from helices III, V, VI, and VII, as well as ECL2. Most of the hydrophobic portion of the binding pocket is lined with short aliphatic residues that define the shape of the pocket and four aromatic residues that provide the potential for specific interactions (Fig. 2). The involvement of some of these residues in the binding and signaling of the S1P receptor was determined previously through molecular modeling and mutagenesis. The acyl chain is precisely structured, which was not expected on the basis of commonly held views of acyl chain flexibility (*28*). This reflects a role for selective hydrophobic interactions within the pocket that result in this preferred low-energy minimum. The previously

Downloaded from www.sciencemag.org on February 16, 2012

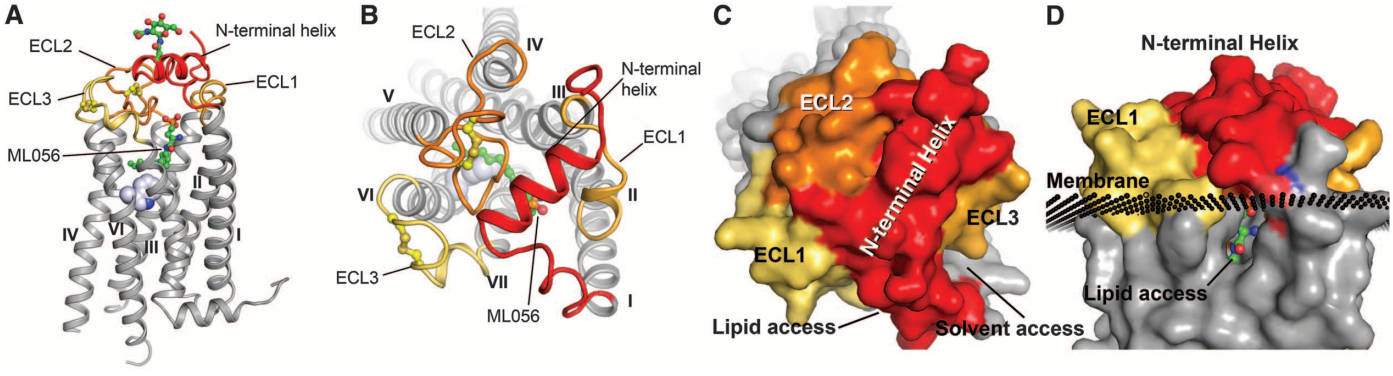

Fig. 1. Overview of the structural features specific to the $S1P_1$ receptor. (**A**) Ribbon trace of the receptor with relevant features highlighted. The receptor folds in a traditional seven-transmembrane helical bundle similar to other class A GPCRs. However, the extracellular domain of the $S1P_1$ receptor adopts a fold that incorporates helical elements from the N terminus (red ribbon), as well as ECL1 (gold ribbon), occluding access to the ligand-binding pocket. ECL2 (orange ribbon) and ECL3 (yellow ribbon) are both constrained by intraloop disulfide bonds (yellow ball-and-stick) and contribute important interactions within the binding pocket. The compound ML056 is shown in green carbon ball-and-stick rendering, and $W269^{6.48}$ is rendered as a space-filling atom in blue as reference point for the binding pocket. The T4L fusion protein was omitted from this figure for clarity. (**B**) Top view of the receptor highlighting the critical role of the N-terminal helix in capping the ligand and limiting solvent access to the binding pocket. There is a sizable access point for ligand entry and exit between helices I and VII. (**C**) Surface rendering of the receptor from the top view highlighting the occluded nature of the binding pocket with two points of access either for lipid or solvent. (**D**) Side view of the lipid access channel relative to the predicted position of the membrane bilayer.

published mutagenesis data for the $S1P_1$ receptor are mostly consistent with the structure of the antagonist-bound receptor.

Structure-activity data from ML056-like compounds reveal an antagonist island that is easily converted to full agonism by small extensions of the acyl chain, suggesting that the volume occupied by the hydrophobic portion of the ligand plays a key role in triggering agonist signaling (*29*). In addition, changing the substitution pattern around the phenyl ring from para to meta switches the pharmacology of the compound series from agonist to antagonist, localizing the effect of hydrophobic volume changes within the binding pocket. Docking studies corroborate these trends in that the ML056 antagonist binding pocket of the $S1P_1$ receptor could not accommodate an acyl carbon greater than nine carbons in length without appreciable ligand strain (Fig. 3A) (*30*, *31*). The increased volume requirements for agonists were accommodated in the model by using an induced fit docking protocol that allowed the side chains of the residues lining the hydrophobic portion of the binding pocket to move in response to a para-substituted regio-isomer of ML056 while holding the S1P head group interactions fixed (Fig. 3B) (*32*–*34*). The largest positional change occurred in $F273^{6.52}$, whose movement along with slight positional changes in $W269^{6.48}$ and $F125^{3.33}$ accommodated binding of the endogenous S1P ligand as well as FTY720-P, suggesting that these residues may be particularly important for signaling (Fig. 4A).

Inspection of known agonists of the $S1P_1$ receptor allows their classification into two basic groups on the basis of receptor interactions: class I ligands that can be either lipid-like compounds mimicking S1P and its sphingophospholipid head-group interactions, as exemplified by FTY720-P, or nonlipid like small molecules possessing polar groups that interact with the S1P head-group region, sharing similar bond lengths and volume to drive affinity and efficacy,

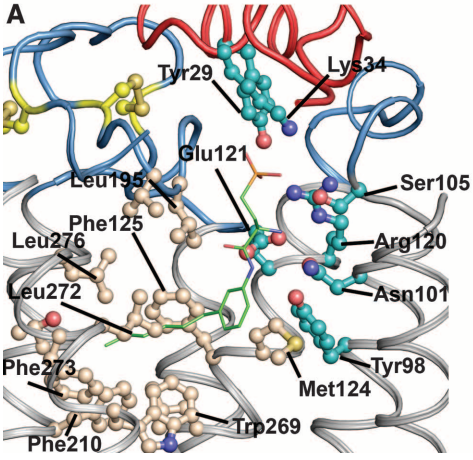

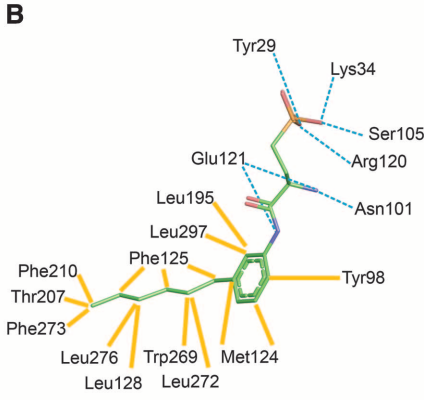

Fig. 2. Detailed structural representation of the interactions between ML056 and the $S1P_1$ receptor. (**A**) ML056 is colored as green carbon sticks. Polar residues within the binding pocket are colored with cyan carbons, whereas residues comprising the hydrophobic portion of the binding pocket are colored with tan carbons, and the two disulfide bonds are shown in yellow ball-and-stick representation. The N-terminal helix and extracellular loops are shown as red and blue ribbons, respectively. (**B**) Two-dimensional residue interaction map illustrating the amino acids within 4 Å of ML056. Polar interactions are represented by dotted cyan lines, whereas hydrophobic interactions are represented as solid yellow lines drawn to the closest atom of the ligand.

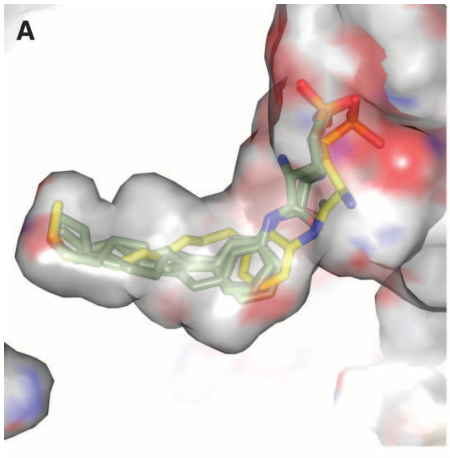

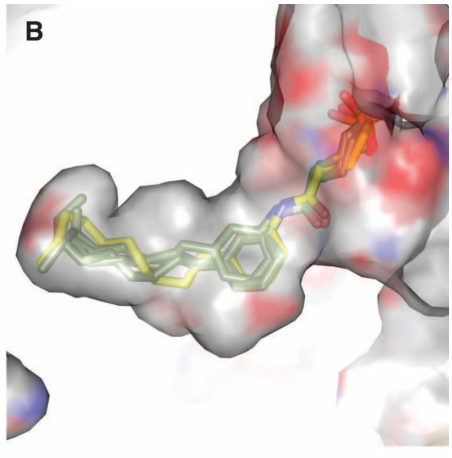

C

Ligand	Antagonist Structure: Docking Score	Antagonist Structure: Calculated ΔG bind (kcal/mol)	Antagonist Structure: Calculated Ligand Strain (kcal/mol)	Induced Fit Modeled Agonist Structure: Docking Score	Induced Fit Modeled Agonist Structure: Calculated ΔG bind (kcal/mol)	Induced Fit Modeled Agonist Structure: Calculated Ligand Strain (kcal/mol)
ML056	-12.4	-95.2	8.3	-13.6	-95.1	11.8
ML056 + 1 carbon	-12.7	-98.9	11.9	-13.7	-102.3	9.5
ML056 + 2 carbons	-13.0	-103.6	11.9	-14.9	-97.6	16.2
ML056 + 3 carbons	-13.1	-98.5	17.7	-15.0	-94.4	23.3
ML056 + 4 carbons	-11.8	-77.1	22.5	-15.0	-97.2	27.0

Fig. 3. Docking study of ML056 analogs (green carbons) with progressively longer acyl chains. A 10-carbon acyl chain (yellow carbons) switches the response from antagonism to agonism. (**A**) Docking each of the five ligands into the antagonist binding pocket resulted in essentially superimposable docking poses for all of the ligands except ML056 + 4 (yellow carbons), which cannot maintain sphingolipid head-group binding interactions due to high ligand strain. (**B**) Docking each of the five ligands into the induced fit agonist-modeled binding pocket reveals that all ligands can bind with reasonable docking scores while maintaining head-group interactions. (**C**) Table of docking and MM-GB/SA (molecular mechanics, generalized born and solvent accesibility) calculations for assessing the quality of the docking poses. The agonist compound ML056 + 4 docked into the antagonist binding pocket generates a steep drop in calculated ΔG_{bind}, along with an increase in calculated ligand strain.

Downloaded from www.sciencemag.org on February 16, 2012

as exemplified by SEW2871; and class II small-molecule agonists that do not require interactions with the polar head-group–interacting region of the receptor, as exemplified by CYM-5442 (*19*, *35*), and instead make specific variant binding interactions. The binding of the endogenous ligand S1P, as well as other head group–containing class I agonists to the $S1P_1$ receptor, involves strong ionic interactions between the zwitterionic head group and a cluster of charged and polar residues from helices II, III, and VII and the N-terminal capping helix of the receptor (*19*, *25*, *36*). The interactions within the S1P binding region are likely similar to those exhibited by the head group of ML056. The length and position of the acyl chain relative to the amino-phosphate or amino-phosphonate groups generally dictate the pharmacology of these compounds (*37*). The class II agonists to the $S1P_1$ receptor were developed in response to the observation that certain library screening hits do not interact with the conserved polar residues, $R120^{3.28}$ and $E121^{3.29}$, which was hypothesized to increase their potential for tuning receptor subtype selectivity while also providing greater variability in physicochemical properties (*19*, *35*). Recently, we reported development of such a ligand, CYM-5442, which does not require interactions with either $R120^{3.28}$ or $E121^{3.29}$ of the $S1P_1$ receptor, yet induces ERK phosphorylation in vitro and potent lymphopenia in vivo with nanomolar potency, and showed noncompetitive inhibition of ERK signaling with ML056 (*19*). In conjunction with structural efforts, we have investigated the mechanism of binding of CYM-5442 to the $S1P_1$ receptor through mutagenesis of the ligand-interacting portion of the binding pocket.

A series of conservative point mutations along the hydrophobic ligand-binding pocket were made to probe for defective binding or signaling in response to either S1P or CYM-5442 (*38*) and complement previous studies (*28*, *39*). Three such $S1P_1$ receptor mutants, $F210^{5.47}L$, $F265^{6.44}L$, and $W269^{6.48}L$ (table S3), decreased or abolished CYM-5442–induced ERK phosphorylation and binding, and only the $W269^{6.48}L$ mutation minimally affected either binding or signaling induced by S1P and other orthosteric ligands (Fig. 4D). This contrasts with the negative effect of $W269^{6.48}A$ on ligand-induced [^{35}S]GTPγS E_{max} (*28*), indicating that S1P binding is highly dependent on hydrophobicity, but not aromaticity, at this position. The class II agonist, CYM-5442, was dependent on the presence of an aromatic residue, displaying a complete disruption of signaling and binding by the $W269^{6.48}L$ mutation (Fig. 4B and table S3). The hierarchy of loss of agonist responsiveness for the $W269^{6.48}L$ $S1P_1$ mutant receptor relative to the wild type (CYM-5442 >> S1P) was preserved for structural analogs of CYM-5442, such as CYM-5181 and CYM-5178 (Fig. 4E and table S2), suggesting an interaction between the 3,4-diethyloxy-phenyl ring common to these compounds and the aromatic ring of $W269^{6.48}$. Results from a radioligand binding competition assay also indicated that $W269^{6.48}$ plays a more critical role in binding CYM-5442 than in binding S1P (fig. S6) (*40*). These mutagenesis data, together with structure-activity data and the structural information, allowed us to model the likely binding orientation of CYM-5442 and rationalize the high selectivity exhibited by this series of ligands (Fig. 4B). These data also suggest that whereas hydrophobic packing interactions are the basis of both retinal and S1P interactions with the conserved tryptophan, the altered aromatic interactions with this highly conserved residue provide differences in ligand orientation and function and, thus, a foundation for specific anchoring in the pocket.

Designing selectivity is an important component of the development process for $S1P_1$

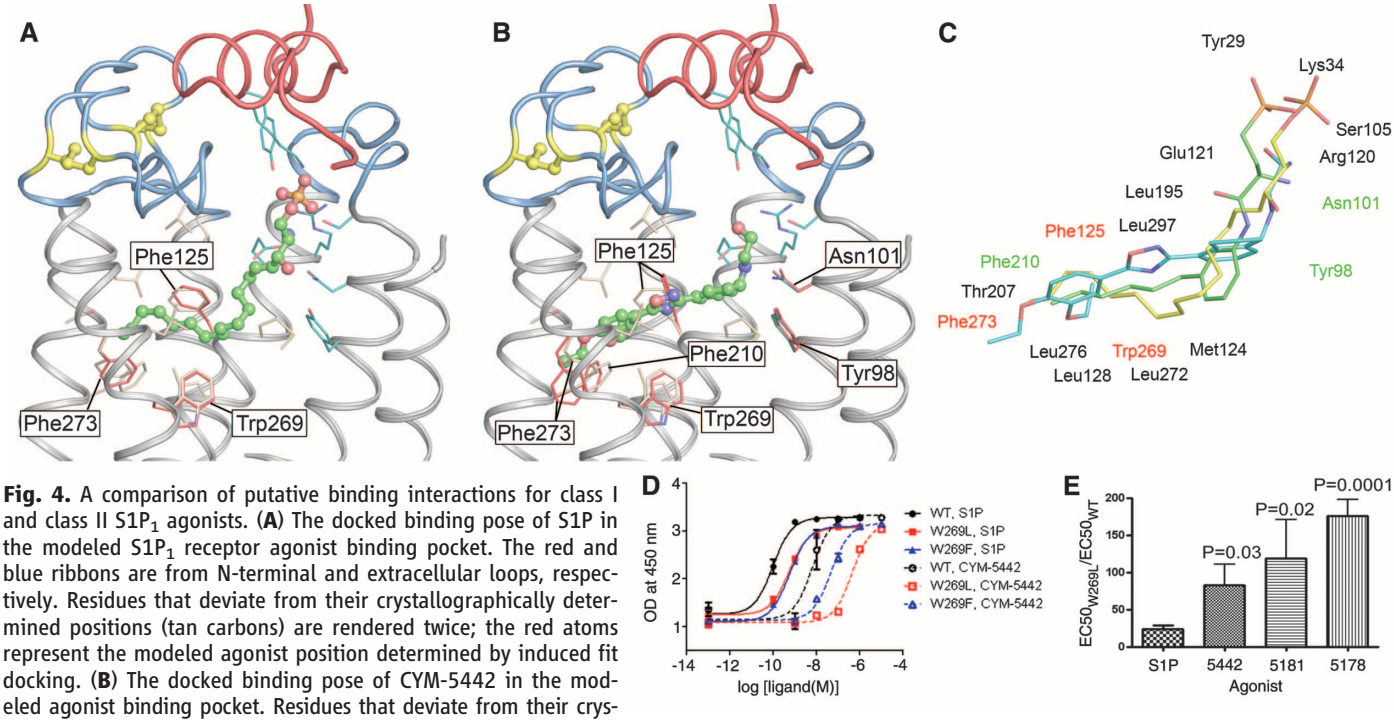

Fig. 4. A comparison of putative binding interactions for class I and class II $S1P_1$ agonists. (**A**) The docked binding pose of S1P in the modeled $S1P_1$ receptor agonist binding pocket. The red and blue ribbons are from N-terminal and extracellular loops, respectively. Residues that deviate from their crystallographically determined positions (tan carbons) are rendered twice; the red atoms represent the modeled agonist position determined by induced fit docking. (**B**) The docked binding pose of CYM-5442 in the modeled agonist binding pocket. Residues that deviate from their crystallographically determined positions (tan carbons) are rendered twice; the red atoms represent the modeled agonist position determined by induced fit docking. The binding pocket must accommodate slightly greater ligand volume in the hydrophobic portion. (**C**) Overlay of the docked ligands S1P (yellow carbons) and CYM-5442 (cyan carbons) compared to the structurally determined conformation of ML056 (green carbons). Binding pocket residues are indicated with black font for those that do not change between the agonist and antagonist binding models, red font for those that change for the agonist induced fit docking model, and green font for those that change conformation induced by CYM-5442 docking. (**D**) Ligand-induced ERK phosphorylation in WT, $W269^{6.48}L$, and $W269^{6.48}F$ Jump-In stable cell lines stimulated with increasing concentrations of either S1P or CYM-5442 (mean ± SD of triplicate samples). The data are from one of three independent experiments showing a minimal effect on S1P signaling. The progressive loss in potency of CYM-5442 tracks with a loss of aromatic π-stacking interactions. (**E**) A differential loss of agonist responsiveness of the mutant W269L $S1P_1$ receptor compared to WT receptor was observed. For each experiment, the EC_{50} for agonist activation of ERK phosphorylation of W269L $S1P_1$ receptor was divided by the EC_{50} of WT $S1P_1$ receptor.

Downloaded from www.sciencemag.org on February 16, 2012

receptor modulators, given that signaling along the other S1P receptor subtypes is associated with a number of clinically adverse events such as bronchoconstriction (*41*). The recently approved therapeutic, Gilenya, is a first-in-class $S1P_1$ prodrug modulator that, once phosphorylated by sphingosine kinase, is a potent agonist for the $S1P_3$, $S1P_4$, and $S1P_5$ receptors. Second-generation therapeutics, derivatives of CYM-5442, currently under development can selectively agonize the $S1P_1$ pathway without loss of potency. The structural basis for this enhanced selectivity can be rationalized directly on the basis of discrete binding pocket substitutions as compared to $S1P_3$ and $S1P_4$. The $S1P_3$ receptor has one notable substitution, $F263^{6.55}$, relative to the $S1P_1$ receptor's $L276^{6.55}$, which occurs further down in the hydrophobic binding pocket, introducing steric clashes with the aromatic ring system of class II agonists. The $S1P_4$ receptor also has only one notable change in the binding pocket, $L125^{3.32}$, relative to the $S1P_1$ receptor's $M124^{3.32}$, which may result in a slight constriction of the binding pocket at a critical location where the phenyl ring of FTY720-P and the indole ring of CYM-5442 are predicted to bind. The binding pocket of the $S1P_5$ receptor is very similar to that of the $S1P_1$ receptor, with no apparent substitutions to inform selectivity, which is consistent with the lack of selectivity exhibited by most, if not all, of the $S1P_1$ agonists. In addition to the S1Px receptors, this structure will be particularly useful for modeling additional members of the EDG family, as well as increasing the repertoire of structural knowledge being collected on class A GPCRs.

By taking advantage of specific aromatic interactions within the hydrophobic binding pocket, class II agonists avoid features that mimic the S1P head group, relying more on shape complementarity to the agonist pocket, thereby allowing more selectivity between receptor subtypes. The ability of the GPCR fold to adapt to multiple diverse chemotypes appears to be driven by topological differences in the extracellular domain. Sphingolipid-binding receptors channel access to the binding pocket, a small region between helices I and VII adjacent to the plasma membrane, where sphingolipid molecules gain access from within the confines of the membrane rather than the extracellular milieu. On the basis of recent work on retinal loading in opsin, activation of the receptor may affect pocket accessibility through slight rearrangement of the transmembrane helices (*42*). Persistent signaling of $S1P_1$ in the presence of certain ligands may be explained by occlusion of ligand egress from the binding pocket after activation.

References and Notes

1. H. Rosen, P. J. Gonzalez-Cabrera, M. G. Sanna, S. Brown, *Annu. Rev. Biochem.* **78**, 743 (2009).
2. J. Chun *et al.*, *Pharmacol. Rev.* **54**, 265 (2002).
3. S. Mandala *et al.*, *Science* **296**, 346 (2002).
4. V. Brinkmann *et al.*, *Nat. Rev. Drug Discov.* **9**, 883 (2010).
5. J. H. Park, P. Scheerer, K. P. Hofmann, H. W. Choe, O. P. Ernst, *Nature* **454**, 183 (2008).
6. S. G. Rasmussen *et al.*, *Nature* **469**, 175 (2011).
7. S. G. Rasmussen *et al.*, *Nature* **450**, 383 (2007).
8. T. Warne *et al.*, *Nature* **454**, 486 (2008).
9. V. Cherezov *et al.*, *Science* **318**, 1258 (2007).
10. E. Y. Chien *et al.*, *Science* **330**, 1091 (2010).
11. V. P. Jaakola *et al.*, *Science* **322**, 1211 (2008).
12. K. Palczewski *et al.*, *Science* **289**, 739 (2000).
13. B. Wu *et al.*, *Science* **330**, 1066 (2010).
14. F. Xu *et al.*, *Science* **332**, 322 (2011).
15. S. G. Rasmussen *et al.*, *Nature* **477**, 549 (2011).
16. G. Lebon *et al.*, *Nature* **474**, 521 (2011).
17. M. G. Sanna *et al.*, *Nat. Chem. Biol.* **2**, 434 (2006).
18. Diffraction data were processed by two different methods, yielding data sets at 3.35 and 2.8 Å resolution. A lower-resolution data set using traditional integration and scaling methods was derived from selecting reflection groups based on resolution shell. A higher-resolution data set was derived from an experimental microdiffraction data assembly method by assembling data based on peak profile correlations. Further details are in the Supporting Online Material.
19. P. J. Gonzalez-Cabrera *et al.*, *Mol. Pharmacol.* **74**, 1308 (2008).
20. M. A. Hanson, R. C. Stevens, *Structure* **17**, 8 (2009).
21. D. P. Hurst *et al.*, *J. Biol. Chem.* **285**, 17954 (2010).
22. S. A. Schadel *et al.*, *J. Biol. Chem.* **278**, 24896 (2003).
23. S. Filipek, R. E. Stenkamp, D. C. Teller, K. Palczewski, *Annu. Rev. Physiol.* **65**, 851 (2003).
24. In addition to numbering residue positions in the primary amino acid sequence, Ballesteros-Weistein numbering is shown as a superscript. The most conserved residue in each transmembrane helix is designated as x.50, where x is the number of the transmembrane helix, and the second number (50) indicates the relative position of the specific residue. The second number decreases toward the N terminus and vice versa. Only residues on transmembrane helices are noted.
25. A. L. Parrill *et al.*, *J. Biol. Chem.* **275**, 39379 (2000).
26. E. Jo *et al.*, *Chem. Biol.* **12**, 703 (2005).
27. K34 does not have strong electron density, and placing its side chain unambiguously in a position interacting with the phosphonate of W146 relies on omit maps rather than standard $2|F_o| - |F_c|$ maps. Its position on the N-terminal capping helix, coupled with modeling and docking studies as well as subsequent mutagenesis, has establish a role for this residue in sphingosine ligand-binding interactions in support of its placement in the weak electron density maps.
28. Y. Fujiwara *et al.*, *J. Biol. Chem.* **282**, 2374 (2007).
29. M. D. Davis, J. J. Clemens, T. L. Macdonald, K. R. Lynch, *J. Biol. Chem.* **280**, 9833 (2005).
30. P. D. Lyne, M. L. Lamb, J. C. Saeh, *J. Med. Chem.* **49**, 4805 (2006).
31. Prime, version 3.0, Schrödinger, LLC, New York, NY, 2011.
32. S. Suite, 2011 Induced Fit Docking protocol; Glide version 5.7, Schrodinger, LLC, New York, 2011; Prime version 3.0, Schrodinger, LLC, New York, 2011.
33. The induced fit model derived by leveraging structure-activity relationships of the VPC compound series was used for subsequent analysis of class I $S1P_1$ agonists without further modifications and was used as the starting point for induced fit modeling of class II ligands.
34. W. Sherman, T. Day, M. P. Jacobson, R. A. Friesner, R. Farid, *J. Med. Chem.* **49**, 534 (2006).
35. S. C. Schürer *et al.*, *ACS Chem. Biol.* **3**, 486 (2008).
36. D. A. Wang *et al.*, *J. Biol. Chem.* **276**, 49213 (2001).
37. SEW2871 also been shown to interact with the head group–binding region of the receptor, likely through a dipole moment interaction, while presenting aromatic ring systems to the hydrophobic binding pocket, and shares the same 15-16 carbon bond length.
38. The Jump-In system was used to provide a quantitative comparison between cell lines with similar surface expression, G protein coupling, and background protein expression.
39. A conservative mutagenesis approach was employed where hydrophobic to hydrophobic substitutions were preferred over substitutions that may drastically change the nature of the binding pocket or the overall protein fold.
40. Given the highly conserved nature of $W269^{6.48}$ in all class A GPCRs and its position directly above the third intracellular loop, a site of G protein binding, the effects of this mutation were rigorously quantified by assaying stable single-cell clones of wild-type (WT) and the $W269^{6.48}L$ mutant using ERK phosphorylation upon stimulation with increasing concentrations of S1P and CYM-5442 (table S3). The WT and $W269^{6.48}L$ EC_{50} (half-maximal effective concentration) values differed by 15-fold when tested by S1P stimulation. They differed by more than 100-fold when ERK phosphorylation was measured in response to CYM-5442 stimulation (table S3). The $W269^{6.48}L$ mutant has a 10-fold greater effect on CYM-5442 signaling than on S1P signaling, suggesting that $W269^{6.48}$ in S1P1 plays a more critical role in CYM-5442–induced receptor activation. An additional stable mutant, $W269^{6.48}F$, was used to examine whether aromaticity at this position is sufficient for ligand-induced ERK phosphorylation in response to the class II agonists (Fig. 4D) The ratio of EC_{50} shifts comparing CYM-5442 to S1P for each mutant ($W269^{6.48}L$ = 12.3 and $W269^{6.48}F$ = 1.3) confirm that the aromatic ring of $W269^{6.48}$ supplies a key interaction for CYM-5442 and the class II agonists.
41. M. Forrest *et al.*, *J. Pharmacol. Exp. Ther.* **309**, 758 (2004).
42. P. W. Hildebrand *et al.*, *PLoS ONE* **4**, e4382 (2009).

Acknowledgments: This work was supported in part by the Protein Structure Initiative (PSI):Biology grant U54 GM094618 for structure production, NIH Roadmap grant P50 GM073197 for technology development, NIH Roadmap Molecular Libraries Probe Production Centers grant U54 MH084512 for antagonist and class II agonist identification, and AI074564 and AI055509 to H.R. and M. B. Oldstone for studying the role of S1P in infection and immunity. The content is solely the responsibility of the authors and does not necessarily represent the official views of the National Institute of General Medical Sciences (NIGMS) or the NIH. We thank E. Chien for preliminary analysis; M. Mileni for critical evaluation of the structure; V. Cherezov, V. Katritch, and I. Wilson for careful review of the manuscript; J. Johnson, A. Leslie, W. Kabsch, and A. Perrakis for discussion and review of the experimental microdiffraction data assembly processing method; and A. Walker for assistance with manuscript preparation. We acknowledge J. Smith, R. Fischetti, and N. Sanishvili at the GM/CA-CAT beamline at the Advanced Photon Source, for assistance in development and use of the minibeam and beamtime. The GM/CA-CAT beamline (23-ID) is supported by the National Cancer Institute (Y1-CO-1020) and the NIGMS (Y1-GM-1104). Atomic coordinates and structure factors have been deposited in the Protein Data Bank with identification code 3V2W and 3V3Y. R.C.S. is a founder and on the Board of Directors, and H.R. is a founder and on the Scientific Advisory Board, of Receptos, a GPCR structure–based drug discovery company with an $S1P_1$ clinical compound. H.R. is an inventor on a patent application by The Scripps Research Institute (TSRI) on CYM-5442 and related S1P receptor modulators (US2010/0010001). Materials will be made available under a Material Transfer Agreement with TSRI.

Supporting Online Material

www.sciencemag.org/cgi/content/full/335/6070/851/DC1
Materials and Methods
Figs. S1 to S6
Tables S1 to S3
References

28 October 2011; accepted 22 December 2011
10.1126/science.1215904

Downloaded from www.sciencemag.org on February 16, 2012

Epithelial Nitration by a Peroxidase/NOX5 System Mediates Mosquito Antiplasmodial Immunity

Giselle de Almeida Oliveira, Joshua Lieberman, Carolina Barillas-Mury*

Plasmodium ookinetes traverse midgut epithelial cells before they encounter the complement system in the mosquito hemolymph. We identified a heme peroxidase (HPX2) and NADPH oxidase 5 (NOX5) as critical mediators of midgut epithelial nitration and antiplasmodial immunity that enhance nitric oxide toxicity in *Anopheles gambiae*. We show that the two immune mechanisms that target ookinetes—epithelial nitration and thioester-containing protein 1 (TEP1)–mediated lysis—work sequentially, and we propose that epithelial nitration works as an opsonization-like system that promotes activation of the mosquito complement cascade.

Mosquitoes become infected with *Plasmodium* when they ingest blood that contains gametocytes. Zygotes form within the lumen of the mosquito midgut and mature into motile ookinetes. To complete their development in the mosquito, ookinetes must traverse the midgut epithelium and avoid being detected and lysed by the mosquito complement system. Thioester-containing protein 1 (TEP1) is a member of the macroglobulin family in *Anopheles gambiae* with a structure similar to complement C3 protein in vertebrates (*1*). In the susceptible *A. gambiae* G3 strain, TEP1 lyses about 80% of *Plasmodium berghei* ookinetes that complete invasion as they encounter the mosquito hemolymph (*2*). TEP1 protein circulates as a stable complex in association with two proteins of the leucine-rich repeat family, LRIM1 and APL1C (*3*–*5*). The mechanism of TEP1 activation is unknown, and it is not clear what determines whether TEP1 will bind to the surface of a given parasite and lyse it.

Ookinete invasion of midgut epithelial cells causes irreversible damage that leads to apoptosis (*6*). Invaded cells mount defense responses such as expression of high levels of nitric oxide synthase (NOS). We previously proposed that the rate of cellular responses to invasion may be critical to *Plasmodium* survival (*6*). Biochemical studies in *A. gambiae* revealed extensive nitration in *Plasmodium*-invaded cells that appears to be a two-step process in which induction of NOS expression is followed by increased peroxidase activity (*7*). The peroxidase activity induced in *Plasmodium*-infected midguts is very stable (remaining active after glutaraldehyde fixation) and can catalyze protein nitration in vitro (*7*) in a reaction similar to that described for myeloperoxidase-mediated nitration in vertebrates (*8*, *9*). In this study, we identify heme peroxidase (HPX2) and NADPH (reduced form of nicotinamide adenine dinucleotide phosphate) oxidase 5 (NOX5) as key enzymes induced in ookinete-invaded midgut cells of *A. gambiae* (G3) that—together with NOS—mediate protein nitration. The HPX2/NOX5 system potentiates nitric oxide (NO) toxicity and is critical for mosquitoes to mount an effective antiplasmodial response. We provide direct experimental evidence that epithelial nitration and TEP1-mediated lysis, which are often thought to be mutually exclusive (*10*), work sequentially, and we propose that epithelial nitration by HPX2/NOX5 modifies ookinetes and makes them "visible" to the mosquito complement system.

Bioinformatic analysis of the *A. gambiae* genome identified 18 genes containing heme-peroxidase (HPX) domains (*11*). Transcription of four of these putative heme peroxidases—HPX2, HPX7, HPX8, and double peroxidase (DBLOX)—and of the dual oxidase (Duox) gene is induced in the midgut in response to *Plasmodium* infection (*7*). We explored the participation of the four inducible peroxidases in antiplasmodial immunity. The role of Duox has been previously reported (*12*).

Transcriptional activation of the four HPX genes by *Plasmodium berghei* ookinete invasion 24 hours after feeding was confirmed (*13*) (Fig. 1A), and their expression was efficiently silenced (by 70 to 90%) by systemic injection of double-stranded RNA (dsRNA) (Fig. 1B). The effect of silencing each of these enzymes on the peroxidase activity of glutaraldehyde-fixed midguts from mosquitoes fed on a healthy or a *Plasmodium*-infected mouse was measured to determine *Plasmodium*-induced enzymatic activity. HPX2 silencing reduced activity induced by infection by 90%, whereas silencing of HPX7, HPX8, and DBLOX had no effect (Fig. 1C). Midgut homogenates from mosquitoes injected with dsLacZ and infected with *Plasmodium* (Fig. 2A, left) and a commercial peroxidase (Fig. 2A, positive control, right) can catalyze bovine serum albumin nitration in vitro; however, nitration was no longer observed when the enzymatic activity was inhibited by addition of sodium azide or when HPX2 expression was silenced (Fig. 2A), indicating that HPX2 is the enzyme induced by *Plasmodium* infection that catalyzes protein nitration in vitro. An enzyme-linked immunosorbent assay (ELISA)–type test was developed to measure in vivo protein nitration using a monoclonal antibody to nitrotyrosine. As expected, midgut nitration increased significantly in response to *Plasmodium* infection (Fig. 2B). Furthermore, silencing HPX2 significantly reduced midgut nitration in *Plasmodium*-infected midguts (Fig. 2B).

Polyclonal antibodies to recombinant HPX2 detect a major protein band (100 kD under native conditions) that is present at higher levels in *Plasmodium*-infected midguts (Fig. 2C), and a second 55-kD band is occasionally observed (Fig. 2D). The signal from both bands (100 and 55 kD) is greatly reduced when HPX2 is silenced (Fig. 2D). HPX2 is highly expressed in ookinete-invaded cells undergoing apoptosis (Fig. 2E), and nitrotyrosine signal is detected in damaged cells protruding into *Plasmodium*-infected midguts that express high levels of HPX2 (Fig. 2F and fig. S1); however, the level of HPX2 and nitrotyrosine signal is very weak in uninvaded cells (Fig. 2F and fig. S1) and in the midguts of mosquitoes fed on a healthy mouse (fig. S1). HPX2 silencing increased the intensity of *Plasmodium* infection by a factor of 3.6

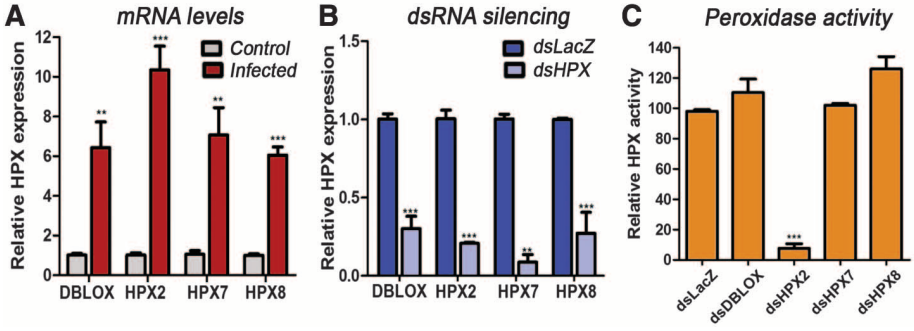

Fig. 1. Expression and activity of midgut heme peroxidases (HPXs). (**A**) mRNA expression of DBLOX, HPX2, HPX7, and HPX8 in the midguts of mosquitoes fed on a healthy (C, control) or a *Plasmodium*-infected (I, infected) mouse 24 hours after feeding and (**B**) in the midguts of infected mosquitoes injected with dsLacZ or with dsRNA from each of the four HPXs 24 hours after feeding. (**C**) Effect of silencing each HPX on *Plasmodium*-induced midgut peroxidase activity (mean ± SEM).

Laboratory of Malaria and Vector Research, National Institute of Allergy and Infectious Diseases, National Institutes of Health (NIH), Rockville, MD 20892, USA.

*To whom correspondence should be addressed. E-mail: cbarillas@niaid.nih.gov

Downloaded from www.sciencemag.org on February 16, 2012

(P = 0.001) (Fig. 2G), whereas HPX8 and DBLOX silencing did not affect the intensity of infection and HPX7 silencing reduced infection to a moderate degree (P = 0.054) (fig. S2). Together, these findings indicate that HPX2-mediated nitration in invaded midgut cells is a major determinant of *Plasmodium* survival.

Heme peroxidases require a source of hydrogen peroxide to be enzymatically active. A single member of the NADPH oxidase (NOX) family, a putative ortholog of the vertebrate NOX5, was identified in *A. gambiae* by BLAST analysis (AGAP008072) (*14*). NOX5 mRNA (Fig. 3A) and protein (Fig. 3B) expression was highly induced in the midgut in response to *Plasmodium* infection, and expression was efficiently silenced at the mRNA (Fig. 3C) and protein (Fig. 3D) levels by dsNOX5 injection. NOX5 silencing significantly reduced nitration in *Plasmodium*-infected midguts (Fig. 3E). NOX5 protein is highly expressed in cells damaged by ookinete invasion (Fig. 3F), and nitrotyrosine staining is detected in damaged cells that express high levels of NOX5 (Fig. 3G and fig. S3). In contrast, the staining is very weak in uninvaded cells (Fig. 3G and fig. S3) or in the midguts of mosquitoes fed on a healthy mouse (fig. S3). Furthermore, NOX5 silencing significantly increased the intensity of *Plasmodium* infection (P = 0.002) (Fig. 3H). Double silencing of HPX2 and NOX5 had the

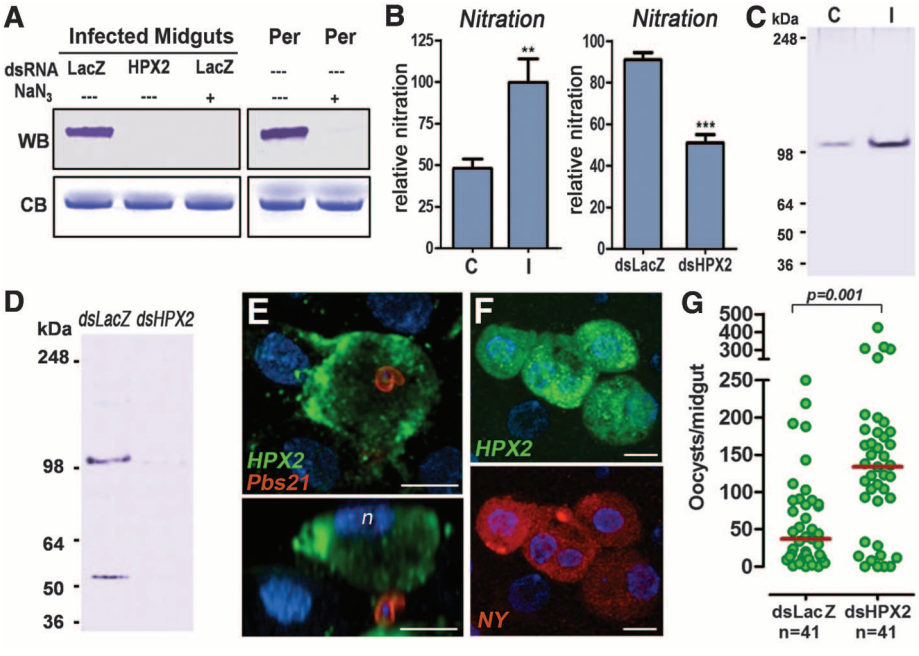

Fig. 2. Localization of HPX2 and effect of HPX2 silencing on nitration and *Plasmodium* infection. (**A**) In vitro bovine serum albumin (BSA) nitration by a commercial peroxidase (Per) or by peroxidase from *Plasmodium*-infected midguts. Inhibition of peroxidase activity by addition of sodium azide (NaN_3) or silencing HPX2 prevent in vitro nitration. Western blot (WB) with an antibody to nitrotyrosine and Coomassie blue (CB) staining of BSA. (**B**) Effect of *Plasmodium* infection (left) and of silencing HPX2 (right) in *Plasmodium*-infected mosquitoes on in vivo midgut nitration (mean ± SEM). Western blot detection of HPX2 protein in midgut homogenates from (**C**) mosquitoes fed on a healthy (C, control) or a *Plasmodium*-infected (I, infected) mouse 24 hours after feeding and (**D**) *Plasmodium*-infected mosquitoes injected with dsLacZ control or dsHPX2 collected 24 hours after feeding. (**E** and **F**) Immunofluorescent staining of *Plasmodium*-infected midguts 24 hours after feeding. (E) Ookinetes stained with antibodies to Pbs21 (red) and HPX2 (green). The lower image shows the side view; n, nuclei of apoptotic cell (blue). (F) HPX2 (top) and nitrotyrosine (bottom) expression in *Plasmodium*-infected midguts (scale bar, 10 μm). (**G**) Effect of HPX2 silencing on *Plasmodium* infection 7 days after feeding. Each circle represents the number of parasites in individual midguts (the red line shows the median).

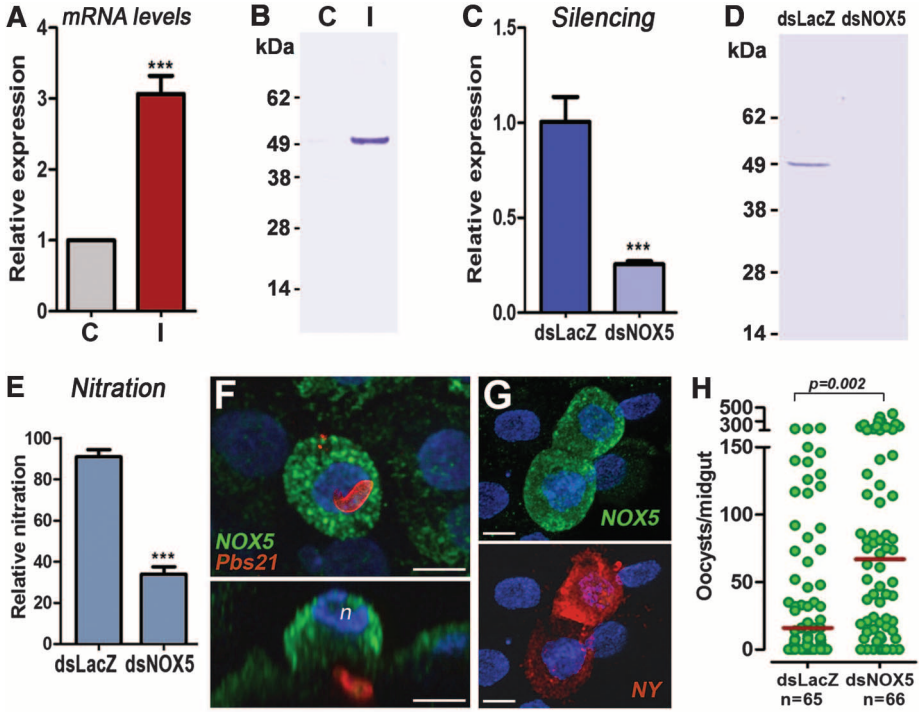

Fig. 3. Expression and localization of NOX5 and effect of NOX5 silencing on *Plasmodium* infection. (**A**) Midgut NOX5 mRNA and (**B**) protein expression 24 hours after feeding in mosquitoes fed on a healthy (C, control) or a *Plasmodium*-infected (I, infected) mouse. (**C**) Midgut NOX5 mRNA and (**D**) protein expression 24 hours after feeding on mosquitoes injected with dsLacZ or dsNOX5. (**E**) Effect of NOX5 silencing on in vivo midgut protein nitration (mean ± SEM). (**F** and **G**) Immunofluorescence staining of midguts 24 hours after feeding on a *Plasmodium*-infected mouse. (F) Ookinetes stained with Pbs21 (red) and NOX5 (green). The lower image shows the side view; n, nuclei of apoptotic cell (blue). (G) Nitrotyrosine (red) and NOX5 (green) expression in cells of *Plasmodium*-infected midguts undergoing apoptosis (scale bar, 10 μm). (**H**) Effect of NOX5 silencing on *Plasmodium* infection 7 days after feeding. Each circle represents the number of parasites in individual midguts (the red line shows the median).

Downloaded from www.sciencemag.org on February 16, 2012

same effect as silencing either HPX2 or NOX5 alone (fig. S4), indicating that they mediate the same antiplasmodial response. We also explored the possibility of a functional link between HPX2 and TEP1. Co-silencing HPX2 and TEP1 had the same effect on *Plasmodium* infection as silencing TEP1 alone, suggesting that the antiplasmodial effect of HPX2 is mediated by TEP1 (Fig. 4A).

We have previously shown that disruption of the IMPer/Duox system, by silencing either gene, results in very high levels of NOS expression and a dramatic decrease in *Plasmodium* survival (*12*). The hypothesis that increased NO levels in IMPer-silenced females accelerate HPX2/NOX5-mediated nitration was investigated. Midgut nitration was significantly higher when IMPer expression was silenced (Fig. 4B). However, although HPX2 or NOX5 silencing did not affect NOS or TEP1 expression (fig. S5), co-silencing IMPer/HPX2 or IMPer/NOX5 decreased nitration to control levels (Fig. 4B), indicating that the HPX2/NOX5 system is required for efficient nitration. Moreover, the antiparasitic effect of IMPer silencing was completely reversed when either HPX2 or NOX5 was co-silenced (Fig. 4C).

We also explored the participation of TEP1 in the antiplasmodial response in IMPer-silenced mosquitoes. Co-silencing TEP1 did not affect midgut nitration in IMPer-silenced midguts (Fig. 4B) but completely reverted the antiparasitic effect (Fig. 4C), indicating that HPX2/NOX5 nitration does not directly kill *Plasmodium* but requires TEP1-activation. TEP1-mediated lysis also did not take place when either HPX2 or NOX5 was silenced (Fig. 4C). We performed immunofluorescence analysis to directly assess whether HPX2-mediated nitration affected TEP1 binding to *Plasmodium* (Fig. 4D). HPX2 silencing significantly reduced the proportion of parasites labeled with TEP1 ($P = 0.003$) (Fig. 4E). Furthermore, *Plasmodium*-induced TEP1 binding to the mosquito midgut was also significantly reduced ($P < 0.001$) (Fig. 4F).

All ookinetes that traverse the midgut epithelium come in contact with the complement system, so it has been difficult to understand why TEP1 lyses some ookinetes while others are spared. Our findings indicate that the nitration response mediated by HPX2/NOX5 is required for effective TEP1-mediated lysis. We propose that nitration modifies ookinetes during their transit through the midgut and that—although TEP1 is an important effector of antiplasmodial immunity—the outcome of infection depends, to a large extent, on the interaction of a given ookinete with the cell(s) it traverses. We have shown that the rate of nitration mediated by HPX2/NOX5 is a major determinant of *Plasmodium* survival. This predicts that physiologic conditions that accelerate nitration, such as faster or higher expression of these enzymes, or that increased the availability of substrates, such as arginine, would be detrimental to the parasite. This is in agreement with previous studies indicating that a higher rate of hydrogen peroxide generation by mitochondria (*15*) or a reduced rate of detoxification (*16*, *17*) promotes ookinete lysis. This model also predicts that ookinetes that migrate faster through invaded cells would be more likely to survive. If ookinetes are not detected by the mosquito complement system, they recover from exposure to toxic nitrogen-reactive species and proceed to transform into oocysts. Our studies reveal that NOS induction is not sufficient to achieve an effective antiplasmodial response and identify HPX2 and NOX5 as strong potentiators of NO toxicity. In humans, increased NOX5 activity has been associated with

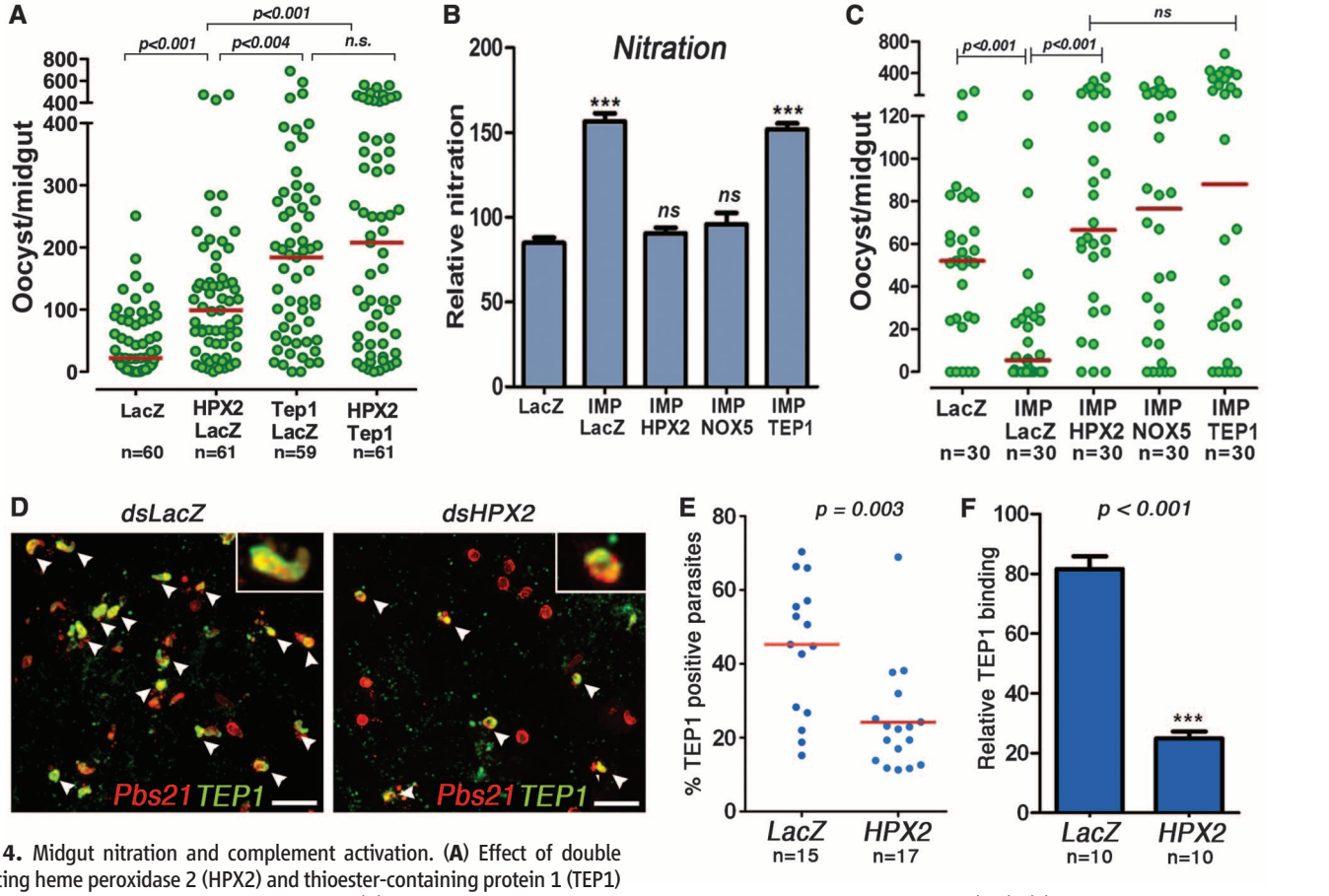

Fig. 4. Midgut nitration and complement activation. (**A**) Effect of double silencing heme peroxidase 2 (HPX2) and thioester-containing protein 1 (TEP1) on *Plasmodium* infection 7 days after feeding. (**B**) Effect of silencing IMPer or co-silencing NADPH 5 (NOX5), HPX2, or TEP1 on in vivo protein nitration and (**C**) *Plasmodium* infection 7 days after feeding. Each circle represents the number of parasites in an individual midgut; the horizontal lines indicate medians. Effect of HPX2 silencing on (**D**) TEP1 staining (green) on ookinetes labeled with an antibody to Pbs21 (red), (**E**) percentage of parasites on individual midguts that stain positive for TEP1, and (**F**) *Plasmodium*-induced TEP1 binding (difference in binding to infected and uninfected midguts) 28 to 30 hours after feeding. Arrowheads indicate examples of TEP1-positive parasites.

Downloaded from www.sciencemag.org on February 16, 2012

coronary artery disease (*18*). Our findings indicate the possibility of a human myeloperoxidase/NOX5 system that would potentiate NO toxicity in endothelial cells and promote complement activation.

References and Notes

1. R. H. Baxter *et al.*, *Proc. Natl. Acad. Sci. U.S.A.* **104**, 11615 (2007).
2. S. Blandin *et al.*, *Cell* **116**, 661 (2004).
3. M. Povelones, R. M. Waterhouse, F. C. Kafatos, G. K. Christophides, *Science* **324**, 258 (2009).
4. M. Povelones, L. M. Upton, K. A. Sala, G. K. Christophides, *PLoS Pathog.* **7**, e1002023 (2011).
5. M. Fraiture *et al.*, *Cell Host Microbe* **5**, 273 (2009).
6. Y. S. Han, J. Thompson, F. C. Kafatos, C. Barillas-Mury, *EMBO J.* **19**, 6030 (2000).
7. S. Kumar, L. Gupta, Y. S. Han, C. Barillas-Mury, *J. Biol. Chem.* **279**, 53475 (2004).
8. S. Pfeiffer, A. Lass, K. Schmidt, B. Mayer, *FASEB J.* **15**, 2355 (2001).
9. J. Byun, J. P. Henderson, D. M. Mueller, J. W. Heinecke, *Biochemistry* **38**, 2590 (1999).
10. S. H. Shiao, M. M. A. Whitten, D. Zachary, J. A. Hoffmann, E. A. Levashina, *PLoS Pathog.* **2**, e133 (2006).
11. R. M. Waterhouse *et al.*, *Science* **316**, 1738 (2007).
12. S. Kumar, A. Molina-Cruz, L. Gupta, J. Rodrigues, C. Barillas-Mury, *Science* **327**, 1644 (2010).
13. Materials and methods are available as supporting material on *Science* Online.
14. T. Kawahara, M. T. Quinn, J. D. Lambeth, *BMC Evol. Biol.* **7**, 109 (2007).
15. J. H. Oliveira *et al.*, *Insect Biochem. Mol. Biol.* **41**, 349 (2011).
16. A. Molina-Cruz *et al.*, *J. Biol. Chem.* **283**, 3217 (2008).
17. G. Jaramillo-Gutierrez, A. Molina-Cruz, S. Kumar, C. Barillas-Mury, *PLoS ONE* **5**, e11168 (2010).
18. T. J. Guzik *et al.*, *J. Am. Coll. Cardiol.* **52**, 1803 (2008).

Acknowledgments: This work was supported by the Division of Intramural Research, National Institute of Allergy and Infectious Diseases, NIH. We thank A. Laughinghouse and K. Lee for insectary support; J. Ribeiro and J. Valenzuela for their comments and insight; and L. Garver and B. Marshall for editorial assistance.

Supporting Online Material

www.sciencemag.org/cgi/content/full/science.1209678/DC1
Materials and Methods
Figs. S1 to S5
Tables S1 to S3
References

13 June 2011; accepted 26 October 2011
Published online 26 January 2012;
10.1126/science.1209678

Structural Basis of TLR5-Flagellin Recognition and Signaling

Sung-il Yoon,[1] Oleg Kurnasov,[2]* Venkatesh Natarajan,[3]* Minsun Hong,[1]* Andrei V. Gudkov,[3,4] Andrei L. Osterman,[2]† Ian A. Wilson[1,5]†

Toll-like receptor 5 (TLR5) binding to bacterial flagellin activates signaling through the transcription factor NF-κB and triggers an innate immune response to the invading pathogen. To elucidate the structural basis and mechanistic implications of TLR5-flagellin recognition, we determined the crystal structure of zebrafish TLR5 (as a variable lymphocyte receptor hybrid protein) in complex with the D1/D2/D3 fragment of *Salmonella* flagellin, FliC, at 2.47 angstrom resolution. TLR5 interacts primarily with the three helices of the FliC D1 domain using its lateral side. Two TLR5-FliC 1:1 heterodimers assemble into a 2:2 tail-to-tail signaling complex that is stabilized by quaternary contacts of the FliC D1 domain with the convex surface of the opposing TLR5. The proposed signaling mechanism is supported by structure-guided mutagenesis and deletion analyses on CBLB502, a therapeutic protein derived from FliC.

Toll-like receptors (TLRs) play a key role in innate immunity by eliciting the first line of defense against invading pathogens (*1*). TLRs are membrane-bound antigen recognition receptors (*2*) that directly recognize highly conserved molecular structures in pathogens using their horseshoe-shaped, leucine-rich repeat (LRR) ectodomains. Each TLR recognizes a different set or subset of antigens with a distinct ligand-binding mechanism (fig. S1). Nonetheless, all known agonist-activated TLR structures form a similar dimer organization, which brings their C-terminal regions into juxtaposition so that their intracellular TIR domains can initiate the signaling cascades (*3*–*6*). To date, structural studies on TLR-ligand recognition have been limited to nonprotein antigens, and the structural basis for protein antigen recognition by a TLR has not been addressed.

TLR5 is the only protein-binding TLR that is conserved in vertebrates from fish to mammals (*7*–*9*). TLR5 responds to a monomeric form of flagellin from β- and γ-proteobacteria that constitutes the whiplike flagellar filament responsible for locomotion (*8*, *10*, *11*). Flagellin (hereafter termed FliC, corresponding to the main flagellin gene product in *Salmonella*) binding to TLR5 induces MyD88-dependent signaling and activates the proinflammatory transcription factor NF-κB in epithelial cells, monocytes, and dendritic cells, which results in activation of innate immune responses against flagellated bacteria (*8*, *12*–*16*).

The key roadblock against TLR5-FliC interaction studies has been the formidable technical challenge in expression of the mammalian TLR5 ectodomain (ECD) in a functionally active, soluble form. We overcame this challenge by testing the expression of a number of TLR5 orthologs (*16*, *17*). Only the zebrafish *Danio rerio* ortholog (*dr*TLR5-ECD) could be successfully expressed in a secreted soluble form in the baculovirus system, but with a low purification yield (<50 μg from 1 liter of culture) (*18*). To improve the yield, we engineered a series of *dr*TLR5-ECD C-terminal deletion variants as chimeric proteins with the C-terminal fragment of hagfish variable lymphocyte receptor (VLR) B.61 using a strategy successfully used for the crystallization of other TLRs (*4*, *19*). Three chimeric proteins containing 6, 12, and 14 N-terminal LRR modules (TLR5-$N6_{VLR}$, TLR5-$N12_{VLR}$, and TLR5-$N14_{VLR}$, respectively) (fig. S2A) were expressed, purified to homogeneity, and tested for their interaction with CBLB502 (*20*) (fig. S2B), a pharmacologically optimized derivative of FliC from *Salmonella enterica* subspecies *enterica* serovar Dublin (*sd*FliC), by size exclusion chromatography and native electromobility shift assay (EMSA) (Fig. 1A). Stable 1:1 complexes with CBLB502 were obtained for TLR5-$N12_{VLR}$ and TLR5-$N14_{VLR}$ (but not TLR5-$N6_{VLR}$) and were used for structural studies.

The largest chimeric protein TLR5-$N14_{VLR}$ inhibited CBLB502-induced signaling as efficiently as full-length *dr*TLR5-ECD in a competitive assay using human embryonic kidney (HEK) 293 cells stably expressing NF-κB–luciferase reporter and human TLR5 (*hs*TLR5) (Fig. 1B). The observed median inhibitory concentrations (IC_{50} values) for both derivatives of *dr*TLR5 (67 and 139 pM; Fig. 1B) were in the same range as the EC_{50} of CBLB502-*hs*TLR5 signaling efficiency (77 pM) measured in the same reporter system (Fig. 1, C and D). Although none of these values can be interpreted as a true dissociation constant, this observation supports the relevance of *dr*TLR5 as a model for *hs*TLR5 interactions with FliC.

To provide the structural basis for TLR5-FliC interaction, we determined the crystal structures of TLR5-$N12_{VLR}$ and a complex of TLR5-$N14_{VLR}$ with a D0 deletion variant of *sd*FliC (*sd*FliC-ΔD0; fig. S2B) at 2.83 and 2.47 Å resolutions, respectively (*21*) (Fig. 2A and table S1). In the TLR5-FliC complex, the FliC D1 domain is located on the lateral side of TLR5, forming an extensive primary binding interface that defines a 1:1 heterodimer. Two heterodimers further oligomerize to a symmetric 2:2 complex where TLR5 from the first heterodimer makes additional, weaker interactions with both FliC′ and TLR5′ from the

[1]Department of Molecular Biology, The Scripps Research Institute, La Jolla, CA 92037, USA. [2]Sanford-Burnham Medical Research Institute, La Jolla, CA 92037, USA. [3]Roswell Park Cancer Institute, Buffalo, NY 14263, USA. [4]Cleveland BioLabs Inc., Buffalo, NY 14203, USA. [5]Skaggs Institute for Chemical Biology, The Scripps Research Institute, La Jolla, CA 92037, USA.

*These authors contributed equally to this work.
†To whom correspondence should be addressed. E-mail: wilson@scripps.edu (I.A.W.); osterman@sanfordburnham.org (A.L.O.)

Downloaded from www.sciencemag.org on February 16, 2012

second heterodimer, forming a secondary dimerization interface. This TLR5-FliC interaction mode is completely different from other TLR interactions with nonprotein ligands with respect to stoichiometry, ligand arrangement, and binding interfaces (*16*). Nonetheless, flagellin binding results in assembly of two TLR5s in a tail-to-tail organization, which juxtaposes the C-terminal tail regions of TLR5-ECD for signaling by analogy with other agonist-bound TLRs (fig. S1). Thus, the TLR5-N14$_{VLR}$/FliC-ΔD0 structure illustrates distinct, as well as conserved, features relative to other TLRs for receptor activation.

TLR5 adopts a single-domain LRR structure that consists of an N-terminal β-hairpin capping motif (LRRNT), 13 complete LRR modules (LRR1 to LRR13), and two residues from LRR14 (*22*) (Fig. 2B and fig. S3). The concave surface displays a smooth, curved β-sheet structure that is formed from two antiparallel β strands of LRRNT and 13 parallel β strands of LRR modules. However, the convex surface is less regular, with an assortment of helices and extended structures. Comparison of TLR5 with other known TLR structures indicates that TLR5 can be better categorized as a TLR3-like LRR structure than as a TLR4- or TLR2-like structure, consistent with the evolutionary closeness of TLR3 and TLR5 (*23*) (fig. S4).

Two of the three FliC-ΔD0 domains, D1 and D2, could be modeled in the complex structure (*24*) (fig. S5), but only D1 is involved in direct interaction with TLR5 (Fig. 2C). The D1 domain consists of four elongated segments that vertically assemble into a long, largely helical rod. The four segments correspond to two N-terminal α helices (αND1a and αND1b), one C-terminal α helix (αCD1), and a segment of β hairpin and extended structure that connects αND1b to the D2 domain (Fig. 2C and fig. S6).

The extensive primary binding interface responsible for the specific recognition of FliC by TLR5 is formed between the ascending lateral surface of TLR5 LRRNT to LRR10 and one side of the three long α helices of FliC D1 with ~1320 Å^2 of buried accessible surface area (b.s.a.) on each side (Fig. 3A). This interface can be described as two adjacent, but spatially separated surfaces, interfaces A and B, and includes residues previously proposed as TLR5 binding sites by a mutational study (*11*) (fig. S7). Moreover, the FliC interface coincides with residues involved in FliC oligomerization in the flagellar filament structure and is therefore well conserved across species of β- and γ-proteobacteria (figs. S6 and S8). These observations support the hypothesis that TLR5 evolved to target a common molecular pattern of FliC that is functionally crucial for flagellar assembly and hence is evolutionarily constrained (*11*).

Interface A is formed between the concave and ascending sides of TLR5 LRRNT to LRR6 and the C-terminal half of FliC αCD1 with ~530 Å^2 b.s.a. (Fig. 3A, bottom, and fig. S9). Interface A narrows from LRRNT toward LRR6, with LRRNT to LRR2 providing three or four residues from both concave and ascending sides, and LRR3 to LRR6 contributing one or two residues only from the ascending side. Interaction in interface

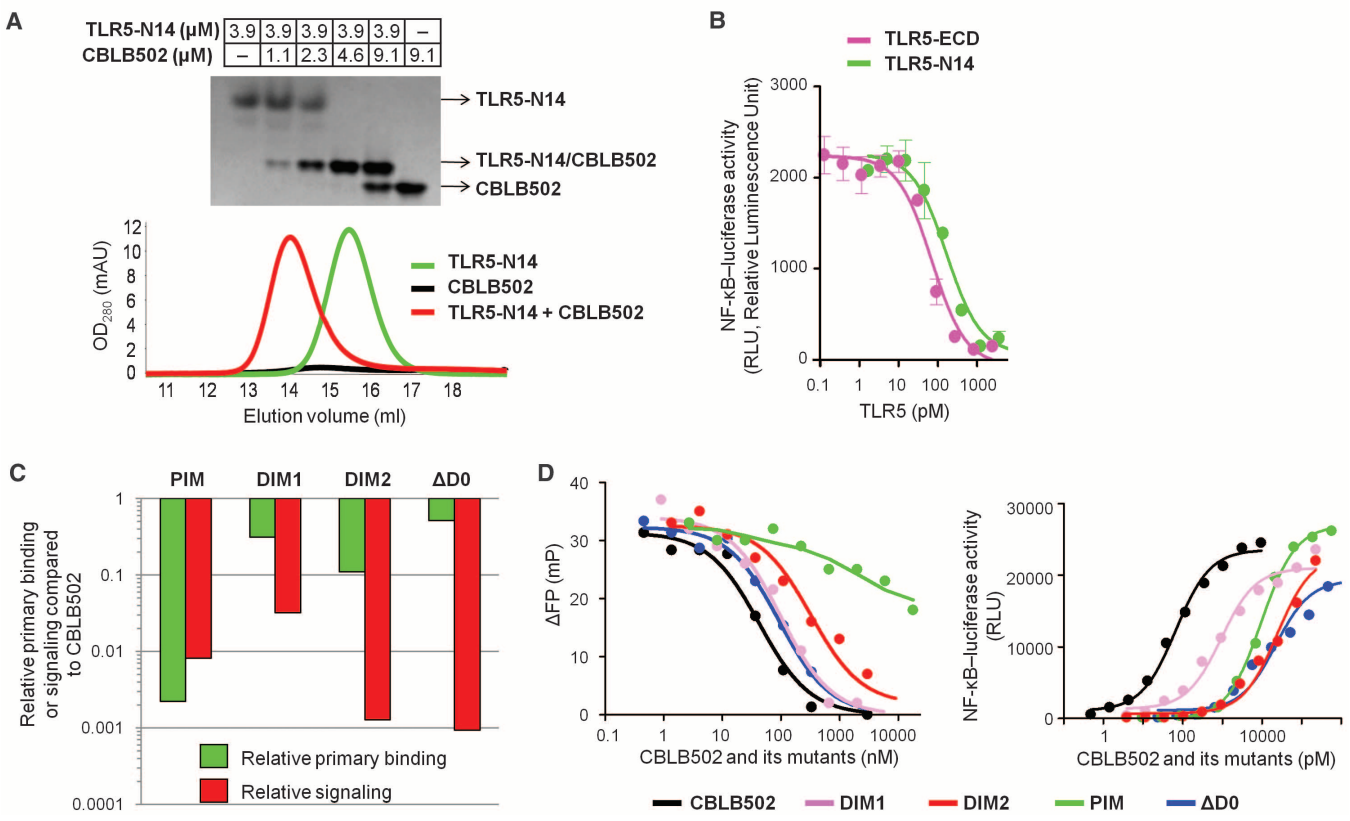

Fig. 1. TLR5-FliC interactions and mutational studies. (**A**) Native EMSA (upper panel) and size exclusion chromatography (lower panel) reveal formation of a 1:1 TLR5-N14$_{VLR}$/CBLB502 heterodimer. (**B**) TLR5-ECD and TLR5-N14$_{VLR}$ display comparable binding for CBLB502, as revealed by a competition assay (IC$_{50}$ values of 67 ± 4 pM and 139 ± 28 pM, respectively, in the presence of 90 pM CBLB502; errors are SD) using HEK293 cells that express NF-κB–luciferase reporter and *hs*TLR5. Data are expressed as means ± SD (n = 3). (**C**) Mutational studies using dimerization interface-disruption mutants (CBLB502-DIM1 and -DIM2) and D0-deletion mutant (CBLB502-ΔD0) demonstrate that both the dimerization interface of the complex structure and FliC D0 domain contribute to formation of an active signaling complex. TLR5 primary binding efficiency was analyzed by a competitive FP assay where TLR5-N14$_{VLR}$ interaction with fluorescein-labeled CBLB502 was inhibited by unlabeled CBLB502 or its mutants. Relative primary binding efficiency was derived from IC$_{50}$ ratio of CBLB502 to mutants. TLR5 signaling was assessed in an NF-κB–dependent luciferase reporter assay, and relative signaling efficiency was assessed by the EC$_{50}$ ratio of CBLB502 to mutants. Smaller ratios correspond to weaker (or less efficient) binding or signaling. (**D**) A competitive FP assay (left) and an NF-κB–dependent luciferase reporter cell assay (right) of CBLB502 and its mutants shown in (C). FP assay results are representative of two independent experiments (left) and cell assay data are expressed as means (n = 2) with SD below 2000 RLU (right).

Downloaded from www.sciencemag.org on February 16, 2012

A is mainly hydrophilic, with five H bonds and three salt bridges (table S2).

Interface B is located on the ascending lateral surface of the central LRR modules (LRR7 to LRR10) of TLR5 and on the upper part of FliC αND1a and αND1b (Fig. 3A, right) and constitutes ~60% (~790 Å^2) of the primary interface (fig. S9, A and B). Interface B is also mainly hydrophilic, with 12 H bonds, and is primarily located at a protruding loop of LRR9 that undergoes structural changes upon FliC binding (fig. S10, A and B). In the TLR5-N12$_{VLR}$ structure, the LRR9 loop is highly flexible, as indicated by high *B* values and poor electron density, but upon FliC binding, the loop undergoes structural rearrangement to form a well-defined groove (Fig. 3B and fig. S10A) that accommodates the absolutely conserved FliC residues Arg^{90} and Glu^{114} (fig. S6). The groove side and rim reinforce FliC binding through diverse H bonds and van der Waals interactions with eight FliC residues at the C-terminal end of αND1a and N-terminal half of αND1b. This groove is responsible for half of the primary-interface H bonds and ~35% of b.s.a. The functional importance of the LRR9 loop was further demonstrated by an LRR9-loop deletion that severely impaired FliC binding in size exclusion chromatography, a competitive fluorescence polarization (FP) assay (by at least three orders of magnitude), and competitive cell-based signaling assays (by two to three orders of magnitude) (fig. S10, C to F). This loop is highly conserved in all species and likely forms the hot spot in the TLR5-FliC interaction (*25*).

The secondary dimerization interface consists of three surfaces: interface α (TLR5′-FliC), its two-fold symmetry–related interface α′ (TLR5-FliC′), and interface β (TLR5-TLR5′); no contacts are made between FliC molecules (*26*) (Fig. 4). Dimerization interface α is located on the convex side of TLR5′ LRR12/13 and on the FliC C-terminal αND1b region and following loop at the bottom of the D1 domain (Fig. 4, left). Dimerization interface β is formed by TLR5 residues mainly on the ascending lateral side of LRR12/13 (Fig. 4, right). The dimerization interface is relatively limited with a total of ~550 Å^2

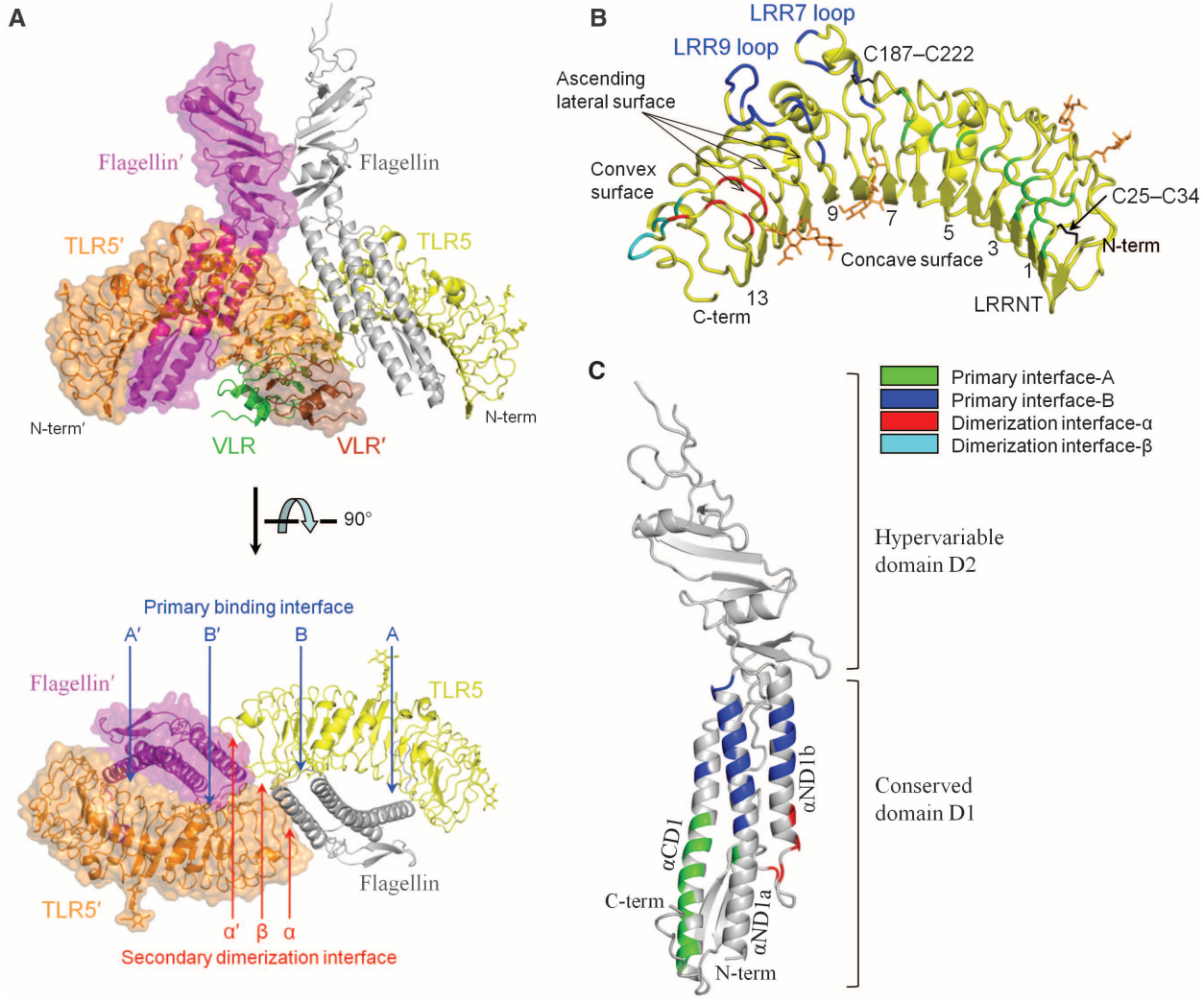

Fig. 2. Overall structure of the 2:2 TLR5-N14$_{VLR}$/FliC-ΔD0 complex. (**A**) TLR5-N14 interacts with FliC-ΔD0 into a 2:2 quaternary complex structure that organizes two TLR5 molecules in a tail-to-tail orientation where their C-terminal regions are disposed in the center of the complex. The 2:2 complex consists of two copies of 1:1 complex, 1:1 TLR5-N14$_{VLR}$/FliC-ΔD0 (ribbons: yellow, TLR5-N14; green, VLR; gray, FliC D1-D2), and 1:1 TLR5-N14$_{VLR}$′/FliC-ΔD0′ (ribbons with translucent surface: orange, TLR5-N14′; brown, VLR′; magenta, FliC′ D1-D2). The prime denotes that the molecule or residue comes from the second 1:1 complex in the 2:2 assembly. The 1:1 complex formation is mediated by the primary binding interface (A, B, A′, and B′) and its homodimerization to the 2:2 complex is mediated by the secondary dimerization interface (α, α′, and β). For clarity, only the TLR5-N14 and FliC D1 domain are shown in the lower panel. (**B**) The TLR5-N14 structure of the complex. Interface residues are color-coded according to the color scheme indicated. Two disulfide bonds and four N-linked glycans are represented by black and orange sticks, respectively. Four N-linked glycans are scattered over the TLR5 surface but are not involved in TLR5-FliC interfaces. LRR7 and LRR9 are atypically long (with 32 and 36 residues, respectively) in contrast to the other LRRs (23 to 27 residues) and protrude as long loops (fig. S3). The ascending lateral surface of the LRR domain refers to the region connecting the C-terminal end of the concave surface to the N-terminal end of the convex surface in each LRR module (*36*). (**C**) The FliC D1-D2 structure observed in the complex. Each α helix is labeled according to previous nomenclature (*37*).

Downloaded from www.sciencemag.org on February 16, 2012

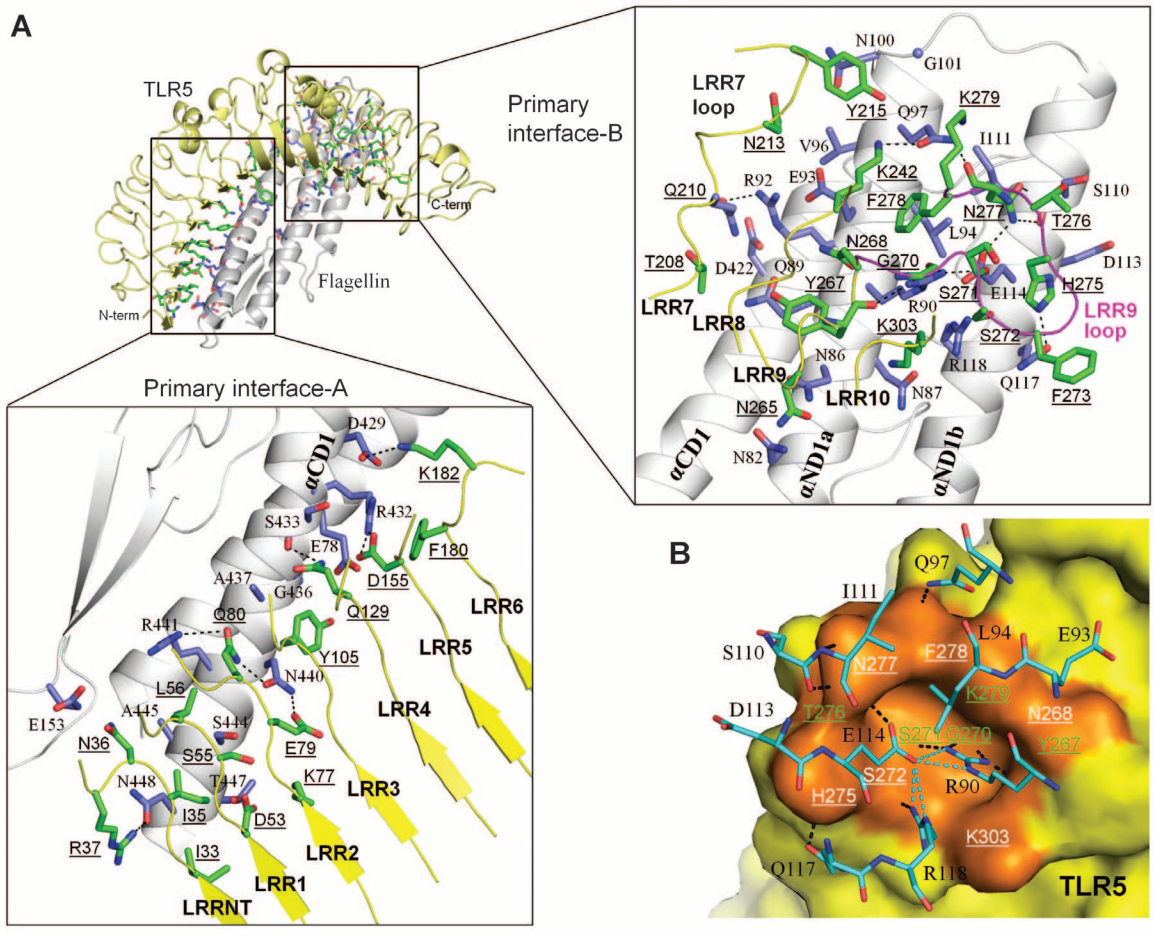

Fig. 3. The primary binding interface of the TLR5-FliC 1:1 complex. (**A**) Residues in primary interfaces A (bottom) and B (right) are shown in sticks (TLR5, green; FliC, light blue) on the 1:1 TLR5-FliC complex (TLR5, yellow ribbon; FliC, gray ribbon). The protruding loop of TLR5 LRR9 is highlighted in magenta. H bonds and salt bridges are represented by dashed lines. TLR5 residues are underlined to distinguish them from FliC residues. Amino acid abbreviations: A, Ala; D, Asp; E, Glu; F, Phe; G, Gly; H, His; I, Ile; K, Lys; L, Leu; N, Asn; Q, Gln; R, Arg; S, Ser; T, Thr; V, Val; Y, Tyr. (**B**) The LRR9 loop forms a groove that provides the major FliC-binding site. FliC Arg^{90} is deeply inserted into the groove and makes four H bonds with carbonyl oxygens of TLR5 Tyr^{267}, Gly^{270}, and Ser^{271} (*38*). FliC Glu^{114} buttresses and orients the Arg^{90} side chain toward the groove via H bonds, and also forms H bonds with TLR5 Asn^{277}. The bottom of the groove is constructed from the main chains of Gly^{270} and Ser^{271}, and its surrounding wall is decorated by eight LRR9 residues (Tyr^{267}, Asn^{268}, Ser^{272}, His^{275}, Thr^{276}, Asn^{277}, Phe^{278}, and Lys^{279}) and an LRR10 residue (Lys^{303}). The LRR9 loop groove is shown in the orange surface; interacting residues are labeled (green labels for residues that engage only main chain in the interaction with FliC; white labels for residues that engage side chains in the interaction). FliC residues that interact with the LRR9 loop groove are shown in cyan sticks. Intermolecular and intramolecular H bonds are represented by black and cyan dashed lines, respectively.

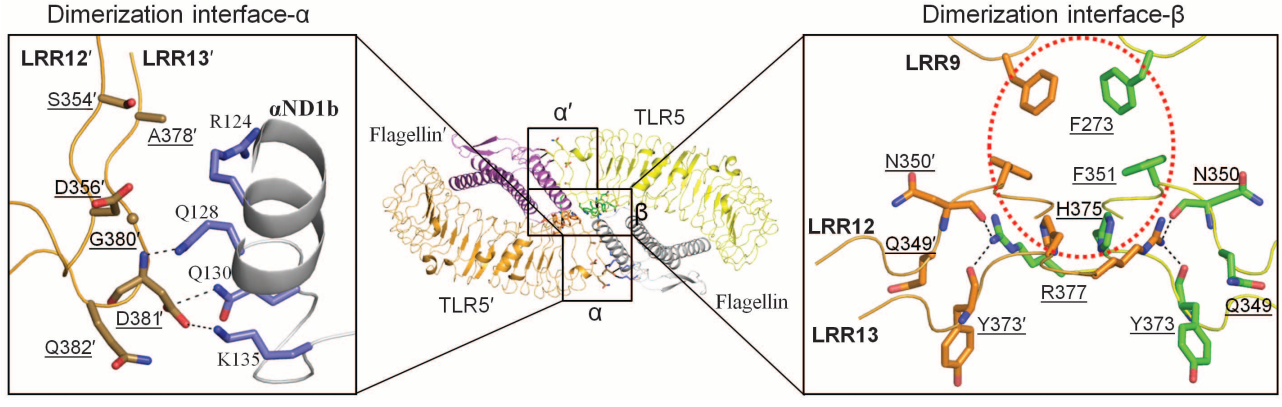

Fig. 4. Secondary dimerization interface in the 2:2 TLR5-FliC assembly. Two of the 1:1 TLR5-FliC complex homodimerize to the 2:2 complex using dimerization interfaces α, α′, and β. The overall 2:2 complex is shown in the center, and enlarged dimerization interfaces α and β are shown in the left and right panels, respectively (TLR5′ residues, brown sticks; TLR5 residues, green sticks; FliC residues, lilac sticks). In interface α, TLR5′ $Asp^{381\prime}$, which is conserved as an acidic residue (Asp or Glu) in all TLR5 orthologs, forms three H bonds with FliC Gln^{128}, Gln^{130}, and Lys^{135}. Interface β is created by van der Waals interactions among two sets of three equivalent aromatic residues (Phe^{273}, Phe^{351}, and His^{375} of TLR5 and TLR5′), which creates a largely hydrophobic core (red dotted circle) that is conserved in all other TLR5 sequences (Phe at residue 273, Leu at residue 351, and His at residue 375; see fig. S3), and by four H bonds (Arg^{377}-$Asn^{350\prime}$, Arg^{377}-$Tyr^{373\prime}$, $Arg^{377\prime}$-Asn^{350}, and $Arg^{377\prime}$-Tyr^{373}).

Downloaded from www.sciencemag.org on February 16, 2012

b.s.a. on each 1:1 complex (α, ~130 Å^2; α′, ~130 Å^2; β, ~290 Å^2), but may be greater in the full-length TLR5-FliC interaction (*16*). This dimerization interface exhibits high sequence conservation among both vertebrate TLR5 orthologs and FliC orthologs from diverse bacteria (figs. S3, S6, and S11), and high shape complementarity (shape correlation statistic S_c, 0.64 to 0.76) (*27*), underscoring its functional importance in the secondary dimerization of TLR5-FliC (*28*).

We used structure-guided mutagenesis to assess whether the observed dimerization interface contributes to TLR5 activation for downstream NF-κB signaling. A series of CBLB502 derivatives with the proposed dimerization surface disrupted by point mutations and/or deletions were tested in two assays: (i) a competitive FP assay to assess primary binding for *dr*TLR5, and (ii) an NF-κB–luciferase reporter assay to assess signaling activity that results from both primary binding and secondary dimerization. The latter assay with *hs*TLR5 in HEK293 cells also provided an opportunity to further validate the *dr*TLR5 structure as a surrogate for *hs*TLR5. The binding and signaling data from the CBLB502 mutants (Fig. 1, C and D, and table S3) support the proposed contribution of the dimerization interface to signaling. Dimerization interface mutant 1 (DIM1; Arg^{124} → Asp, Gln^{128} → Ala, Gln^{130} → Ala, and Lys^{135} → Ala mutations in αND1b at the dimerization interface α, Fig. 4) shows a factor of ~30 decrease in signaling, but essentially no decrease in binding (factor of ~3). For the second mutant (DIM2; deletion of residues 126 to 128 and Thr^{129} → Gly, Gln^{130} → Gly, and Lys^{135} → Glu mutations to disrupt αND1b and connecting loop structures and introduce charge repulsion), the disruption in signaling efficiency is even more pronounced (a factor of ~800 decrease, versus only a factor of 9 decrease in binding). In the control mutant CBLB502-PIM (with Gln^{89}, Arg^{90}, and Gln^{97} mutated to Ala in the primary interface), comparable decreases in primary binding (by a factor of 450) and signaling efficiency (by a factor of ~120) were observed (*29*). Decoupling of antigen binding and receptor signaling was also observed for CBLB502-ΔD0, used as a control, where a minor (factor of 2 to 3) change in binding affinity both for TLR5-$N14_{VLR}$ and TLR5-ECD contrasts with a factor of ~1000 decrease in signaling efficiency (Fig. 1, C and D, and fig. S12). Thus, both dimerization interface mutants (CBLB502-DIM1 and -DIM2) clearly correlate in activity with the signaling-impaired CBLB502-ΔD0 mutant rather than with the primary binding–impaired CBLB502-PIM mutant.

Our results indicate that the D1 domain makes substantial contributions to both high-affinity binding and TLR5 signaling (*16*), whereas D0 contributes to TLR5 activation, but has no or little effect on binding. Furthermore, the TLR5-FliC structure and unique features of ligand recognition and activation provide a template to enhance the therapeutic activity of the radioprotective drug (CBLB502) or flu vaccine (VAX102) in clinical trials, as well as to design new vaccine adjuvants or antagonistic therapeutics for hyperinflammatory diseases.

References and Notes

1. K. Takeda, T. Kaisho, S. Akira, *Annu. Rev. Immunol.* **21**, 335 (2003).
2. There are 10 functional human TLRs (TLR1 to 10) and 12 functional mouse TLRs (TLR1 to 9, TLR11 to 13).
3. L. Liu *et al.*, *Science* **320**, 379 (2008).
4. M. S. Jin *et al.*, *Cell* **130**, 1071 (2007).
5. B. S. Park *et al.*, *Nature* **458**, 1191 (2009).
6. This tail-to-tail TLR dimerization is believed to be a prerequisite for signal transduction, consistent with lack of signaling by antagonist-bound TLR 1:1 complexes and a head-to-head TLR dimer of a TLR4 regulator, RP105 (*19*, *30*–*32*).
7. O. W. Stockhammer, A. Zakrzewska, Z. Hegedûs, H. P. Spaink, A. H. Meijer, *J. Immunol.* **182**, 5641 (2009).
8. F. Hayashi *et al.*, *Nature* **410**, 1099 (2001).
9. M. Iqbal *et al.*, *Infect. Immun.* **73**, 2344 (2005).
10. E. Andersen-Nissen *et al.*, *Proc. Natl. Acad. Sci. U.S.A.* **102**, 9247 (2005).
11. K. D. Smith *et al.*, *Nat. Immunol.* **4**, 1247 (2003).
12. A. T. Gewirtz, T. A. Navas, S. Lyons, P. J. Godowski, J. L. Madara, *J. Immunol.* **167**, 1882 (2001).
13. T. K. Means, F. Hayashi, K. D. Smith, A. Aderem, A. D. Luster, *J. Immunol.* **170**, 5165 (2003).
14. P. F. McDermott, F. Ciacci-Woolwine, J. A. Snipes, S. B. Mizel, *Infect. Immun.* **68**, 5525 (2000).
15. T. Eaves-Pyles *et al.*, *J. Immunol.* **166**, 1248 (2001).
16. See supplementary material on *Science* Online.
17. Human, mouse, frog, trout, and zebrafish TLR5 ectodomains were screened for expression in a baculovirus system. In addition, human and mouse TLR5 ectodomains were also tested in an HEK293 cell expression system.
18. Zebrafish contains two highly homologous *tlr5* genes, *tlr5a* and *tlr5b*. Previous *tlr5a/b* knockdown embryo experiments showed that TLR5a/b are responsible for FliC-specific immune responses (*7*). TLR5b was used for this study.
19. H. M. Kim *et al.*, *Cell* **130**, 906 (2007).
20. CBLB502 contains only D0 and D1 domains from *sd*FliC, which consists of four domains (D0, D1, D2, and D3). CBLB502 activates TLR5 as FliC and protects the hematopoietic system and gastrointestinal tissues from radiation-induced damage, creating opportunities for therapeutic applications (*33*).
21. Despite the tight complex formation, cocrystallization trials of *dr*TLR5 chimeric proteins with *sd*FliC and CBLB502 failed to yield diffractable crystals, most likely because of the excessive flexibility of the D0 domain, which appeared dispensable for formation of a 1:1 complex with TLR5 as assessed by binding of CBLB502-ΔD0 in a competitive FP assay (fig. S12). Although CBLB502-ΔD0 also failed to yield diffractable cocrystals, *sd*FliC-ΔD0 in complex with TLR5-$N14_{VLR}$ was successful in producing diffraction-quality crystals.
22. The TLR5 structures in TLR5-$N12_{VLR}$ and FliC-bound TLR5-$N14_{VLR}$ superimpose well, except for the protruding loop of LRR9, which undergoes substantial conformational changes upon FliC binding (Cα-RMSD without the loop, 0.56 Å). Thus, for TLR5 structure analysis, the TLR5-$N14_{VLR}$ structure is described unless otherwise specified.
23. N. D. Temperley, S. Berlin, I. R. Paton, D. K. Griffin, D. W. Burt, *BMC Genomics* **9**, 62 (2008).
24. The FliC D3 domain could not be built because of poor electron density, although it exhibits an apparent molecular envelope (fig. S5).
25. Although the protein-to-protein binding interface is generally extensive, most of the binding stability and free energy are provided by a small cluster of hotspot residues. We propose that the binding hotspot of the primary *dr*TLR5-FliC binding interface is located in the LRR9 loop, given that deletion of the LRR9 loop almost completely abrogates FliC binding. Moreover, the LRR9 loop sequence is more conserved than other primary interface residues (fig. S3). Accordingly, the LRR9 loop is anticipated to also function as a key determinant in human TLR5 interaction with FliC. About 62% of the total interactions observed at the *dr*TLR5 LRR9 loop would be conserved in human TLR5, with 8 out of 10 H bonds recapitulated (fig. S13). In contrast, other interface residues from LRRNT to LRR8 show lower sequence conservation, consistent with our observation that a TLR5-VLR hybrid (TLR5-$N6_{VLR}$) that contains a majority of interface-A residues from LRRNT to LRR6 does not form a tight complex with FliC or CBLB502 in solution. Therefore, the network of *hs*TLR5-FliC interactions in this region could be somewhat different. Only ~34% of the total interactions observed at the *dr*TLR5 region from LRRNT to LRR8 would be formed in human TLR5, with 2 out of 10 H bonds functionally conserved. The conservation of the key interactions in the TLR5-flagellin interface is supported by our mutagenesis data (PIM-mutant of CBLB502) using a reporter system with *hs*TLR5 (Fig. 1, C and D), as well as by highly efficient, competitive inhibition of CBLB502-induced *hs*TLR5 signaling by *dr*TLR5-ECD (Fig. 1B).
26. The secondary dimerization interaction is very weak in solution for these ectodomain constructs. The 2:2 complex was not detectable by size exclusion chromatography and native EMSA even with full-length TLR5-ECD and FliC proteins. Only a trace amount of the 2:2 complex was observed between the full-length TLR5-ECD and CBLB502 with a K_d of ~0.5 mM in analytical ultracentrifugation, which suggests the instability of the secondary dimerization in solution. Nonetheless, we anticipate that FliC-mediated TLR5 dimerization would be enhanced on the cell surface, possibly as a result of the constraint of two-dimensional movement in the membrane (*34*), engagement of intracellular and transmembrane domains of TLR5, or contribution of other unknown co-receptor/adaptor molecules.
27. M. C. Lawrence, P. M. Colman, *J. Mol. Biol.* **234**, 946 (1993).
28. The secondary dimerization interface of TLR5-N14/FliC extends to interactions between VLR and VLR′ (b.s.a., ~370 Å^2), between VLR and FliC′ (b.s.a., ~100 Å^2), and between VLR′ and FliC (b.s.a., ~40 Å^2) in the TLR5-$N14_{VLR}$/FliC-ΔD0 structure. However, the VLR interactions exhibit very low shape complementarity (0.42, 0.16, and 0.04 of S_c values, respectively) and do not include any specific H bonds and salt bridges. These observations suggest that they make minimal contributions to TLR5-$N14_{VLR}$/FliC-ΔD0 dimerization.
29. Individual alanine mutations at FliC Gln^{89}, Arg^{90}, and Gln^{97} reduced TLR5 signaling by factors of 4.1, 7.4, and 5.6, respectively, in a previous study (*11*).
30. S. Divanovic *et al.*, *Nat. Immunol.* **6**, 571 (2005).
31. S. I. Yoon, M. Hong, I. A. Wilson, *Nat. Struct. Mol. Biol.* **18**, 1028 (2011).
32. U. Ohto, K. Miyake, T. Shimizu, *J. Mol. Biol.* **413**, 815 (2011).
33. L. G. Burdelya *et al.*, *Science* **320**, 226 (2008).
34. M. Gavutis, E. Jaks, P. Lamken, J. Piehler, *Biophys. J.* **90**, 3345 (2006).
35. E. Andersen-Nissen, K. D. Smith, R. Bonneau, R. K. Strong, A. Aderem, *J. Exp. Med.* **204**, 393 (2007).
36. J. Bella, K. L. Hindle, P. A. McEwan, S. C. Lovell, *Cell. Mol. Life Sci.* **65**, 2307 (2008).
37. F. A. Samatey *et al.*, *Nature* **410**, 331 (2001).
38. Amino acid variations at groove-forming residue 271 (Ala^{267} in human, Pro^{268} in mouse, and Ser^{271} in zebrafish) were implicated in human versus mouse differences in the cellular response to FliC (*35*). The same study also showed that mutations of two TLR5 aspartate residues (Asp^{294} of LRR10 and Asp^{366} of LRR13 in human TLR5) modulated the FliC response. However, these two acidic residues are not in the TLR5-FliC interface, but are instead located in the middle of the concave β strands and are involved in intramolecular interactions with nearby serine residues and the Asn^{346}-linked glycan, suggesting a critical role in TLR5 protein folding or stability. Thus, it is expected that the mutations would indirectly affect FliC response through modulation of TLR5 protein integrity, rather than directly through FliC binding.

Downloaded from www.sciencemag.org on February 16, 2012

Acknowledgments: We thank Y. S. Choo for critical comments on the manuscript, H. Tien and D. Marciano for automated crystal screening, X. Dai and M.-A. Elsliger for expert technical assistance, and K. Namba and K. Yonekura for generously sharing coordinates of flagellar filament. X-ray diffraction data sets were collected at SSRL beamline 11-1 and APS beamlines 23ID-B and 23ID-D. Supported by NIH grants AI042266 (I.A.W.), R01 AI080446 (A.V.G.), and RC2 AI087616 (A.V.G.); the Skaggs Institute for Chemical Biology (I.A.W.); and research grants from Cleveland BioLabs Inc. (CBLI) to Roswell Park Cancer Institute (A.V.G.) and Sanford-Burnham Medical Research Institute (A.L.O.). A.L.O. is a paid consultant for and holds stock options in CBLI which has developed the flagellin derivative CBLB502 into a radiation countermeasure. U.S. patent 8,007,812 for pharmacologically optimized FliC derivative CBLB502 is licensed to CBLI by Cleveland Clinic. Reagents are available under a materials transfer agreement. This is Scripps Research Institute manuscript 21369. The data presented in this paper are tabulated in the main paper and the supplementary material. Structure factors and coordinates for TLR5-N12$_{VLR}$ and TLR5-N14$_{VLR}$/FliC-ΔD0 are deposited in the Protein Data Bank under accession codes 3V44 and 3V47, respectively.

Supporting Online Material
www.sciencemag.org/cgi/content/full/335/6070/859/DC1
Materials and Methods
SOM Text
Figs. S1 to S14
Tables S1 to S3
References (*39*–*54*)

20 October 2011; accepted 4 January 2012
10.1126/science.1215584

Survival Analysis of Faculty Retention in Science and Engineering by Gender

Deborah Kaminski[1]* and Cheryl Geisler[2]

Individual assistant professors (a total of 2966 faculty) hired in science and engineering since 1990 at 14 United States universities were tracked from time of hire to time of departure by using publicly available catalogs and bulletins. Results of survival analysis showed that the chance that any given faculty member will be retained over time is less than 50%; the median time to departure is 10.9 years. Of all those who enter as assistant professors, 64.2% were promoted to associate professor at the same institution. Overall, men and women are retained and promoted at the same rate. In mathematics, however, faculty leave significantly earlier than other disciplines, and women leave significantly sooner than men, 4.45 years compared with 7.33 years.

U.S. universities are concerned about faculty retention in science and engineering (*1*–*4*). When a faculty member leaves prematurely, they suffer disruptions in teaching and mentoring as well as significant economic losses (*1*). Start-up costs in engineering and natural sciences can range from $110,000 to nearly $1.5 million (*3*), and it may take up to 10 years to recoup this investment (*4*).

Retention rates for faculty in the United States have been consistent. From 1971 through 1989, faculty members were retained at rates of 90 to 92% for associate and full professors and 84 to 86% for assistant professors (*5*). In 1996–1997 and 2001–2002, the retention rates for associate professors were again in the range of 90 to 92% (*6*).

Problems with the retention of women in science and engineering in the United States have been well documented. Like a leaky pipeline, each career stage in engineering and the natural sciences shows the retention of women lower than the stage before it (*3*, *7*). In particular, although women are increasingly represented among those with earned doctorates, they lag behind in representation in the academic faculties (*8*).

The problem appears to lie in differential application rates. Once women apply for or are in consideration for a career move, they are equally likely to succeed, but they are often not in the pool (*3*, *9*–*11*). Men have been found to be significantly more likely to receive tenure or move to positions outside of academia, whereas women are significantly more likely to be unemployed or to exit the tenure track for adjunct positions (*3*). Women with Ph.D.s in science, technology, engineering, and mathematics (STEM) disciplines have also been found to be less likely than men to be employed full time, although equally likely to succeed if they apply (*11*).

Women have also been shown to have greater intentions to leave the STEM disciplines (*12*), although not academia as a whole (*13*), and to leave for different reasons. Whereas salary is the number one reason for men, women cite more interpersonal and family reasons (*14*, *15*). Delays in tenure resulting in lower salaries could account for women leaving before tenure (*16*), but department climate is a primary reason why women are less satisfied and more likely to quit (*4*).

Significant disciplinary variations exist in the retention of women in science and engineering. In the disciplines included in this study, the rate of growth in earned doctorates, the level of representation in the pool of Ph.D.s, and representation in the ranks of assistant professors all showed marked disciplinary differences between men and women (*8*). At research I universities in six of the nine fields included in this study, the mean percentage of those who applied, were interviewed for, and were made offers to was closer to the percentage of women in the relevant doctoral pool for electrical engineering, mathematics, and physics, where their representation was lowest, than in chemistry and biology, where their representation in the pool was highest (*11*).

Women's representation among earned doctorates is particularly high in the biological sciences (*8*). Between 1972 and 1991, representations of women in all levels of academics was highest for life sciences and lowest for engineering, with physical science in between (*9*). The probability of having a tenure-track position 10 years after Ph.D. is significantly smaller for women in the life sciences but about the same for those in physical and engineering sciences (*9*). In the biological and life sciences, where women are most heavily represented, they have an 8 to 9% less chance of getting a tenure-track job, getting tenure, or getting promoted to full professor (*9*). In terms of retention, one study reports that women and minority faculty have higher turnover intentions in the pure and applied life sciences as well as in the pure physical sciences, but not in the applied science areas that include the engineering fields (*1*).

In this study, we tracked 2966 science and engineering faculty from 14 universities from time of hire to the time they left the university. All data were obtained from publicly available

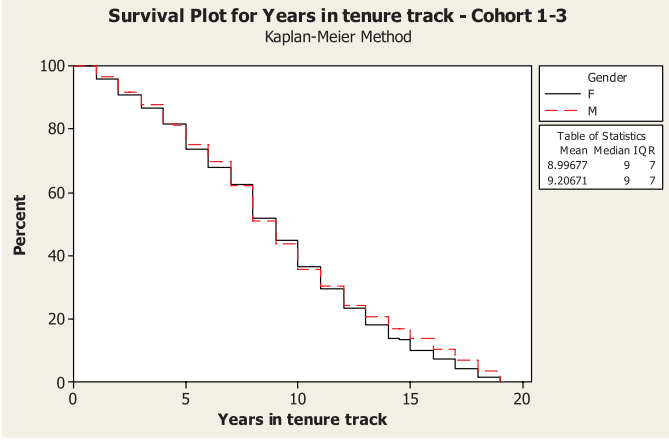

Fig. 1. Nonparametric survival curve for faculty who entered between 1990 and 2002 by gender. IQR, interquartile range.

[1]Department of Mechanical, Aerospace, and Nuclear Engineering, Rensselaer Polytechnic Institute, Troy, NY 12180, USA. [2]Faculty of Communication, Art, and Technology, Simon Fraser University, Harbour Centre 7410, 515 West Hastings Street, Vancouver, BC V6B 5K3, Canada.

*To whom correspondence should be addressed. E-mail: kamind@rpi.edu

Downloaded from www.sciencemag.org on February 16, 2012

college catalogs and bulletins (*17*). We divided our sample into five cohorts, beginning with those who entered from 1990 to 1993 and ending with those entering from 2006 to 2009. The sample size and composition of each cohort can be found in table S1. The question of retention was examined by using the first three cohorts, who arrived between 1990 and 2002 (*18*), as specified in table S2.

Figure 1 shows the Kaplan-Meier survival curve for cohorts 1 to 3. Large declines appear at years 5, 8, and 10; there is no significant difference between men and women. The data are correlated in Fig. 2, which includes parametric survival curves, probability density functions, and hazard functions. A log normal distribution provided the best fit to data, with a correlation coefficient of 0.983. The probability density function shows that departure rates are higher in the first 10 years. In the first 3 years, departure rates are somewhat lower, whereas in the next 3 years, departure rates are high. The survival function shows a rather steeper decline in faculty at early times and a more moderate descent at later times. It is apparent that posttenure faculty leave at a lower rate than pretenure faculty. The hazard function tells a similar story. This is the rate of attrition at a given point in a faculty career, and it peaks at about 6 years. The differences between men and women are small.

Table 1 gives the median time to departure for cohorts 1 to 3 by gender. Half of all entering faculty have departed by 10.9 years. There is no statistically significant difference between men and women. The 95% confidence intervals (CIs) on the median for men and women are nearly coincident.

Another perspective on faculty retention is available by examining promotion rates. The percentage of faculty in the first two cohorts who were promoted to associate professor is given in table S3. For the full population of 1032 faculty, 64.2% ± 3.65% were promoted to associate professor. There is no significant variation by cohort or by gender. For the first cohort, the average number of years to promotion to full professor was 10.73 for men and 10.91 for women.

These results give a broad view of parity between men and women in the areas of retention and promotion, consistent with several other studies (*1*, *11*). Women on the whole are less satisfied than men (*15*, *19*), but this dissatisfaction does not manifest as increased rates of departure.

There was no significant change in retention patterns from 1990 to 2002. There has been a substantial increase in the percentage of women hired into STEM faculty positions since 1990, as shown in fig. S1. These two facts together imply an increased presence of women in STEM departments over the long run. Those who are hired tend to stay, and the number hired is increasing. The time constant for the change in department gender composition is, however, very long.

Although there are no significant differences in retention by gender for the entire population, there are some disciplinary variations. Table 2 lists the median time to exit for men and women by discipline. A log-rank and Wilcoxon test for significant difference between two survival curves (*20*) shows no differences except in the case of mathematics, where $P = 0.0522$ and 0.008, respectively. Because of the choice of weighting function, the log-rank test puts more emphasis on differences at long times, and the Wilcoxon puts more emphasis on differences at short times. A Cox proportional hazards model was used to detect differences among disciplines regardless of gender. Two disciplines were significantly different. In mechanical engineering, faculty leave later than those in other disciplines ($P = 0.0006$), but gender differences are not significant. In mathematics, by contrast, faculty leave earlier than those in other disciplines ($P < 0.0001$), and the difference between men and women is stark. The median for men is 7.33 years, and the median for women is 4.45 years.

The Kaplan-Meier survival curve for mathematics faculty is presented in Fig. 3. Women leave at a significantly greater rate than men, including a dramatic decline at 5 years. The data were correlated with a log normal function, as shown in fig. S2. There is little overlap in the 95% confidence intervals for the men and women, indicating statistically significant differences. The correlation coefficients of 0.967 and 0.975 are high. The probability density function, the survival function, and the hazard function for mathematics faculty are given in fig. S3. The probability density function shows that women are much more likely to leave very soon after hiring than are men. This results in a survival curve in which very few women persist to the 20-year mark.

Previous large-scale analyses of the retention of academic faculty in the United States have relied on aggregate data or surrogate variables to track year-to-year turnover in STEM disciplines. The large-scale analysis reported here, which tracked the retention of individual faculty across time, confirmed some of the earlier results but points to new areas of concern. Although the use of college catalogs and bulletins as a data source is time-intensive, previous work has made the case for the value of using publicly available sources to monitor institutional change (*21*).

An early study based on American Association of University Professors data (*5*) found average attrition rates of 0.15 for assistant professors and 0.08 for associate professors. The values for assistant professors are much higher than our hazard function values, indicating that retention of assistant professors may have improved since 1990. In a more recent study (*6*), the attrition rates for all associate professors averaged 0.077. From our data, the hazard function at 10 years (representative of associate professors) was 0.0709, and at 8.5 years it was 0.073, consistent with the two earlier studies.

Our work confirms the importance of the late pretenure period as a period of critical risk in the retention of faculty in STEM. Like earlier analyses, we find that posttenure faculty members are overall less likely to depart than pretenure faculty. Overall, the chances that any

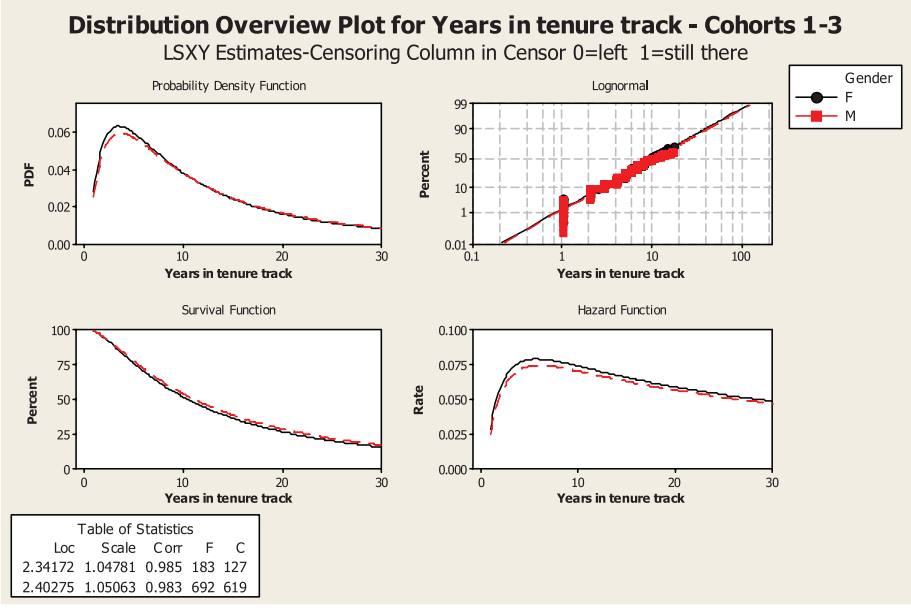

Fig. 2. Survival analysis of faculty who entered between 1990 and 2002 by gender. LSXY, least squares; F, number that left; C, number still remaining.

Table 1. Median times to exit the tenure track by gender, cohorts 1 to 3.

	Median time to exit, years	95% Normal CI	
		Lower	Upper
All	10.94	10.3	11.61
Men	11.05	10.34	11.81
Women	10.40	9.094	11.89

Downloaded from www.sciencemag.org on February 16, 2012

Table 2. Median times to exit the tenure track by gender and discipline for cohorts 1 to 3. CIs are for medians.

Discipline	Median years men	Lower 95% CI	Upper 95% CI	Median years women	Lower 95% CI	Upper 95% CI	*P* log rank test	*P* Wilcoxon test
Elec Eng	12.92	10.51	15.88	10.68	6.49	17.59	0.641	0.576
Physics	11.14	9.00	13.79	9.41	6.61	13.40	0.118	0.739
Mech Eng	16.19	12.80	20.46	10.41	7.10	15.24	0.109	0.153
Chemistry	12.46	10.07	15.41	10.53	7.57	14.64	0.980	0.847
Math	7.33	6.20	8.68	4.45	3.34	5.93	0.0522	0.0083
Comp Sci	9.32	7.64	11.39	10.25	6.87	15.28	0.5156	0.548
Civil Eng	8.68	7.01	10.76	10.74	7.48	15.43	0.970	0.262
Biology	11.96	9.30	15.37	16.36	9.20	29.10	0.0664	0.197
Chem Eng	11.64	9.00	15.05	9.78	5.95	16.08	0.393	0.687

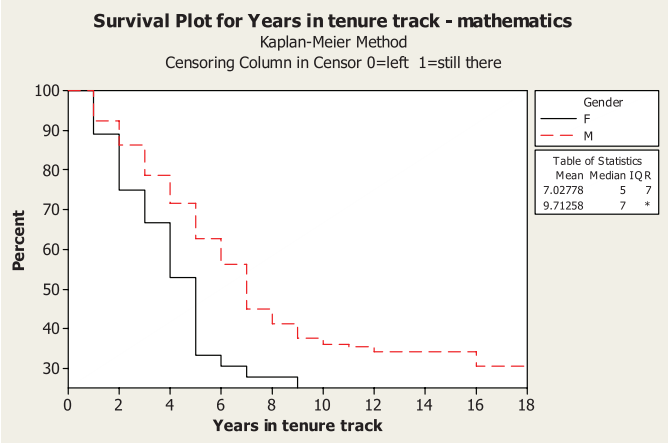

Fig. 3. Kaplan-Meier survival plot for mathematics faculty by gender, cohorts 1 to 3.

given faculty member will be retained over time is less than 50%; the median time to departure is 10.9 years. These retention data are rather stable over the 12-year period studied and may be resistant to change. Further work will need to be done to establish how much of this mobility results from the pull of better opportunities or the push of concern over tenure and how much results in a decision to leave the tenure track or the academic sector altogether.

Given the high economic and institutional costs of failures to retain, these low retention rates represent a substantial burden on institutions of higher education. Universities must be prepared to replace departing faculty and must plan for the high cost of start-up packages. If a university expects to grow its faculty, it has an even greater challenge. Simply staying the same size requires considerable hiring and mentoring, even without considering retirement.

The lack of gender effects in retention and promotion in our data is good news and confirms the patterns found in recent aggregate and indirect analyses (*1*, *3*). For all STEM disciplines considered together, the percentage of women hired is lower than men, but the retention rates are comparable. This indicates that, if the women are hired, they will likely persist and that recruitment is a more pressing issue than retention in achieving gender parity. However, the long span of faculty careers provides considerable inertia in the system. Marschke *et al*. (*22*) estimate that it would take about 40 years for a department to match the gender composition of the hiring pool because of the long length of faculty careers. Although our data do show an increase in percentage of women hired, the goal of 50% women may not be achieved until as late as 2050. Thus, if current trends continue, it may take 100 years before women are 50% of the faculty in STEM departments.

In our data, the discipline of mathematics stands out in two ways with respect to retention. First, it has the quickest departure rates in any discipline we studied. Second, there are statistically significant differences in the retention rates of men and women faculty. The median time to departure for men is 7.33 years, and for women it is 4.45 years. No other discipline shows gender effects at the 95% confidence level. Annual surveys of the discipline by the American Mathematical Society (*23*) track the recruitment of new doctoral recipients into academic mathematics but have not examined retention. Our data suggest that there are significant retention issues in the discipline deserving of further scrutiny.

References and Notes

1. Y. J. Xu, *Res. Higher Educ.* **49**, 607 (2008).
2. University of Colorado at Boulder, "Faculty recruitment and retention task force report" (2001), www.colorado.edu/AcademicAffairs/fac_recruit/fac_recruit.doc.
3. National Academy of Sciences, National Academy of Engineering, and Institute of Medicine, *Beyond Bias and Barriers: Fulfilling the Potential of Women in Science and Engineering* (National Academies Press, Washington, DC, 2007).
4. R. R. Callister, *J. Technol. Transf.* **31**, 367 (2006).
5. R. Ehrenberg, H. Kasper, D. Rees, *Econ. Educ. Rev.* **10**, 99 (1991).
6. M. Nagowski, *Am. Econ.* **50**, 69 (2006).
7. V. Valian, *Why So Slow? The Advancement of Women* (MIT Press, Cambridge, MA, 1998).
8. D. Nelson, D. Rogers, "A national analysis of diversity in science and engineering faculties at research universities" (University of Oklahoma, Department of Chemistry, 2006), http://faculty-staff.ou.edu/N/Donna.J.Nelson-1/diversity/briefings/Diversity%20Report%20Final.pdf.
9. T. J. Ley, B. H. Hamilton, *Science* **322**, 1472 (2008).
10. W. W. Ding, F. Murray, T. E. Stuart, *Science* **313**, 665 (2006).
11. National Research Council Committee on Gender Differences in the Careers of Science, Engineering, and Mathematics Faculty; Committee on Women in Science, Engineering, and Medicine; and Committee on National Statistics; *Gender Differences at Critical Transitions in the Careers of Science, Engineering, and Mathematics Faculty* (National Academies Press, Washington, DC, 2010).
12. Y. J. Xu, *Res. Higher Educ.* **49**, 40 (2008).
13. Y. Zhou, J. F. Volkwein, *Res. Higher Educ.* **45**, 139 (2004).
14. A. E. Preston, *Leaving Science: Occupational Exit from Scientific Careers* (Russell Sage Foundation, New York, 2004).
15. S. Gardner, *J. Professoriate*; available online at http://umaine.academia.edu/SusanGardner/Papers/464281/Cumulative_negativity_Reasons_for_women_faculty_departure_from_one_research_institution.
16. D. K. Rausch, B. P. Ortiz, R. A. Douthitt, L. L. Reed, *CUPA J.* **40**, 1 (1989).
17. Methods are available as supporting material on *Science* Online.
18. Faculty in the most recent two cohorts have not been in position long enough to provide useful data for most of our research questions.
19. V. J. Rosser, *Res. Higher Educ.* **45**, 285 (2004).
20. D. W. Hosmer, S. Lemeshow, S. May, *Applied Survival Analysis* (Wiley, Hoboken, NJ, 2008).
21. C. Geisler, D. Kaminski, R. A. Berkley, *NWSA J.* **19**, 145 (2007).
22. R. Marschke, S. Laursen, J. M. Nielsen, P. Dunn-Rankin, *J. Higher Educ.* **78**, 1 (2007).
23. R. Cleary, J. W. Maxwell, C. A. Rose, *Not. Am. Math. Soc.* **57**, 1306 (2010).

Acknowledgments: We thank T. Willemain and K. Bennett for help with the analysis. This work was supported by NSF ADVANCE award 0548354. The data reported in this paper are archived in the supporting online material.

Supporting Online Material

www.sciencemag.org/cgi/content/full/335/6070/864/DC1
Materials and Methods
Figs. S1 to S3
Tables S1 to S8
References
Data

4 October 2011; accepted 22 December 2011
10.1126/science.1214844

Downloaded from www.sciencemag.org on February 16, 2012

New Products

THERMAL CYCLER

The new G-Storm thermal cycler, GS482, embraces a sleek, black styling and features an enlarged screen to improve the user interface and experience. The new, cost-effective system is equipped with a number of enhanced features that increase the instrument's flexibility and functionality. The two independent 48-well blocks, both with sprung heated lids that adapt to both tubes and high profile 48-well plates within the GS482, enables two programs to be run independently or one program simultaneously on both blocks. Both of the GS482's thermal blocks feature two independent temperature control sensors and four peltier heating units to ensure accurate temperature control and uniformity across the block surface. Active Sample Cooling also ensures that samples are cooled until the heated lid reaches its target temperature. Onboard software features a Program Wizard that can store up to 1,000 programs.

Labtech International
For info: +44-(0)-1273-814888 | www.labtech.com

DISPOSABLE SYRINGE FILTERS

A new range of disposable syringe filters provide fast and efficient filtration of cell culture media. Manufactured in a Class 100000/ISO Class V clean room to ISO 9001:2008 and EN ISO 13485:2003 manufacturing standards ensures all Porvair syringe filters are free from DNA/RNA, DNAse/RNAse, and Pyrogen contamination. Stringent quality testing means each syringe filter performs reliably to specification. With three membranes to choose from an optimized syringe filter is available for most applications. Polyethersulfone membrane syringe filters exhibit a low affinity for proteins and extractables making them ideal for pre-filtration and filtration of buffers and culture media. The mixed Cellulose Ester membrane efficiently binds trace proteins making them the syringe filters of choice for filtration of aqueous solutions. Porvair's hydrophobic Nylon membrane offers excellent chemical compatibility across a wide pH range enabling it to be used for the filtration of either aqueous or organic solvents.

Porvair Sciences
For info: +44-(0)-1372-824290 | www.porvair-sciences.com

WESTERN BLOT STRIPPING SOLUTION

Based on G-Biosciences' popular Western ReProbe, this modified single component system is specifically formulated to dissociate and remove stubborn, high-affinity antibodies from membrane-bound proteins without destroying the antigenic-binding affinity. Western ReProbe PLUS saves time and money by eliminating the need to rerun gels and transfer processes and by offering you the ability to reuse Western blots. G-Biosciences' Western ReProbe PLUS eliminates the need for boiling, denaturants, or SDS. The membrane-bound protein is retained on the membrane and the matching antibodies are washed away. Once the antigen-antibody bonds are broken, the membrane-bound protein is free to accept new antibodies. G-Biosciences' Western ReProbe PLUS allows screening of the same blot with different antibodies, repeated analysis and correction of unsatisfactory blots with multiple probes, and comparison of phosphorylated and total protein on the same blot. Each 100 mL supply is sufficient for up to 30 standard size Western blots.

G-Biosciences
For info: 314-991-6034 | www.gbiosciences.com

SAMPLE DRYING

Available for use with Genevac evaporators, Dri-Pure technology enables scientists to rapidly dry their samples without cross-contamination or loss of sample due to solvent bumping. Dri-Pure offers significant benefits to scientists, especially those working in synthesis and purification. Other methods of solvent removal tend to be very laborious or lead to unacceptable cross-contamination. Dri-Pure running on a Genevac evaporator gives smooth, controlled solvent removal in optimum time. The patented Dri-Pure technology is available for all current models of Genevac centrifugal evaporators, from the affordable EZ-2 through to the production-scale HT-24. Genevac's unique anti-bumping system works by carefully controlling the reducing pressure in the evaporation chamber in combination with an increase in rotor speed to achieve greater g-force. In addition, heat flow to the samples must be reduced during the pressure ramping stage. Dri-Pure achieves all this via the embedded instrument software and hardware that makes such an elegant solution easy to apply.

Genevac
For info: +44-(0)-1473-240000 | www.genevac.com

2-D CODED TUBES

Identifying your sample via a code on the tube can be done in a number of ways. However the most reliable in terms of long-term identification and tracking of samples is via a 2-D coding on the bottom of the tubes. Barcodes on Micronic 2-D Data Matrix and 2-D TraXis coded tubes are permanently laser-etched into the tube surface making them especially resistant to solvent attack and wear. Uniquely manufactured from a single component, the code in Micronic laser encrypted 2-D codes cannot fade or peel off even when subjected to repeated handling and freeze-thaw cycles. Because code clarity will remain unchanged throughout the lifetime of a Micronic 2-D coded tube, they offer unmatched secure sample traceability. Manufactured to industry-leading strict tolerances, the precision and tube-to-tube consistency of Micronic sample storage tubes maximizes uptime when used with automated handling systems.

Micronic
For info: 724-941-6411 | www.micronicna.com

Electronically submit your new product description or product literature information! Go to **www.sciencemag.org/products/newproducts.dtl** for more information.

Newly offered instrumentation, apparatus, and laboratory materials of interest to researchers in all disciplines in academic, industrial, and governmental organizations are featured in this space. Emphasis is given to purpose, chief characteristics, and availability of products and materials. Endorsement by *Science* or AAAS of any products or materials mentioned is not implied. Additional information may be obtained from the manufacturer or supplier.

Downloaded from www.sciencemag.org on February 16, 2012

How they contribute to society through science and technology?

"Healthcare and Medical Technology" Field

Development of a new therapeutic drug targeting cancer-specific molecules

"Provides dramatic effectiveness as a treatment for chronic myelogenous leukemia and offers increased hope for the future development of cancer treatment drugs."

Dr. Janet D. Rowley, USA

Dr. Brian J. Druker, USA

Dr. Nicholas B. Lydon, USA

"Environment, Energy and Infrastructure" Field

Development of the world's highest performance Nd-Fe-B type permanent magnet

"Achieves a massive improvement in the efficiency of motors with wide-ranging applications, contributing to energy conservation on a global scale."

Dr. Masato Sagawa, Japan

This is an important element in the Japan Prize selection criteria.

The Japan Prize is awarded to scientists and engineers from around the world who are recognized as having achieved original and dramatic accomplishments that greatly enhance the progress of science and technology, thereby contributing to the peace and prosperity of mankind.

JAPAN PRIZE

▶ Search for "Japan Prize" to access announcement of the 2012 laureates.

JAPAN PRIZE Search

JAPAN PRIZE

sysmex

Prospective Protein Provider

ProCube

Evolution comes, suddenly.

Bringing unprecedented efficiency to pharmaceutical development:
Introducing ProCube, a service that assists the analysis of protein interactions.

You want to outsource search and quality control processes. But you need the work done quickly, and you want to keep a lid on costs. ProCube is designed to meet the demands of this type of development environment. We offer high-quality, ready-to-use analytical tools based on proprietary specimen testing technology and protein production technology that uses silkworms. This approach streamlines business processes from search to quality control. The evolution of the pharmaceutical development environment starts with Sysmex.

Features of ProCube

- **Validation data**
  We provide peace of mind and earn customers' trust by centralizing immobilization work and including interaction analysis results.
- **Multi-variety, high-volume samples**
  We can accommodate a broad range of applications using silkworm technology.

www.procube.sysmex.co.jp

Sysmex Corporation

LOCATION: Jackson Park Health Club
ARTICLE: *An Electronic Second Skin*
DATE: Sep 21, 7:43am

LOCATION: University Faculty Lounge
ARTICLE: *The Visual Impact of Gossip*
DATE: Sep 21, 4:22pm

LOCATION: Gyro King
ARTICLE: *Cavemen Craved Carbs, Too*
DATE: Sep 21, 1:13pm

LOCATION: Hemlock Bar
ARTICLE: *Quantum Simulation of Frustrated Classical Magnetism in Triangular Optical Lattices*
DATE: Sep 21, 9:21pm

LOCATION: Bed
ARTICLE: *Consciousness: What, How and Why*
DATE: Sep 21, 10:56pm

A new way to look at science

The new *Science* Reader app for iPad® from AAAS puts *Science* in your hands, wherever you go. Read abstracts, career advice, and highlights from our newest journals, *Science Signaling* and *Science Translational Medicine*. Plus, AAAS members can access full text articles from *Science*. Visit iTunes App Store℠ or content.aaas.org/ipad for details.

Available on the App Store

Science
AAAS

NEW ENGLAND BioLabs® Inc.
enabling technologies in the life sciences

Mix it up.

RE-Mix™ Restriction Enzyme Master Mixes

Restriction enzyme digests are now even easier! The same high quality restriction enzymes that you have come to trust from New England Biolabs are now available in master mix format; simply add your DNA and digest.

With RE-Mix Master Mixes take advantage of:

- Simplified and shortened protocols
- Fast digestion in 15 minutes (Time-Saver qualified)
- High product quality with reproducible results

RE-Mix Master Mixes – just add your DNA and mix

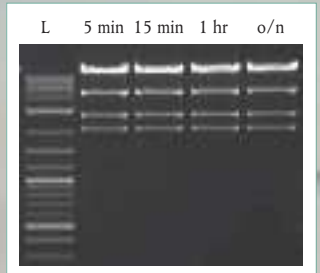

pXba DNA was digested with EcoRV-HF™ RE-Mix™ according to the recommended protocol. Lane L is the TriDye™ 2-Log DNA Ladder (NEB #N3270). The same results are obtained whether incubated for 5–15 minutes, 1 hour or overnight.

For more information, visit
www.NEBREMIX.com

Blue-footed Booby (Sula nebouxii)
© Tui De Roy

INDIA'S NO.1 RANKED NON-PROFIT PVT. UNIVERSITY

AMITY UNIVERSITY

Part of India's Leading Education Group

95,000 STUDENTS, 3,500 FACULTY, 5 UNIVERSITIES, 7 INTERNATIONAL CAMPUSES, 60,000 ALUMNI AND 2 DECADES OF EXCELLENCE IN EDUCATION.

250	250	300	300	240
patents filed by faculty in the last years	Govt. funded research projects	case-studies developed by faculty in the last one year	state-of-the-art labs	programmes across 50 disciplines

Established by the Chauhan Family more than twenty years ago, the Amity Education Group is a leading education group today, offering globally benchmarked education right from pre-schools to Ph.D. level. Starting with campuses in India, Amity today has campuses around the world and aims to add more in 25 countries over the next few years.

Amity, one of the few universities in India to offer 240 UG & PG degrees, has brought together some of the most eminent scientists, research scholars and corporate leaders from across the world, who are doing research in diverse, cutting-edge areas of science, technology and industry. Such focus on path-breaking innovations, a globally benchmarked infrastructure and outstanding faculty have resulted in Amity institutes being ranked amongst the top by India's most respected surveys.

SOME OF AMITY'S ACHIEVEMENTS

3,500 faculty & scientists – At Amity, a vibrant community of 3,500 distinguished faculty of scientists, professors, researchers and corporate professionals has been drawn from different walks of the industry who have been credited with publishing over 3,400 research papers and authoring over 500 books.

Highest number of patents filed – The Amity faculty have been credited with filing the highest number of patents by any university in India in the last one year.

India's Largest Fellowship Programme – Furthering its goal of excellence in research, Amity also offers India's Largest Ph.D. and Post-Doctoral Programme.

International Linkages – To keep abreast of the latest developments, Amity has tie-ups with over 100 global Universities, Laboratories and Research Centres spanning USA, Europe and Australia in areas of research, faculty & student exchange and curriculum development.

Recognition for research – Amity has been recognized as a Scientific & Industrial Research Organisation (SIRO) by the Govt. of India, a unique achievement by any Indian University and is a reflection of its unique initiatives in hi-end research.

State-of-the-art academic environment - Setting benchmarks only against the best universities globally, a hi-tech experience is drawn at Amity from a mix of 5 million sq.ft. of buildings, 300 state-of-the-art labs across 35 science disciplines, libraries with 4,00,000 books, periodicals & 17,000 online journals.

7 international campuses - Amity has emerged as India's only education group with international campuses in London, New York, Singapore, California, Mauritius, Dubai & Romania. Through centrally located campuses, the highest rating & accreditations and globally recognised degrees, these campuses carry forward Amity's rich legacy of excellence in education.

AMITY UNIVERSITY CAMPUSES IN INDIA

DELHI NCR

GURGAON

LUCKNOW

JAIPUR

GWALIOR

Amity conducts research & offers UG & PG degree programmes in over 35 disciplines of Science & Technology including: Aerospace I Agriculture I Applied Sciences I Biotechnology I Engineering - Automobile/Civil/Computer Science/Control Systems/Electronics & Comm./Electrical & Electronics/Information Technology/Instrumentation/Mechatronics/Mechanical & Automation/Optoelectronics & Optical Comm./Power Systems/ Telecom/VLSI/Wireless Comm. | Environment I Food Tech. I Forensic Sciences I Green Technology I Herbal Research & Studies I Horticulture I Marine Sc. I Medical & Allied Sc. I Microbial Sc. I Nanotechnology I Nuclear Science & Technology I Pharmacy I Physiotherapy I Post Harvest Tech. & Cold Chain Management I Space Sciences I Telecom I Virology & Immunology *(For complete programme list, visit www.amity.edu)*

Universities or Faculty/Scientists interested in collaboration with Amity may contact at partnerships@amity.edu | Faculty interested in teaching at Amity may contact at globalfaculty@amity.edu

Learn how current events are impacting your work.

***Science*Insider, the new policy blog from the journal *Science*,** is your source for breaking news and instant analysis from the nexus of politics and science.

Produced by an international team of science journalists, *Science*Insider offers hard-hitting coverage on a range of issues including climate change, bioterrorism, research funding, and more.

Before research happens at the bench, science policy is formulated in the halls of government. Make sure you understand how current events are impacting your work. Read *Science*Insider today.

www.ScienceInsider.org

*Science*Insider

Breaking news and analysis from the world of science policy

Science

AAAS

New Products

THERMAL CYCLER

The new G-Storm thermal cycler, GS482, embraces a sleek, black styling and features an enlarged screen to improve the user interface and experience. The new, cost-effective system is equipped with a number of enhanced features that increase the instrument's flexibility and functionality. The two independent 48-well blocks, both with sprung heated lids that adapt to both tubes and high profile 48-well plates within the GS482, enables two programs to be run independently or one program simultaneously on both blocks. Both of the GS482's thermal blocks feature two independent temperature control sensors and four peltier heating units to ensure accurate temperature control and uniformity across the block surface. Active Sample Cooling also ensures that samples are cooled until the heated lid reaches its target temperature. Onboard software features a Program Wizard that can store up to 1,000 programs.

Labtech International
For info: +44-(0)-1273-814888 | www.labtech.com

DISPOSABLE SYRINGE FILTERS

A new range of disposable syringe filters provide fast and efficient filtration of cell culture media. Manufactured in a Class 100000/ISO Class V clean room to ISO 9001:2008 and EN ISO 13485:2003 manufacturing standards ensures all Porvair syringe filters are free from DNA/RNA, DNAse/RNAse, and Pyrogen contamination. Stringent quality testing means each syringe filter performs reliably to specification. With three membranes to choose from an optimized syringe filter is available for most applications. Polyethersulfone membrane syringe filters exhibit a low affinity for proteins and extractables making them ideal for pre-filtration and filtration of buffers and culture media. The mixed Cellulose Ester membrane efficiently binds trace proteins making them the syringe filters of choice for filtration of aqueous solutions. Porvair's hydrophobic Nylon membrane offers excellent chemical compatibility across a wide pH range enabling it to be used for the filtration of either aqueous or organic solvents.

Porvair Sciences
For info: +44-(0)-1372-824290 | www.porvair-sciences.com

WESTERN BLOT STRIPPING SOLUTION

Based on G-Biosciences' popular Western ReProbe, this modified single component system is specifically formulated to dissociate and remove stubborn, high-affinity antibodies from membrane-bound proteins without destroying the antigenic-binding affinity. Western ReProbe PLUS saves time and money by eliminating the need to rerun gels and transfer processes and by offering you the ability to reuse Western blots. G-Biosciences' Western ReProbe PLUS eliminates the need for boiling, denaturants, or SDS. The membrane-bound protein is retained on the membrane and the matching antibodies are washed away. Once the antigen-antibody bonds are broken, the membrane-bound protein is free to accept new antibodies. G-Biosciences' Western ReProbe PLUS allows screening of the same blot with different antibodies, repeated analysis and correction of unsatisfactory blots with multiple probes, and comparison of phosphorylated and total protein on the same blot. Each 100 mL supply is sufficient for up to 30 standard size Western blots.

G-Biosciences
For info: 314-991-6034 | www.gbiosciences.com

SAMPLE DRYING

Available for use with Genevac evaporators, Dri-Pure technology enables scientists to rapidly dry their samples without cross-contamination or loss of sample due to solvent bumping. Dri-Pure offers significant benefits to scientists, especially those working in synthesis and purification. Other methods of solvent removal tend to be very laborious or lead to unacceptable cross-contamination. Dri-Pure running on a Genevac evaporator gives smooth, controlled solvent removal in optimum time. The patented Dri-Pure technology is available for all current models of Genevac centrifugal evaporators, from the affordable EZ-2 through to the production-scale HT-24. Genevac's unique anti-bumping system works by carefully controlling the reducing pressure in the evaporation chamber in combination with an increase in rotor speed to achieve greater g-force. In addition, heat flow to the samples must be reduced during the pressure ramping stage. Dri-Pure achieves all this via the embedded instrument software and hardware that makes such an elegant solution easy to apply.

Genevac
For info: +44-(0)-1473-240000 | www.genevac.com

2-D CODED TUBES

Identifying your sample via a code on the tube can be done in a number of ways. However the most reliable in terms of long-term identification and tracking of samples is via a 2-D coding on the bottom of the tubes. Barcodes on Micronic 2-D Data Matrix and 2-D TraXis coded tubes are permanently laser-etched into the tube surface making them especially resistant to solvent attack and wear. Uniquely manufactured from a single component, the code in Micronic laser encrypted 2-D codes cannot fade or peel off even when subjected to repeated handling and freeze-thaw cycles. Because code clarity will remain unchanged throughout the lifetime of a Micronic 2-D coded tube, they offer unmatched secure sample traceability. Manufactured to industry-leading strict tolerances, the precision and tube-to-tube consistency of Micronic sample storage tubes maximizes uptime when used with automated handling systems.

Micronic
For info: 724-941-6411 | www.micronicna.com

Electronically submit your new product description or product literature information! Go to **www.sciencemag.org/products/newproducts.dtl** for more information.

Newly offered instrumentation, apparatus, and laboratory materials of interest to researchers in all disciplines in academic, industrial, and governmental organizations are featured in this space. Emphasis is given to purpose, chief characteristics, and availability of products and materials. Endorsement by *Science* or AAAS of any products or materials mentioned is not implied. Additional information may be obtained from the manufacturer or supplier.

2013 AAAS ANNUAL MEETING
14–18 February ▸ Boston
www.aaas.org/meetings

Call for Symposium Proposals

Symposium proposals for the 2013 AAAS Annual Meeting are now being solicited. To submit a proposal, visit www.aaas.org/meetings. ***The deadline for submission is Thursday, 26 April 2012***.

The Beauty and Benefits of Science

The theme for the meeting points to the "unreasonable effectiveness" of the scientific enterprise in creating economic growth, solving societal problems, and satisfying the essential human drive to understand the world in which we live.

The phrase, "unreasonable effectiveness," was coined in 1960 by physicist Eugene Wigner, who explored the duality of mathematics — both beautiful unto itself, and also eminently practical, often in unexpected ways.

The scientific program will highlight the rich and complicated connections between basic and applied research, and how they bring about both practical benefits and the beauty of pure understanding.

Student Poster Competition

The competition recognizes the individual efforts of students actively working toward an undergraduate, graduate, or doctoral degree. ***Online entries will be accepted beginning 14 May 2012***.

For information about exhibits and sponsorships, contact meetings@aaas.org.

AAAS
ADVANCING SCIENCE, SERVING SOCIETY

SIGMA-ALDRICH®

SIGMA® Life Science Where bio begins™

Bioidentify.

Pinpoint the functional gene targets for your miRNA with the MISSION® Target ID Library.

The MISSION Target ID Library enables transcriptome-wide identification of gene targets regulated by microRNA and other non-coding RNA. Simplify target identification with these easy steps: transfect library, select, transfect miRNA and select target clones.

sigma.com/targetid

biosilencing

©2012 Sigma-Aldrich Co. LLC. All rights reserved. SIGMA and SIGMA-ALDRICH are trademarks of Sigma-Aldrich Co. LLC, registered in the US and other countries. MISSION is a registered trademark of Sigma-Aldrich Co. LLC. Where bio begins is a trademark of Sigma-Aldrich Co. LLC.

Science Careers Advertising

For full advertising details, go to ScienceCareers.org and click For Employers, or call one of our representatives.

Tracy Holmes
Worldwide Associate Director
Science Careers
Phone: +44 (0) 1223 326525

UNITED STATES & CANADA
E-mail: advertise@sciencecareers.org
Fax: 202-289-6742

Tina Burks
Midwest/West Coast/
South Central/Canada
Phone: 202-326-6577

Elizabeth Early
East Coast & Corporate
Phone: 202-326-6578

Marci Gallun
Sales Administrator
Phone: 202-326-6582

Online Job Posting Questions
Phone: 202-312-6375

EUROPE & REST OF WORLD
E-mail: ads@science-int.co.uk
Fax: +44 (0) 1223 326532

Simone Jux
Phone: +44 (0)1223 326529

Lucy Nelson
Phone: +44 (0)1223 326527

Kelly Grace
Phone: +44 (0) 1223 326528

JAPAN
Makiko Hara
Phone: +81 (0) 90-9853-9982
E-mail: mhara@aaas.org
Fax: +81 (0) 3-6369-4491

CHINA & TAIWAN
Ruolei Wu
Phone: +86-1367-1015-294
E-mail: rwu@aaas.org

All ads submitted for publication must comply with applicable U.S. and non-U.S. laws. *Science* reserves the right to refuse any advertisement at its sole discretion for any reason, including without limitation for offensive language or inappropriate content, and all advertising is subject to publisher approval. *Science* encourages our readers to alert us to any ads that they feel may be discriminatory or offensive.

Science Careers
From the journal *Science* AAAS

THE CHINESE UNIVERSITY OF HONG KONG

Dean of the Faculty of Science

Founded in 1963, The Chinese University of Hong Kong is a forward-looking and vibrant university, aspiring to be acknowledged regionally and internationally as a first-class comprehensive research university. With a team of over 2,000 full-time teaching and research staff, the University offers a broad spectrum of programmes up to PhD level in various disciplines organized under eight Faculties (viz. Arts, Business Administration, Education, Engineering, Law, Medicine, Science and Social Science). In 2011-12, undergraduate and postgraduate enrolment in publicly-funded programmes reaches 11,300 and 3,100 respectively (*http://www.cuhk.edu.hk*).

The Faculty of Science comprises four Departments: Chemistry, Mathematics, Physics, and Statistics, and two Schools: Chinese Medicine and Life Sciences, and also offers a number of multidisciplinary and interfaculty programmes. The Faculty has 300 full-time teaching and research staff, 1,740 undergraduate students and more than 490 postgraduate research students. Detailed information on the Faculty is available at *http://www.cuhk.edu.hk/sci/*.

The University now invites applications and nominations of qualified candidates for the Deanship of the Faculty. The Dean will be a member of the University senior management team reporting to the University Council via the Vice-Chancellor/President or the Provost. As the academic and executive head of the Faculty, the Dean will provide academic leadership and discharge administrative responsibilities in respect of academic, staff, financial and student matters.

Candidates should be academics with established scholarship appropriate for appointment at Professor level in an academic department, with an appreciation of the breadth of research and educational developments in the fields relevant to the Faculty. They should have demonstrated capability for academic leadership and management at an appropriate level in higher education institutions, long-term vision for the development of the Faculty, and excellent interpersonal and communication skills.

Salary and fringe benefits for the post will be highly competitive, commensurate with qualifications and experience.

Please send applications/nominations under confidential cover, with the post marked, to the Search Committee for the Dean of the Faculty of Science, c/o Provost's Office, The Chinese University of Hong Kong, Shatin, N.T., Hong Kong [fax: (852) 3943 1462; e-mail: *SCDeanship-Sc@uab.cuhk.edu.hk*]. All applications/nominations will be treated in strict confidence. The Personal Information Collection Statement will be provided upon request.

Consideration of applications/nominations will continue until the post is filled. The University reserves the right to fill the post by invitation.

Faculty Position

Department of
Biomedical Engineering
The Johns Hopkins University
www.bme.jhu.edu

The Johns Hopkins Department of Biomedical Engineering invites applications for a tenured or tenure-track faculty position. Hopkins BME has a long history of excellence in scientific discovery and teaching at the undergraduate and graduate levels. The priority research areas targeted by this search are: systems biology, cardiovascular systems, tissue engineering, neuroscience, neuroengineering, instrumentation, and imaging. Biomedical Engineering enjoys the position of a department in both the Johns Hopkins School of Medicine and the Whiting School of Engineering and our faculty have laboratories within both schools. There are ample opportunities for inter- and cross-departmental collaboration through a variety of research institutes, centers and informal research teams.

The new faculty position will have a primary appointment in the Whiting School of Engineering. Successful applicants will be expected to establish independently funded research programs and participate in undergraduate and post-graduate education and research training. Please submit via email a *curriculum vitae*, a statement of research goals, and the names, e-mail addresses and phone numbers of three references to: **Dr. Elliot McVeigh, Chairman, Department of Biomedical Engineering, bmefacultysearch@jhu.edu**.

The Johns Hopkins University is an Equal Opportunity/Affirmative Action Employer. Women and minorities are strongly encouraged to apply.

Gastrointestinal Immunologist

The Department of Medicine at Georgetown University seeks an outstanding MD, PhD or MD/PhD at the Assistant or Associate Professor rank. The ideal candidate will be a clinician and/or laboratory scientist with a strong interest in translational research in gastroenterology especially with a focus on immunological disorders such as inflammatory bowel disease. The candidate will have a successful program of research demonstrated by their publication record and participation as PI or co-I on peer-reviewed extramurally funded research. The candidate will establish and lead a translational immunology program that integrates with clinical and basic science investigators within the university community and benefits from the Georgetown - Howard Universities Center for Clinical and Translational Science. Nearby federal institutions including the NIH, FDA and VA serve to enrich the academic environment while our location in the heart of the Nation's capitol offers an unparalleled social, recreational and cultural lifestyle. Please send your cover letter and curriculum vitae by **May 31, 2012** to: **Ms. Tolise Miles (Tel: 202.687.7380; E-mail: tcm9@georgetown.edu)**.

Georgetown University is an Affirmative Action/Equal Opportunity Employer.

Department of Health and Human Services
National Institutes of Health / National Eye Institute
Associate Director, GS-601-15
(Organizational Title: Associate Director of the Office of Science Communications, Public Liaison, and Education)

POSITION: The National Eye Institute (NEI), a major component of the National Institutes of Health (NIH) and the Department of Health and Human Services (DHHS), is seeking exceptional candidates for the position of Associate Director of the Office of Science Communications, Public Liaison, and Education. The NEI is responsible for a national and international program to conduct and support research, training, health information dissemination, and other programs with respect to blinding eye diseases, visual disorders, mechanisms of visual function, preservation of sight, and the special health problems and requirements of individuals who are visually impaired.

The incumbent reports directly to the Director, NEI and is the chief technical and policy advisor on health information dissemination. The Associate Director will conduct planning, management, and evaluation of a dynamic, nationally visible science communications, public liaison, and education program in eye health and vision disorders and will (1) interpret, develop and produce scientific and lay publications, reports, articles, exhibits and other materials on institute research, activities, and programs; (2) utilize the latest health and consumer communications strategies to translate research results to the health care and academic communities and the general public; (3) respond to inquiries from the public, patients and families, health professionals, and government and non-government organizations; (4) plan, implement, and evaluate nationwide vision research and eye health media programs and media-related materials; (5) develop and oversee the NEI public and internal communication websites; (6) establish and maintain collaborative partnerships with professional organizations and patient and community groups; and (7) oversee the Congressionally-mandated National Eye Health Education Program.

Applicants should be known and respected within their profession, both nationally and internationally.

QUALIFICATIONS REQUIRED: Applicants must possess a degree in an academic field related to the health sciences, allied sciences, or health science communications appropriate to the work of the position. Experience in academic, professional society, and/or industry settings is important for the level of liaison and collaboration required with constituents from sectors such as ophthalmic and optometric health service organizations, government agencies, members of the press and public, national and international public interest organizations, and community patient and advisory groups.

SALARY AND BENEFITS: GS-15 salary range is $123,758 - $155,500. Full Federal benefits are available including leave, health and life insurance, long-term care insurance, retirement, and retirement savings plan (401K equivalent).

HOW TO APPLY: Interested candidates may apply at **www.usajobs.com** to vacancy announcement **NIH-NEI-DE-12-571550**, beginning February 22, 2012. Applications must be received by midnight **March 7, 2012**. For questions, contact **Aurelia Spencer, Human Resources Specialist, Office of Human Resources** at **spenceau@mail.nih.gov**.

The NIH encourages the application and nomination of qualified women, minorities, and individuals with disabilities.
DHHS, NIH and NEI ARE EQUAL OPPORTUNITY EMPLOYERS.

Health and Human Services
National Institutes of Health
EUNICE KENNEDY SHRIVER NATIONAL INSTITUTE OF CHILD HEALTH AND HUMAN DEVELOPMENT
Program in Genomics of Differentiation
Postdoctoral Positions Available

Fully funded postdoctoral positions are available in the Program in Genomics of Differentiation (PGD), Eunice Kennedy Shriver National Institute of Child Health and Human Development (NICHD), National Institutes of Health, Health and Human Services (NIH), Bethesda, MD. The PGD is a diverse and highly interactive program in basic cellular, molecular, and developmental biology research at the NIH just outside of Washington, DC. The 19 laboratories making up the PGD encompass a wide variety of research areas, with strong emphasis on developmental patterning and differentiation, chromatin dynamics and epigenetics, the immune system, the viral life cycle, DNA replication, gene regulation, and RNA metabolism. Program investigators perform research using a wide variety of models including viruses, bacteria, mammalian cell culture, yeast, fruit flies, zebrafish, frogs, and mice. Environment, resources, and stipend support are excellent. For additional information on the PGD and its researchers, including contact information for individual researchers, see **http://science.nichd.nih.gov /confluence/display/pgd/Home**. Interested applicants with a M.D, or Ph.D., and less than 5 years' postdoctoral experience should email a CV, bibliography, cover letter with a brief description of research experience and interests, and the names of 3 references (with phone numbers) to individual investigators listed below.

Sohyun Ahn – Neurogenesis in the developing and mature nervous system of the mouse
Harold Burgess – Analysis of neural circuits controlling behavior in zebrafish
Mike Cashel – Molecular regulation of the prokaryotic stress response
Ajay Chitnis - Early neural and lateral line development, Notch signalling
David Clark – The role of chromatin structure in gene activation in yeast
Robert Crouch – RNase H function in health and disease
Igor Dawid – Early embryonic development and patterning in the frog and zebrafish
Melvin DePamphilis – Regulation of DNA replication in normal and in cancer cells in the mammal
Bruce Howard – Experimental and bioinformatic analysis of epigenome structure
Judith Kassis – Gene silencing by Polycomb group genes (PcG) in Drosophila
James Kennison – Drosophila developmental genetics
Judith Levin – HIV-1 replication; reverse transcription, host restriction, and viral assembly
Paul Love – Genes regulating mammalian hematopoiesis
Richard Maraia – RNA metabolism, the La protein and RNA Polymerase III
Keiko Ozato – Gene regulation in innate immunity
Karl Pfeifer – Epigenetic regulation of gene expression and cardiac development in mice
Thomas Sargent – Epidermal and neural crest development in frog and fish
Brant Weinstein – Vascular development in the zebrafish

The HHS and NIH are Equal Opportunity Employers.

2012 Call for Applications for the Directorship of New IBS Research Centers

The Institute for Basic Science (IBS) was established by the Korean government in November 2011 with the goal to create a world-class research institute in the basic sciences. IBS invites applications for the position of Director for a number of research centers. These centers will foster the growth of world-class basic science research in order to advance the creation of knowledge and the basis of future technologies.

Feb. 2012
President of the IBS, Se-Jung Oh

1. Research Areas: Top-tier, world-class basic science research will focus on large-scale and long-term group programs, presently not available at universities or government- supported institutes.

2. Requirements:
- A candidate for the position of a director should have world-renowned research achievements, or should have the potential for such achievements.
- A candidate should be able to devote to research activities over a long period of time.
- A candidate should be capable of directing and managing a research group.

3. Our Offers:
- Directors will be given autonomy in hiring and organizing scientific staff and carrying out research.
- Directors will be offered a tenure-track position at IBS, or a full-time professorship or a permanent position at a partner institute.
- The annual salary of directors will be decided upon negotiations with the President of IBS and will become effective upon signing the contract.

4. The Budget and Evaluation of Research:
- The research budget will vary according to the research plan.
- An evaluation of research achievements will take place every three years and will affect the support for center (the first evaluation will take place after five years).

5. Regulations for Research Implementation:
- Directors are required to work full time in their institutes and members of research centers are generally expected to conduct research at the location of the institute.
- On publications by researchers who participate in IBS research center programs, the IBS should be cited as the primary affiliation.

For more information, refer to FAQ (frequently asked questions) with regard to the selection and management of IBS research centers.

6. Procedures of Selection

Steps	Procedures	By
Candidate Recruitment	• Open Invitation • Candidate recommendation from the Scientific Advisory Board (SAB)	President
Evaluation	• Pre-Screening of candidates for in-depth evaluation • Formation of review panets for each selected candidate • Peer review (open sysmposium and discussion, reference letter) • SEC's recommendation	Selection and Evaluation Committee (SEC)
Consultation and Appointment	•Consultation with the SAB •Final choice of directors and negotiations •Appointment of directors	President

7. Schedule:
- Application: Candidates may file an application at any time by using on the IBS web-site.
- 2012 Schedule (Schedule is subject to change)
  March 2012~: 1st round of evaluation on candidates
  May, 2012: Appointment of the first IBS Directors
  June 2012~: 2nd round of evaluation on candidates
  September 2012~: 3rd round of evaluation on candidates

8. Submission of Applications: Please send your application in English with necessary documents as a single PDF to: **http://www.ibs.re.kr/en/apply** (for more information, please visit **http://www.ibs.re.kr/en**). If you have questions, please contact by phone at **+82-42-878-8141** or by e-mail at **hjchoi@ibs.re.kr**.

AMITY UNIVERSITY

India's No. 1 Ranked non-profit Pvt. University

FACULTY POSITIONS

Amity University is part of India's leading global education group with 95,000 brilliant students, over 240 Graduate & Post Graduate degrees and 3,500 faculty comprising distinguished researchers, scientists and industry professionals.

Amity University and its institutions in Biotechnology, Engineering & Telecom have been ranked amongst the top-10 in India by leading surveys on myriad parameters like infrastructure, academic excellence & research.

Focus on Research:
The faculty and scientists at Amity have filed the highest number of patents in the last year, more than any other University in India and are carrying out over 250 Govt. funded research projects. Further, Amity is recognised as a Scientific & Industrial Research Organisation (SIRO) by Govt. of India and has research collaboration with over 80 leading global universities, besides the largest number of Fellowships for Ph.D. and Post Doctoral Research in India.

For its University campus in India and Dubai, Amity invites applications from candidates who enjoy working in a dynamic, growth-oriented environment and with a strong teaching/ research portfolio.

Positions exist in the following disciplines:

Aerospace I Agriculture I Applied Sciences I Biotechnology I Engineering I Environment I Food Tech. I Forensic Sciences I Green Technology I Herbal Research & Studies I Horticulture I Marine Sc. I Medical & Allied Sc. I Microbial Sc. I Nanotechnology I Nuclear Science & Tech. I Pharmacy I Physiotherapy I Post Harvest Tech. & Cold Chain Management I Space Sciences I Telecom I Virology & Immunology. (For complete programme list, visit www.amity.edu)

Faculty interested in teaching at Amity campuses, may e-mail their curriculum vitae to globalfaculty@amity.edu (mentioning the name of the campus they wish to apply to).

VILLANOVA UNIVERSITY

Villanova University's College of Liberal Arts and Sciences invites applications for two **Mendel Science Experience Post-doctoral Fellows** (see **http://www1.villanova.edu/villanova/artsci/faculty_staff/chairs_professorships_fellowships.html**)

The Fellows program is designed to enhance the College's teaching of science to non-science majors through the Mendel Science Experience program and to foster the professional development of recent Ph.D. recipients on a career path leading to faculty positions. Positions are 50:50 teaching and research. Fellows will team-teach a non-science-majors course with their faculty mentor as well as upper level undergraduate or graduate-level (M.S.) courses, will conduct research in collaboration with the faculty mentor, and will have opportunities to supervise undergraduate research. The positions begin in August 2012.

Applicants should contact mentors (**Dr. Anthony Lagalante, Chemistry, http://www3.villanova.edu/anthony.lagalante/; Dr. Michael Russell, Biology http://www.homepage.villanova.edu/michael.russell/; or Dr. Nathaniel Weston, Geography and the Environment, http://www.homepage.villanova.edu/nathaniel.weston/**) prior to submitting applications, as the applications must include information on the nature of the relationship between the mentor and post-doc.

Applications must include a curriculum vitae, official transcripts of all undergraduate and graduate work, and a cover letter that includes: a statement of career goals, a personal professional development plan, a plan for research that indicates collaboration with the potential faculty mentor, a proposal for teaching that includes a Mendel Science Experience course for non-science-majors and an upper level science course (possibly team-taught with the faculty mentor) and names and contact information for three references. Applicants must apply online at **https://jobs.villanova.edu**. We seek to fill two positions. Review of applications will begin on **2 March 2012**; the search will remain open until the positions are filled.

Villanova is a Catholic university sponsored by the Augustinian order. An AA/EEO Employer, Villanova seeks a diverse faculty committed to scholarship, service, and especially teaching, who understand, respect, and can contribute to the University's mission and values.

WPI Advanced Institute for Materials Research (AIMR)
of Tohoku University
Recruitment of Researchers
(Assistant Professor/Postdoctoral Researcher)

Tohoku University WPI Advanced Institute for Materials Research (AIMR) was established on October 1st, 2007 as one of the top five research centers in Japan under the World Premier International Research Center Initiative (WPI Program) run by the Ministry of Education, Culture, Sports, Science and Technology.

The institute aims to establish a new paradigm of Material Research fused with Physics, Chemistry, Biology, Engineering and Mathematics. AIMR's ultimate objective in science is to discover new principles via collaborative researches between materials science and mathematics and create predictable materials science based on the discovered principles, and finally develop new functional materials through the new materials science. As a path to achieving this objective, AIMR sets up the **three target projects** below and opens positions for those who engaged in the projects becoming a bridge between materials scientists and mathematicians. AIMR's official language is English and AIMR has supporting staff for those from abroad.

Three target projects:
(1) Non-equilibrium Materials based on Mathematical Dynamical Systems
(2) Topological Functional Materials
(3) Multi-Scale Hierarchical Materials based on Discrete Geometric Analysis
(See our website for details: **http://www.wpi-aimr.tohoku.ac.jp/en/modules/staff/**)

Number of positions: Three Assistant Professors and five Postdoctoral Researchers
Starting date: April 1st, 2012 or earliest possible date
Application deadline: February 29th (Wednesday), 2012

Research Fields:
Assistant Professor: Theoretical Physics, Theoretical Chemistry, Mathematical Physics, Mathematics, and Materials Science/Engineering.
Postdoctoral Researcher: Physics, Chemistry, Mathematical Physics, Mathematics, Materials Science, and Engineering.

To stay in an experimental laboratory and become an interface bridging between the experimental scientists and mathematicians, we have four research groups: **Bulk Metallic Glasses, Materials Physics, Soft Materials, and System/Device**, together with the Mathematics Unit (See our website for more details) **http://www.wpi-aimr.tohoku.ac.jp/en/index.php**.

Employment conditions:
(1) **Salary:** an annual income system is employed according to the rules of Tohoku University.
(2) **Research fund:** Cooperative research together with the PI who manages the research fund is recommended, but independent research proposals for assistant professors are also encouraged.
(3) **Term:** Assistant Professor: in principle five year term but there is review process every two years. Postdoctoral researcher: annually renewed, up to three years.

Documents for application:
(1) CV (Including current address, telephone number and e-mail)
(2) Publication list
(3) Outline of research accomplishments, and research proposal at AIMR
(4) Two reference letters
(5) 2 copies of major papers, up to three titles

The files of the above documents (pdf) should be sent to the following e-mail address: **koubo2012 _at_ wpi-aimr.tohoku.ac.jp**, or the printed-out documents should be sent via regular mail to the following address: **General Affairs Section, WPI Advanced Institute for Materials Research, Tohoku University, Katahira 2-1-1, Aoba-ku, Sendai, 980-8577, Japan**

When you submit your application, please state clearly which position you are applying to, Assistant Professor or Postdoctoral Researcher. You are allowed to apply to both.

Applications from, or nomination of, women and minority candidates are encouraged. Tohoku University WPI-AIMR is an Affirmative Action/Equal Opportunity Employer.

One of America's Top Hospitals.
Make Cleveland Clinic Your Choice.

CHAIR DEPARTMENT OF CANCER BIOLOGY

LERNER RESEARCH INSTITUTE THE CLEVELAND CLINIC

We are seeking a Chair for the Department of Cancer Biology in the Lerner Research Institute. An endowed chair accompanies this position. The department currently consists of 8 faculty members with funded research programs in brain, prostate, and colorectal cancer in the areas of cell cycle control and signaling and mitotic spindle control. The ideal applicant for this position will have an outstanding national reputation in an area that complements the strengths of the department. Due to the pivotal role of Cancer Biology research to translational research and patient care, the successful chair will lead Cancer Biology to integrate with the translational, clinical trials and clinical care programs in the Taussig Cancer Institute as well as the Case Comprehensive Cancer Center. An affiliate position with the Case Comprehensive Cancer Center may accompany this post. The Lerner Research Institute with over 160 independent investigators in 11 departments and an annual budget of greater than $250 million has a commitment to excellence in basic and translational research. The Chair will be provided with a highly competitive salary, generous start-up support, and recruitment packages for additional faculty. Curriculum vitae and the names and addresses of three references should be sent to:

Kandice Kottke-Marchant, MD, PhD.
Search Committee for the Chair of Cancer Biology
Chair, Pathology and Laboratory Medicine Institute
9500 Euclid Avenue, L21
Cleveland, OH 44195
Visit us on the Web at http://www.lerner.ccf.org/cancerbio/
E-mail: marchak@ccf.org

Cleveland Clinic is an equal opportunity employer and is committed to increasing the diversity of its faculty. It welcomes nominations of and applications from women and members of minority groups, as well as others who would bring additional dimensions to its research, teaching, and clinical missions. Cleveland Clinic is a smoke/drug free work environment.

Cleveland Clinic

UNITED NATIONS UNIVERSITY

The United Nations University (UNU) is the academic arm of the United Nations system. Its mission is to contribute through collaborative research and postgraduate education, dissemination of knowledge and advisory services, to efforts to resolve the pressing global problems of human survival, development and welfare that are the concern of the United Nations, its Peoples and Member States. The University functions as a think-tank for the United Nations system and for UN Member States providing knowledge-based policy advice.

DIRECTOR, D-1 Level
UNU- INTERNATIONAL INSTITUTE FOR GLOBAL HEALTH (UNU-IIGH)

(DUTY STATION: KUALA LUMPUR, MALAYSIA)

The UNU-IIGH Director serves as the Chief Academic and Administrative Officer of the Institute and has overall responsibility for the direction, organization, administration and programmes of the Institute, under the direction of the Rector of the UNU.
Qualifications: a Doctorate in the field of Health Systems and Policies, Public Health, Epidemiology or other health related discipline with high impact publications in nationally and internationally recognized journals or books edited by internationally recognized publisher. Associate or Full Professorship or equivalent appointment at an academic institution.
Experience: Broad knowledge in the field of Public Health with proven experience in promoting successful PhD theses. Has postgraduate teaching experience and didactical qualities.

CLOSING DATE: 31 MARCH 2012

The successful candidate will have at least 10 years of management experience, ideally in a leadership role within an academic institution or international organization. Candidates should possess excellent communication skills with fluency in English and at least one other official language of the United Nations.
Applications from suitably qualified women candidates are particularly encouraged.
Please visit **http://www.unu.edu/employment** for the full job description, requirements and application procedures. Application by email is highly encouraged.

WestVirginiaUniversity

School of Dentistry

The West Virginia University School of Dentistry seeks applications for four (4) tenured or tenure-track faculty positions at the Assistant/Associate Professor level in the following areas:
• Cariology • Biomaterials/Nanotechnology • Salivary Diagnostics • Oral Pathology/Inflammation

As part of the Robert C. Byrd Health Sciences Center, the West Virginia University School of Dentistry is investing significant resources to advance our basic and translational research capacity. The School of Dentistry's five-year strategic plan includes the development of new clinical, and basic and translational research capabilities to augment the teaching mission. These tenure or tenure-track positions will be at the Assistant or Associate Professor levels. Successful applicants will have up to 80% of their time protected for research. The candidate will have a DDS/DMD degree, and research experience (MS and/or PhD), reasonable potential for external grant funding, and demonstrated success in teaching and/or clinical practice. He/she must also show demonstrated abilities in working with people of diverse backgrounds, teaching, and leadership. The applicant will be eligible for a West Virginia dental license **http://www.wvdentalboard.org**.

The West Virginia University School of Dentistry is located in the historic community of Morgantown, West Virginia, approximately 80 miles south of Pittsburgh, PA and is easily accessible to major metropolitan areas in the East and Midwest. The School of Dentistry is one of 14 colleges in a major land-grant research University and is part of a comprehensive Health Sciences Center which includes the Schools of Medicine, Nursing, Pharmacy, and Dentistry, the Mary Babb Randolph Cancer Center, and West Virginia University Hospitals. WVU has initiated establishment of a new School of Public Health. Currently, the WVU School of Medicine's accredited public health programs have enrolled over 100 MPH students and more than 20 PhD students. Additionally, plans are underway to develop a DDS/MPH degree, as well as several other combined degrees, including a DDS/PhD. The Health Sciences Center campus is home to the Blanchette Rockefeller Neuroscience Institute and a state-of-the art Library/Learning Resource Center. For more information on the School of Dentistry and Health Sciences Center see **http://www.hsc.wvu.edu/sod/** or **http://www.hsc.wvu.edu**.

Review of applications will begin immediately and will continue until all positions are filled by qualified candidates. Salary and academic rank will be commensurate with qualifications and experience. Applicants should send a letter of interest, research statement, and curriculum vitae with the names, addresses, and phone numbers of three references to: **Richard J. Crout, DMD, PhD, Associate Dean for Research, Chair, Search Committee, West Virginia University School of Dentistry, PO Box 9448, Morgantown, WV 26506-9448** or email to **rcrout@hsc.wvu.edu**.

West Virginia University is an Affirmative Action/Equal Opportunity Employer. It is also the recipient of an NSF ADVANCE award for gender equality. WVU Health Sciences Center is a smoke free campus.

WOMEN IN SCIENCE

forging new pathways in green science

Read inspiring stories of women working in "Green Science" who are blending a unique combination of enthusiasm for science and concern for others to make the world a better place.

Download this free booklet ScienceCareers.org/LOrealWiS

Science AAAS

This booklet is brought to you by the AAAS/*Science* Business Office in partnership with the L'Oreal Foundation

INTERNATIONAL IBERIAN NANOTECHNOLOGY LABORATORY

INL-MIT Program

INL – International Iberian Nanotechnology Laboratory (INL), based in Braga (Portugal), is the first fully international research organization in Europe in the field of nanoscience and nanotechnology. As part of a collaboration with the Massachusetts Institute of Technology, the INL is currently seeking candidates for **two Group Leader positions**. The first position will focus on research in the area of **biological approaches to templated self-assembly and nanopatterning.** The second position will lead the effort on **graphene-based nanoelectronic sensor devices** at INL.

Candidates with outstanding CVs and demonstrated excellence in these scientific topics will be especially considered. Candidates with an excellent research track record are sought. Previous industrial laboratory experience will be valued. The work location is Braga (Portugal), but candidates must show availability for temporary relocation between Massachusetts (US) and Braga (Portugal). The start-up package and remuneration scheme is in line with those offered by other International Organizations and according to candidate experience and background. Applicants should forward the application material indicated to the INL directly, with a copy to *inl-mit@mtl.mit.edu.*

The detailed position announcement can be found at http://inl.int/job_offers

INL-MIT-2012-05
Nanotemplating of Biomolecular Structures
(Group Leader)

INL-MIT-2012-06
Graphene Based Nanoelectronic Sensor Devices
(Group Leader)

DEADLINE: April 9th, 2012

THE UNIVERSITY of York

DEPARTMENT OF BIOLOGY

Lectureship in Molecular Biophysics

Ref: 2205

As part of a major expansion in biological and biomedical research activity at York, we are seeking to appoint a lecturer in Molecular Biophysics.

Applications are invited from outstanding and dynamic scientists with a demonstrated track record of internationally competitive research. Applicants should be addressing important biological or biomedical questions using ensemble solution biophysical/structural methods and/or single-molecule detection methods. You should be ambitious, keen to work in a collaborative environment and have the capacity to teach across a broad spectrum of biophysical science. Areas of particular interest include protein-nucleic acid and protein-protein interactions, but other applications in molecular biophysics are also strongly encouraged.

You will be expected to develop an independent research programme of international standing and to engage in teaching in related areas.

For informal enquiries please contact Professor Jennifer Potts (jennifer.potts@york.ac.uk; 01904 328679) or the Head of Department, Professor Deborah Smith (biohod@york.ac.uk; 01904 328555).

Salary within the range: £35,938 - £44,166 per annum.

For further information and to apply on-line, please visit our website: https://jobs.york.ac.uk Alternatively contact HR Services on +44 (0)1904 324835.

Closing date: 16 March 2012.

The University of York is committed to promoting equality and diversity.

www.york.ac.uk

CERCA

Call for applications: Director, ICN2

The Catalan Institute of Nanoscience and Nanotechnology (ICN2), with a staff over 150 people, is a Research Institution supported by the public foundation Generalitat-CSIC-UAB. The ICN2 was recently created from the merger of two prior research institutes in nanotechnology: ICN (**www.icn.cat)** and CIN2 (**www.cin2.es**). The mission of ICN2 is to pursue frontier research in the nanoscience area, including nanomaterials synthesis, nanoelectronics, nanomedicine and applications for ICT and the environment, among other areas.
ICN2 is located on the UAB campus in Bellaterra (Barcelona), Spain.

Candidate profile and contact information:
ICN2 is seeking applicants with a distinguished record of scientific excellence and the innovative thinking necessary to lead a dynamic and diverse organisation.

Applicants must have a PhD or comparable degree. Salary will be commensurate with experience.

Applicants should send a CV and a cover letter by e-mail to the **Chair of the ICN2 Scientific Advisory Board (SAB), at: hr@icn.cat**. The appointment will be for a period of 5 years, which could be extended up to a maximum of 10 years.

Job description for the position of Director
The Director will have the following duties:
- Provide the scientific vision and strategic goals for ICN2
- Submit the Institute's Research Activities Programme and annual operational budget to the Board of Trustees.
- Represent the Institute at official scientific and social events in the absence of the Chair of the Board of Trustees, or when no other Trustee has been delegated by the President
- Maintain close contact with CERCA, CSIC and UAB (stakeholders) in relation to the Institute's progress
- Any other functions approved by the Board of Trustees.

The Director will be responsible for:
- Devising a strategic plan and monitoring its implementation
- Negotiating ICN2's Programme Contract with funding stakeholders
- Presenting the Director's Report at the Board of Trustees meetings
- Periodically calling and chairing meetings of the Executive Committee
- Proposing to the Board of Trustees the appointment of members of the Scientific Advisory Board (SAB), keeping them informed about major changes, and organizing their regular meetings
- Coordinating periodic scientific assessments of ICN2's research programmes and core facilities, and implementing the SAB's recommendations
- Supervising the financial aspects of budget implementation
- Negotiating contracts of new group leaders or programme coordinators, whenever appropriate
- Participating in strategic decision-making, such as for strategic alliances with other research institutions of with industry, in line with ICN2's mission

Pre-selection of candidates:
Suitable candidates will be pre-selected by the SAB with the support of the experts that the SAB might require. Candidates included in the short list will be invited to visit ICN2 and meet the SAB for a final interview. The results of these interviews will be presented to the Board of Trustees, who will then designate the new Director.

Calendar:

3 Feb	Call for applications opens
5 Mar	Application deadline
12-19 Mar	Short list of pre-selected candidates chosen
16-23 Apr	Candidates visit ICN2 and have final interview with the SAB
24-30 Apr	Appointment announced

Science Careers online @sciencecareers.org

Get a Career Plan that Works.

An exceptional career requires insightful planning and management. That's where *Science* Careers comes in. From job search to career enhancement, *Science* Careers has the tools and resources to help you achieve your goals. Get yourself on the right track today and get a real career plan that works. Visit **ScienceCareers.org**.

Science Careers
From the journal *Science* AAAS

ScienceCareers.org

DREXEL UNIVERSITY
COLLEGE OF MEDICINE

DEAN AND SENIOR VICE PRESIDENT, MEDICAL AFFAIRS

A vital component of Drexel University, one of America's most innovative and entrepreneurial research universities, the Drexel University College of Medicine is embarking on a comprehensive national search to find its next leader who will take the College to the next level of excellence in teaching, research, and clinical activities. The next Walter and Lenore Annenberg Dean—one of a few endowed Deanships within the Association of American Medical Colleges—and Senior Vice President, Medical Affairs will have an outstanding opportunity to lead and to steward the College of Medicine. The Dean and the Senior Vice President will report to John A. Fry, the President of Drexel University, and will serve as a member of President Fry's senior leadership team.

A leader in curriculum development and educational technology, the College of Medicine is recognized for its commitment to the broadest form of diversity, its emphasis on service and the care of medically underserved communities, and its engagement in significant interdisciplinary research, all enhanced by Drexel University and its exceptional reputation in engineering and technological innovation. Located in the vibrant city of Philadelphia, the College of Medicine has 1,066 medical students (the largest enrollment of any private medical school in the country), is the academic sponsor for approximately 645 residents and fellows, and has 826 full-time and 69 part-time, non-faculty staff. The College of Medicine has an endowment of $154.8 million and an operating budget of $227 million.

Possessing an engaging personal style that encourages collaboration and teamwork among faculty and professional staff, the most qualified candidates will have a distinguished and successful professional career that engenders credibility and respect. The individual must be a visionary leader who can recruit, retain, empower, and inspire a team of people and can set the right tone at the top, to fulfill the mission of the College of Medicine and to achieve its goals and aspirations. The next Dean must understand the business and economics of healthcare today, and business and financial acumen are required. The person must possess a proven track record of both strategic thinking and executing and achieving results. The next Dean should collaborate across boundaries and functions within a complex environment in an effective manner. Finally, the person must be equally committed to the education, clinical and research missions of Drexel's medical school.

Please direct all correspondence, including applications, nominations, and general inquiries to the attention of **Judith von Seldeneck, Joseph Frick, and Andrew Wheeler, Consultants to the Search Committee, via email at drexeldean@divsearch.com or via the phone for Carol Burke at 215 656-3571.** Interested individuals should provide an electronic version of their curriculum vitae, a cover letter addressed to the Drexel University College of Medicine Search Committee describing their interest in and qualifications for the position, and a list of references. References will not be contacted without prior knowledge and approval of the candidate. All candidate information will be held in **strict confidence.**

Scan QR code for more information.

Drexel is an Equal Opportunity, Affirmative Action Employer.
Nominations and applications from women and minorities are encouraged.

DiversifiedSearch

REGIONAL CENTRE FOR BIOTECHNOLOGY
an institution of education, training & research

Adv. No.1/12
YOUNG VISITING SCIENTISTS AWARD

The Regional Centre for Biotechnology (RCB) invites applications for Young Visiting Scientists Award from the eligible candidates residing in the regional member countries of UNESCO (other than India). The Young Visiting Scientists Award will be initially for one year extendable for another year on merit basis.

The Regional Centre for Biotechnology (RCB) has been established by the Department of Biotechnology, Govt. of India under an agreement with UNESCO as its Category II Centre. It is designed to be a Centre of excellence in biotechnology with intimate contributions from the countries of the region and academic institutions from the rest of world. It provides a meeting place where innovation, enterprise and industrial development will germinate.

The objective of the Young Visiting Scientists Award is to identify and nurture outstanding young scientists with innovative ideas and desirous of pursuing research in frontier areas of biotechnology related but not limited to structural, systems and synthetic biology, nano science & technology, cellular and molecular biology, disease biology and data-intensive discovery research under the mentorship of senior faculty at the Regional Centre for Biotechnology. Young Scientists below the age of 35 having PhD degree in any discipline of natural science are eligible to apply. The candidates selected for the Young Visiting Scientists Award will be given one to and fro international fare, leased residential accommodation and medical coverage in addition to the Award of Rs. 40,000/- per month. The Awardee shall not be entitled to draw any other remuneration, fellowship or salary. They will have to obtain inter-governmental clearances and international passport and visa on their own. However necessary documents will be provided to them for the purpose.

Interested candidates may submit their applications in the prescribed format which can be downloaded from the website **www.rcb.res.in** , to the **Registrar, Regional Centre for Biotechnology, 180, Udyog Vihar, Phase- I, Gurgaon-122016, Haryana (India)** so as to reach latest by **March 15, 2012**. A copy of the duly filled in application form should also be sent on the email ID **registrar@rcb.res.in**.

FACTS & FICTION

Careers in Industry and Academia

Trying to figure out the next step in your career? Join us for a roundtable discussion that will look at facts and fiction surrounding academic and industry career options for PhD-level scientists. Get some nuts and bolts advice on how to research career options, what questions to ask, and how to best prepare for various careers.

- Do industry and academic careers require different skill sets?
- Do industry jobs have better compensation? Less autonomy?
- Do academic scientists have less work/life balance?

For answers view our roundtable discussion for free at:

ScienceCareers.org/webinar

Science Careers

From the journal *Science* AAAS

Produced by the *Science*/AAAS Business Office.

SYMPOSIUMS

28TH NATIONAL SPACE SYMPOSIUM
SPACE FOUNDATION
The Premier Gathering of the Global Space Community
April 16 - 19, 2012
The Broadmoor Hotel • Colorado Springs, Colorado

THE ONE BUSINESS and NETWORKING EVENT
You can't miss!

FEATURED SPEAKERS

Photo Courtesy of Topfoto.uk

Mr. Charles F. Bolden, Jr.
Administrator National Aeronautics and Space Administration (NASA)

Gen. C. Robert Kehler, USAF
Commander United States Strategic Command (USSTRATCOM)

Dr. Neil deGrasse Tyson
Well-known for his enthusiastic and clever explanations of the mysteries of space

FEATURED EVENTS

CYBER 1.2
A Space Foundation event

Featured Speaker
Lt. Gen. Michael J. Basla, USAF
Vice Commander, Air Force Space Command, Peterson AFB
(Requires separate registration)

SPACE TECHNOLOGY HALL OF FAME DINNER
Co-sponsored by SPACEX

Featured Speaker
Mr. Mark Stevenson
Best-Selling Author and Futurist
"An Optimist's Tour of the Future"
(Ticket purchase may be required.)

Register Today!

THE SPACE REPORT 2012

www.NationalSpaceSymposium.org/SciMag1
+1.800.691.4000
Secure Online Registration

POSITIONS OPEN

ILLINOIS
UNIVERSITY OF ILLINOIS AT URBANA-CHAMPAIGN

Assistant or Associate Professor of Integrative Insect Biology School of Integrative Biology

The School of Integrative Biology and the Department of Entomology at the University of Illinois, Urbana-Champaign invite applications for a full-time, nine-month, tenure-track faculty position in integrative insect biology at the rank of Assistant or Associate Professor. The position starts as early as August 2012. We seek a broadly trained biologist working on insects who will develop an internationally recognized, externally funded research program that integrates evolutionary approaches into any aspect of insect biology, including but not limited to chemical ecology, developmental genetics, plant-insect interactions, physiology, neuroscience, and behavior. Applicants should be familiar with a diversity of modern techniques, including molecular and genomic methods. The successful candidate will have the opportunity to be part of dynamic and well-established communities of integrative biologists with interests spanning a wide range of taxa in the School of Integrative Biology, as well as in a number of interdisciplinary programs across the campus. Participation in both undergraduate and graduate education is required. A Ph.D. in Biology or related discipline is required by start date, and postdoctoral experience is desirable. Salary is commensurate with qualifications and experience.

To ensure full consideration, please create your candidate profile through **http://go.illinois.edu/InsectBiology** and upload your application letter, curriculum vitae, summary of research and plans, teaching philosophy and experience, and contact information for three professional references by **March 15, 2012**. Referees will be contacted electronically upon the submission of the application. Applicants may be interviewed before the closing date; however, no hiring decision will be made until after the date. For further information contact **Insect Biology Search Chair, sib@life.illinois.edu**.

Illinois is an Affirmative Action/Equal Opportunity Employer and welcomes individuals with diverse background, experiences, and ideas who embrace and value diversity and inclusivity. (www.inclusiveillinois.illinois.edu)

PRIZES

The 2012 Martha T. Muse Prize for Science and Policy in Antarctica

The "Martha T. Muse Prize for Science and Policy in Antarctica" is a US$ 100,000 unrestricted award presented to an individual in the fields of Antarctic science or policy who has demonstrated potential for sustained and significant contributions that will enhance the understanding and/or preservation of Antarctica. The Prize is inspired by Martha T. Muse's passion for Antarctica and is intended to be a legacy of the International Polar Year 2007-2008.

The prize-winner can be from any country and work in any field of Antarctic science or policy. The goal is to provide recognition of the important work being done by the individual and to call attention to the significance of understanding Antarctica in a time of change. A website with further details, including the process of nomination, closing date and selection of the Prize recipients is available at **www.museprize.org.**

The Prize is awarded by the Tinker Foundation and administered by the Scientific Committee on Antarctic Research (SCAR). The Tinker Foundation have committed to funding the Prize for at least five years.

TFI TINKER FOUNDATION INCORPORATED

Nominations open until 12 April 2012

SCAR

POSITIONS OPEN

ASSOCIATE OR FULL PROFESSOR
Obesity Research
University of Iowa

The University of Iowa Carver College of Medicine is seeking a full-time faculty member in the Department of Surgery, Division of Gastrointestinal, Minimally Invasive, and Bariatric Surgery at the level of Associate or Full Professor in the tenure-track. The successful candidate for this position will be expected to participate actively in an ambitious new University of Iowa Obesity Initiative, which is a multidisciplinary initiative in obesity research and education. New faculty with expertise in basic biomedical research and in translational and community based obesity research will complement the University's existing expertise in these areas to form the core of this innovative multidisciplinary initiative. Participation in the Obesity Research Initiative will be an important component in performance evaluations. The new hire will be among the first new faculty appointments to the Fraternal Order of Eagles Diabetes Research Center.

Candidates must possess a M.D. and/or Ph.D. (or equivalent). Candidates must have an established record of research excellence, including a record of sustained external research funding with R01 funding being highly desirable and ongoing scholarly productivity. Candidates must have experience working effectively in a diverse environment and should have excellent interpersonal and leadership skills.

The new hire may be eligible for appointment as Vice Chair of Research for the Department of Surgery, appointment to a basic science department, as well as appointment to the Dr. Edward and Dordana Mason Professorship.

To apply for this position visit the University of Iowa **website: http://jobs.uiowa.edu, requisition #60275.**

The University of Iowa is an Equal Opportunity/Affirmative Action Employer. Women and minorities are strongly encouraged to apply. Applicant credentials are subject to verification; background checks will be conducted on final candidates for all positions in the University of Iowa Hospitals and Clinics.

DEPARTMENT OF PEDIATRICS
School of Medicine
Georgetown University Medical Center

A postdoctoral position is available in the laboratory of **Dr. N'Gouemo** at Georgetown University Medical Center, Washington, D.C., to investigate the role of L-type Ca2+ channels in the etiology of alcohol withdrawal seizures in rodents. An integrated approach combining patch-clamp electrophysiology, behavior, stereotaxic surgery, protein biochemistry, RNA interference, and molecular techniques is used on various brain preparations. Candidate must have a Ph.D. or M.D.-Ph.D. in neuroscience or related field and experience track record of using electrophysiological (single neuron, brain slice recordings) and molecular (gene and protein expression, phosphorylation assays) techniques. Georgetown University Medical Center offers state-of-the-art equipment and a stimulating research environment. Curriculum vitae, brief statement of relevant experience, and names of three references can be sent as a single PDF file to **Dr. Prosper N'Gouemo** at **e-mail: pn@georgetown.edu, telephone: 202-687-8464, fax: 202-444-7161, or addressed: 3900 Reservoir Road NW, Washington DC 20057-1443.**

CAREER OPPORTUNITY—Doctor of Optometry (O.D.) degree in 27 months for Ph.D.s in science and M.D.s. Excellent career opportunities for O.D./Ph.D.s and O.D./M.D.s in research, education, industry, and clinical practice. This unique program starts in March of each year, features small classes, and 12 months devoted to clinical care.

Contact the Admissions Office, **telephone: 800-824-5526** at **the New England College of Optometry, 424 Beacon Street, Boston, MA 02115.** Additional information at **website: http://www.neco.edu, e-mail: admissions@neco.edu.**

POSITIONS OPEN

ELECTROPHYSIOLOGY RESEARCH ASSOCIATE
Yale University

Position available for Ph.D. or M.D. with expertise in patch-clamp electrophysiology, to join multidisciplinary team studying pathophysiology of ion channels, at the Center for Neuroscience and Regeneration Research, Yale Medical School. Prior experience and publications on patch-clamp analysis of ion channels, preferably in sensory neurons and/or on voltage-gated channels, are essential. Experience with both voltage-clamp and current-clamp analysis, and with functional profiling of channel mutations, is desirable. Superb opportunity to work collaboratively with cell and molecular biologists, pharmacologists, etc. Send statement of interest, curriculum vitae, and three letters of reference to: **Stephen Waxman,** M.D.-Ph.D., electronically to **e-mail: stephen.waxman@yale.edu,** and/or via post to: **Neuroscience & Regeneration Research Center of Yale University, VA Connecticut, 950 Campbell Avenue, Bldg. 34, West Haven, CT 06516.** *Equal Opportunity/Affirmative Action Employer.*

KOCH POSTDOCTORAL TEACHING FELLOW

The Department of Ecology and Evolutionary Biology (EEB) at Tulane University seeks to fill the inaugural Koch Postdoctoral Teaching Fellowship in Plant Ecology And Evolution, pending budgetary approval (**website: http://tulane.edu/sse/eebio/about/kochfellow.cfm**). The position is a two-year appointment, with faculty status and a start date of July 1. The department aims to recruit outstanding researchers with a Ph.D. and prior postdoctoral research experience who will merge excellence in teaching (30%), research (60%), and service (10%). Applicants are encouraged to identify a potential faculty collaborator in EEB, although those interested in independent research will be given consideration. Applicants should describe botanical courses they would be able to teach, including courses that are not in the existing curriculum and could be taught as special topics. An application (curriculum vitae, statement of research interests, and statement of teaching philosophy and interests) and three letters of recommendation focusing on both research excellence and teaching potential should be submitted electronically to the Search Committee (**e-mail: ecolevol@tulane.edu**). Please write "Koch Fellow" in the subject line. Application review will begin immediately, and the position will remain open until filled.

Tulane University is an Equal Employment Opportunity/Affirmative Action/ADA employer committed to excellence through diversity. All eligible candidates are invited to apply.

ASSISTANT/ASSOCIATE/FULL PROFESSOR OF NEUROSCIENCE
Washington State University

The Program in Neuroscience at Washington State University, which is housed in the Department of Veterinary and Comparative Anatomy, Pharmacology and Physiology (VCAPP), seeks to fill a tenure-track, full-time, position available in neuroscience at the rank of Assistant/Associate/Full Professor to begin January 2013. This position is a permanent state-funded nine-month position with summer funding available for the first two years of appointment. Salary and rank are dependent upon qualifications. A generous startup package is available. Laboratory space will be assigned in a newly built (completion 2012) state-of-the-art research building specifically designed for neuroscience-based research.

Screening of applications will begin March 16, 2012. For job duties and application process, go to website: **http://www.wsujobs.com/applicants/Central?quickFind=56758.** Electronically send inquiries to **e-mail: kinslow@vetmed.wsu.edu.** *Equal Employment Opportunity/Affirmative Action.*

POSITIONS OPEN

ASSISTANT PROFESSOR/ASSOCIATE PROFESSOR/PROFESSOR
Cardiovascular/Heart Failure Researcher

New York College of Osteopathic Medicine (NYCOM) of New York Institute of Technology (NYIT) seeks a new faculty member with research expertise in the area of Cardiovascular Disease or Heart Failure. Applicants will be considered at all ranks, with extramural funding expected for senior level appointment. The successful candidate will focus primarily on research, with the remaining effort in teaching and service. He/she will have access to a confocal microscope, histology services, physiology core services including echocardiography/hemodynamics, and an animal facility which currently accommodates rats, mice, and zebrafish.

New York Institute of Technology (NYIT) is a private, non-profit, independent institution of higher learning for 14,000 students enrolled in more than 90 programs of study leading to undergraduate, graduate, and professional degrees. Students attend classes at NYIT's Manhattan and Long Island campuses as well as five global campuses. In 2010 and 2011, NYIT was named a "Great College to Work For" by The Chronicle of Higher Education. For more information, visit **website: http://www.nyit.edu.**

The successful candidate will possess a Ph.D., M.D., DVM, or D.O. and three-plus years of postdoctoral research experience. To apply, please electronically send cover letter and resume to: **Dr. A. Martin Gerdes,** Chair of Biomedical Sciences at **e-mail agerdes@nyit.edu. P.O. Box 8000 Northern Blvd, NY 11568-8000.** *Equal Opportunity Employer Minorities/Females/Persons with Disabilities/Veterans.*

POSTDOCTORAL FELLOWSHIPS AND JUNIOR FACULTY POSITIONS in Diabetes and Beta Cell Biology
University of Pittsburgh
Division of Endocrinology & Metabolism

Pancreatic beta cell-diabetes group seeks postdocs and junior faculty, M.D. or Ph.D., with excellence in cell biological techniques (including co-IP, immunohistochemistry, confocal imaging, and intracellular trafficking) and molecular techniques (including adenoviral and retroviral gene delivery). Send resume to: **Andrew Stewart, M.D., Chief, Endocrinology, University of Pittsburgh School of Medicine, USA,** via **e-mail: kal134@pitt.edu.**

The University of Pittsburgh is an Affirmative Action/Equal Opportunity Employer.

Help employers find you. Post your resume/cv.

Science Careers
From the journal *Science* AAAS

www.ScienceCareers.org

MARKETPLACE

Widely Recognized Original & Guaranteed

KlenTaq1

8¢/u Truncated Taq DNA Polymerase Withstand 99°C

US Pat #5,436,149
Call: **Ab Peptides**
Fax: 314•968•8988

e-mail: abpeps@msn.com
1•800•383•3362
www.abpeps.com